TIME DISTANCE ANALYSIS OF A MINE SCALE EVENT

By

Benjamin Ollila

A thesis submitted in partial fulfillment

of the requirements for the degree of

Master of Applied Science (M.A.Sc.) in Natural Resources Engineering

The Office of Graduate Studies

Laurentian University

Sudbury, Ontario, Canada

THESIS DEFENCE COMMITTEE/COMITÉ DE SOUTENANCE DE THÈSE
Laurentian Université/Université Laurentienne
Faculty of Graduate Studies/Faculté des études supérieures

Title of Thesis Titre de la thèse	TIME DISTANCE ANALYSIS OF A MINE SCALE EVENT
Name of Candidate Nom du candidat	Ollila, Benjamin
Degree Diplôme	Master of Science
Department/Program Département/Programme	Natural Resources Engineering
Date of Defence Date de la soutenance	February 25, 2022

APPROVED/APPROUVÉ

Thesis Examiners/Examinateurs de thèse:

Dr. Marty Hudyma
(Co-Supervisor/Co-directeur(trice) de thèse)

Dr. Laura Brown
(Co-Supervisor/Co-directeur(trice) de thèse)

Dr. Dean Millar
(Committee member/Membre du comité)

Approved for the Office of Graduate Studies
Approuvé pour le Bureau des études supérieures
Tammy Eger, PhD
Vice-President, Research (Office of Graduate Studies)
Vice-rectrice à la recherche (Bureau des études supérieures)

Dr. Brad Simser
(External Examiner/Examinateur externe)

ACCESSIBILITY CLAUSE AND PERMISSION TO USE

Abstract

Mining induced seismic events greater then Nuttli Magnitude 3.0 are difficult to understand, have high potential consequences and are becoming increasingly common in Canada. The term mine scale event (MSE) is used to describe a seismic event in which the mechanisms and processes involved take place on a scale similar to that of the mine.

A MSE from Nickel Rim South Mine was investigated using seismic data to explain its time, location and large magnitude. A novel tool, Time Distance Analysis was developed to identify spatial-temporal trends in seismicity around the MSE. Guidelines were developed to account for the unknown spatial and temporal extent of the processes that led to and were affected by the MSE.

The results showed that preceding seismicity tended to coalesce around the eventual hypocenter of the MSE while subsequent seismicity migrated away. The coalescence was interpreted to represent the deterioration of a fault asperity, leading to an eventual rupture. After the MSE occurred, the dispersion of seismicity was interpreted to represent an unloading of the source region.

Keywords

Mine seismicity, mining, rock mechanics

Acknowledgements

Thank you Dr. Marty Hudyma for your inspiration, support and guidance through this research. Your practical experience and theoretical knowledge set me on the right path from the beginning and I greatly enjoyed the process of exploring and learning about the field of mine seismicity.

Thank you Dr. Laura Brown for the discussions, ideas and critiques. Your guidance was a great help to narrow my focus in completion of this thesis.

Thank you to the Australian Center for Geomechanics for providing the seismic data analysis software used in this research, mXrap.

I would like to thank Glencore for use of the high-quality seismic data from Nickel Rim South Mine.

Financial support was provided by the Bharti School of Engineering and Kirkland Lake Gold.

Table of Contents

List of Tables

List of Figures

1 Introduction

Large seismic events have been reported in Canadian mines for almost 100 years (Hedley, 1992). Many of these events have been greater than magnitude 3.0, and in some cases greater than 4.0. Events of these magnitudes are commonplace in earthquake seismology but are very serious occurrences in mining. While earthquakes tend to occur far below the surface, mining related events often occur proximally to the underground workings. Many of these events have resulted in severe damage to the mine workings, and in some cases, loss of life.

The problem of large seismic events and rockbursting first became prevalent in the mining camps of Sudbury and Kirkland Lake in in the 1930's. Beginning in the 1980's, large seismic events became more widely recorded across Canada, in Ontario, occurring in Red Lake, Timmins, Hemlo, Thunder Bay, in Quebec, Rouyn, Val D'or, and the Jonquiere area, and in New Brunswick in Bathurst.

In Canada, it is often easier to continue extraction from an operating mine than for greenfields development, resulting in mining taking place at ever greater depths. Building a new mine has always been an extremely expensive endeavour, but difficulties are not purely financial. In the past 40 years, environmental standards have increased and a greater degree of scrutiny is placed on the environmental impact of mining, often resulting in a long permitting process. Additionally, new discoveries of large or high grade orebodies have become increasingly rare, and are more and more likely to be in remote, hard to access locations. The ever growing global metal demand has resulted in a tendency for Canadian mines to increase extraction from established mines rather than attempt to build new mines. While it is generally a positive outcome that existing mines continue to operate, the potential for large seismic events tends to increase with maturity and depth. Greater extraction often means deeper, higher stress, and higher hazard orebodies will be extracted. Improved technology has enabled mining at greater depths, with battery

powered electric equipment reducing the ventilation limitations and an evolution of ground support to better handle dynamic ground conditions. The two deepest mines in Canada, Agnico-Eagle's LaRonde and Glencore's Kidd Creek, have both had numerous events greater than magnitude 3.0. As the current reserves of these already deep orebodies nears completion, both companies have recently announced funding for ultra deep exploration programs (Boyd, 2021; Grech, 2021), indicating the need, will and ability to mine at greater depths. This tendency for ultra deep mining is underscored by the fact that large seismic events already occur at these mines and are likely to continue to occur. These large seismic events can have a high consequences and are difficult to understand with much certainty. As Canadian mines become deeper and more mature, large events are becoming more prevalent, resulting in a greater need for research.

1.1 Mine Scale Event Definition

The term "mine scale event" (MSE) will be used to describe seismic events influenced by processes that exist on a scale that includes a significant part of the mine. These events are the most rare, largest and potentially most damaging instances of seismicity in mining. While smaller scale seismicity (Moment Magnitude (Mw) < 2.0) can be caused by a rockmass failure process induced by the excavation of a single tunnel or stope, a MSE is influenced by accumulated mining on a much larger scale. This research will explore the influence that mining has on the processes that generate these events in the domains of space, time and energy.

For the purposes of this thesis, the term MSE will be used to describe an event greater than Nuttli Magnitude (Mn) 3.0 (Nuttli, 1973).

1.2 The Problem of Mine Scale Events

MSEs have historically been one of the great problems in underground mining ground control. These events, though relatively uncommon, have the unfortunate combination of potential for high consequence and limited or incomplete data, often leaving ground control practitioners with a

poor or weak understanding of the forces and mechanisms involved. There is often inability to observe the damage at the source, or to observe the fracture that produced the seismic wave. In general, failure of brittle material depends on that material's load bearing capacity versus the induced load. In mining related rockmass failure, the *in situ* stress conditions, the strength of the rockmass and strength of the discontinuities vary significantly and are often poorly understood. There are factors affecting the stability of the rockmass that can be unknown, for example, unidentified faults or lithological rock units. The timing of large seismic events is often not understood. Some large events are strongly related to mine blasting, some are poorly related, and some have no relation whatsoever and appear to occur randomly.

In all cases of mining related seismicity there are geologic influences, such as the pre-mining stress regime and the structural history imprinted in the rockmass through geological discontinuities. The mining influence is predominantly the mining related induced stresses that can substantially increase the loads on the rockmass. The extent of geologic influence to MSEs likely exists on a spectrum, with a completely natural earthquake on one end and a completely mining induced seismic event on the other end. A deterministic viewpoint suggests that in most cases, a Mn 3.0 that occurs near a mine is not a natural earthquake, yet it is not always clear to what extent mining influence has in generating these events.

Compared to earthquakes, a Mn 3.0 event is only a minor event. The difference in consequence, however, exists due to the fact the natural earthquakes of this size are often tens or hundreds of kilometres below surface, while the hypocenter of a MSE can be near or within the mine workings. Figure 1 shows just a small part of the damage caused by a Mn 3.8 that occurred at Kidd Mine in 2011.

Figure 1. Kidd Mine Mn 3.8 Rockburst (Duan, Wesseloo and Potvin, 2015)

Photos of the worst damage caused by MSEs – wholesale tunnel collapse – are uninteresting in that the damage dimensions can't be observed; the tunnel simply ends in a large muck pile. While Figure 1 does not show anything close to the worst damage caused by MSEs, it provides a good indication of how extensive the damage can be, existing on both heavily supported walls and stretching into the distance. The most obvious risk of a MSE is that to the safety of underground personnel. While an individual could have conceivably survived the damage shown in Figure 1, it is highly unlikely that person would have walked away unscathed. The secondary risk of a MSE is financial, which can have impact the mine ranging from simple rehabilitation of damage to abandonment of reserves to complete loss of mine excavations. The damage shown in Figure 1 can be exceedingly difficult to repair, and it often makes sense to simply abandon the tunnel and develop a new one. In some cases, mine scale events have resulted in the mine operators abandoning equipment, development, significant ore reserves, or even shutting down an entire

mine. A series of large seismic events, including a Mn 3.8, resulted in the early closure of Macassa Mine in 1999 (Blake and Hedley, 2001). This mine closure not only negatively impacted the mine operator, Kinross Gold Corp., it devastated the economy of the small town of Kirkland Lake in which the mine was located. The IAMGOLD Westwood mine closed for several months following a large event in 2020. Events Mn ≥ 3.0 do not always cause damage to mine excavations; factors involved in damage mechanisms are complex, having been studied by Kaiser, McCreath and Tannant, 1996; Heal, Potvin and Hudyma, 2006; Kaiser and Cai, 2013, among others. While MSEs do not always cause significant damage, the potential for damage by MSEs tends to be much greater than for smaller mining related events.

An unfortunate attribute of seismicity is that for very large mining events, the general understanding of contributing factors tends to be uncertain (Ortlepp, 2005). In many cases, MSEs have occurred at times when there is no clear trigger, which can come as a surprise to the mine operators. April 23, 2020 a Mn 3.5 seismic event occurred at Creighton Mine shortly after a development blast (Sudbury.com, 2020). The resultant stress change from the blast could not supply the energy released in a seismic event of this magnitude, leaving open the questions of what process supplied the energy and why did the event occur at the time of such a small blast. It seems likely that there may be a tectonic component to the energy supply of some of these events, but deterministically understanding how close a fault is to slipping prior to mining is near impossible given the uncertainties involved. Once a MSE event occurs, the nature of the rockmass damage at the source is usually unknown, with multiple potential explanations. Spatial description of rockmass damage is limited to what can be observed from the mine workings and is often only secondary damage.

The occurrence of mine scale events is becoming increasingly prevalent in Canada. Figure 2 shows that in Canada, the number of large events (Mn ≥ 3.0) per year has undergone a significant increase since 2011.

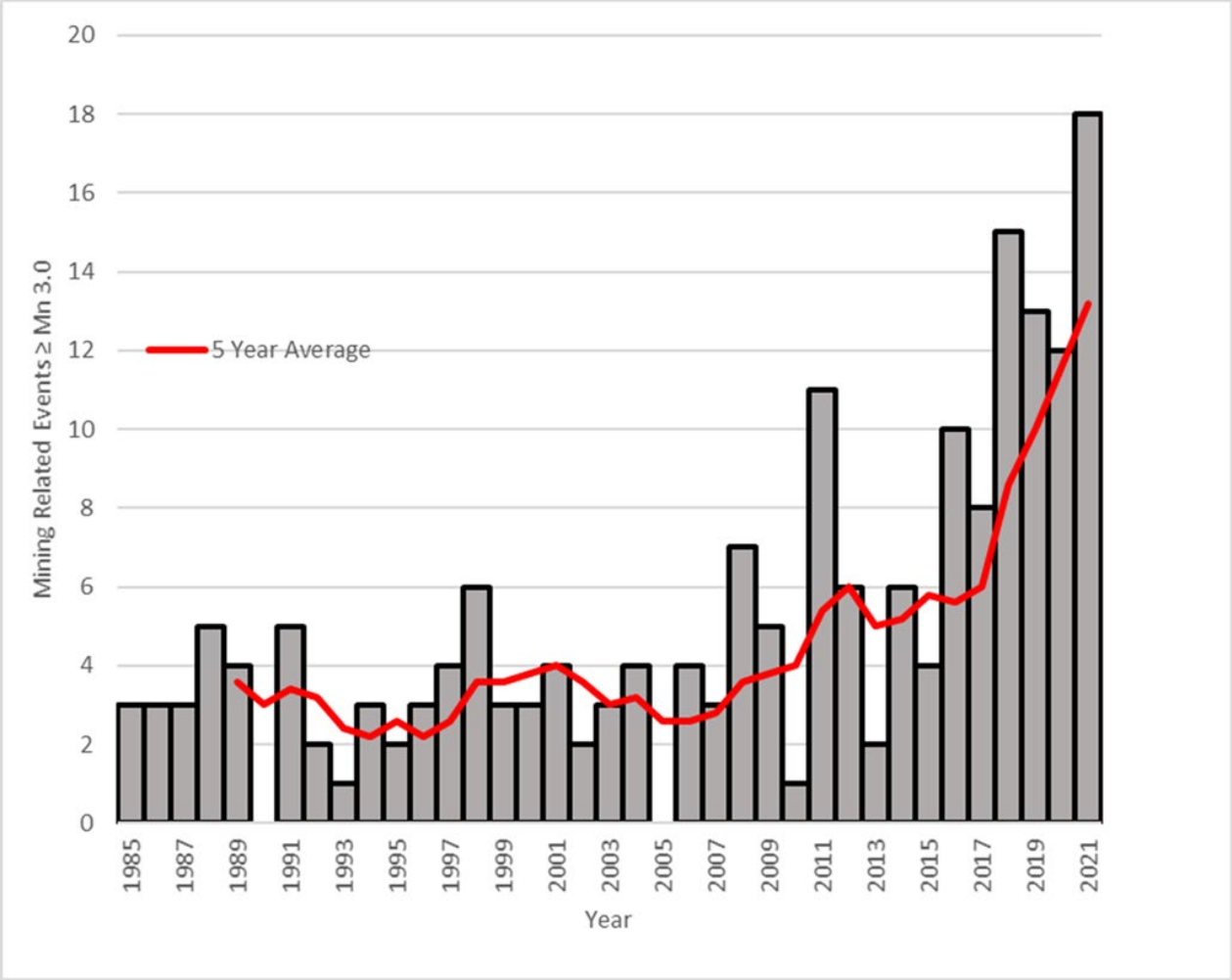

Figure 2. Mining related events Mn ≥ 3.0 in Canada (Earthquakes Canada, 2021)

The historical average was 3.2 events per year from 1985 – 2011. In the past 10 years, the average number of events per year was 8.7, and appears to be increasing.

Possible factors for the increase in rate of large events include the high level of maturity of many Canadian operations as well as the tendency for deeper and higher stress extraction. Locations for events since 2010 include at least eight mines that are still operational, six of which have had multiple events Mn ≥ 3.0 (Earthquakes Canada, 2021). Beyond speculating as to the cause of the greater frequency of large events, the critical fact is that conditions that generate MSEs exist in Canadian mining and appear to be increasingly common.

1.3 Thesis Objective

An underpinning assumption behind this research is that MSEs do not occur randomly and are part of larger rockmass failure process that can be studied and characterized using source parameters of seismic events. These rockmass failure processes lead to and are impacted by MSEs, therefore identification and characterization of these processes over time can improve understanding of MSEs. A novel tool, Time-Distance Analysis (TDA), was developed to identify and understand spatial trends in source parameters of seismicity around MSEs over time. The objective of this thesis is to understand MSEs as a part of a larger rockmass failure process using TDA. A case study of a large seismic event from Nickel Rim South mine features the use of TDA.

1.4 Scope

The scope of this research is limited to observation and manipulation of source parameters of seismicity and comparison with geologic and mining data. This thesis is focused on development and use of a novel method, TDA, to further understand the relation seismicity, geology and mining can have in the occurrence of MSEs.

The focus of the research is on the use of source parameters rather than improvement of collection techniques or improvement of their reliability.

This work is constrained to the use of inferred seismic analysis techniques, derived from spectral analyses. Other methods of understanding large events exist, such as waveform analysis techniques and numerical modeling. These methods, while shown to be useful for back analysis, require more specialized knowledge, and are less commonly performed in-house at mine sites. An objective of this research was to improve methods of practical back analysis for ground control practitioners at mine sites.

1.5 Research Approach

This thesis employed a deductive approach to meet the research objectives. A research strategy was developed to determine if a MSE could be explained by the theoretical asperity model for fault slip. This strategy consisted of development of a novel tool (TDA) and guidelines for use. The tool was applied to back analyze a MSE case study from Nickel Rim South Mine and results were discussed.

1.6 Thesis Structure

This section will describe the organization of the thesis.

Chapter 2 consists of a literature review, which describes seismicity in mines, calculation of seismic source parameters, seismic data analyses and a brief description of some earthquake concepts.

In Chapter 3, a brief background is given to Glencore's Nickel Rim South in Sudbury, Ontario.

Chapter 4 introduces a MSE that occurred at Nickel Rim South and identifies unanswered questions. The asperity model for fault slip is introduced as a potential failure mechanism for the MSE. A novel technique, Time-Distance Analysis is introduced to understand if the MSE is an asperity failure. A methodology for use of Time-Distance Analysis is presented. The methodology is applied to the case study and results are presented.

Chapter 5 discusses the implications, assumptions and results of the thesis.

Chapter 6 briefly summarizes the feature case study and recommends areas for further study.

2 Literature Review

2.1 Seismicity in Mines

The study of mine seismicity attempts to understand and characterize the interaction between rockmass failure processes and mining operations with the goal of minimizing risk. The questions for study often involve the:

- Timing of seismicity
- Location of seismicity
- Magnitude or size of seismicity

Full understanding of the causes of time, location and magnitude of seismicity is not always possible. Analysis methodologies in mine seismicity attempt to quantify the uncertainty and improve understanding of the influences. The results of these analyses can be used to refine and improve strategies to reduce impact of seismicity on mining.

This section will describe causes of seismicity, how seismicity is manifested and the effects of seismicity.

2.1.1 Stress

The occurrence of seismicity is related to stress in the rock. Stress levels near to or greater than the strength of the rock can result in rock failure and the radiation of seismic waves (Cook, 1976).

In the natural environment, stress magnitude at a given point tends to be anisotropic; it varies with direction. Common practice is to summarize the stress tensor to three orthogonally oriented principal stresses: σ_1 (primary), σ_2 (intermediate), and σ_3 (minimum).

Prior to mining activities taking place, a rockmass is under a natural state of stress referred to as the *in situ* stress. The magnitude and directions of *in situ* stress are dependent on the weight of the overlying rock, tectonic forces as well as the loading conditions imposed through geologic history (Brady and Brown, 2004)

The excavation of mine tunnels and voids alters the stress regime in the rockmass. As mining takes place and new voids are created, the load that was previously carried by the mined rock is redistributed to the surrounding rockmass. The total state of stress then becomes the summation of the *in situ* stresses and the mining induced stresses (Gibowicz and Kijko, 1994). Figure 3 illustrates modeled stress redistribution around two underground excavations.

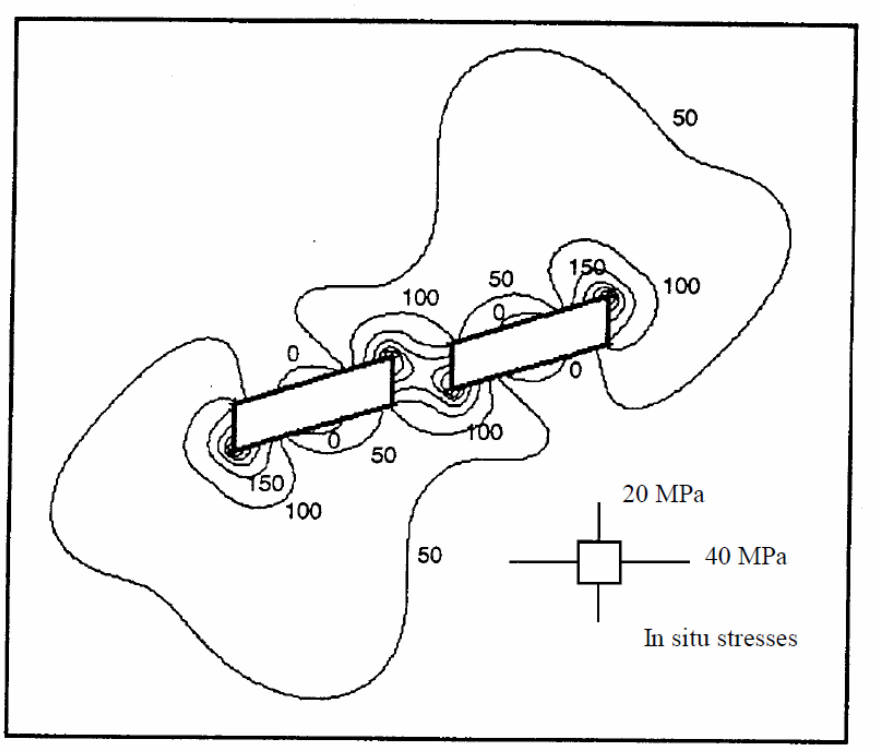

Figure 3 Primary stress around two trapezoidal shaped excavations in rock (Hoek, Kaiser and Bawden, 1995)

Figure 3 shows contours of primary stress around two trapezoidal shaped excavations. While the *in situ* principal stress is 40 megapascals (MPa), the additional stress induced by mining exceeds 150 MPa in the vicinity of the excavation. As the distance from the excavation increases, the

stress levels decrease back to the undisturbed *in situ* stress levels. The stress contours tend to wrap the excavations and are highest at the outer corners of the excavations and in the central pillar.

While increases in stress are often seen as a driver of rock failure, leading to seismicity, a decrease in confining stress or a change in stress direction can also cause seismicity (Gibowicz and Lasocki, 2001; Castro, Carter and Lightfoot, 2009). It has long been recognized that strength of rock is dependent on confinement, and peak loads that a rock can withstand tend to increase with greater confinement (Coulomb, 1776). A drop in confinement can reduce the strength of a previously stable rockmass, permitting rock yield and potentially seismicity. Often in analytical or numerical analyses, confinement dependent deviatoric stress (σ_1 - σ_3) is used to assess the stability of a rockmass.

2.1.2 Seismic Rock Failure Process

A seismic event is the near instantaneous release of elastic potential energy through an inelastic deformation process (Mendecki, 1993). Hard rock, when loaded, deforms elastically, storing strain energy. Through either an increase in load or a decrease in strength, sudden failure of that rock results in a near instantaneous rebound to static equilibrium. The elastic potential energy is released in three ways: through heat, inelastic deformation and elastic ground motions (Kanamori and Rivera, 2006).

Acoustic emissions, like seismic events, are elastic waveforms produced by inelastic deformation in the rockmass (Lockner, 1993). While seismicity and acoustic emissions are both a type of near-instantaneous rock failure, acoustic emissions take place on a much smaller scale, and are usually measured in a laboratory setting. In comparison of magnitude, acoustic emissions are usually measured below Mw -6, while recorded mining events are usually Mw > -3 (Goodfellow and Young, 2014). Though seismicity is generated by physical instances of rockmass failure, it is difficult to directly measure the stress and strain at the source of an event. Total stress and strain,

however, are measurable in sample scale testing and acoustic emissions can provide learnings how seismicity responds to stress and strain. Knowledge of how acoustic emissions occur at different stages of the rock failure process can improve understanding of seismicity at a larger scale (Lockner, 1993). Figure 4 shows a typical stress strain curve with measured acoustic emissions for the loading of a brittle rock sample.

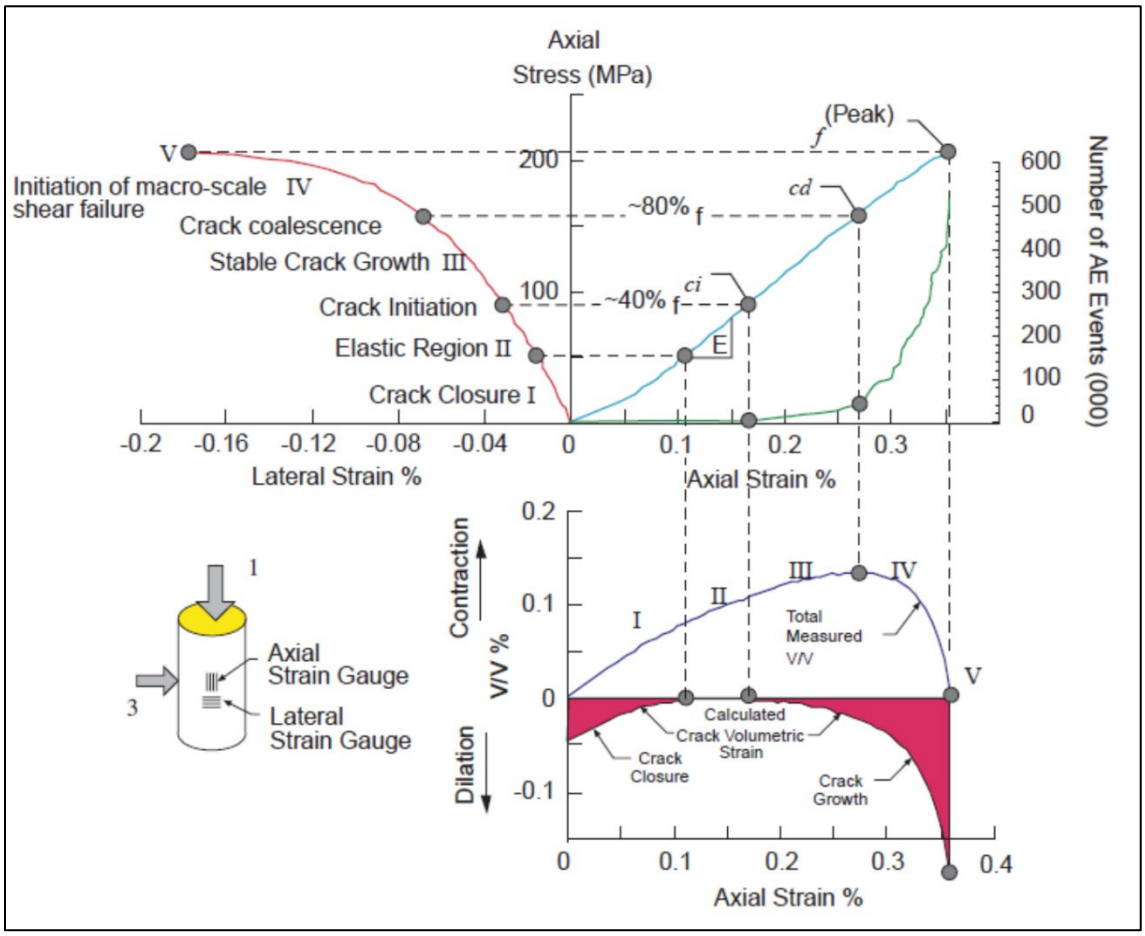

Figure 4 Characteristic stress-strain curve for the failure of brittle rock under axial load (Martin, Christiansson and Soederhaell, 2001)

Figure 4 shows a rock sample under axial load, with measurements of axial strain, lateral strain, axial stress and cumulative acoustic emission count. Several stages of rock failure can be observed. The following discussion is summarized from (Martin and Chandler, 1994; Martin, Christiansson and Soederhaell, 2001)

Crack closure: Rock samples typically have some degree of preexisting damage or cracking. As the load is initialized, these cracks close, which results in gradually decreasing strain. Strain generally takes place without new cracking or acoustic emissions at this stage.

Elastic region: Rock response to increase or decrease in load in a linear elastic manner. Strain is recoverable upon removal of the load.

Crack initiation: As the load increases, inelastic damage begins at the crack initiation point. Acoustic emissions start to increase.

Stable crack growth: As load continues to increase past the crack initiation point, cracking damage and acoustic emissions occur in a stable manner.

Crack coalescence: Cracks begin to interact and single cracks begin to merge into larger cracks. After this point, strain and number of acoustic emission increase more dramatically. Martin and Chandler (1994) suggested that above point of crack coalescence (*cd),* failure will eventually occur if loading conditions are constant, making *cd* indicative of long term strength.

Initiation of macro scale shear failure: Further loading produces growth of fractures towards the final rupture geometry.

Peak: At peak loading, acoustic emissions and stress are at the highest point. After this point, stress begins to decrease due to failure of the rock sample.

Figure 4 shows the stress-strain curve up to peak stress. After peak stress, as the rock sample fails, accurate measurements are difficult to achieve in brittle rock samples in the laboratory setting and have historically been limited by the testing equipment (Hou *et al.*, 2021). Diederichs, Kaiser and Eberhardt (2004) demonstrated post peak behavior using a numerical simulation of a stress-strain curve with acoustic emissions (Figure 5).

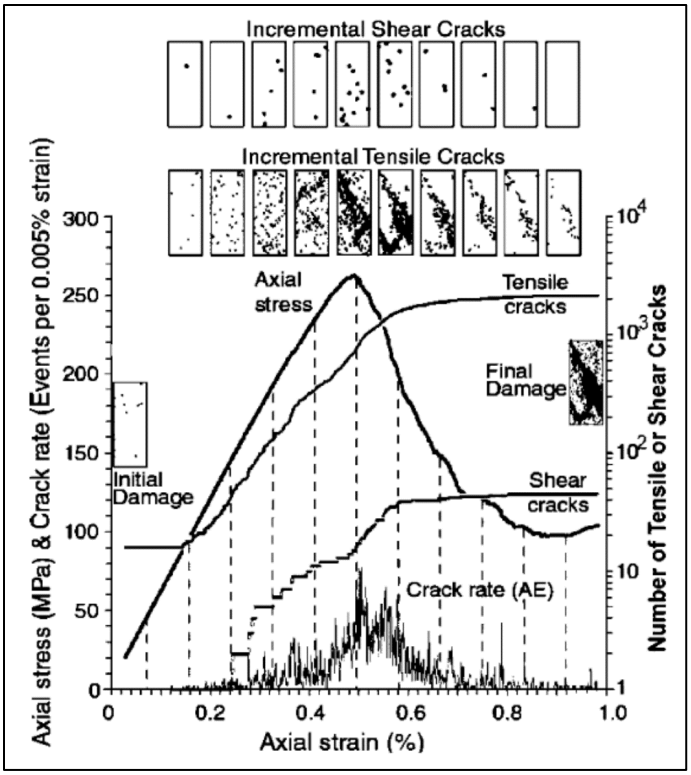

Figure 5 Numerical simulation of acoustic emissions associated with the failure of intact granite (Diederichs, Kaiser and Eberhardt, 2004).

While Figure 4 showed the pre peak, stiffening response of a rock sample, Figure 5 adds information by showing post peak, softening behaviour. Several characteristics of the rock failure process can be observed and their potential meanings for mine seismicity are discussed.

- The crack rate is low (aseismic) during the initial elastic loading period. The strain response due to stress is dominantly elastic. The implication is that during dominantly elastic loading, a rockmass can store substantial energy without emitting significant seismicity.
- Damage locations, viewed as incremental tensile and shear cracks, tend to concentrate and coalesce as peak stress is approached and passed, due to an increasing tendency for the propagation of existing fractures to consume less energy than the formation of new fractures. This behaviour is similar to the concept of crack coalescence from Figure 4.

- The highest crack rate occurs just after peak axial stress is reached and stress begins to decrease. The regime changes from dominantly elastic energy storage to inelastic energy release. The implication is that the greatest seismic activity may take place as the rockmass is being unloaded rather than loaded.
- The crack rate becomes low (aseismic) once again as the residual stress is reached. A failed rockmass should become aseismic.

2.1.3 Seismic Source Mechanisms

Seismicity in mines is not a random process. Each seismic event is an instance of inelastic deformation that is part of a physical rockmass failure process (Hudyma and Potvin, 2010). Mining and geological factors can influence these rockmass failure processes, therefore seismicity is often spatially or temporally associated with an influential factor. Common locations of seismic events in mining are:

- Excavation abutments (Disley, 2014; Carusone, 2018)
- Development blasting (Drover and Villaescusa, 2019)
- Pillars (Hudyma *et al.*, 1994; Townsend and Sampson-Forsythe, 2014; Disley, 2018)
- Faults (White and Whyatt, 1999, Van Aswegen and Meijer, 1994)
- Lithological contacts (Lebel, Quesnel and Glover, 1987; Counter, 2017)
- Stiff dykes (James, Rangasamy and Petho, 2007)

A fundamental law of seismicity is that as event magnitude increases, the frequency of occurrence of that event size tends to decrease (Gutenberg and Richter, 1944). The largest events are relatively rare in mining and can only occur in locations where conditions permit them. The amount of rockmass deformation that occurs during a seismic event tends to increase with magnitude, implying that larger mining events should be increasingly related to rockmass failure

systems that can generate greater amounts of deformation. Figure 6 shows locations of large events reported in a deep South African mine.

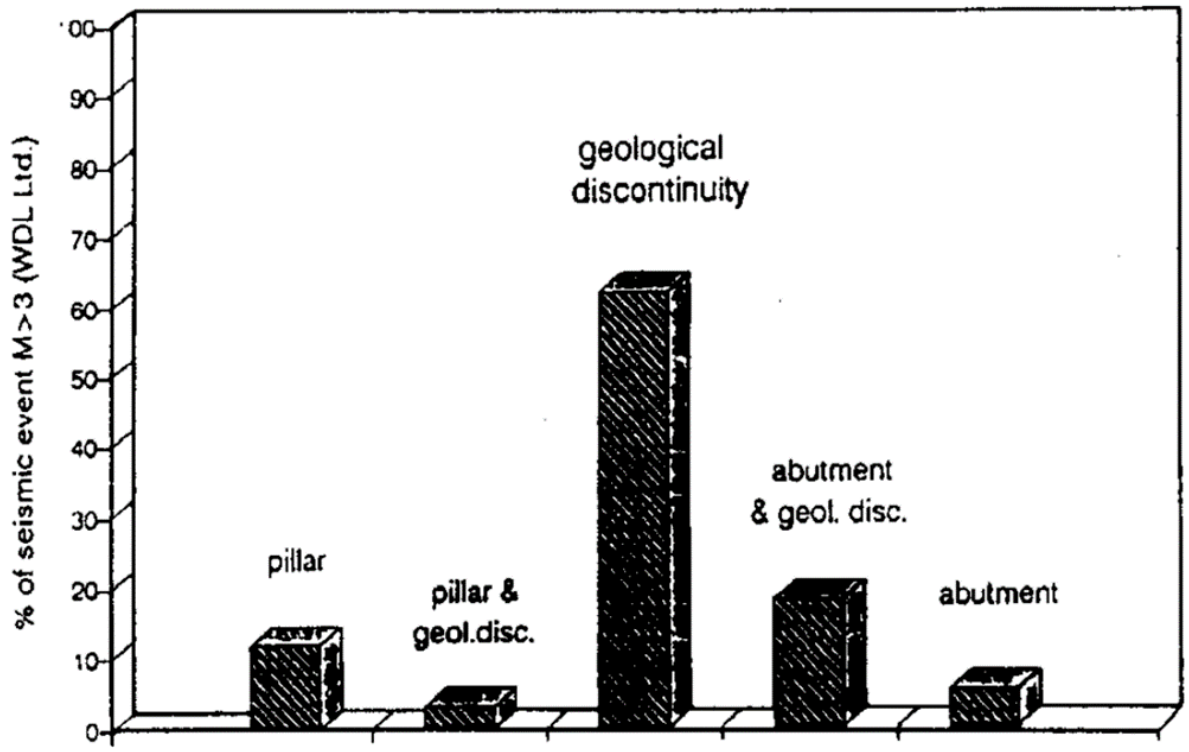

Figure 6 Locations of large seismic events (Mw > 3) at Western Deep Levels, South Africa (Lenhardt, 1988)

More than 50% of events occur in proximity to geological discontinuities, while other common locations include abutment-discontinuity interactions and mine pillars. It's clear that the largest events most commonly involve geological structure, but the possibility of large events occurring without mapped structure still exists.

The term seismic source mechanism describes the dominant rockmass failure process that generates seismicity (Gibowicz and Kijko, 1994). Characterization of seismic events as part of specific sources helps define the seismic hazard; when and where large events are most likely to occur (Heal, Hudyma and Vezina, 2005; Hudyma and Potvin, 2010; Mendecki, Lynch and Malovichko, 2010). Figure 7 diagrammatically shows several common source mechanisms found in mines.

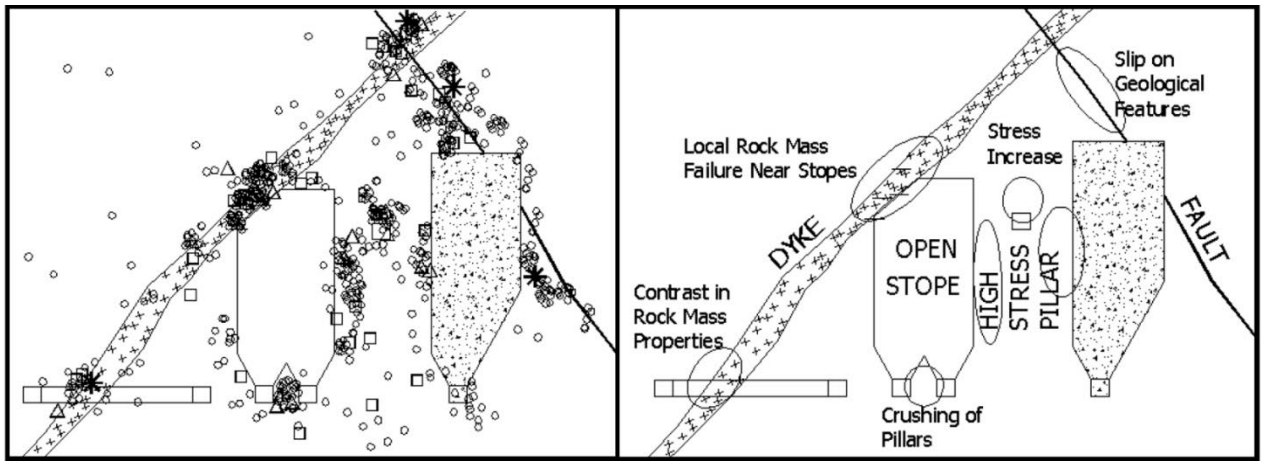

Figure 7. Populations of mine seismicity (left) and labeled source mechanisms (right) (Hudyma, Mikula and Heal, 2003)

The left diagram of Figure 7 shows typical locations of seismicity around geological features and mining excavations, while the right diagram illustrates how the occurrence of the events are explained in terms of rockmass failure mechanisms.

Hedley (1992) classified mechanisms as either volumetric or contact failure. Volumetric failure is defined as overstressing of a geometric component of the mine, such as a pillar or abutment. Contact failure describes shear along a preexisting discontinuity, such as a fault or contact.

Another way to describe seismic source mechanisms is by their relative connection with mining. Gibowicz (1990) stated that in general terms, there are two main types of events in mining; those directly associated with mining induced rockmass failure processes and those that exist on large scale, pre-mining discontinuities such as faults and weak contacts. Rockmass failure processes that are related to mining are usually near excavations, are associated with blast-induced stress change and tend to be better understood than seismicity on geologic discontinuities, which is often distant from the excavations, and in the short term, unrelated to timing of blast induced stress change (Hudyma, 2008; Brown, 2018).

Classifying populations of seismicity by source mechanism not only helps characterize rockmass failure processes, but it can also give an indication of the level of hazard presented by the event population, since the type of rockmass failure mechanism tends to control the amount of deformation and energy that can be released by a single event. Table 1 proposes typical behaviors for seismic events of varying size.

Table 1. Suggested characteristics of typical seismic source mechanisms in mines. Redrawn after (Ortlepp, 1998) by (Hudyma, Mikula and Heal, 2003)

SEISMIC SOURCE MECHANISM					
Event Type	Strain-Burst	Buckling	Face-Crush, Pillar Burst	Shear Rupture	Fault-Slip
Richter Magnitude	upto 0	0 to 1.5	1.0 to 2.5	2.0 to 3.5	2.5 to 5.0
Instability Process	Spalling, buckling	Euler-type instability	Slabbing, crushing, dilation	"Stick-slip" release of energy from strained rock around slip surface	
Seismic Signature	Implosive	Implosive	Implosive plus shear	Double-couple fault slip	
Postulated Source Mechanism	Superficial spalling with violent ejection of fragments	Outward expulsion of large slabs pre-existing parallel to surface of opening	Violent expulsion of rock from stope face or pillar sides	Violent propagation of shear fracture through intact rock mass	Violent renewed movement on existing fault or dyke contact
Required Condition for Event to Occur	Failure very close to free surface	Free surface >> lamina thickness	Stress > strength in destoyed volume	Shear stress exceeds shear strength of rock	Shear stress exceeds resistance to sliding

Events that can be explained by the mining induced stress change caused by newly created underground excavations tend to have source mechanisms with spatial and temporal relation to those excavations. Examples illustrated in Figure 7 include stress increase around development, local rockmass failure around stopes and high stress in pillars, which are associated with strain bursting, buckling, face crush and pillar bursts. The timing of stress increase events usually shows a strong relation to blast influences (Hudyma, 2008). These types of failure processes tend to respond temporally to changes in mine geometry caused by blasting. The locations of stress change events often occur near underground excavations in locations where blast induced stress change has the most influence (Brown and Hudyma, 2018).

Table 1 provides a general guideline that describes maximum sizes for events of different mechanisms, but magnitudes have been found to vary. Canadian pillar events have been

recorded up to magnitudes of ML 3.5 (Blake and Hedley, 2001), an order of magnitude greater than that given by Ortlepp in Table 1. Lenhardt (1992) also suggests pillar related events can occur at ML > 3.0. Though pillar events may be possible at higher magnitudes, Figure 6 and Table 1 seem to indicate the majority of very large events occur on geologic discontinuities, which may be due to the potential of a preexisting discontinuity to release a greater amount of strain energy upon rupture.

Structurally related seismicity occurs through shear on preexisting geologic discontinuities and tend to be less responsive to mining influences than stress increase related sources (Hudyma, 2008). The largest events may become more common later in a mine life, as the extracted volume grows (Hedley *et al.*, 2013) . Potential for damage from fault slip events generally extends over a greater spatial area than stress change events (Hedley *et al.*, 2013). The condition for fault slip in Table 1 states that an event occurs due to higher shear stress than resistance to sliding. It follows that this condition could be reached in two ways: an increase in shear stress or a decrease in resistance to sliding. A decrease in resistance can be due to reduction in normal, clamping stress on the structure (Castro, Carter and Lightfoot, 2009) or through a material change. Dieterich (1978,1972) performed block and spring experiments as an analogue for fault slip, suggesting that the frictional material property of a fault should not be assumed as a constant over the plane, and that the friction on a fault plane was to some degree time dependent due to strain induced deterioration of the rock at the fault interface.

The shear rupture seismic source mechanism has not been extensively documented outside of South Africa. A shear rupture describes a seismic event that causes shearing of previously intact ground to form a new mining induced fault (Gay and Ortlepp, 1978). South African experience has been that these event mechanisms are possible under high stress, strong massive rock and tabular mining. Documentation of shear ruptures outside of South Africa has been limited. In Canada, mine geometry, in-situ stress and geologic conditions are quite different than in South

African, which could potentially impact the defining characteristics of shear rupture type failure. A shear rupture mechanism for large events has been proposed at two Canadian mines: Kidd Creek mine (Counter, 2014; Disley, 2014), as well as the Williams mine (Coulson, 2009; Bewick, 2013). Both of these cases were associated with regional pillars.

2.1.4 Seismic Waves

Ground motions generated by seismicity consist of body waves: Primary (P) waves and Secondary (S) waves, and surface waves: Love waves and Raleigh waves. Generally, only the body waves, P and S, are of interest in the near field in mines. Figure 8 illustrates a typical seismic waveform composed of the two waves.

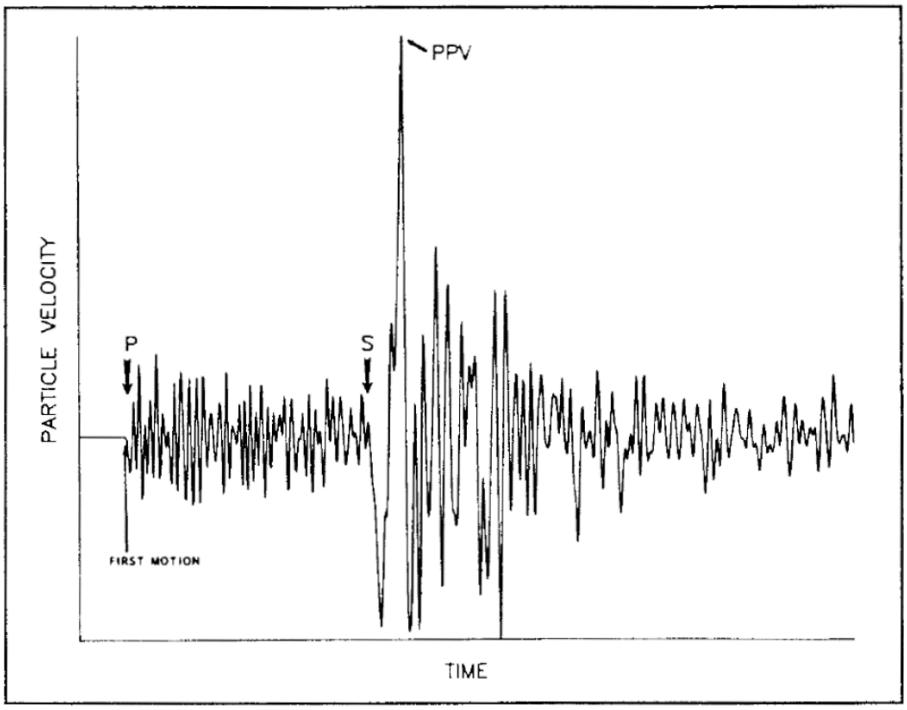

Figure 8. P and S Waves (Hedley, 1991)

P waves are longitudinal, meaning that the direction of the wave motion is in the direction of travel. S waves are transverse, meaning the direction of the wave motion is perpendicular to the direction of travel. P and S waves have individual velocities that depend on the characteristics of the rock.

P waves have a higher velocity than S waves, therefore a typical seismic trace will show a later arrival time for the S wave, as illustrated in Figure 8.

An important characteristic of seismic waves is attenuation of amplitude with distance from the event hypocenter. Seismic waves attenuate with distance for three primary reasons (Cormier and Gupta, 1990):

- Geometric spreading: increase in radiation area with distance from their origin
- Intrinsic attenuation: loss of energy through inelastic deformation of the medium
- Scattering attenuation: the energy of the wave is dispersed during transfer though heterogeneous mediums

2.1.5 Relation between Seismicity and Mining

Seismicity in mining is related to the excavation process of the mine. Hedley (1992) observed that the largest events tended to occur after approximately 80% extraction of an orebody, suggesting that the cumulative mining void is influential in generation of large events. Prior to mining, rock is usually in a near-equilibrium state, evidenced by the lack of seismicity. The stress change due to the excavation of mine voids induces local rockmass failure and destabilises pre-existing geological processes, causing seismicity.

The effect of mine blasting on seismicity is manifested in two ways: through inducing events that are related to the failure processes caused by that blast and by triggering events that are a part of larger scale failure processes (McKinnon, 2006). Figure 9 shows an illustration of the relation between blasting and induced and triggered seismicity.

Figure 9 Seismic response of blasting illustrating induced events (blue) located near the blast and triggered events located on a fault distant from the mine blast (Brown, 2018)

Induced seismic events are related to blast induced stress change. The size of these events are proportionate to the stress change caused by the blast (McGarr, Simpson and Seeber, 2002). Induced events tend to have temporal and spatial relation to blasting.

Triggered events are caused by larger scale failure process, potentially including the influence of a larger part of the mine geometry and/or premining tectonic forces. The primary characteristic of a triggered event is a disproportionate energy release relative to the stress change cause by blasting (McGarr, Simpson and Seeber, 2002). Triggered events may be poorly related or unrelated to blasting in space and time.

Brown (2018) introduced a third term, complex seismicity, for those events that have a disproportionate energy to a blast, but are very close to the blast in space and time. These events tend to locate on geologic features that are spatially close to the blast.

Work on identifying and differentiating triggered and induced events has been completed by many authors, including, Brown (2018), Woodward and Wesseloo (2015), McGarr, Simpson and Seeber (2002).

Hazard mitigation is inherently more difficult for triggered events than for induced events. Simple experience can give an indication of the maximum size of induced events, since these events tend to have proportional energy release to blast induced stress change. Triggered events are caused by rockmass failure processes that develop over larger time and space as the cumulative effect of mining and geologic influences. Recognizing the development of a large scale failure before it occurs is difficult. Prediction of these events, in terms of specifying the time, location and size, is currently impossible (Spottiswoode, 2010). Simser (2006) found that at the Craig mine, approximately 40% of damaging events occurred shortly after blasting, 30% had some kind of precursory trend in seismicity indicating instability and 30% completely lacked any precursory short term events. Blake and Hedley (2001) contrast stress related seismicity and structurally related seismicity, stating that while stress related failures sometimes exhibit signs of precursory instability, structurally related failures tend to occur without prior warning. They go on to suggest that the triggering mechanism for slip events may more commonly be a reduction in clamping force rather than an increase in shear stress.

The term mine scale event by definition suggests a triggered mechanism. The energy release associated with MSEs are usually not usually proportional to stress change caused by a single blast; rather, they are caused by a larger scale failure process that may or may not have an identified blast trigger. The release of energy during a MSE is disproportionate to stress change caused by the moderately sized stope blasting that is common in Canadian hard rock mining. Individual blasts of the size that could induce MSEs are generally avoided and conditions with the potential to induce MSEs are not common, and potentially not feasible.

2.1.6 Rockbursting

The study of seismicity in mines exists primarily due to a potential consequence, called rockbursting. A rockburst is defined as damage to an excavation that is caused by a seismic event (Kaiser, McCreath and Tannant, 1996; Gibowicz and Kijko, 1994). Seismicity can exist

without rockbursting, however, a seismic event must occur in order for a rockburst to happen. Characterising the seismic response to mining is fundamental to understanding rockburst location, time and damage potential.

Ground motion from large scale seismicity is thought to be a significant factor in rockburst damage (Kaiser, McCreath and Tannant, 1996). Figure 10 illustrates three types of damage mechanisms from seismicity.

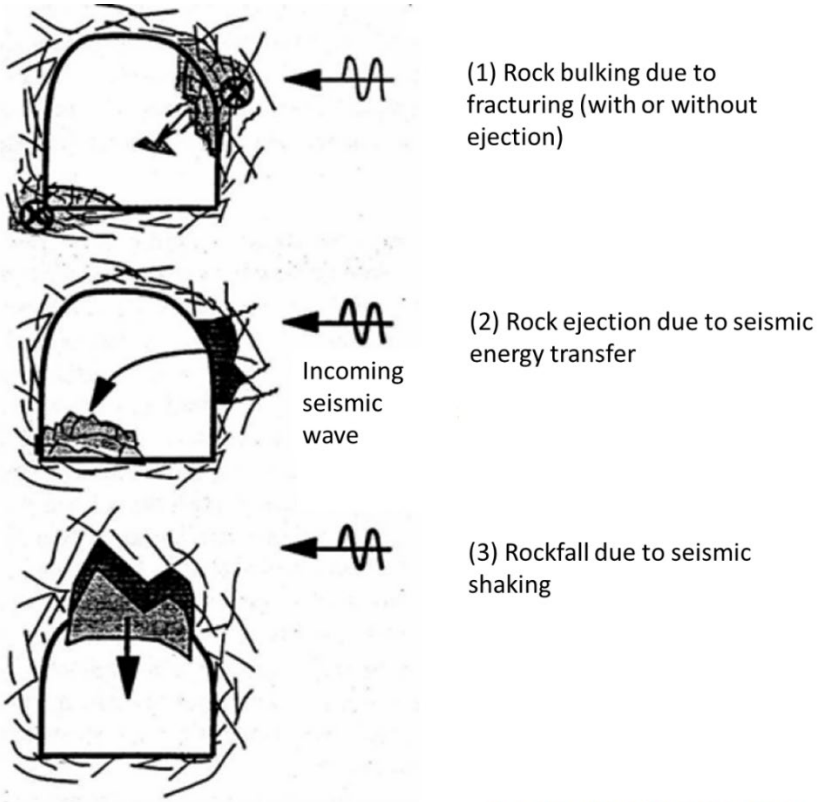

Figure 10 Rockburst damage mechanisms (Kaiser, McCreath and Tannant, 1996)

Figure 10 shows how incoming ground motions from a seismic event distant from an excavation can cause damage. Damage mechanisms (2) and (3) are caused entirely by incoming ground motions that critically load blocky ground around an excavation. Mechanism (1) is a caused by a local overstressing of the excavation, called a strainburst. Kaiser and Cai (2013) further divide mechanism (1) into three categories:

- Self initiated strainburst: The cause of failure is purely local overstressing. The hypocenter of the seismic event coincides with the damage.
- Seismically triggered strainburst: A critically loaded system is triggered to fail by the stress wave associated with a distant seismic event. The stress wave only triggers failure and does provide a significant part of the failure energy.
- Dynamically loaded strainburst: The stress wave from a distant seismic event causes a local overstressing of the rockmass, resulting in a strainburst. The stress wave provides a significant part of the failure energy.

It is intuitive that as the magnitude of seismic events increase, the potential for rockburst damage will be greater. There is a relation between event size and potential for damage, but other factors play key roles. Heal, Potvin and Hudyma (2006) listed some of the most important factors as stress conditions, ground support capacity, influence of geological structure and excavation span. Given several events of a similar size, a wide range of damage could be expected.

Figure 11 shows documentation of several years of rockburst damage in Ontario.

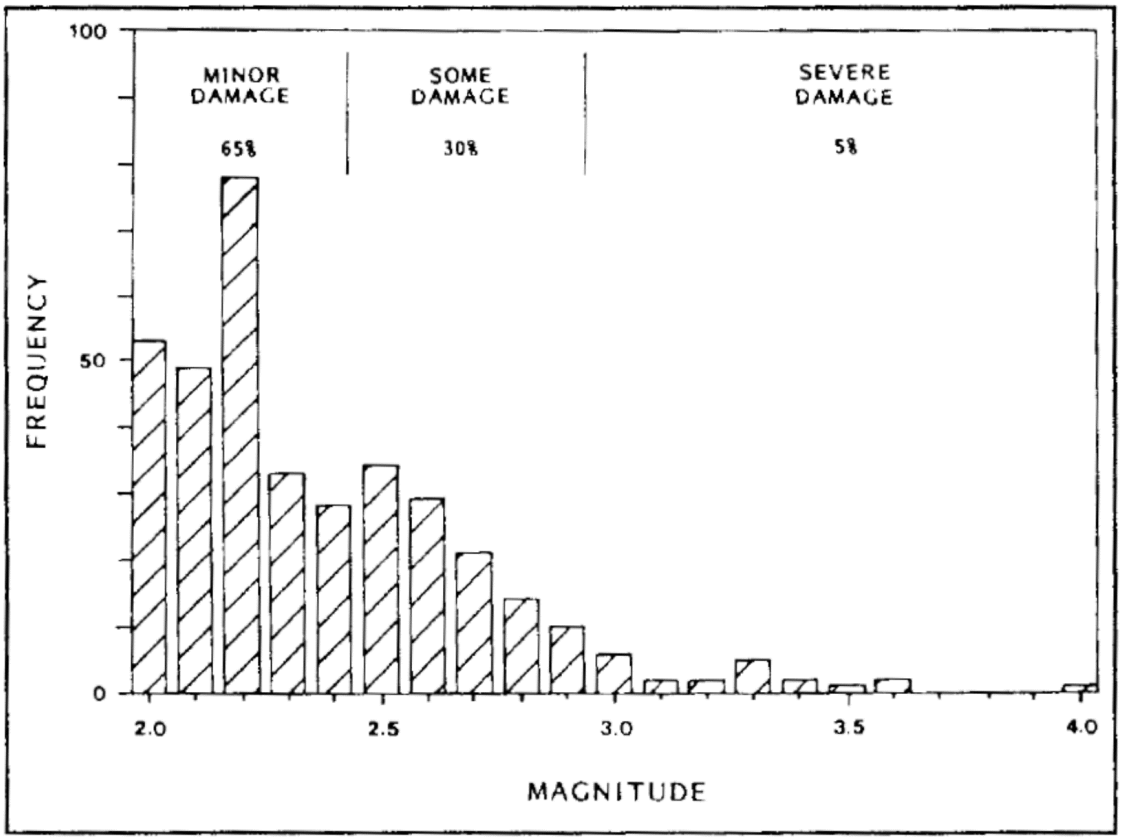

Figure 11 Rockburst damage associated with event magnitude for Ontario 1984-1989 (Hedley, 1991)

Ninety-five percent of damaging events were Mn < 3.0, with damage ranging from very minor to about 10 tonnes of displaced rock. Only 5% of damaging events were Mn > 3.0, but the damage could be much more severe, with displaced tonnage up to two orders of magnitude greater (Hedley, 1991).

MSEs do not always cause damage, but generally, as the magnitude of a seismic event increases, the greater the probability of damage and of increased severity of damage (Hudyma, Brown and Cortolezzis, 2016). In a study of rockburst damage from three Sudbury mines, Morissette (2015) found that events Mn > 3.0 only resulted in damage greater than 10 tonnes of displaced rock about 30% of the time. A fundamental property of seismicity is that as the size of the event increase, the frequency of occurrence decreases (Gutenberg and Richter, 1944). An event of Mn 2.0 and an event of Mn 3.0 both have the potential to cause damage in most mines. The Mn 3.0 may be more likely to cause damage than a single Mn 2.0, but according to the frequency-

magnitude relation there should be approximately 10 events of about Mn 2.0 for each Mn 3.0 event. While it is clear that large events don't always cause damage, an examination of Canadian rockbursting history shows that the potential for severe or catastrophic damage by a Mn > 3.0 event is much higher than a Mn 2.0.

2.1.7 Mine Scale Events in Canada

Rockbursting has become a major problem in mining in the last 100 years, with the first Canadian rockburst being recorded in January 1928 at Sudbury's Frood Mine (Hedley, 1992). Rockbursting was recognized as a significant problem in the Kirkland Lake mines from 1939-1964. Over this time period, some of the largest events in Canadian mining history occurred, with damage that resulted in significant loss of life and finances. Causes of the large events were generally poorly understood. These events destroyed levels, shafts, and in some instances closed mines. Early on, seismic hazard mitigation strategies were largely experience based, with many "rules of thumb" or guidelines being developed to reduce the seismic hazard (de la Vergne, 2008). A combination of better mining practices and the closure of problematic Kirkland Lake mines significantly reduced the occurrence of exceptionally large events by the late 1960's (Blake and Hedley, 2001).

In Canada, the modern era of rockbursting and the historical era are separated by a relatively quiet 20 year span, from 1964 to 1984. This period also predates the systematic collection of data, so the period of quiet may be considerably influenced by lack of data recording and record keeping. Standardized record keeping of mining related events started in the Geological Survey of Canada (GSC) in 1985.

The modern era of Canadian rockbursting began in Sudbury in 1984, with MSEs occurring at Falconbridge and Creighton mines in Sudbury, and Quirke Mine in Elliot Lake. Due to multiple fatalities that year, substantial effort began into rockburst research. Since 1984, the occurrence

of MSEs has not been reduced, but the available tools to analyse and mitigate large events has greatly increased.

The late Dave Hedley documented and compiled case histories of rockburst in Canadian Mining (Hedley, 1991; Hedley, 1992; Blake and Hedley, 2001; Hedley *et al.*, 2013). The following paragraphs consist of brief summary of some of the more notable large seismic events in Canadian mining. Unless otherwise cited, the documentation can be found in the most recent compilation (Hedley *et al.*, 2013).

1939-09-19, a Mn 4.4 occurred at Lakeshore Mine in Kirkland Lake. The event resulted in extensive damage to levels over a 630m vertical distance. Levels between 1400 and 2575 were cut off from shaft access by falls of ground. This event was followed by a Mn 3.7 nine minutes later. No trigger is listed, but the event was preceded 19 days prior by a Mn 3.5 and 17 days prior by a Mn 4.3, both locating in a shaft pillar. The large magnitude and vertical alignment of the damage suggest a fault slip mechanism, though this was only recognized as a potential mechanism in the 1980's.

1951-12-21, a Mn 4.3 occurred at Lakeshore Mine in Kirkland Lake. The event resulted in damage over 760m vertical extent. There was no understood trigger or cause for the event. The event was followed by a Mn 3.7 shortly afterwards. A fault slip mechanism is likely.

1957-01-01, a Mn 4.1 occurred at Lakeshore Mine in Kirkland Lake. The damage resulted in loss of access to 8 levels. No cause or trigger was noted. The event most likely had a fault slip mechanism.

1957-11, two events Mn 3.1 occurred in a span of 15 minutes at Teck-Hughes Mine in Kirkland Lake. These events occurred in the shaft pillar and damages resulted in the loss of the shaft.

1961-03-01, a Mn 4.3 occurred at Lakeshore Mine in Kirkland Lake. This event had similar damage and mechanism to the 1957 Lakeshore event.

1964-08-14, a Mn 3.1 occurred at Wright-Hargreaves Mine in Kirkland Lake. This event located in the shaft pillar, resulting in the collapse of a stope, in which two miners were killed. Shortly afterwards, a Mn 4.2 occurred. The damage from the Mn 4.2 included loss of access to 11 levels, loss of a shaft and the eventual closure of the mine. The event mechanism for the Mn 4.2 was thought to be fault slip. The event sequence was likely triggered by a blast in the same shaft pillar stope in which the fatalities occurred.

1984-1985, a sequence of events up to Mn 3.5 occurred at the Quirke Mine in Elliot Lake. These events were related to a spreading region of pillar failures, with some of the large events occurring on an overlying hanging wall fault. There was a loss of access to the central pillar failure area and an inflow of water into the mine through a fault from an overlying lake.

1984-06-20, a Mn 3.5 occurred at Falconbridge Mine in Sudbury. This event resulted 4 fatalities, and over 1000 tonnes of displaced material. The mine was later closed. The event had no clear trigger and was thought to have a fault slip mechanism. The event was followed by Mn 3.5 and Mn 3.2 events within 2 hours.

1984-07-06, a Mn 4.0 occurred at Creighton Mine in Sudbury. The event resulted in displacement of over 1000 tonnes of material in development spread over 240m vertically in the mine. The event had no clear trigger, occurring during a summer shutdown. The mechanism is thought to be fault slip. A series of large events followed over the next 1.5 hours.

1993-11-26, a Mn 2.5 occurred at Macassa Mine in Kirkland Lake. The event resulted in a 22,000 tonne collapse of backfill in a stope, killing two miners. The event mechanism was likely a pillar failure, triggered by a blast in the pillar 16 hours prior.

1997-04-12, a Mn 3.8 occurred at Macassa Mine in Kirkland Lake, resulting in severe damage to the shaft. The mechanism is thought to be a pillar foundation failure. The event occurred 7 minutes after a blast and was shortly followed by a Mn 3.7. Mining was restricted below the 5000

Level by the Ministry of Labour and the mine was closed in 1999. The mine has since reopened, but is not mining at the same depths.

1999-10, a Mn 3.3 occurred at Brunswick Mine in Bathurst. Numerous shotcrete posts failed as a result of the event. The event occurred simultaneously with a massive 352,800 tonne blast of a low grade, high stress pillar. The source mechanism was thought to be shearing of a metasedimentary contact in the mine hanging wall.

2003-09-13, a Mn 3.5 occurred at the Williams Mine in Hemlo with only minor damages. No trigger is listed. The event was part of a multi year sequence of large events in a regional pillar. Coulson (2009) and Bewick (2013) suggest a shear rupture mechanism.

2008-09-11, a Mn 3.8 occurred at the Copper Cliff North Mine in Sudbury. Damage consisted of 2500 tonnes displaced over several locations. The event occurred immediately after a crown pillar blast. The event mechanism was unclear.

2008-10-03, a Mn 3.2 occurred at the Red Lake Mine in Red Lake, resulting in damage to 6 locations. The fault slip event occurred 1 hour after a blast.

2008-12-05, a Mn 3.1 occurred at Garson Mine in Sudbury, displacing 400 tonnes of material in the region of a crown pillar. The event likely had a fault slip mechanism and was possibly a delayed reaction to a blast in a crown pillar.

2009-01-06, a Mn 3.8 occurred at Kidd Creek Mine in Timmins, resulting in extensive damage over 9 levels (360m vertical). The event had a complex mechanism, locating on a historically active fault, but much of the damage locating on a conjugate shear rupture. The event was theorized to be a delayed response to a blast.

2011-09-13, a Mn 3.8 occurred at Kidd Creek Mine in Timmins. Damage over 5 levels displaced approximately 1000 tonnes. The event was very interesting in that it involved very similar

structure and mining sequencing as the 2009-01-06 Kidd Mn 3.8. The event is thought to be a delayed reaction to a blast 4 days prior.

2015-05-25 a Mn 3.2 occurred at Westwood Mine in Rouyn, caused several falls of ground and damage on 8 levels. The event was followed by events Mn 2.7 and 2.4 within 40 hours. There was no blast trigger. This event is unlike others in that it occurred early in the mine life, less than a year after production commenced. Kalenchuk, Mercer and Williams (2017) suggested that the event mechanism was a pillar failure created by high horizontal stress between vertically aligned development.

A few characteristics of these large events can be observed. Undoubtedly, the worst Canadian rockbursting period was 1939-1964 in the deep Kirkland Lake gold mines. The largest events during this time period were greater than Mn 4.0, with damage occurring over very large areas of the mines. In the modern era of rockbursting (1984-2021), only three events Mn > 4.0 have occurred despite deeper mining and greater extraction ratios, possibly suggesting that modern strategies of mine sequencing are beneficial in limiting the size of the events.

Most of the large events either have a proposed fault slip mechanism or the mechanism is unclear.

Large events often occur in sequences, preceded by or followed by other large events. This behaviour could be interpreted as either a triggering mechanism between different failure processes or a single, large scale failure process that fails in multiple instances. In either case, it seems likely that MSEs can significantly alter the stress regime over a large spatial area.

Damage sometimes has a better alignment with aftershocks than the main, large event. This may be due to increased uncertainty of location with magnitude or triggering of secondary failure processes by the large event. A consequence is that damage and location of aftershocks may not be a reliable indicator of the main shock failure mechanism.

Large, structurally related events often have damage that aligns with the structure over several levels, such as the very large Kirkland Lake events, which resulted in damage zones intersecting levels for over 700m. Theoretical earthquake models suggests that source radius for MSEs can be 100m+, which would easily intersect multiple levels since mining levels are commonly 20-40m apart. Damage to excavations is thought to be due to the induced stress wave near the source where vibrations are highest (Kaiser, McCreath and Tannant, 1996), but could potentially be part of the source a large fault slip event.

The timing of MSEs can be strongly or poorly related to blasting. Sometimes a MSE can be thought to have a link to a blast that occurred a significant time before the event. Often MSEs can occur at the same time as blasting.

Because the magnitude of MSEs approach earthquake sizes, event location can be estimated by the national seismic network. The GSC has a continuous record of monitoring large mining events since 1985. Cross reference of the event locations with known operating mines can give an indication of which Canadian mines have had MSEs (Figure 12).

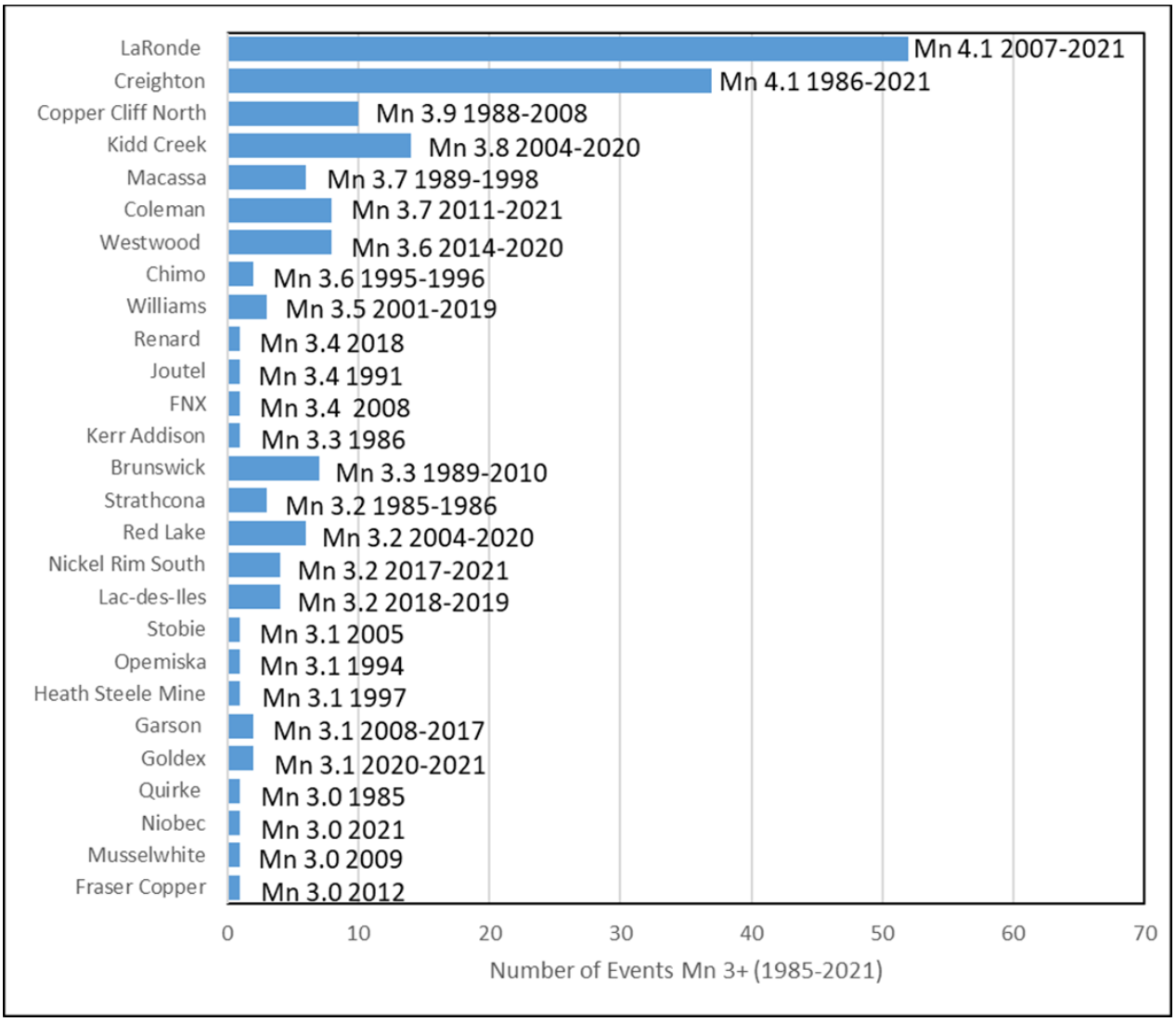

Figure 12 GSC recorded number of events Mn ≥ 3.0 per mine, 1985-2021 (Earthquakes Canada, 2021). The mines are ordered by largest magnitude event, and include the year of the first and last MSE.

Twelve of the 27 mines had only one MSE, suggesting that for many mines, MSEs are singular, one in a mine occurrences. However, nine of the 27 mines have had more than five MSEs.

The number of Mn ≥ 3.0 occurring at each mine appears to be related to the magnitude, with larger events tending to occur at mines with more MSEs. Creighton and LaRonde mine stand out from the rest, having almost 50% of the total events Mn ≥ 3.0. Kidd Creek Mine has the third most events Mn ≥ 3.0. As of 2021, LaRonde, Kidd Creek and Creighton were the three deepest operations in Canada, and among the top ten deepest in the world (Mining Technology.com,

2019). High *in situ* stress due to depth seems to play a role, but is not likely the only factor. LaRonde and Kidd Creek are both operating at 3000m+ depth, but LaRonde has had almost three times as many events Mn ≥ 3.0 as Kidd. Kidd Creek is deeper than Creighton, but Creighton has many more large events than Kidd Creek. LaRonde and Creighton have a similar number of large events, but Creighton has been active significantly longer than LaRonde, suggesting LaRonde had a higher rate of large events.

2.2 Seismic Source Parameters

Seismic source parameters describe characteristics of the rock failure mechanism that generated the event. Mendecki (1993) stated that the minimum quantitative description of a seismic event consists of the event time, location, and two other independent source parameters. There are five independent source parameters: time, location, moment, radiated energy and source size. Useful secondary source parameters exist as manipulations of the five independent parameters.

2.2.1 Location and Time

Determination of location and time are intrinsically linked and will be discussed in the same section.

The time of a seismic event is the exact time the event occurred. After a seismic event occurs, a transient stress wave travels a distance through the rock and is recorded by sensors as an arrival time. There are four wave phases for a large seismic event, the compression wave (P-wave), shear wave (S-wave), raleigh waves and love waves. For seismicity in mines, generally only the compression and shear waves are relevant. Figure 13 shows a recording of seismic waves by stations at several different locations.

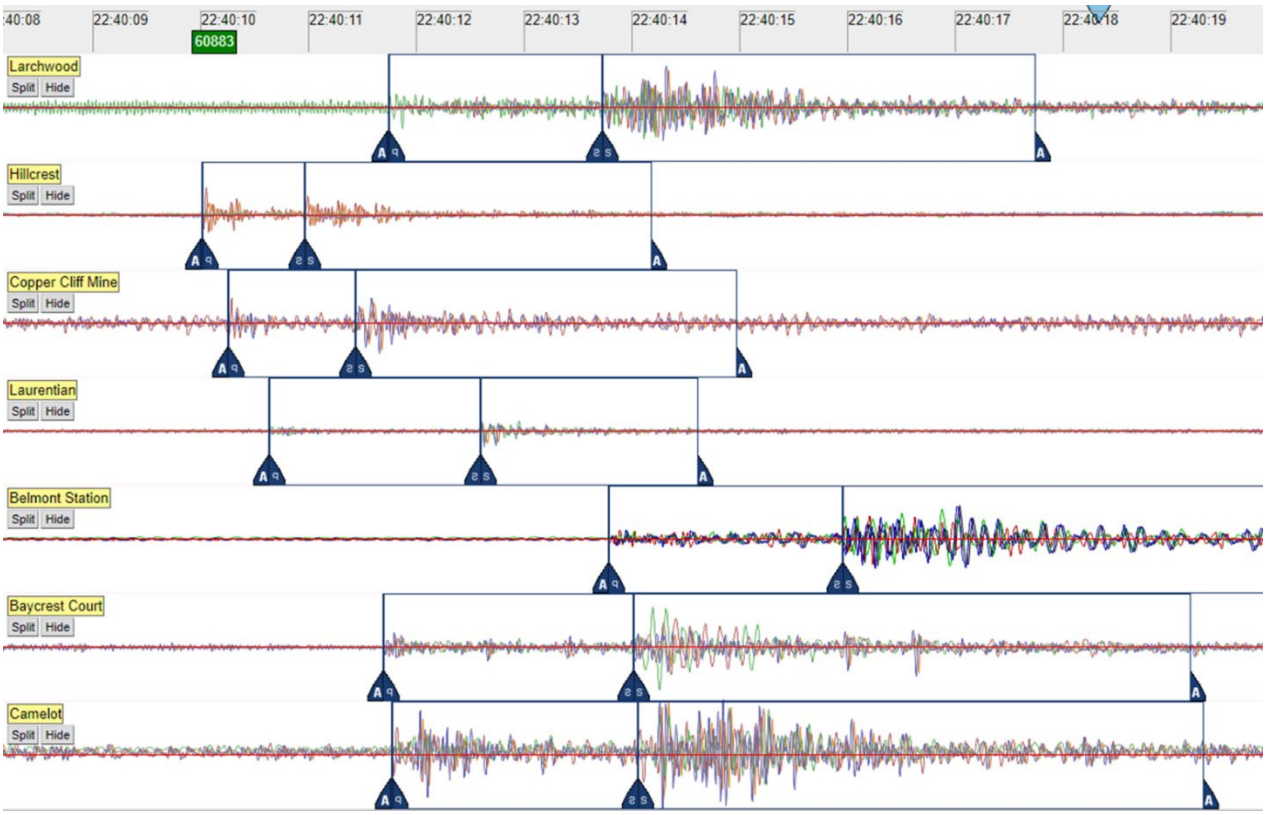

Figure 13 Arrival time of waveforms on the Sudbury Regional Seismic Network.

The location of a seismic event is approximated using knowledge of the seismic wave velocities in the rockmass. If the individual velocities of the P-wave and the S-wave are known, the distance from a station can be back calculated based on the time between the P- and S-wave arrivals. The level of agreement between multiple stations can then be used to approximate the event hypocenter, as illustrated in Figure 14.

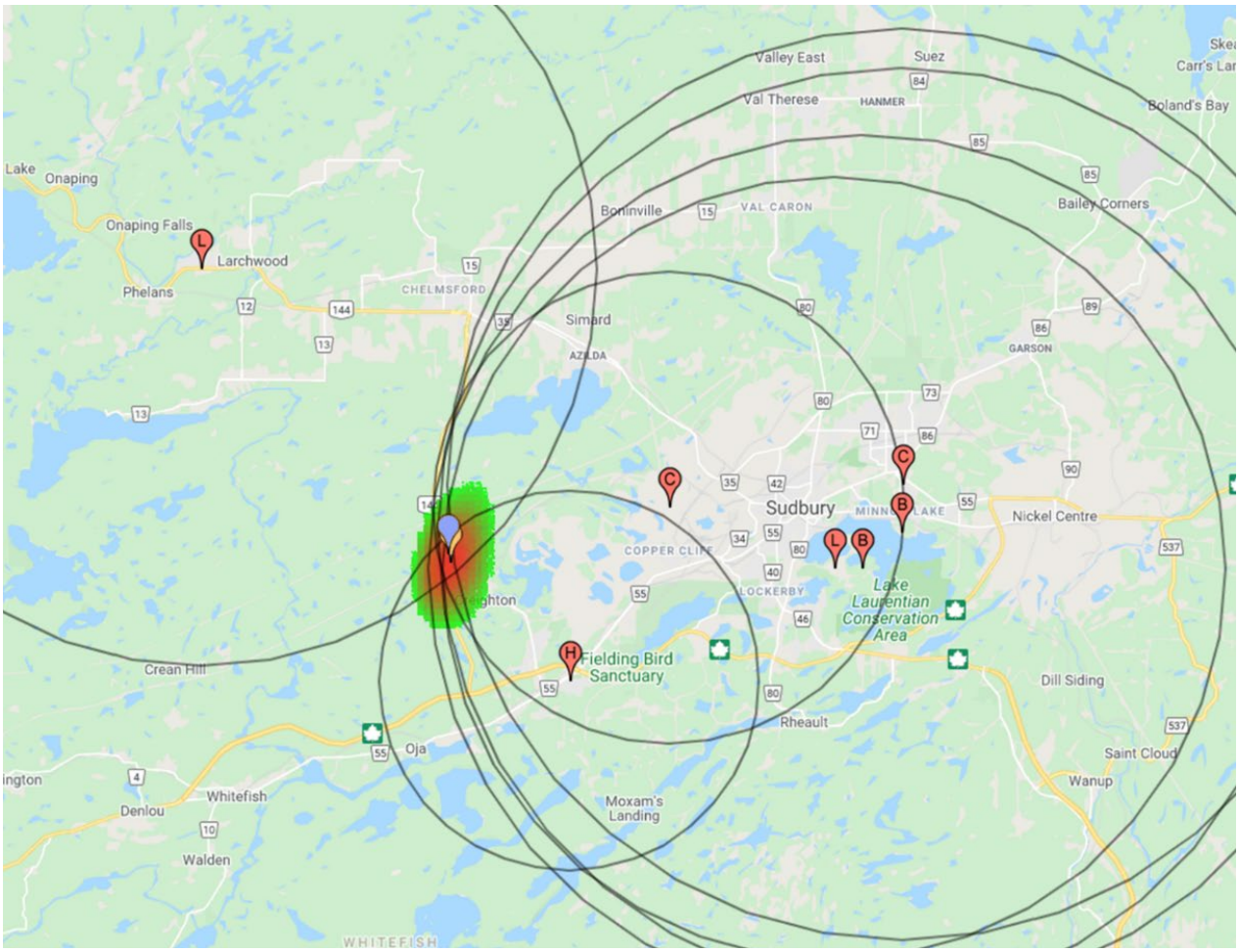

Figure 14 Approximate location of event, indicated by blue pin, on the Sudbury Regional Seismic Network. Sensor locations are indicated by red pins.

Event location is arguably the most important source parameter as calculation of most other source parameters relies to some degree on an accurate location. Arrival time residual is the difference between theoretical and actual arrival time for an event (Gibowicz and Kijko, 1994). Multiple methodologies exist to calculate the location of a seismic event, all of which attempt to minimize the location error, or arrival time residual of that event (Gibowicz and Kijko, 1994).

Commonly at mining operations, seismic processing software will automatically pick P- and S-wave arrival times, but manual refinement can still reduce location error. Figure 15 demonstrates how the residuals of seismic events can be reduced by manually picking arrival times.

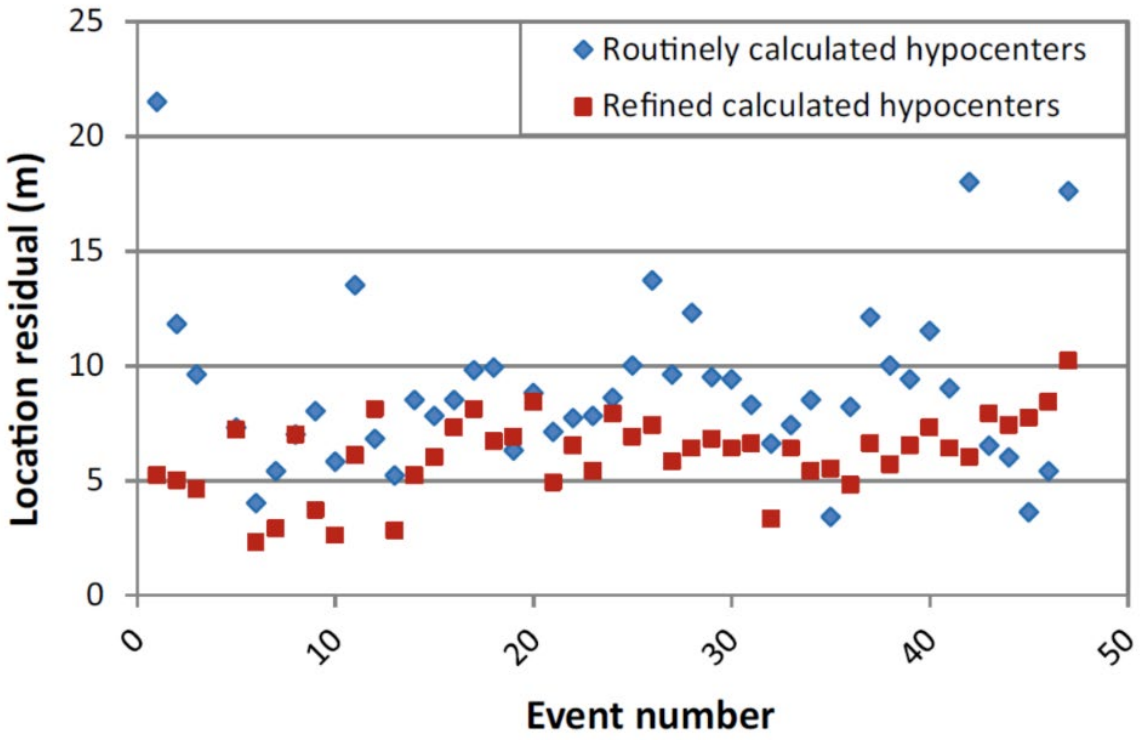

Figure 15 Manual vs. automatic P- and S-wave picks (Nordström, Dineva and Nordlund, 2017)

For practical purposes, residual is often given as a distance rather than a time, calculated by multiplying the time residual by the average rock velocity. Figure 16 shows results from a survey of location accuracy in metres from several Canadian mines.

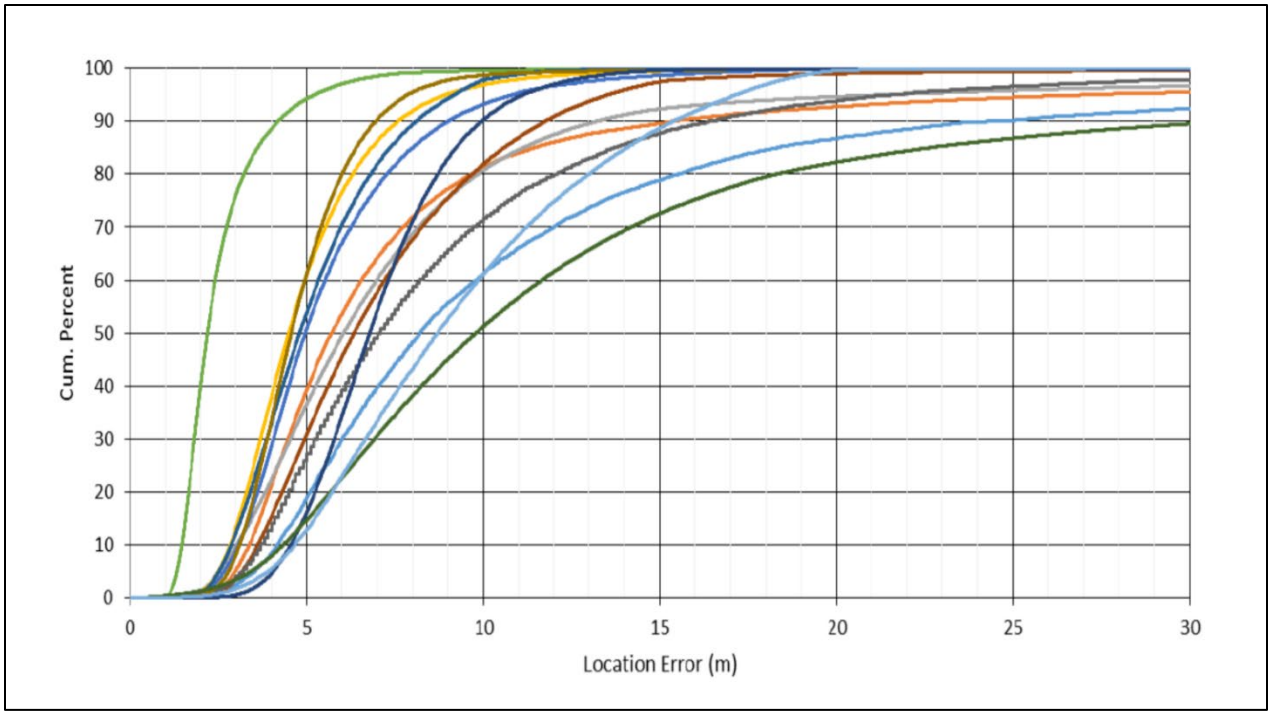

Figure 16 Cumulative residual error (m) of 13 Canadian mines (Brown and Hudyma, 2018)

The data show that for Canadian mines, the median error residual varies from 3 to 10 metres, while the most accurate seismic systems in Canadian mining is under 5m median error residual.

2.2.2 Seismic Moment

Seismic moment is a measurement of the physical deformation of the rockmass, providing the best descriptor for the overall force involved in a seismic event (Gibowicz and Kijko, 1994). Seismic moment describes co-seismic deformation for a pure shear event, but is commonly used for seismic events of all mechanisms. Aki (1966) defined seismic moment as:

$$M_0 = \mu A(\Delta u) \qquad [1]$$

Where,

M_0 = seismic moment (Nm)

μ = shear modulus of rock (Pa)

A = area of rupture (m^2)

Δu = average displacement of rupture (m)

Figure 17 shows a cartoon of how [1] is physically represented.

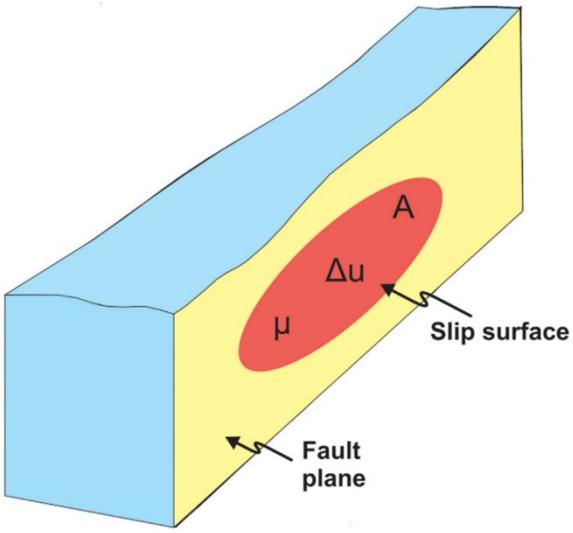

Figure 17 Physical representation of a ruptured fault plane (Gudmundsson, 2014)

Direct calculation of seismic moment is impractical, as measurement of the rupture area (A) and average displacement (Δu) are generally not possible. Waveform techniques are used to provide an approximation. Seismic moment can be calculated as (Gibowicz and Kijko, 1994):

$$M_0 = 4\pi\rho c^3 \Omega_0 / F_c \qquad [2]$$

Where,

M_0 = seismic moment (Nm)

ρ = rock density (kg/m^3)

c = velocity of elastic wave in rock (m/s)

Ω_0 = low frequency plateau

F_c = empirical radiation coefficient

The low frequency plateau Ω_0, is found by converting the seismic waveform from the time domain to the frequency domain (see Figure 18).

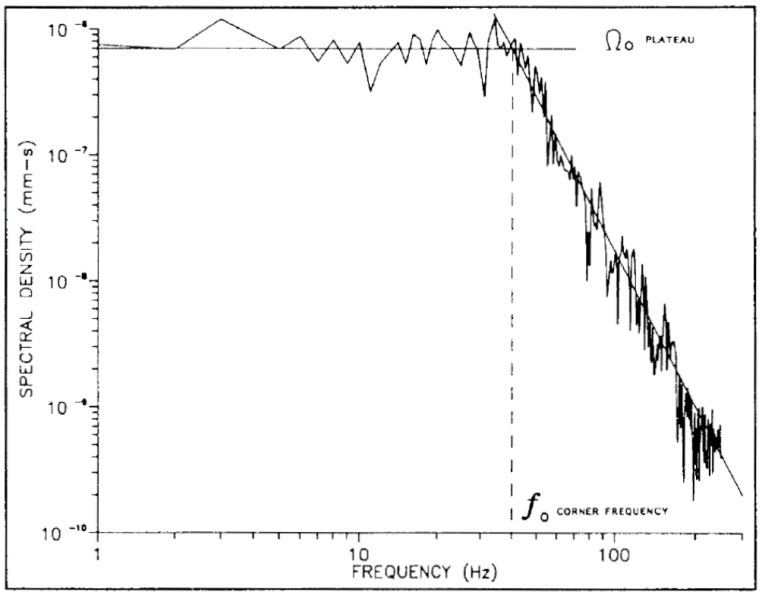

Figure 18 Seismic signal converted to the frequency domain (Hedley, 1991)

2.2.3 Radiated Energy

Seismicity changes the state of energy in the rockmass through inelastic deformation, production of heat and an elastic stress wave (Kanamori and Rivera, 2006). Radiated energy is the total measured energy of the elastic strain wave (Gibowicz and Kijko, 1994). For a constant rupture area, the amount of radiated energy is dependent on the velocity of the rupture, with a higher rupture speed resulting in a greater amount of radiated energy (Mendecki, Malovichko and Malovichko, 2013).

Radiated energy for a seismic event is the summation of the energy of the P- and S-waves. According to Gibowicz and Kijko (1994), the calculation for each wave can be defined by [3].

$$E = 4\pi\rho c R^2 J_c / F_c^2 \qquad [3]$$

Where,

E = radiated energy (joules)
ρ = rock density (kg/m³)
c = velocity of elastic wave in rock (m/s)
R = distance from hypocenter to receiver (m)
J_c = integral of the square of the rock velocity
F_c = empirical radiation coefficient

2.2.4 Source Dimensions

The dimensions of a shear event are inversely proportional to the corner frequency of the seismic wave (Brune, 1970). Source radius can be calculated by [4] (Gibowicz and Kijko, 1994).

$$R_0 = K_c\beta_0/2\pi f_0 \qquad [4]$$

Where,

K_c = constant

β_0 = S-wave velocity (m/s)

f_0 = corner frequency (Hz) (see Figure 18)

Figure 19 illustrates the relation between corner frequency, seismic moment and source size.

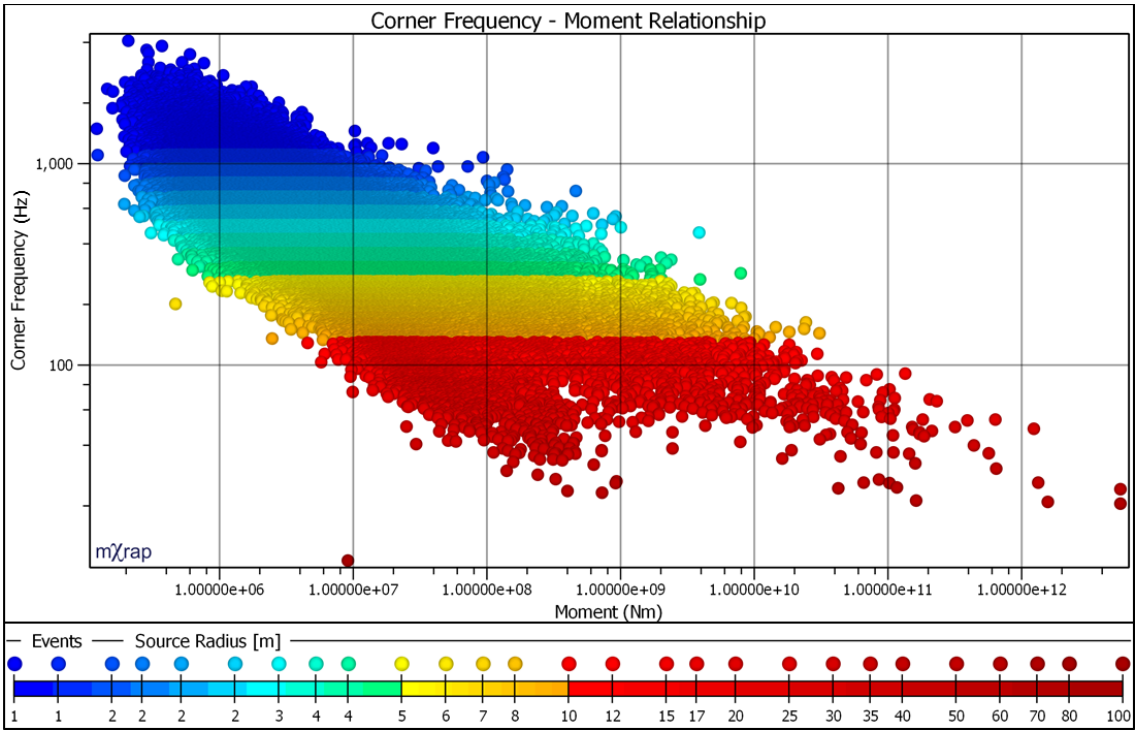

Figure 19 Corner frequency vs. moment, coloured by source radius, recorded in a Canadian mine.

As the size of the source increases, the corner frequency decreases. It can be observed from Figure 19 that a given source radius can exist over a range of moments, suggesting that the size of moment for a given source radius must depend on driving stress conditions at the source. Eqn.

[1] shows that for a given source radius, an increase in moment means a higher displacement, therefore it is logical that the driving stress to generate the higher displacement must be greater.

2.2.5 Magnitude

In practice, magnitude is one of the most widely used descriptors of a seismic event. It is a unitless, easily understood quantification of the size of a seismic event. As discussed in Sections 2.2.2 - 2.2.4, a single parameter does not completely describe a seismic event, but a magnitude scale is useful to approximate the size of an event in easily understood terms.

The best known magnitude is the Richter scale. Seismic waves attenuate with distance, meaning the amplitude decreases with distance between the event hypocenter and the receiver. Richter magnitude is calculated from the peak displacement of a seismic wave and a normalized distance between the event and receiver (Richter, 1935). Since the Richter magnitude scale was the first of its kind to be developed, most subsequent magnitude scales have attempted to provide a numerically similar approximation of Richter magnitude.

In a seismically active mine, underground workers experience seismicity through vibration and sound. Table 2 provides a qualitative description of how events feel for 6 orders of magnitude.

Table 2 Qualitative description of how events of certain magnitude feel (Hudyma, 2008)

RICHTER MAGNITUDE	QUALITATIVE DESCRIPTION
-3.0	▪ Small bangs or bumps felt nearby. Typically only heard relatively close to the source of the event. ▪ This level of seismic noise is normal following development blasts in stressed ground. ▪ Event may be audible but vibration likely too small to be felt. ▪ Undetectable by a microseismic monitoring system.
-2.0	▪ Significant ground shaking. ▪ Felt as good thumps or rumbles. May be felt more remote from the source of the event (i.e. more than 100 m away). ▪ May be detectable by a microseismic monitoring system.
-1.0	▪ Often felt by many workers throughout the mine. ▪ Major ground shaking. ▪ Similar vibration to a distant underground secondary blast. ▪ Should be detectable by a microseismic monitoring system.
0.0	▪ Vibration felt and heard throughout the mine. ▪ Bump commonly felt on surface (hundreds of metres away), but may not be audible on surface. ▪ Vibration felt on surface similar to those generated by a development round.
1.0	▪ Felt and heard very clearly on the surface. ▪ Vibrations felt on the surface similar to a major production blast. ▪ Can be detected by regional seismological sensors located hundreds of kilometres away.
2.0	▪ Vibration felt on the surface is greater than large production blasts.
3.0	▪ The largest mining-induced seismic events recorded in Australia registered about Richter 3 to Richter 4

The Nuttli magnitude (Mn) scale was developed specifically for the attenuating properties of the earth's crust in Eastern North America (Nuttli, 1973). Earthquakes Canada uses Mn for regional monitoring of earthquakes and mining events in the Canadian Shield, and Canadian mine sites will often use the recorded Nuttli magnitude to confirm the size of their largest events. Hedley, (1992) noted that Mn is commonly 0.3 - 0.6 units less than Richter magnitude.

Globally, the most common magnitude scale among seismologists is Moment magnitude (Mw or M). Moment magnitude attempts to approximate the size of an event to Richter magnitude by a relation with the seismic moment (Hanks and Kanamori, 1979).

$$Mw = 2/3 \log (M) - 6.1 \qquad [5]$$

Where,

Mw = moment magnitude

M = seismic moment (Nm)

In practice at operating mines, magnitude is often calculated from a combination of moment and energy or singularly from moment (Mendecki, Malovichko and Malovichko, 2013). In most cases the mine will attempt to correlate its magnitude scale with that of a regional magnitude dataset.

2.3 Seismic Data Analysis

Seismic data analyses attempt to understand the rockmass failure process and to quantify seismic hazard with the goal of managing operational risk. Use of seismic data analysis techniques to describe the response of the rockmass to mining can provide a description of the state of the rockmass failure process (Mendecki, 1993)

One of the challenges in mine seismology is to distinguish the source mechanism of populations of events in space and time, or where and when individual rockmass failure processes are taking place. Multiple methods of seismic source evaluation have been used to characterise mining related seismicity. Seismic source mechanisms have characteristic tendencies and behaviours that can be inferred by analysis techniques. The best approach to characterise a seismic source through inferred analyses techniques uses multiple methods of analysis (Hudyma and Potvin, 2010).

This section will describe the meaning and common use of several of the most common inferred techniques in mine seismology.

2.3.1 Three Dimensional Visualization of Location

This section describes what can be learned from visual observation of seismic event locations. Three dimensional visualisation of seismicity shows where events occur relative to potential seismic sources. 3D visualization:

- Shows where rockmass failure is occurring (Cai, Kaiser and Martin, 2001)
- Shows regions where events are not occurring (aseismic), which can indicate either a stable or failed rockmass (Jalbout and Simser, 2014)

- Shows locations of high mining induced stress (Cook, 1976)
- Shows where the population of events occurs relative to the mine and to geological features (Vezina and Leslie, 2001), (Hudyma *et al.*, 1994)
- Shows most likely areas to be damaged after a large event (Kaiser, McCreath and Tannant, 1996)

The location of an event or population of events is possibly the most important indicator of source mechanism. Events strongly cluster based on the source (Hudyma, Mikula and Heal, 2003), therefore proximity of an event or event cluster to a fault, pillar, dyke or abutment can be a strong indicator of source mechanism. Figure 20 shows a population of seismic events recorded over 3 months at Nickel Rim South Mine (Jalbout and Simser, 2014).

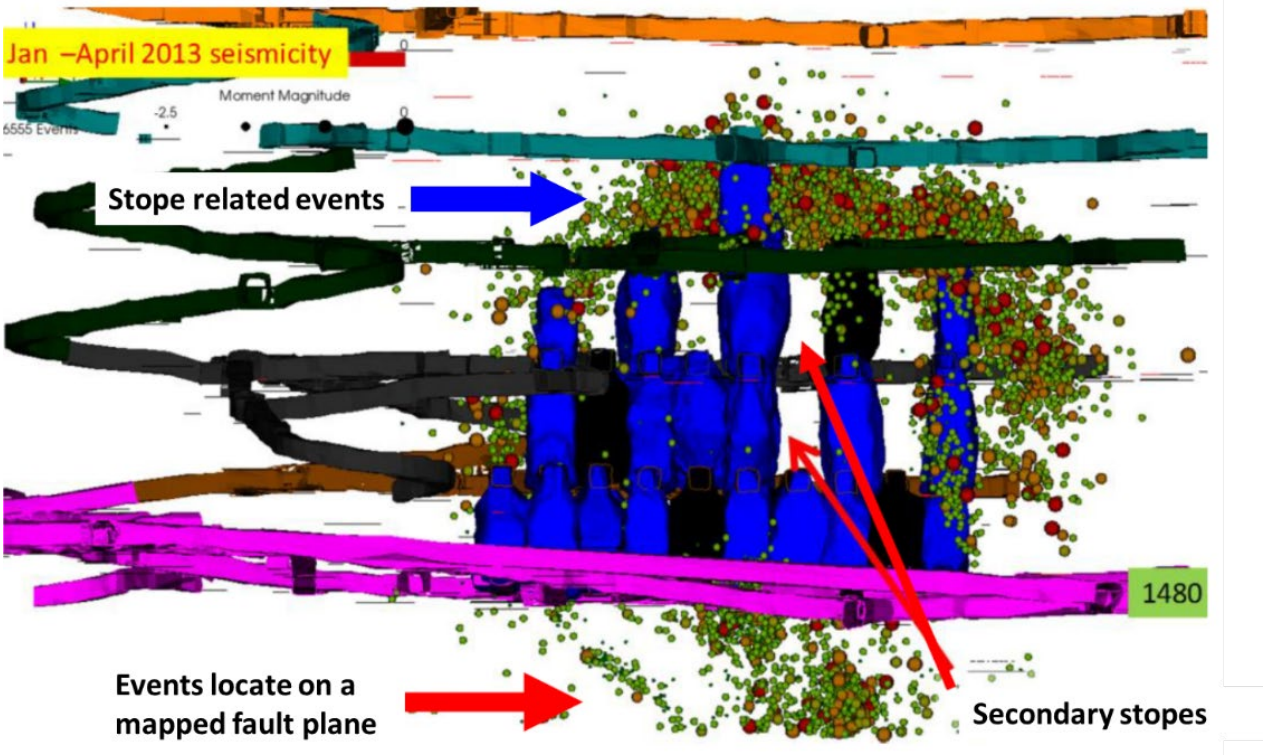

Figure 20 Locations of seismic events (Jalbout and Simser, 2014)

Three observations can be readily made from event locations:

- There is a population of stope related seismicity that clearly follow the outline of the stoping sequence
- Secondary stopes lack seismic events, possibly indicating ground has yielded and become aseismic
- A population of fault related events form a plane on a mapped fault

A lack of seismicity can also provide valuable information about the state of the rockmass, either indicating that the rockmass is intact and not yet undergoing stress induced failure or that the rock has yielded and become de-energized. The absence of seismicity after rock failure has been verified by acoustic emission monitoring during loading and failure of laboratory scale samples (Diederichs, Kaiser and Eberhardt, 2004), (Martin and Chandler, 1994). The secondary stopes illustrated in Figure 20 are interpreted to be yielded pillars, which were seismically active at one point, but have likely yielded as mining progressed on both sides (Jalbout and Simser, 2014). Aseismicity can coincide with high stress conditions as well as failed rock. Rock under high confinement has a higher capacity for load, therefore may be highly stressed, but not actively failing. A region becoming aseismic is not a clear indicator of a de-stressed rockmass, because, as Hudyma and Potvin (2010) point out, a source may simply be dormant due to a lack of disturbance by blasting.

2.3.2 Diurnal Analysis

Stress change related rockmass failure processes tend to have a strong temporal relation to blasting, while seismicity on geologic structure is often less related to blasting (Hudyma, 2008). Diurnal analysis is a technique to asses the relation between seismicity and blasting of a seismic source (Hudyma, 2008), (Cook, 1976). A diurnal chart is a histogram with a 24 hour clock on the horizontal axis and an event count on the vertical axis, shown in Figure 21. Significant blasts at modern mines occur at shift changes, and tend to remain fairly constant. Seismic events that

have a strong temporal relation to blasting tend to occur shortly after blasting, while those that have less relation to blasting tend to occur at more random times of the day. The response of a seismic source to blasting can be characterised using diurnal analysis, and can sometimes provide insights into the type of source mechanism (Hudyma, 2008).

While microseismicity tends to be associated with blast times, the larger the event, the more random the time of occurrence (Brummer, 1999). Relation of seismicity with blasting is often scale dependent and can be tested using diurnal analysis by filtering events by magnitude. Figure 21 illustrates two very differently behaving seismic sources, with data series “All Events” in blue compared to “Significant Events” in red.

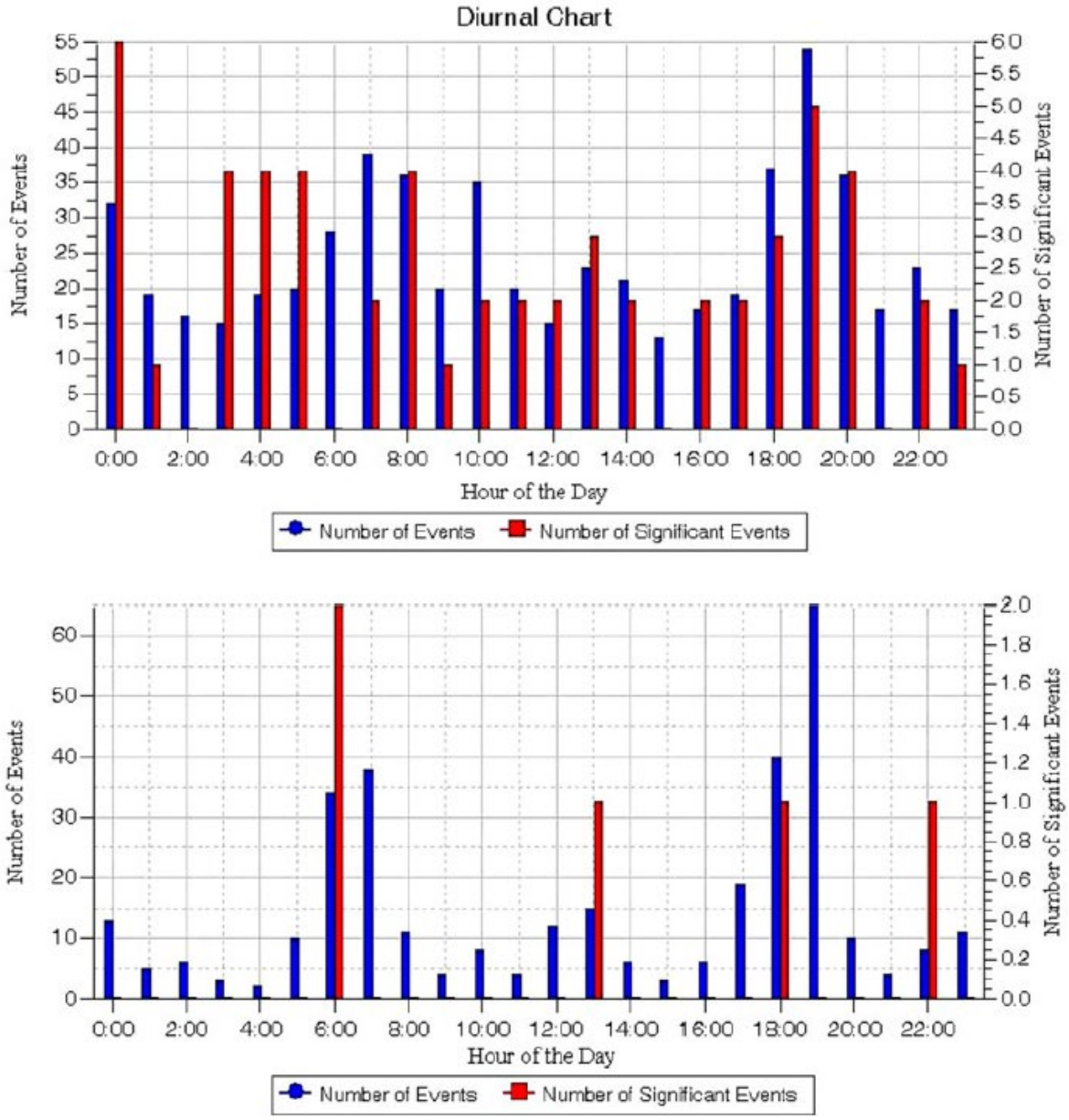

Figure 21 Diurnal chart that shows seismic sources with poor relation to blasting (top) and strong relation to blasting (bottom) (Hudyma and Potvin, 2010)

Event series in the top figure have much more random times of occurrence and a much higher number of significant events. From previously discussed source behaviours, two source types may be inferred from just these two charts. The top figure has two common characteristics of structurally related seismicity: large events and poor relation with blasting. The bottom figure

behaves like a stress fracturing related source, with a lower seismic hazard and a higher relation of events with blasting. Fault events have been observed to have larger potential magnitude than stress fracturing related events (Ortlepp and Stacey, 1994). Fault events often have less relation to blast induced stress change (Hudyma, 2008). Larger events tend to occur at more random times (Brummer, 1999). What is not clear is whether large events occurring more randomly is a characteristic of the size of the event or because large events are more likely to be fault slip events.

A poorly studied but possibly important effect is that of stress magnitude on the relation between blasting and seismicity. Lenhardt (1992) suggested that with higher stress, the inelastic deformation process associated with blasting should take place at a faster rate, giving events a higher temporal relation with blasting. He observed that in an upper reef (1500 – 2500m) of the Western Deep levels, 70% of Mw ≥ 3.0 events occurred more than four hours after the blast, while in the lower reef (2300-3500m), 70% of Mw ≥ 3.0 occurred within four hours of blasting. While Lenhardt suggests that the change may be due to higher stress with depth increasing the deformation rate, the observation has not widely been confirmed.

It has been observed that an increased rate of extraction can often increase the rate of seismicity (Cook, 1976; Hedley, 1991). Since seismicity is often directly related to the creation of new excavations, it is logical that a faster change in mine geometry would result in an increased rate of rockmass failure and a higher rate of seismicity.

2.3.3 Magnitude Time History

Magnitude time history (MTH) analysis is one of the most informative methods to look at a population of seismic events over time. MTH typically has the date on the horizontal axis, magnitude on the primary vertical axis and a cumulative number of events on the secondary vertical axis, as shown in Figure 22.

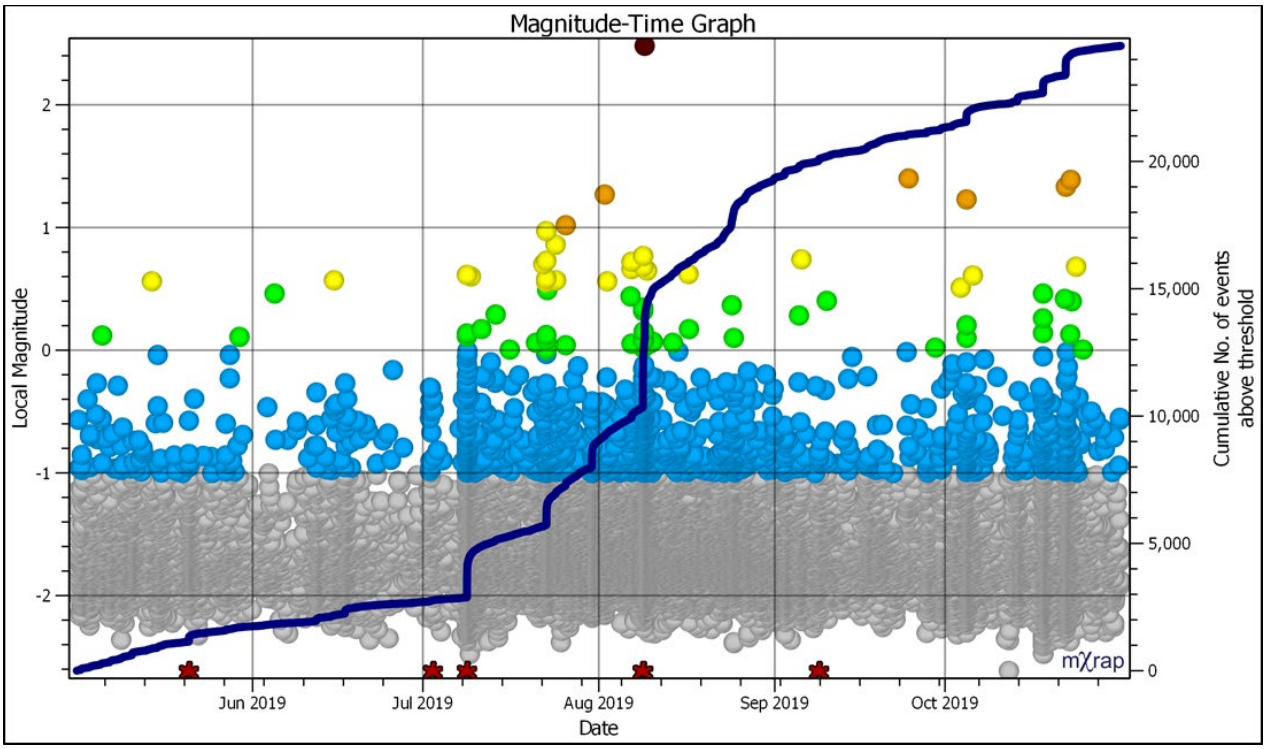

Figure 22 Magnitude Time History Chart

Figure 22 shows how the size of events can be studied temporally. An unseen component is the volume in which the events occurred. Blasts are illustrated on the date axis (red stars). It can be observed that an increase in event rate and the occurrence of larger events is often linked to blasting. The largest event in the sequence occurred at the same time as a blast but was preceded by several large events and an increase in event rate.

A MTH chart for a single seismic source will show a record of the seismically active component of the rockmass failure process. MTH can also be used to infer source mechanism. Hudyma (2008) listed the following usages for MTH charts:

- Indicates the seismic hazard of population and whether it is increasing or decreasing
- Steep increases or steps in the cumulative number of events line show a relation between the rate of the rockmass failure process and blast induced stress change

- An unresponsive event rate with respect to blasting can be a sign of structurally controlled seismicity

Variations to Magnitude-Time history charts can provide further insights into the rockmass failure mechanisms. Figure 23 is a Magnitude-Time history chart that shows a change in source mechanism from stress fracturing to shearing.

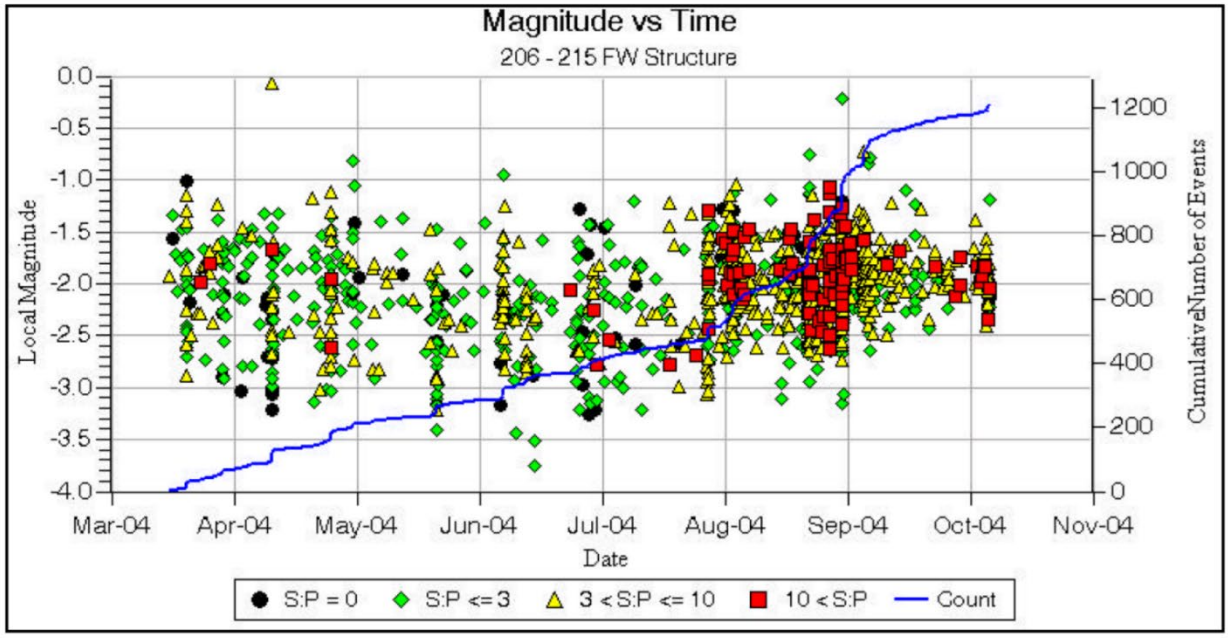

Figure 23 Magnitude-time history graph for LaRonde mine (Heal, Hudyma and Vezina, 2005)

Events in Figure 23 are coloured by S:P ratio. Low S:P (<3) can represent a non-shear mechanism (Hudyma and Potvin, 2010), while high S:P (>10) represents a shearing mechanism (Boatwright and Fletcher, 1984). Up to mid July, event rate is low and responds to blasting, characterised by steps in the event rate. S:P tends to be low, with only a few shear related events. This information indicates the dominant source mechanism may be related to stress induced fracturing. In late July, the event rate sharply increases. There are still steps in the event rate related to blasts, but the event rate remains high between the steps. The proportion of shear related events (S:P > 10) drastically increases, which is consistent with shear on a geologic discontinuity.

2.3.4 *Frequency-Magnitude Relation*

A characteristic of seismicity is that smaller events occur more frequently than large events. Gutenberg and Richter, (1944) found that a power law existed between the occurrence of seismic events and their magnitude, proposing equation [5].

$$\text{Log } N = a - bM \qquad [5]$$

Where,

N = number of events

M = magnitude

a & b are constants

The nature of the frequency-magnitude relation applies for seismicity over the measurable frequency range, from small, laboratory scale high frequency acoustic emissions to large, low frequency earthquakes occurring on plate boundaries (Scholz, 1968; Mogi, 1962).

Figure 24 shows a large population of seismic events that follow the power law.

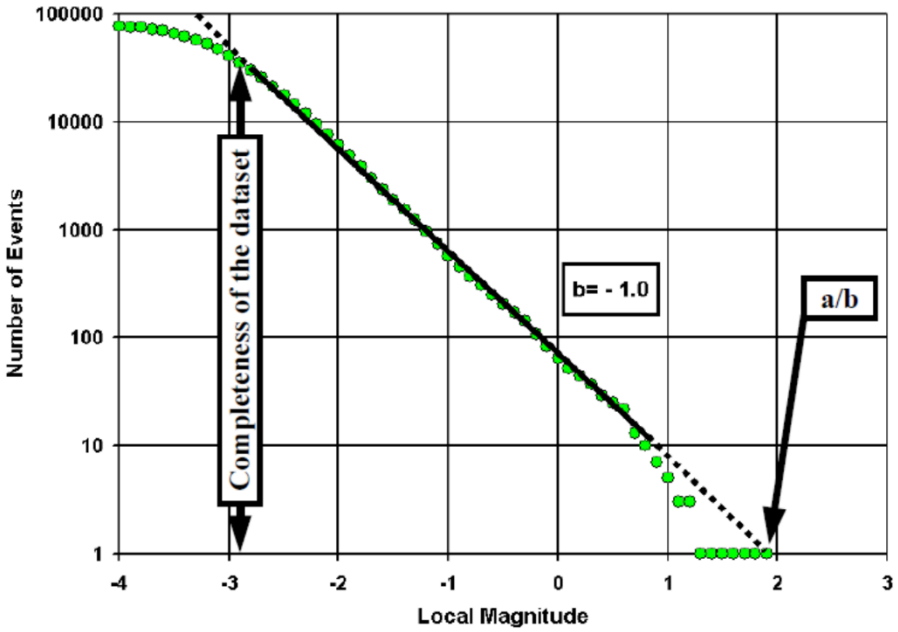

Figure 24 Frequency-magnitude relation for a reliable, well behaved data set (Hudyma, 2008)

Magnitude is a logarithmic measure of size, making the frequency-magnitude plot essentially a log-log chart. Several observations can be made about Figure 24:

- The relation is linear over a majority of the recorded magnitude range. The slope of the linear portion of the graph can give an indication of the proportion of large events to small events for a given population. For a large population of events, b typically tends towards 1 (Hudyma, 2008)
- The magnitude axis intercept, a/b, fits well with the largest recorded event, M_{max}. a/b can give an indication of the expected maximum magnitude of a population (Gibowicz and Kijko, 1994; Kijko and Funk, 1994).
- For M < -3.0, the population deviates with the best fit relation due to the decreasing ability of the seismic sensor array to record events below a certain magnitude. The magnitude that the deviation begins to occur is M_{min}. The magnitude equal to M_{min} is commonly considered to identify the completeness of the dataset.

In order for the dataset to be considered well behaved, the data should have follow a linear power law for at least 2 orders of magnitude, and a reliable dataset generally requires a completeness of at least 2000 events (Hudyma, 2008).

Two unseen factors in a frequency-magnitude chart are the time span over which the data was collected and the volume in which the events occurred. Larger time spans and volumes tend to result in b-values approaching 1, but behavior of the relation has been found to vary significantly for individual seismic sources. Legge and Spottiswoode (1987) suggest higher b-values are typical for 3-dimensional volumes of events and lower b-values are often associated with planar populations of events. Separate behaviours are often found in structurally related sources versus stress fracturing seismic sources. Figure 25 shows frequency-magnitude relations for two populations with very distinctly different behaviours.

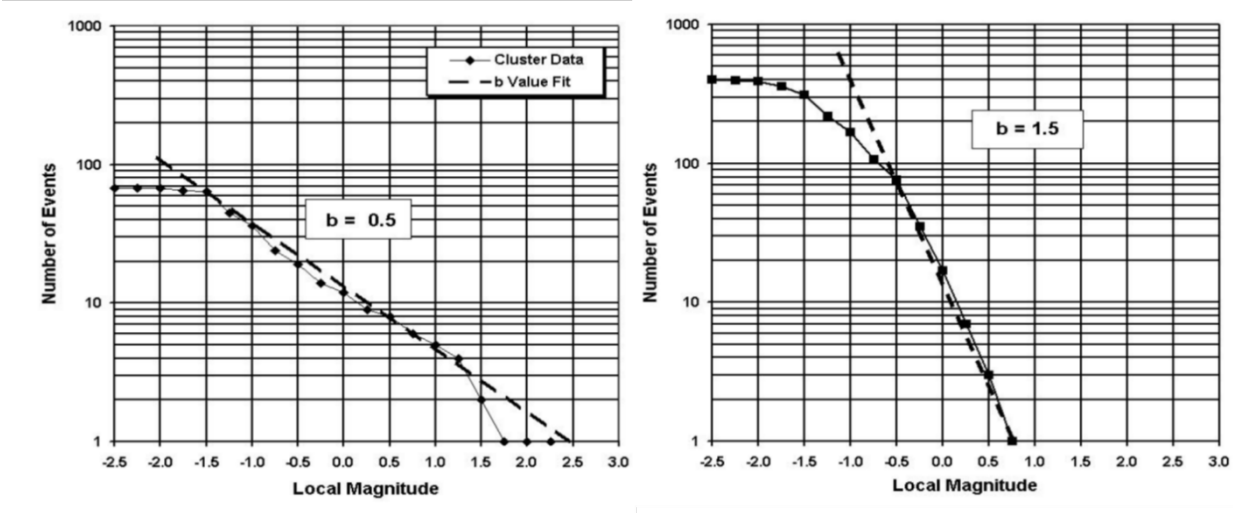

Figure 25 Frequency-magnitude relation for a fault slip source (left) and stress related source (right) (Hudyma, Mikula and Heal, 2003)

The population on the left is from a fault, having a greater hazard, indicated by a/b of 2.5 and a largest event magnitude of 2.3. Fault related seismicity has often been found to have a low b-value, often less than 0.8 (Hudyma, 2008). The population of events on the right is related to blast induced stress fracturing. Stress fracturing related events often have a much higher b-value, typically greater than 1.2 (Legge and Spottiswoode, 1987; Heal, Potvin and Hudyma, 2006). a/b and the largest recorded event are much lower than for the fault related population, indicating the seismic hazard of the population is less than that of the fault.

Self-similarity for the frequency-magnitude relation occurs while the event population fits with equation [5]. Separate rockmass failure processes can be manifested by bi-modal behaviour, depending on the spatial and temporal limits of the event population (Amidzic, 2001). Self-similarity can give an indication of fit between a large event and other supposedly related events. If a large event is part of a failure process that can be represented by a well behaved frequency-magnitude relation, the large event should fit with that dataset in order to be self similar. If the large event does not fit with the dataset, it is possibly part of a failure set that involves a different time or space. Self-similarity of an event with a frequency-magnitude relation can indicate if that event fits with the rest of the population.

Boettcher, McGarr and Johnston (2009) found that at the Tau-tona mine, self similar events exist for the same failure process over the magnitude range -2.0 < Mw < 3.0. The implication of this observation for analysis of seismicity suggests that microseismicity can be studied to understand macroseismicity. If this observation is consistent, the problem still exists, however, of ensuring the right microseismic events are analyzed, as small events are often ubiquitous in the mine, while the largest events are only associated with certain failure processes.

Variance in b-value has been hypothesised to be due to heterogeneity of the rockmass, with a high b-value thought to be representative of an increasingly heterogeneous environment (Mogi, 1962). This idea works well with the behaviour of fault slip vs. stress related sources illustrated in Figure 25. A fault is fundamentally limited to a single surface, and inherently less heterogeneous than an intact rockmass undergoing failure.

In lab experiments, b-value has been found to vary inversely with stress (Scholz, 1968; Lockner, 1993). Urbancic, Bawden and Young (1992) found that low b-value had a spatial correlation with greater stress drops. The relation between b-value and stress has been found to be consistent in earthquake seismology, shown by decreasing b-value with greater depth, which is explained by increased stress (Mori and Abercrombie, 1997; Scholz, 2015).

b-value has also been found to have a correlation with the rigidity of the deformation system. Soft systems are thought to have lower b-values and stiff systems higher b-values (Mendecki and Van Aswegen, 1998). b-value has been thought to sometimes decrease prior to large earthquakes (Hirata, Satoh and Ito, 1987). A study of large events from Creighton and Kidd Creek found decreasing b-values prior to large events (Ma *et al.*, 2018). In terms of proposed physical influences – stress and heterogeneity – this drop in b-value could be explained by increasing rockmass damage. Yielding of asperities, breaking of rock bridges, etc. reduces the heterogeneity of the eventual failure surface, essentially softening the system and permitting a greater degree of freedom for large deformation events.

To summarise:

- The proportion of large events to small events is often greater for fault related seismicity than for stress fracture related (Legge and Spottiswoode, 1987; Hudyma, Mikula and Heal, 2003)
    - Fault related b < 0.8
    - Stress fracturing b > 1.2
- The frequency-magnitude relation can be used to indicate the degree of fit between an event and a seismic population (Hudyma, 2008)

2.3.5 S:P Analysis

The partition of energy between the S-wave and the P-wave (Figure 7) has been shown to be dependent on seismic source mechanism. The ratio between the S- and P-wave (S:P), tends to be greater than 10 for a shear event (Boatwright and Fletcher, 1984). Non-shear seismic events, such as volumetric or tensile fracturing, tend to have a higher proportion of P-wave energy (Hudyma and Potvin, 2010). Hudyma and Potvin (2010) suggest a S:P less than 3 can be used to indicate a non-shear mechanism.

S:P analysis is often used to help characterize the failure mechanism of a seismic source. Figure 26 illustrates how cumulative percentage of S:P ratio can be used to provide an indication of mechanism for a population.

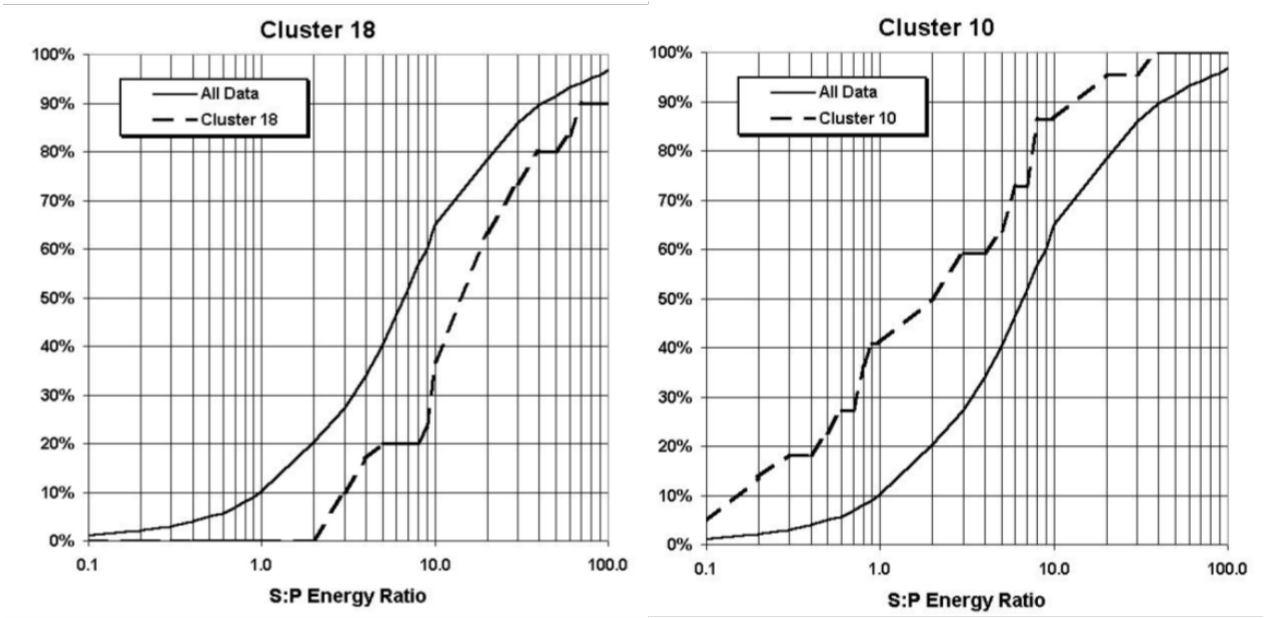

Figure 26 S:P relation for a fault slip source (left) and a stress related source (right) using cumulative frequency distribution (Hudyma, Mikula and Heal, 2003). The solid line represents the S:P relation for the whole mine.

Cluster 18 (left) has been taken from a population of events on a fault and shows a high proportion of events with S:P > 10 (dashed line). The population of events in Cluster 10 (dashed line) has been taken from a stress failure related source and has high proportion of low S:P events.

Another observation from Figure 26 is that both seismic sources have significant proportions of events that do not follow the guideline S:P for mechanism. A population of seismic events can sometimes indicate the dominant mechanism in the population, but S:P analysis for single events may be less reliable.

Source mechanisms of different type can overlap in space and time. As indicated in Figure 6 and Table 1, recorded event magnitude can be scale dependent based on seismic source mechanism. Since S:P has been shown to rely on source mechanism, S:P can be a scale dependent parameter when multiple mechanisms exist in a population. Hudyma (2008) warned of the potential for small, stress fracture related events to dominate the type of analysis illustrated in

Figure 26 and suggested that S:P scale dependence can be used to test for multiple mechanisms overlapping spatially or temporally.

S:P analysis has been shown to often have inconsistent behavior between mine seismic systems (Morkel, Wesseloo and Potvin, 2019). They suggest that use of S:P analysis as an indicator of source mechanism for a single event is unreliable and the commonly established S:P guidelines for source mechanism is not universal across mining operations. The following factors may have an impact on reliability of S:P analysis:

- Uniaxial sensors used to calculate energy (Hudyma, 2008)
- Number of triaxial sensors used to calculate energy (Hudyma, 2008)
- Path dependence of seismic waves (Hudyma, 2008)
- Data processing software (Morkel, Wesseloo and Potvin, 2019)
- Skill of operator at selecting manual S- and P-wave picks (Morkel, Wesseloo and Potvin, 2019)
- Frequency range of sensors (Morkel, Wesseloo and Potvin, 2019)

Morkel, Wesseloo and Potvin (2019) do not dispute the validity of S:P behavior for a seismic source mechanisms in general, just the consistency of the parameter as a source mechanism indicator between datasets from different mines. This leaves open the idea that the behavior of S:P may be useful within a dataset from a single mine. Hudyma (2008) recommended that S:P of populations of seismic events are compared to indicate tendency for shear or crushing. No guidelines exist on what proportion of events in a population are required to define a population as stress based or shear based. In practice, the deviation of S:P behavior for a population from the mine average is often used as indicator of source type, with those of higher S:P than mine average tending towards shear related and those with lower S:P than mine average tending to indicate a non-shear mechanism (Hudyma, 2008).

To summarize:

- S:P > 10 can indicate a shearing mechanism (Boatwright and Fletcher, 1984)
- S:P < 3 can indicate a crushing mechanism (Hudyma and Potvin, 2010)
- The reliability of S:P can vary for different seismic systems (Morkel, Wesseloo and Potvin, 2019)
- Relative variations in S:P can be a useful indication of source mechanism (Hudyma, 2008)

2.3.6 Apparent Stress Time History

This section will outline the meaning and use of Apparent Stress Time History (ASTH) analysis.

Apparent stress describes the stress release associated with a seismic event, shown by [6] (Wyss and Brune, 1968).

$$\sigma_a = \mu E/M \qquad [6]$$

Where,

σ_a = apparent stress (MPa)
μ = shear modulus (Pa)
E = radiated energy (J)
M = seismic moment (Nm)

Boatwright (1984) compared five methods of estimating coseismic stress release and confirmed the use of apparent stress, stating that use of seismic moment and dynamic stress drop provided a reasonable measure of stress release at the source. Dynamic stress drop refers to the change in shear stress that results in radiation of a seismic stress wave (Mendecki, Malovichko and Malovichko, 2013). Apparent stress is not model dependent, meaning that it is not based on a singular rupture model and avoids the inherent assumptions of those rupture models (Hanks and Thatcher, 1972).

ASTH uses apparent stress to give an indication of variations in stress in the rockmass that are caused by mining. The source parameter apparent stress provides a measure of the stress

release associated with a seismic event (Wyss and Brune, 1968). For a given magnitude, apparent stress can vary extensively. Figure 27 shows a population of equal magnitude seismic events from a South African Mine that are sized according to their apparent stress.

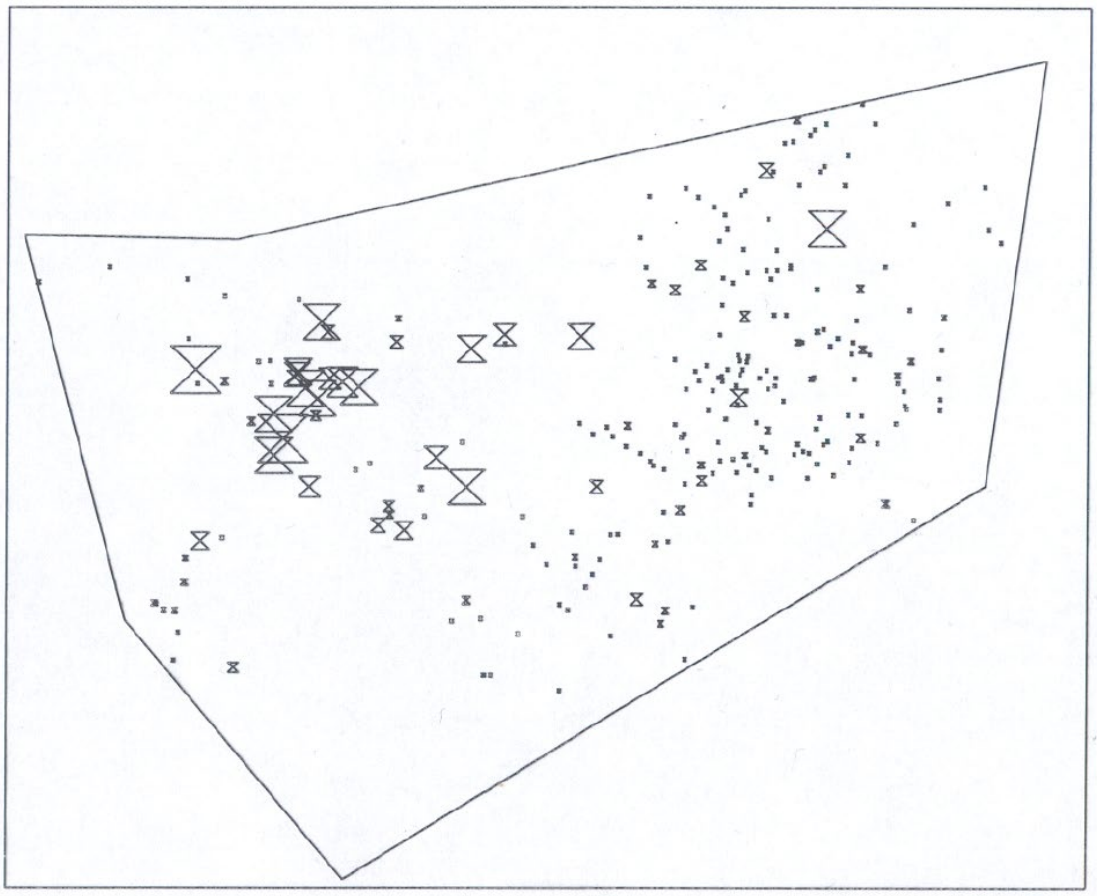

Figure 27 Shows a population of events with an equal ML 1. Event markers are sized by apparent stress, which varies by a factor of 100. (Mendecki, Lynch and Malovichko, 2010)

It can be observed that for the events of the same magnitude, there is a large variation in apparent stress, and that often events of similar apparent stress tend to locate together. High apparent stress events tend to occur in regions that undergo relatively high mining induced stress change (Van Aswegen and Butler, 1993). It could be inferred from Figure 27 visualization that the events on the left of the figure are from a higher stress area than those on the right. Comparison of Figure 27 with mine geometry and structural geology would likely add even more insight.

The purpose of ASTH is to identify time periods of high or increasing apparent stress, which is done by identifying events to those above a certain apparent stress threshold. The top 10-20 percentile of events in a population is usually used as high apparent stress threshold (Hudyma, 2008). Apparent stress frequency (ASF) is a trailing average number of high stress events in a time period, which is usually set to 24 hours. ASTH charts show date on the horizontal axis, apparent stress on the primary vertical axis and apparent stress frequency on the secondary vertical axis as seen in Figure 28.

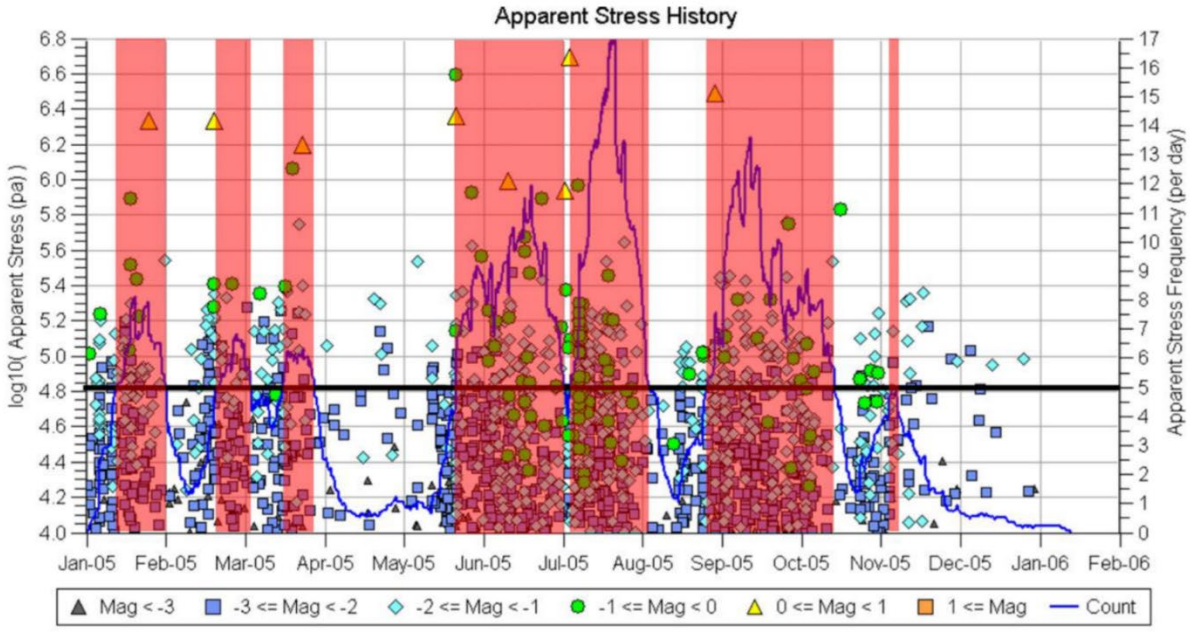

Figure 28 ASTH from a mine showing a relation between large magnitude events and periods of high apparent stress frequency (Hudyma, 2008). Time periods in which the Apparent Stress Frequency (ASF) exceed a threshold of 5 events per day is shaded in red.

It can be observed that all events in the chart greater than magnitude 0 occurred during time periods of high ASF. To illustrate high ASF, a black horizontal line was drawn across the chart at ASF of 5.

ASTH charts give insights into rockmass failure, with high ASF thought to indicate high or increasing stress in the rockmass (Hudyma, 2008). Figure 28 shows that the periods of high ASF, or high stress change in the rockmass, often coincide with large events (Mag>0).

ASTH charts are also useful to show stress increase with blasting (Hudyma, 2008; Carusone and Hudyma, 2017; Hudyma and Brown, 2020). Figure 29 shows an ASTH chart from LaRonde Mine, with superimposed blast times marked as stars with dashed lines.

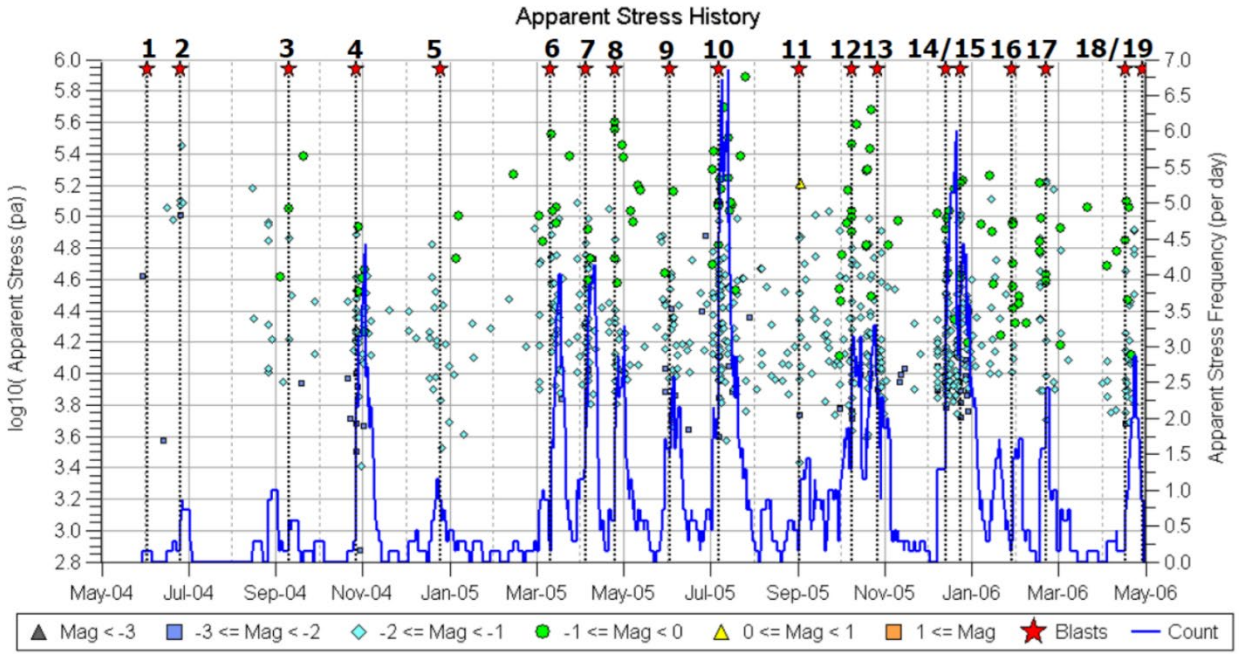

Figure 29 ASTH from LaRonde Mine showing a relation between Apparent Stress Frequency and blasting (Hudyma, 2008)

Figure 29 shows a two year monitoring period with 19 blasts occurring. Periods of high stress are inferred by time periods with high ASF. There is a clear relation between increases in ASF and blasting, with spikes in ASF often occurring soon after a blast. Blasting induces a redistribution of stress in the rock mass, which can cause coseismic rock mass failure. While apparent stress is not a direct measure of stress conditions at a seismic source, a greater number of high apparent stress events can be observed to coincide with time periods of expected blast

induced stress redistribution, leading to the conclusion that a blast induced increase in stress may be a cause of increase in the apparent stress of the associated seismicity.

Hudyma (2008) suggested that the increase in ASF was due to redistributed or increased stress after blasting, and the drop in ASF sometime after the blast indicated the stress redistribution was complete. A further observation was that ASF was affected closest to blasting, and ASF was often unrelated to events occurring at significant distance from blasting (Hudyma, 2008). Carusone and Hudyma (2017) found that there was an initial spike in apparent stress close to blasting followed by a gradual increase in apparent stress at greater distances from blasting, which could correspond to stress increase and rock yield immediately around the excavation, with gradual redistribution of stress further into the rockmass.

To summarise:

- High apparent stress is often related to blasting (Hudyma, 2008), (Disley, 2014), (Carusone and Hudyma, 2017)
- High apparent stress can be linked to elevated seismic hazard (Hudyma, 2008), (Nordström, Dineva and Nordlund, 2020)
- High apparent stress events can be related to mining induced stress increase in the rockmass (Hudyma, 2008), (Brown and Hudyma, 2017)

2.3.7 Instability Analysis

The relation between radiated energy and seismic moment can give a relative indication of the state of stress at an event hypocenter. Even for dynamic, near-instantaneous rock failure there is a length of time over which a shear event or new fracture occurs. For a given seismic moment, a slower event generates a lower frequency seismic wave with less radiated energy, while a very fast rupture velocity event produces a high frequency, high energy wave (Mendecki, 1993). Since source radius is inversely proportional to corner frequency, the lower the corner frequency, the

greater the size of the rupture area. As was noted in equation [6], higher stress release is related to a higher ratio of radiated energy to seismic moment. Simply put, a higher stress seismic event results in a faster rupture with a higher corner frequency. Because independently calculated seismic moments and energies exist for each event, a relation between energy and moment can be plotted for a population of seismic events, shown in Figure 30.

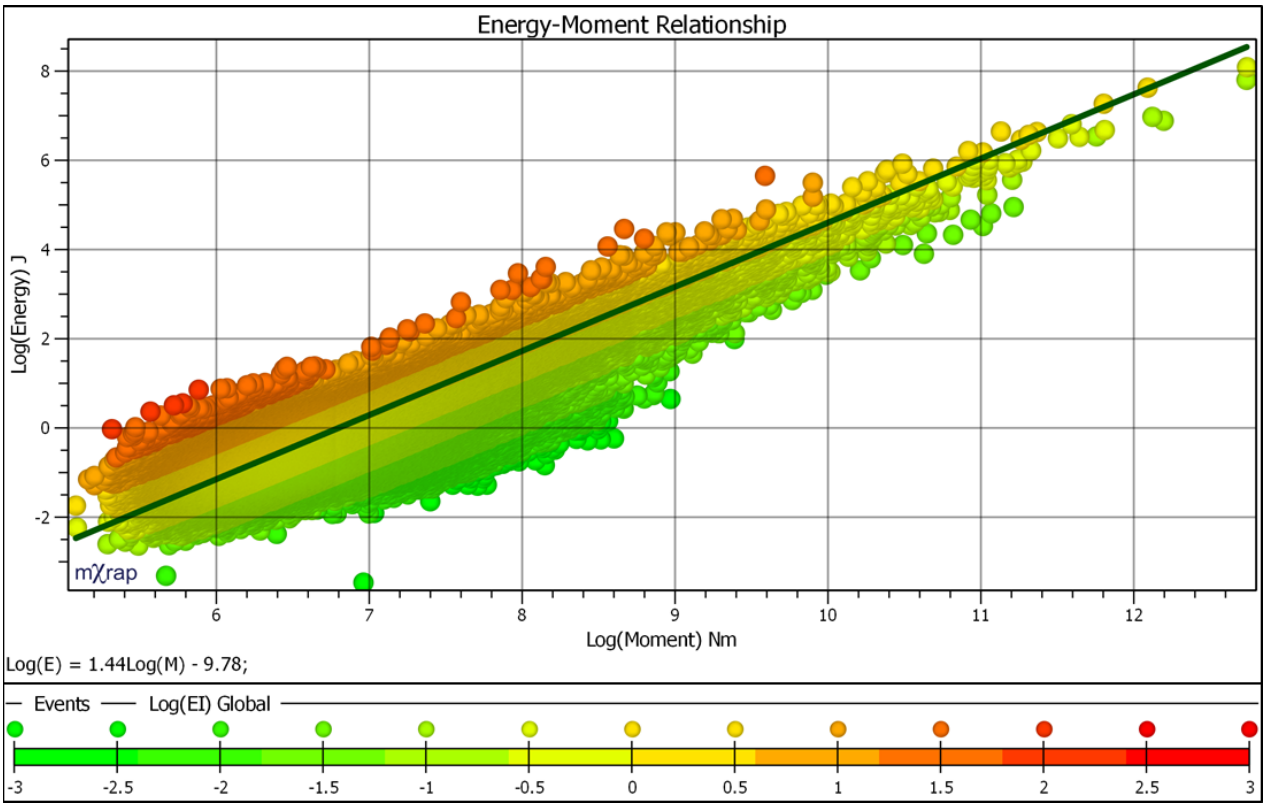

Figure 30 Energy-moment relation coloured by energy index for a Canadian mine.

Radiated energy and moment are only somewhat related for a given seismic event; radiated energy can vary by multiple orders of magnitude for an event of a given moment (Van Aswegen and Meijer, 1994).

Energy index (EI) was defined as the ratio of radiated energy of an event to the average energy of events of the same moment (Van Aswegen and Butler, 1993).

$$Log(EI) = Log(E/E(M)) \qquad [7]$$

Where,

EI = energy index

E = radiated energy of event (joules)

E(M) = average energy for events of the same moment (joules)

EI provides a relative, unitless description of the driving stress conditions that contributed to the event (Mendecki, Malovichko and Malovichko, 2013). Log(EI) greater than 0 describes higher than average stress conditions while Log(EI) less than 0 describes lower than average stress conditions.

Apparent stress is similar to EI in that it can be an indicator of stress, but differs in that it provides an actual measure of stress release while EI is a relative measure. Apparent stress is scale dependant, with larger events having greater apparent stress, while EI has no scale dependency. Figure 31 shows an example of an energy moment relation with events coloured by apparent stress.

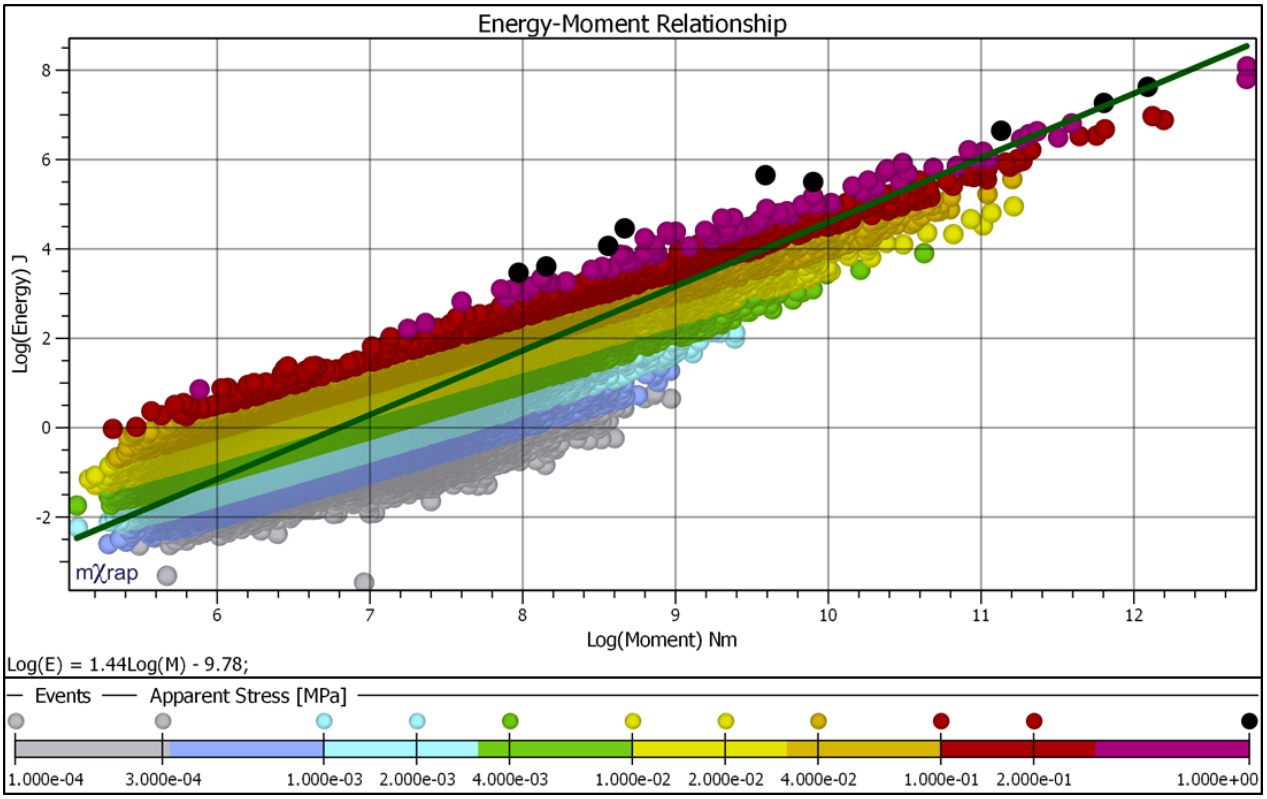

Figure 31 Energy-moment relation coloured by apparent stress

Higher AS is indicated by the progression from lighter to darker colours. While variations in EI in Figure 30 shows alignment with the line of best fit indicating scale independence, AS in Figure 31 is scale dependent, with larger moment events tending to have higher AS.

Apparent volume is a measure of inelastic deformation occurring at the source of an event [8] (Mendecki, 1993).

$$V_A = M^2/(2\mu E) \quad [8]$$

Where,

V_A = apparent volume (m^3)
M = moment (Nm)
μ = shear modulus (GPa)
E = radiated energy (joules)

Energy index and apparent volume plotted over time can provide insights into the state of rockmass failure of a volume of rock. EI is typically plotted as a trailing average of a certain number of events or for a fixed time period. Apparent volume plotted cumulatively (CAV) can show time periods of high or increasing deformation. An EI/CAV chart is called instability analysis. Since EI is an indicator for relative stress and CAV is a measure of deformation, an EI/CAV chart roughly behaves like stress-strain a plot over time (Figure 32).

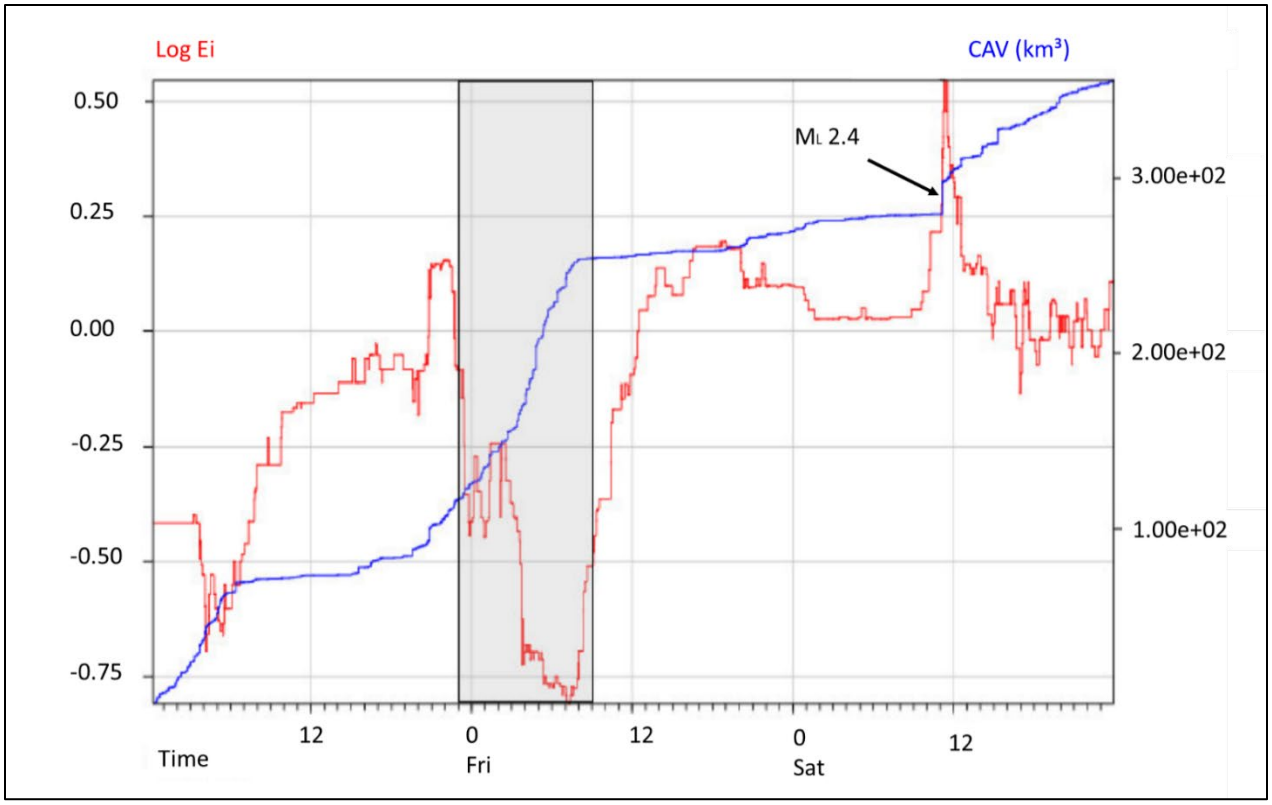

Figure 32 Instability analysis at Tau-tona Mine. Modified from (Lynch and Mendecki, 2001)

It can be observed that that periods of increasing EI tend to occur when increases in CAV are lowest. Attention is called to the shaded grey time period in which there is a significant drop in EI and steep increase in CAV, which was interpreted as a sign of a yielding rockmass or instability. Twenty-six hours after the unstable trend, a large event occurred (ML 2.4).

An initial purpose of EI/CAV was to recognize time periods of instability, during which large events may be more likely to occur. The instability of a volume of rock supplied with mining induced potential energy has been purported to undergo a softening phase prior to some larger events (Van Aswegen and Butler, 1993; Lynch and Mendecki, 2001; Rebuli and Van Aswegen, 2013). The softening phase may be identified by increasing CAV, decreasing EI or a combination of both (Mendecki, Malovichko and Malovichko, 2013). The greyed-out area of Figure 32 shows a large decrease in EI and an increase in the rate of change of CAV, supposedly representing an early warning of instability. An obvious limitation of instability analysis for early warning of large events

is it relies on seismicity to occur to generate data, while large events frequently occur with few or no precursory events. Another issue visible in Figure 32 is that between the early warning and the large event, EI/CAV does not provide any meaningful information, which begs the question: how long after a drop in EI could a large event occur?

Stiffness of a rockmass is its resistance to strain. Hou *et al.* (2021) showed that unstable failure in a laboratory setting is strongly influenced by the stiffness (or softness) of the loading system. The concept can be applied to mine scale loading systems, with stiff systems having low extraction ratios and softer system having high extraction ratios (Kaiser, McCreath and Tannant, 1996). Lynch and Mendecki (2001) applied the concept of system stiffness and softness to rockmasses, noting that in the case of a large mining pillar, large events are less frequent while the pillar was stiffer and became increasingly common as the pillar softened.

The benefit of instability analysis is that it has the potential to offer relatively simple insight into the state of rockmass failure. Figure 33 shows a multi-year instability analysis chart for a diminishing shaft pillar at Tau-tona Mine.

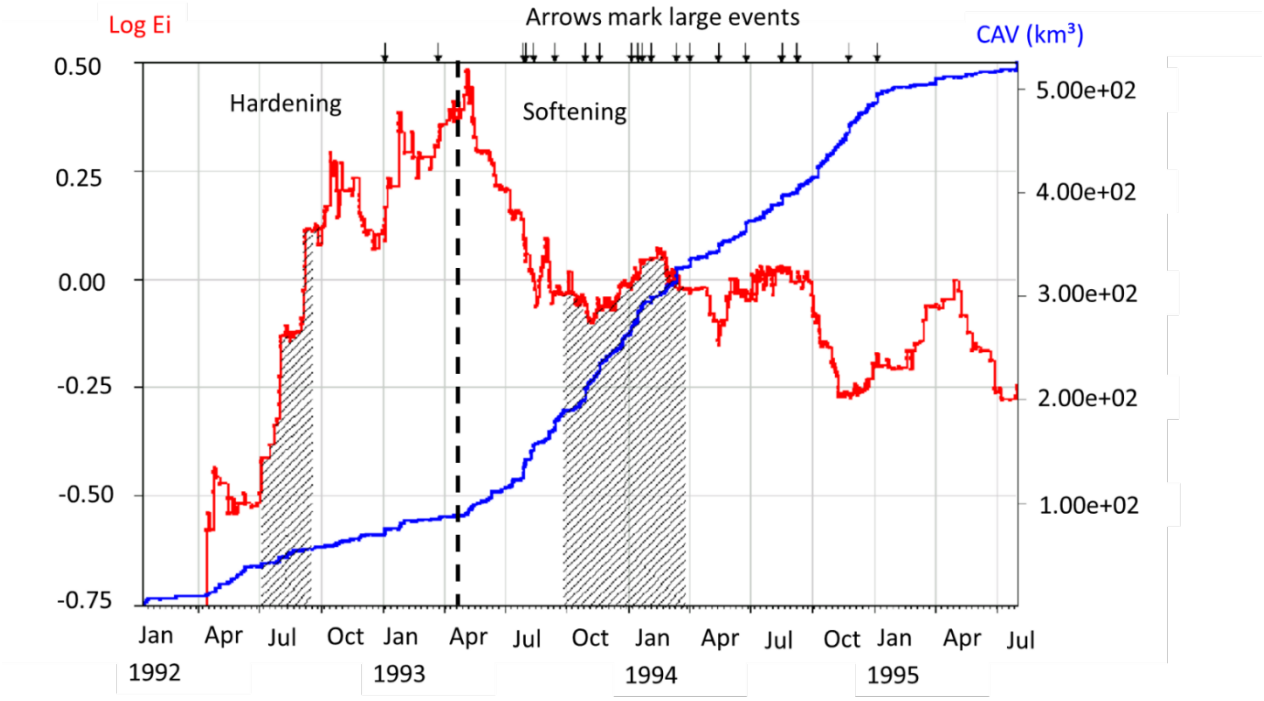

Figure 33 Instability analysis for a diminishing pillar. Modified from (Lynch and Mendecki, 2001)

The long term instability analysis chart in Figure 33 is divided into two time periods, hardening and softening. The hardening time period is characterized by increasing or high EI and comparatively low changes in CAV. The softening period has the opposite behavior; decreasing or low EI and greater changes in CAV. The timing of large events are marked on the top horizontal axis (small black arrows), and are more frequent during the softening time period.

Strain softening can occur through either an increase in driving stress or a decrease in confinement. For a case of a diminishing pillar, increase in driving stress is likely to occur as the loaded volume of rock in the pillar decreases. It can be observed in Figure 33 that early in pillar mining, EI increases quickly while CAV only increases slowly. This hardening phase was interpreted to correspond with an increase in driving stress and a low amount of deformation or yield. The pillar behavior in April 1993, changes to a softening phase, represented by dropping EI and increase in rate of CAV. The frequency of large events is found to increase during the

softening phase. After January 1995, the CAV rate decreases and EI stays low, indicating lower stress and low deformation, possibly indicating the pillar has yielded.

EI is not scale dependent. Because EI is a unitless relative indication of stress, small events have the same weighting as large events in a trailing average. The frequency of events decreases with increase in magnitude, therefore average trailing EI tends to be dominated by the smallest events. As discussed in 2.1.3, maximum event size varies with source mechanism. A trailing EI trend can become confused by inclusion of multiple source mechanisms e.g. a mine scale fault slip mechanism and local stress induced failure around new development. CAV scales with magnitude and therefore is not as sensitive to the occurrence of many small events.

To summarise:

- CAV is a measure of inelastic deformation (Mendecki, 1993)
- Changes in EI can be the result of changes in stress conditions, with log(EI)>0 indicating increasing or higher stress and log(EI)<0 indicating decreasing or lower stress (Van Aswegen and Butler, 1993)
- EI and CAV plotted over time can indicate softening or hardening of the rockmass (Mendecki and Van Aswegen, 1998)
- A drop in EI and increase in CAV is thought to sometimes precede large events (Lynch and Mendecki, 2001)

2.4 Earthquake Concepts

Earthquake seismology and mine seismology both involve the dynamic failure of rock, but the degree of similarity of rock failure mechanisms varies. Because there is some degree of overlap between the fields, learnings in one can have implications for the other (McGarr, Simpson and Seeber, 2002). The largest earthquakes take place on faults at crustal boundaries. As noted by Ortlepp and Stacey (1994) and Lenhardt (1992), events ML ≥ 3.0 have a tendency to be related

to geological features. Seismic events related to mining can also take place on faults, which predate mining, having been formed by natural processes. Fault related seismicity may have the most overlap between mining seismology and earthquake seismology, warranting a discussion of a few concepts that exist in the field of earthquake seismology.

This section will give an overview of some fault slip earthquake concepts that may have application to large mining events.

2.4.1 Barriers and Asperities

The conceptual asperity and barrier models physically describe how the strength of a fault changes due to fault slip events. The surface of a fault plane is irregular and heterogeneous to some degree; consisting of regions of variable resistance to shear deformation. The strong areas are referred to as barriers or asperities. A strong or stable area on a fault could be caused by a number of things, including:

- Healed fault surface (McBeck, Mair and Renard, 2021)
- Rough area of fault surface (Lay and Kanamori, 1981)
- Area of fault under normal stress (Selvadurai and Glaser, 2015), including mining induced normal stress (Castro, Carter and Lightfoot, 2009).

In reference to seismology, Mendecki ***et al.*** (2001) defined an asperity simply as: "*A region of a fault where a high stress drop can occur relative to the surrounding regions.*"

Figure 34 illustrates the barrier/asperity models with the hatched area representing the stressed, strong area of the fault and the white area representing a low stress, slipped area.

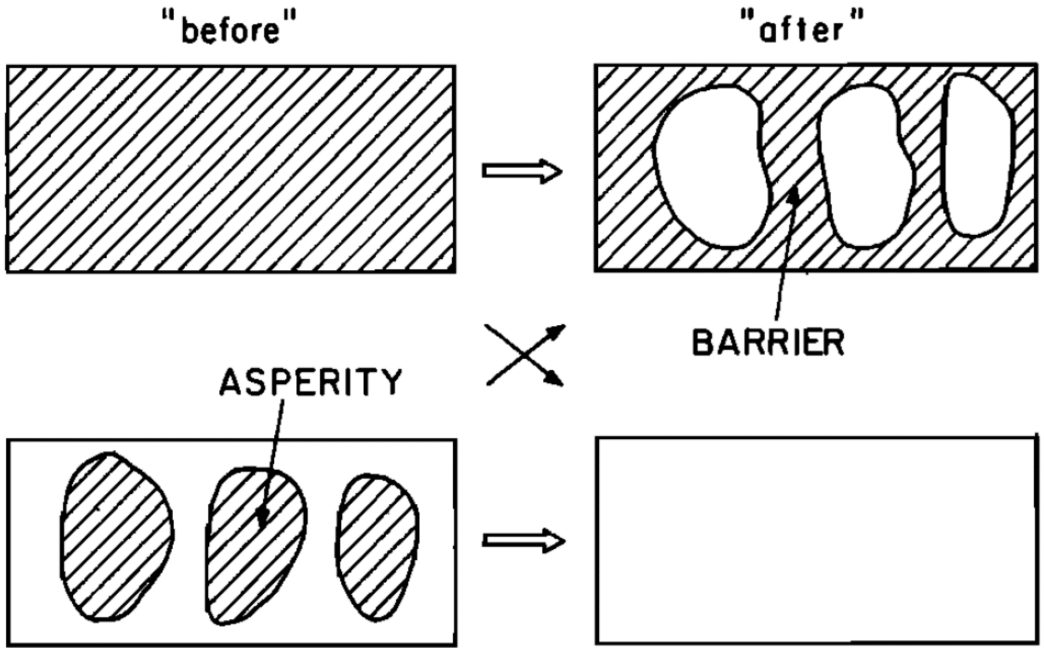

Figure 34 Barrier model (upper) and asperity model (lower) (Aki, 1984). An area on a fault plane is illustrated, with hatched areas representing high resistance to shear and blank areas representing low resistance to shear.

The upper part of Figure 34 illustrates the barrier model, showing that prior to slip, the fault plane is unbroken or resistant. As coseismic displacement takes place, the fault become increasingly heterogeneous, with weak areas and strong barriers. As barriers break, the weak area expands. The lower part of Figure 34 illustrates the asperity model, in which rough patches on the fault resist shear deformation. Seismic events take place coincident with deterioration or failure of asperities. As asperities break, the fault plane becomes increasingly homogeneous. Figure 34 shows a simplified representation of reality, only weak and strong areas of the fault. In reality, the strength of the fault likely exists on a spectrum between the weak and strong end members (Schwartz and Ruff, 1987).

Smalley Jr., Turcotte and Solla (1985) suggested that natural asperities were scale invariant, and that the size of asperities existed over a range, evidenced by the power law relation between the frequency of occurrence and magnitude of seismicity. They compared the failure of an asperity

to the failure of a cable made out of many individual strands. At a certain load, individual strands of the cable break. The total load is not changed, therefore the load carried by broken strands is transferred to the remaining strands until the entire cable catastrophically ruptures. The difference between the cable model and an asperity in the views of Smalley Jr., Turcotte and Solla (1985), is that the strands of a cable are the same scale, while asperities on a fault are thought to be variable.

The asperity model aligns with the idea that large events can occur during a softening rockmass failure system. Mendecki and Van Aswegen (1998) reported that large events have a tendency to occur as a rockmass failure system becomes softer, meaning the deformation response to stress increases. This suggests that as asperities on a fault deteriorate, the freedom for that fault to slip should increase.

Van Aswegen and Mendecki (1993) give a progression of how mining, geology, stress and strain may contribute to the failure of a single asperity:

1. Mining advances towards a fault
2. Mining induced shear stress on the fault gradually increases
3. Shear stress on the fault starts to approach shear strength on part of the fault
4. Weaker areas of the fault start to creep. A stronger area – asperity – undergoes strain hardening as its peak strength is approached.
5. The asperity begins to yield and stress cannot increase. The asperity softens, with changes in stress inducing greater shear deformation.
6. The asperity ruptures, with slip occurring over both the failed area and the weak areas of the fault

7. The source area becomes weak and deforms in response to stress. The weak area on the fault expands with greater deformation.

2.4.2 Foreshocks

Foreshocks are part of an accelerating sequence of seismic activity that occur prior to the largest event, or main shock (Helmstetter and Sornette, 2003). Maeda (1999) lists two possible relations between foreshocks and a main shock:

1. Foreshocks are a sign of a general increase in stress in the region which also causes the main shock.
2. The occurrence of foreshocks transfers stress to the region that yields in the main shock.

The asperity model (Figure 34), describes strong, stressed asperities surrounded by areas that have already slipped or become weak. Foreshocks and preslip are thought to contribute to the asperity failure process (Aki, 1984).

While the occurrence of foreshocks can sometimes can provide early warning of a large event (Berberian, 2014), prediction is limited by the fact that increased event rates often occur without large events and large events frequently occur without any foreshocks (Kayal, 2008). In a study of mining related seismicity at Kiirunavaara Mine, an increase in event rate was noted prior to 71% of large events (Nordström, Dineva and Nordlund, 2020). Similarly, Simser (2006) found that at the Craig mine, approximately 30% of rockbursts occurred without any unusual precursory activity.

The cascade model of foreshocks compares foreshocks to domino-like behaviour, where each event consists of additional rupture on a plane, which eventually leads to a large event (Ide and Aochi, 2005). In this case, the size of the main shock cannot be predicted by foreshocks because the final rupture area can keep increasing as long as conditions permit (Kamogawa *et al.*, 2019).

The nucleation model of foreshocks theorizes that the occurrence of foreshocks is a deterministic process related to the final rupture area (Olson and Allen, 2005). The magnitude of the main shock should be predictable because it is related to the area that is prepared by the foreshocks (Kamogawa *et al.*, 2019)

Foreshocks have been found to sometimes migrate towards the main shock, spatially becoming closer prior to rupture (Helmstetter and Sornette, 2003). Kagan and Knopoff, (1976) also observed migration of seismicity towards a large event and dispersion of aftershocks.

2.4.3 Aftershocks

After a large event, an increase of seismicity above the normal event rate is almost always observed. Events occurring after a main shock are termed aftershocks. Aftershocks are generally more numerous than foreshocks (Utsu, 2002; Kagan and Knopoff, 1976). A very large seismic event redistributes stress through the rockmass both statically and dynamically. The physical cause of aftershocks is thought to be redistribution of strain energy, which triggers other smaller seismic events (Stein, 1999).

Omori's Law states that aftershocks have a behaviour decay according to a power law (Omori, 1894). Experience has shown, however, that sequences of related large events can exist, both in macro scale earthquakes (Scholz, 2010) and in mining (Hedley *et al.*, 2013) that are not part of a Omori decay process.

Triggered secondary earthquakes can occur by static stress change (King, Stein and Lin, 1994) or by the dynamic stress change caused by a transient seismic wave (Gonzalez-Huizar and Velasco, 2011). Theories exist for delayed dynamic stress triggering as well, which suggests that the stress wave from large earthquake could trigger a time dependent weakening process in another source, eventually leading to another large earthquake (Parsons, 2005).

A further complication to understanding the behaviour and meaning of aftershocks is that creeping fault deformation has been found to sometimes take place after the main event without signs of seismicity. Aseismic afterslip has been observed by movement of GPS stations after large earthquakes (Hsu *et al.*, 2006). Afterslip can also result in aftershocks on the same fault plane as the main shock (Hsu *et al.*, 2006).

Henry and Das (2001) observed that for fault slip events, aftershocks are often observed in the outer edges of the main slip. Wetzler *et al.* (2018) found that in some cases, aftershocks could be absent from the hypocenter of the main shock and increase towards the outer edges. These observations are consistent with the unloading of the hypocenter of the main shock.

2.4.4 Seismic Gaps

The seismic gap hypothesis states that a fault area that should theoretically be seismically active, yet remains aseismic has an increased likelihood of producing a large earthquake (McCann *et al.*, 1979). Kagan and Knopoff (1976) found that a seismic gap, or absence of seismicity, could occur prior to and immediately after a great earthquake. Essentially, the probability of occurrence of the largest event on a fault is lowest after one has occurred and increases with time after the last large event. Mogi (1979) referred to two kinds of gaps: a spatial gap on a fault between seismically active areas and a temporal gap, which is an absence of seismicity in the time before a large main shock. The basis for this theory is that the quiet area causing the gap is storing strain energy for an eventual large event. If deformation along a plate boundary is known to occur, but there have been no recent large earthquakes, strain energy may be building for a large release of energy. This theory is somewhat controversial, having been rejected as a forecasting model by Kagan and Jackson (1991), whose methodology was later criticized by Wyss and Wiemer (1999).

The applicability of the seismic gap hypothesis to mining related events has not been widely investigated, but large seismic events have been frequently noted to occur without preceding

seismic activity. Simser, (2006) noted 1/3 of rockbursts at Craig mine occurred without foreshocks, while conversely, Nordström, Dineva and Nordlund, (2020) noted 71% events above ML 0.8 had an unusually high precursory activity rate. These studies show that while most events appear temporally linked to foreshocks, a significant portion of large events occur without precursory events and therefore may have a precursory gap in space and time. The seismic gap hypothesis is unlikely to have much value to mining in a predictive sense but as a conceptual model is an interesting way to think about large events that occur following a quiet space and/or time.

The asperity model is related to the seismic gap hypothesis (Schwartz and Ruff, 1987). A lack of seismicity has been sometimes thought to indicate resistance to deformation. Van Aswegen (2005) suggests that the concepts behind the seismic gap theory can be used to describe certain "stiff" areas where a high co-seismic strain rate is expected, but absent. He gives an example of a large, dyke-related event, which was thought to be related to rupture of an asperity. This region showed signs of high stress but lacked signs of substantial energy release until the large event occurred. The seismic gap theory may not be directly applicable to mine seismicity in a predictive sense but is interesting in that it suggests that large events can occur unexpectedly in regions that are not exceptionally seismically active.

3 Nickel Rim South Mine

The focus of Chapters 3 and 4 is on a back analysis of a large seismic event that took place at Nickel Rim South Mine (NRS). Chapter 3 contains background information on NRS. Chapter 4 contains the analyses, which includes a novel tool to back analyse large events.

NRS is located in the nickel mining region of Sudbury, Ontario Canada. NRS was discovered in 2001 and went into full production in 2010 (Jalbout and Simser, 2014). The mine operates at a planned extraction rate of 3,500 tonnes per day (Glencore, 2018).

3.1 Geology

This section will give an overview of the regional, site and structural geology.

3.1.1 Regional Setting

NRS is one of several mines in the located in the nickel-rich Sudbury basin. The Sudbury basin is located near the southern boundary of the Precambrian Superior Province of the Canadian Shield. Figure 35 shows a geologic map of the Sudbury Basin and the location of NRS.

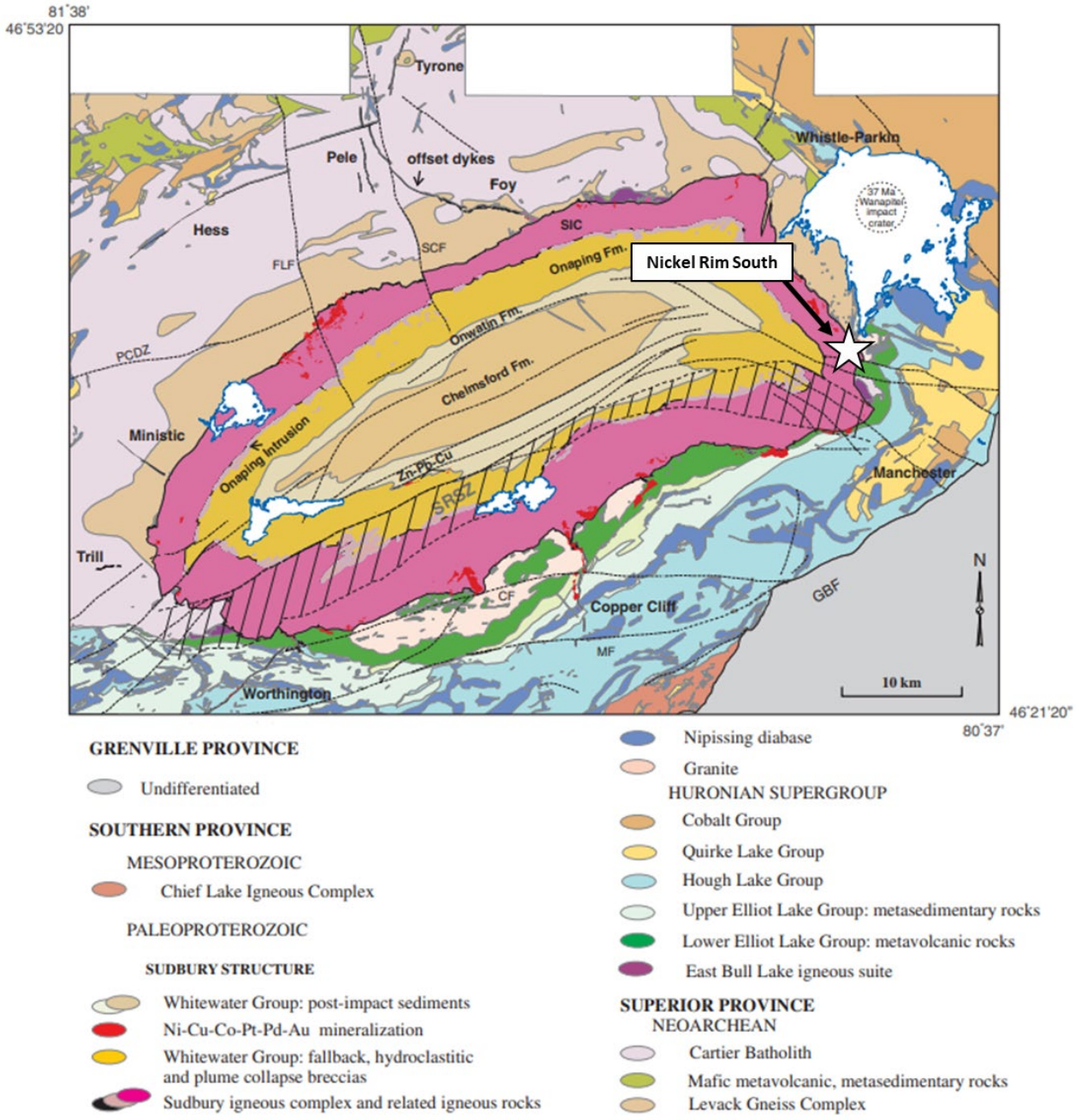

Figure 35 Regional geology of the Sudbury Basin and location of Nickel Rim South Mine (modified from Ames, Davidson and Wodicka, 2008). Fault abbreviations: PCDZ – Pumphouse creek deformation zone, SCF – Sandcherry Creek fault, FLF – Fecunis Lake fault, MF – Murray Fault, CF – Creighton fault, SRSZ – South Range shear zone, GBF Grenville Front boundary fault.

The Sudbury Basin is thought to have formed as the result of a meteorite impact (Ames, Davidson and Wodicka, 2008). The basin consists of impact melt-related rocks called the Sudbury igneous

complex (SIC), overlying impact related breccias of the Whitewater Group and younger metasedimentary rocks of the Onwatin and Chelmsford formations.

Economic mineralization in Sudbury is often associated with the SIC. The SIC consists of 4 lithologies, which ordered from upper to lower are: granophyre, quartz-gabbro, norite, and the sulphide-bearing noritic contact sublayer (Therriault, Fowler and Grieve, 2002). Archean metagranite and metavolcanics underly the SIC to the north, while the south is bounded by metasedimentary and metavolcanic rocks of the Huronian Supergroup (Therriault, Fowler and Grieve, 2002).

The primary economic mineral of the Sudbury basin is nickel, but copper and other secondary metals can be found in mineable grades. Mineralization is often either hosted by the contact sublayer or associated with Sudbury Breccia.

3.1.2 Mine Lithology

NRS is located on the eastern end of the Sudbury basin. Figure 36 shows a cross section of NRS geology.

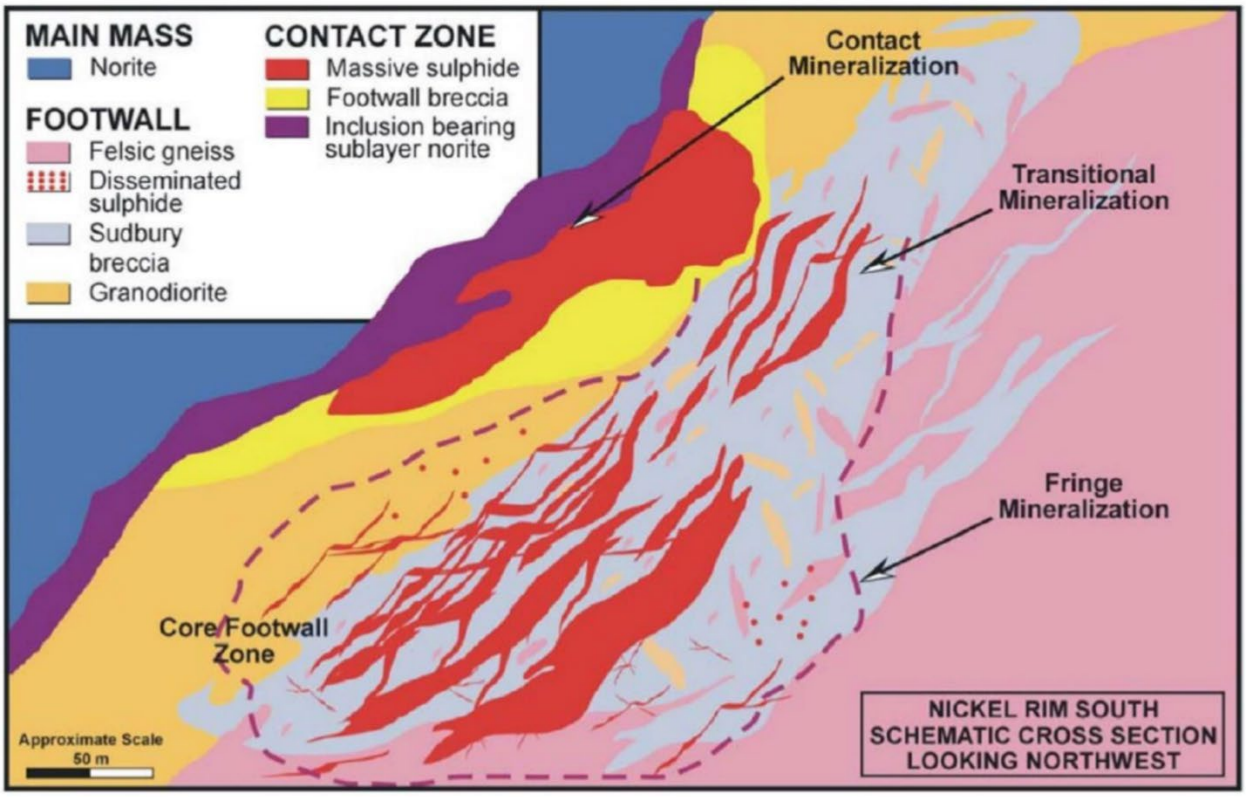

Figure 36 Geological cross section of the Nickel Rim South orebody (McLean, Straub and Stevens, 2005)

The hanging wall (HW) of the NRS orebody is norite of the SIC, while the footwall (FW) is felsic gneiss of the Superior Province. Two zones of mineralization are mined at NRS, called the contact zone and the FW zone. The ore in the contact zone is nickel-bearing massive sulphide and semi massive sulphide (Jalbout and Simser, 2014). The footwall zone is a copper-bearing massive sulphide hosted by Sudbury Breccia (Jalbout and Simser, 2014). Figure 37 illustrates the location of the orebodies relative to mine infrastructure.

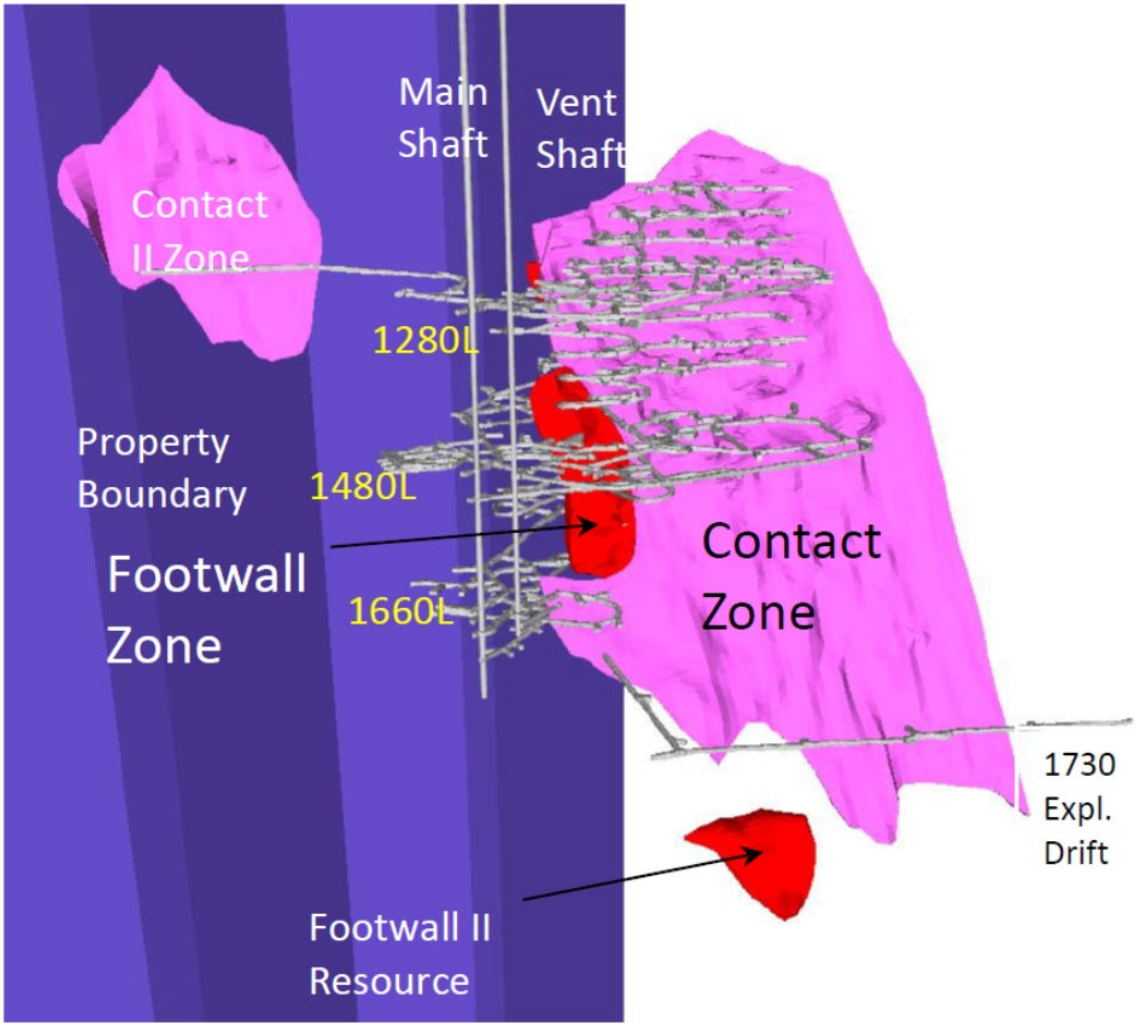

Figure 37 Nickel Rim South orebodies (Jalbout and Simser, 2014)

The width of the combined Contact and Footwall zones is under 125m and the strike length is a maximum of 300m. The orebodies are steeply dipping, allowing the mine operator to use the mining method of blasthole open stoping. Mine reserves are dominated by the Contact Zone and the Footwall Zone, though other smaller deposits exist. Mine levels (L) refer to their depth in metres below surface. The operating levels in the Contact and Footwall Zones extend from 1160 to 1680, typically with 25-30m spacing.

3.1.3 Structural Geology

Several faults intersect the NRS orebody. Figure 38 illustrates faulting in the main mining area.

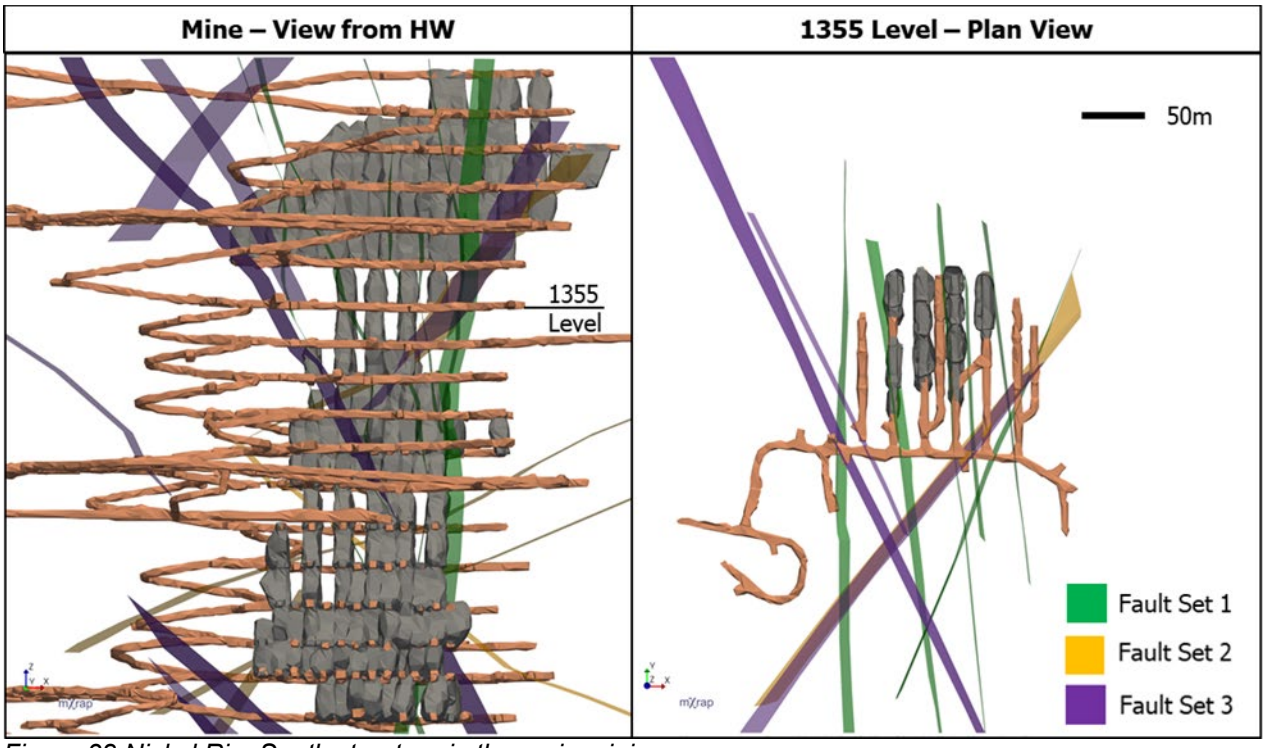

Figure 38 Nickel Rim South structure in the main mining area

Jalbout and Simser, (2014) describe three brittle fault sets in the main part of the mine, which include:

- Fault set 1: North-south group, sub-vertical faults
- Fault set 2: Low angle group
- Fault set 3: Northeast and Southeast striking sub-vertical faults

Fault sets 1 and 3 are more pervasive than fault set 2. Fault set 1 is oriented approximately normal to the strike of the orebody. Fault set 3 is oriented at an oblique angle to the orebody.

The plan view of 1355L shows that the north-south group of faults strikes sub parallel to the cross cuts. Mining width can be up to 125m, exposing a significant strike length of the N-S faults.

3.2 Rock Mechanics

This section will give a brief overview of the rockmass strength and quality of the main lithologies, and the magnitude and direction of in-situ stress at NRS.

3.2.1 Rockmass Properties

Rock quality at NRS is generally very good. Table 3 lists strength and NGI rockmass quality for rock units at NRS.

Table 3 Nickel Rim Rockmass Properties (Jalbout and Simser, 2014). Abbreviations: FGN – Felsic gneiss, FNOR – Felsic norite, SDBX – Sudbury breccia

	UCS (MPa)		Rock quality tunnelling index typical range				
Rock type	**Point Load**	**Core Test**	**RQD**	**Jn**	**Jr**	**Ja**	**Jw**
FGN	178	250	75-100	6-9	1-3	1	1
FNOR	263	215	75-100	6-9	1-3	1	1
Late granite breccia (LGBX)	190	206	75-100	6-9	1-3	1	1
SDBX	200	383	75-100	6-9	1-3	1	1
Semi massive sulphide Ni	153	196	75-100	6-9	0.5-3	1	1
Massive sulphide Ni	84	89	75-100	6-9	0.5-3	1-3	1
High grade copper	49	28	50-75	6-9	0.5-3	1-3	1
Dark norite breccia	229	160	75-100	6-9	0.5-3	1-3	1
Diabase	290	–	75-100	6-9	1-3	1	1
Dark norite	234	160	75-100	6-9	1-3	1	1
Gabbo	284	279	75-100	6-9	1-3	1	1
Grand norite	240	226	75-100	6-9	1-3	1	1

The host lithologies are generally strong and competent. The massive sulphide ore and high grade copper ore are generally weaker than the HW and FW norite and gneiss.

3.2.2 In Situ Stress

The stress regime at NRS has a sub-horizontal principal stress direction, which is typical for the Canadian Shield. The principal stress orientation, originally thought to be east-west (Jalbout and Simser, 2014), is now recognized as trending approximately azimuth 020° mine grid, with a 20° plunge (Glencore, 2018). Seismic stress inversion by Abolfazlzadeh and McKinnon, (2017) generally agrees with this orientation. The orebody dips to the north, putting the principal stress direction an oblique angle to strike.

Table 4 lists approximate magnitudes of the *in situ* stress gradient.

Table 4 Stress magnitudes at Nickel Rim South (from Jalbout and Simser, 2014)

	Magnitude
σ_1	$1.6*\sigma_3$
σ_2	$1.3*\sigma_3$
σ_3	0.026 MPa/m depth

Mining induced stresses likely vary a great deal from the approximations given in Table 4.

3.3 Mining

This section will provide a brief overview of the mining method and sequence at NRS.

3.3.1 Mining Method

The mining method used at NRS is blasthole open stoping with post mining cemented hydraulic backfill. Figure 39 shows a vertical cross section of stope outlines, drill rings and access drifts.

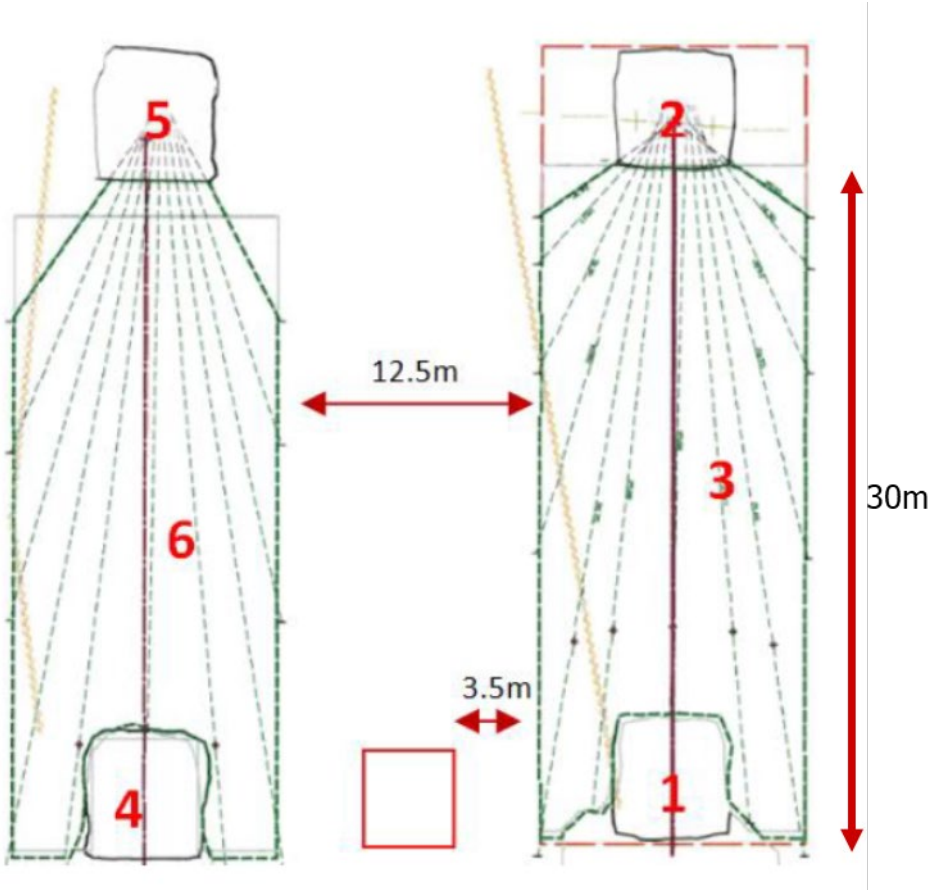

Figure 39 Primary-secondary blasthole open stoping (modified from Jalbout and Simser, 2014). Grey dashed lines represent planned drill rings.

Figure 39 illustrates a typical cross section of stoping at NRS. Labels 3 and 6 are primary stopes, with a 12.5m secondary pillar between planned to be mined at a later date. Labels 1 and 4 are mucking horizons, used to extract the blasted ore. Labels 2 and 5 are drilling horizons, from which blasthole rings are drilled and blasted. After 3 and 6 are drilled, blasted, mucked and backfilled, 2 and 5 become mucking horizons for the stope above. The stopes are typically extracted in two blasts consisting of a 7000t toe shot and a 21000t final blast (Carusone, 2018). The initial blast is usually, taken to about a third of the stope height and the second final blast breaks through to the level above (Carusone, 2018). Stope dimensions are typically 12.5 along strike, 30m height and 30m length.

3.3.2 *Mining Sequence*

Figure 40 to Figure 44 show the NRS mining sequence from 2011-2020.

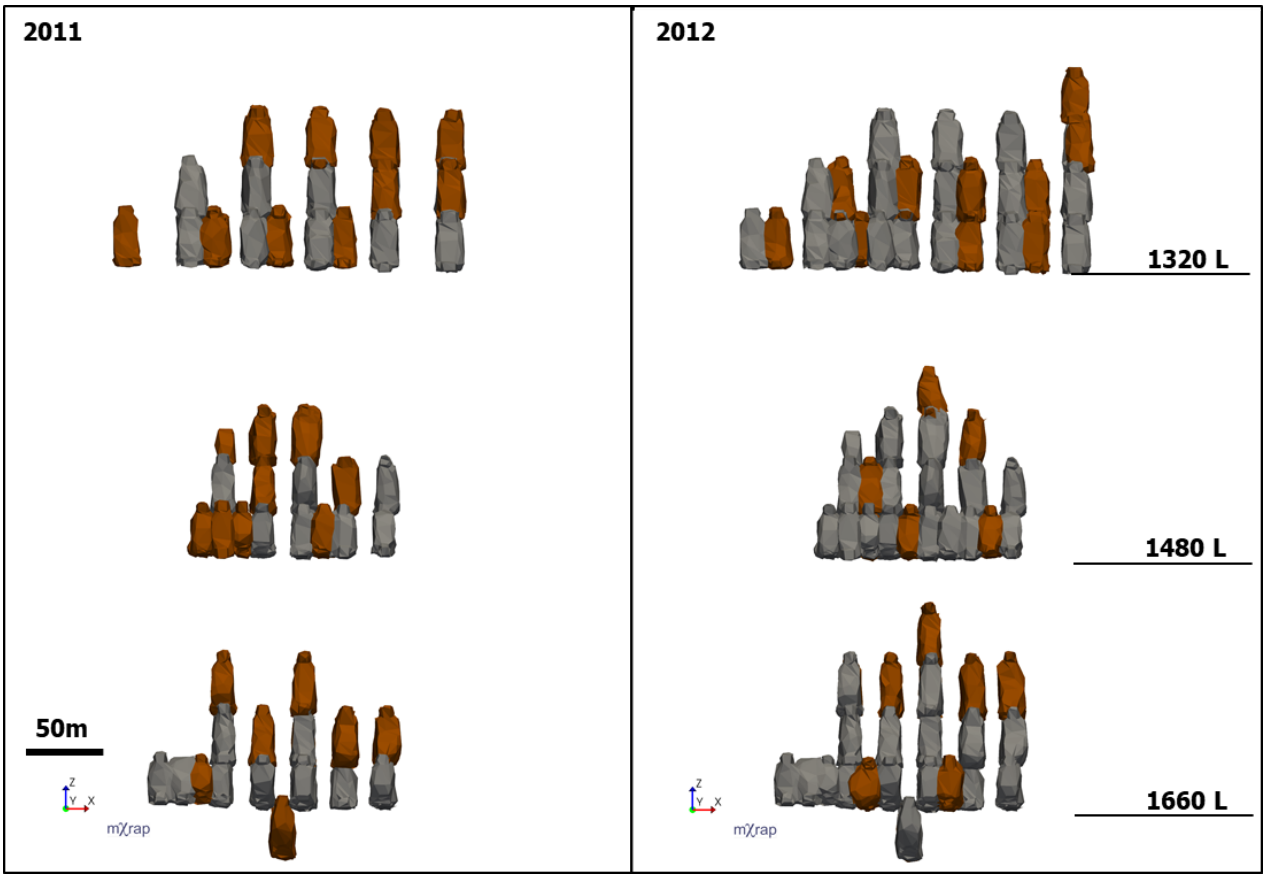

Figure 40 2011-2012 mining shown in brown, looking from HW

Mining was initiated using bottom-up sequences in the main orebody at NRS from mining horizons on 1320L, 1480L and 1660L. These sequences will be referred to as the 1660 sequence, the 1480 sequence and the 1320 sequence. There are two main sills, the temporary regional pillars below 1320L and 1480L. These will be referred to as the 1320 sill and the 1480 sill.

Above 1415L, stopes are accessed from the HW, with stopes mined sequentially in 2-3 stopes, retreating from the FW. Mining below 1415L retreats from the HW towards the FW.

The 1320 sequence used a primary-secondary-tertiary sequence. The 1480 and 1660 sequences utilized a chevron shaped primary-secondary sequence. One level has been mined below 1660L using a pillarless sequence.

Use of pillars in a mining sequence has economic benefits, but the shape of the pillars is often governed by geomechanical constraints. In seismically active mines, it can be more advantageous to have weaker pillars than stronger pillars (Hedley, 1992). Strong squat pillars can promote storage of significant strain energy and be prone to seismicity while slender pillars tend to yield early. Development and stope mining tend to be easier in a yielded, lower stress pillar than a high stress pillar.

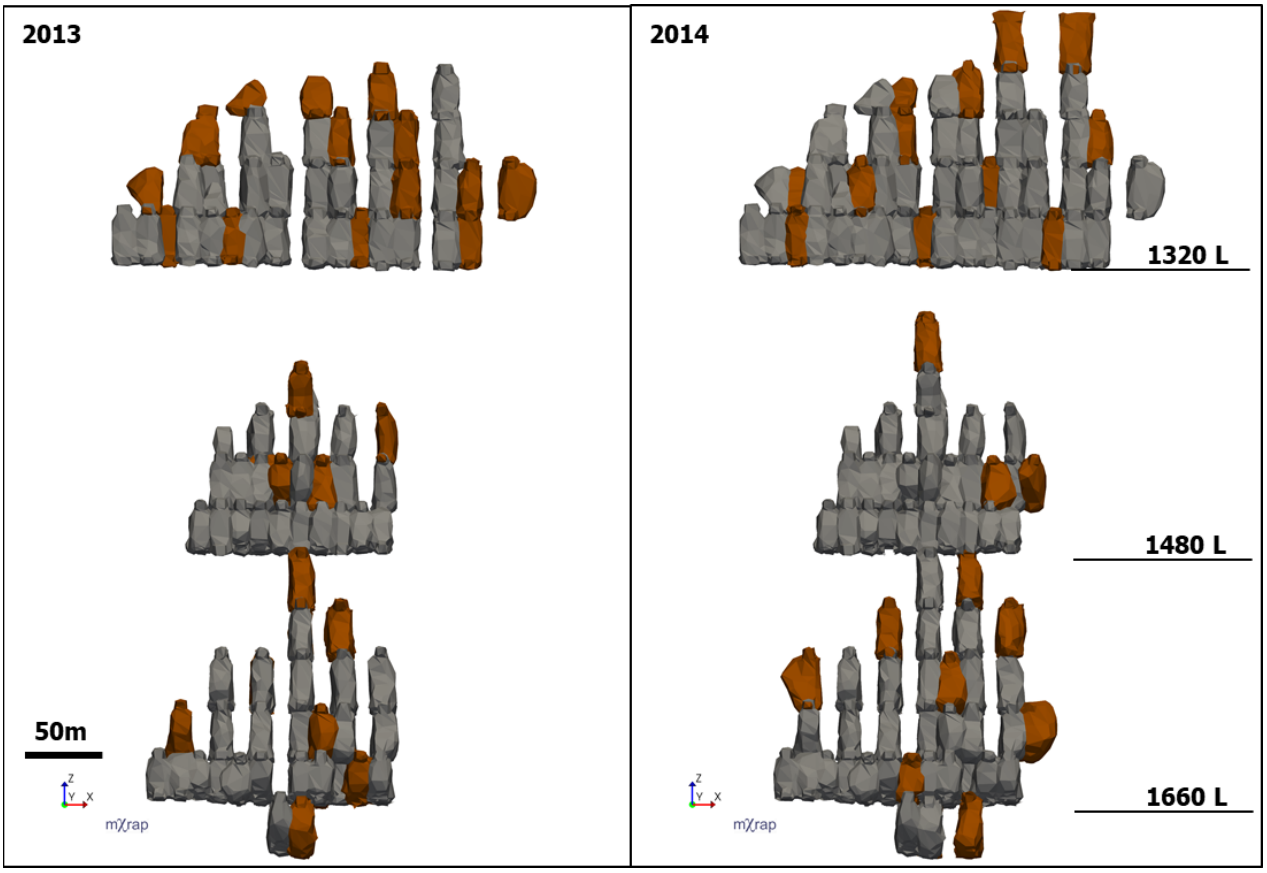

Figure 41 2013-2014 mining shown in brown, looking from HW

Figure 41 shows that the 1480 sill was breached in 2013, with primary mining beginning to progress outwards towards the abutments in 2014. The 1480 sequence was dominantly primary mining.

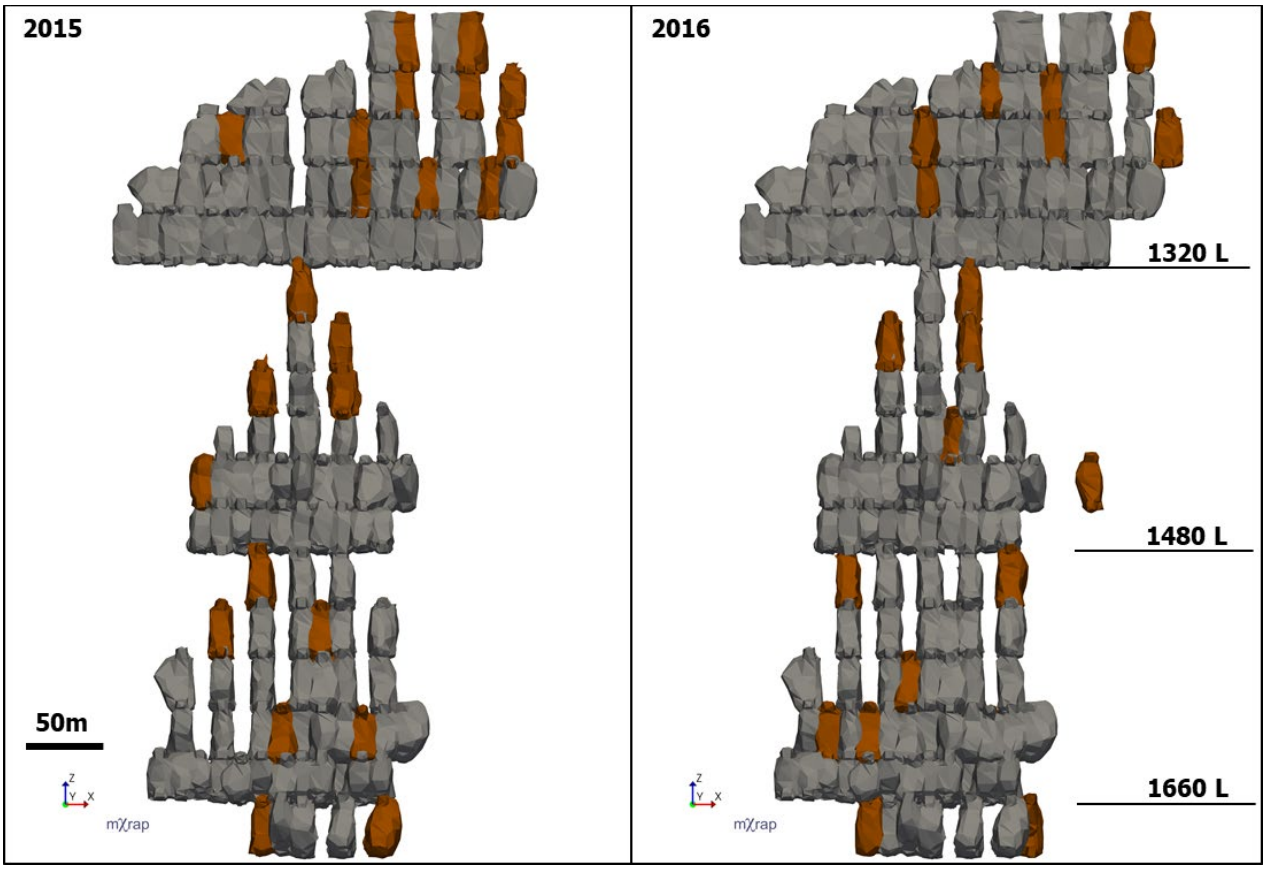

Figure 42 2015-2016 mining shown in brown, looking from HW

Figure 42 shows the 1320 sill was breached in 2015, and expanded along strike in 2016. The 1660 sequence changed from mostly primary mining to mostly secondary mining.

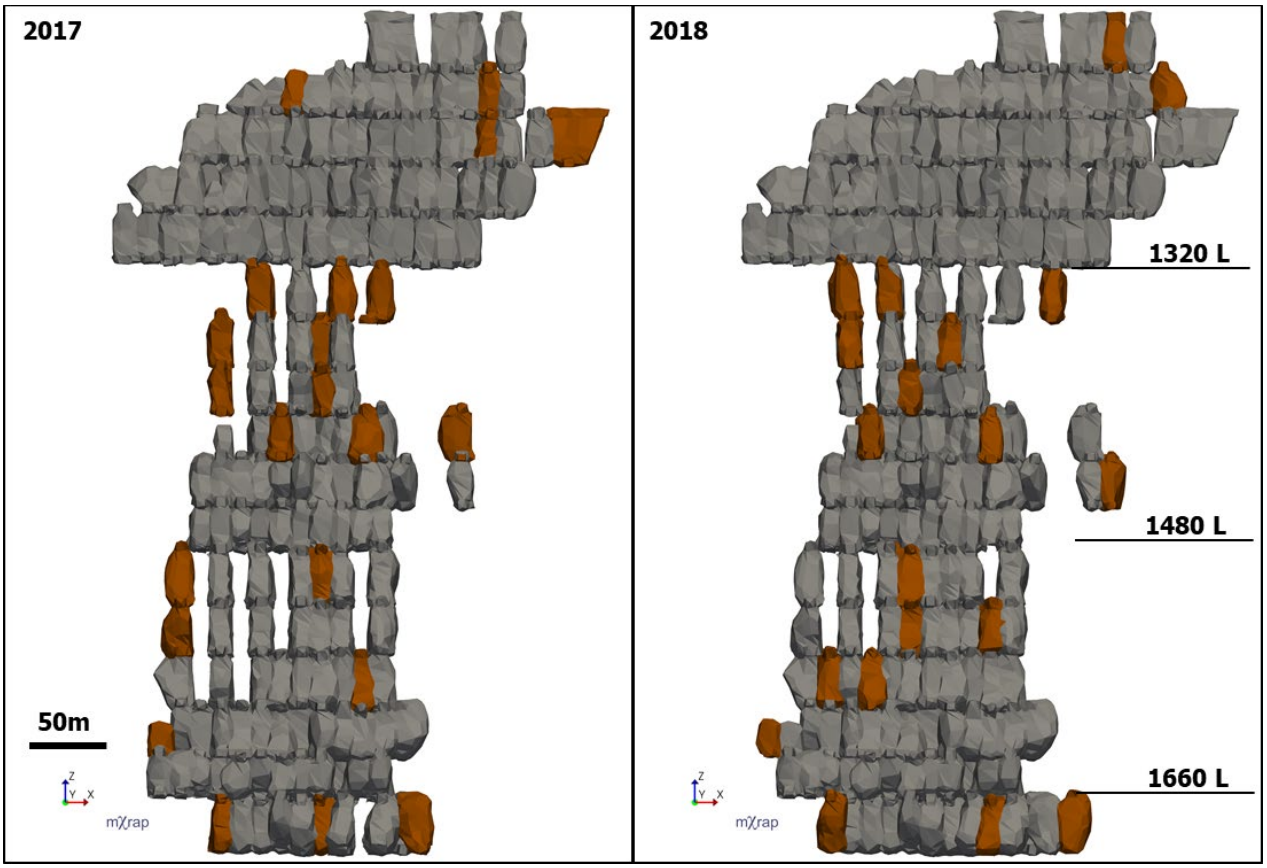

Figure 43 2017-2018 mining shown in brown, looking from HW

In 2017-2018, the 1480L sill was completed to full strike length. Significant primary extraction was completed in the 1320L sill.

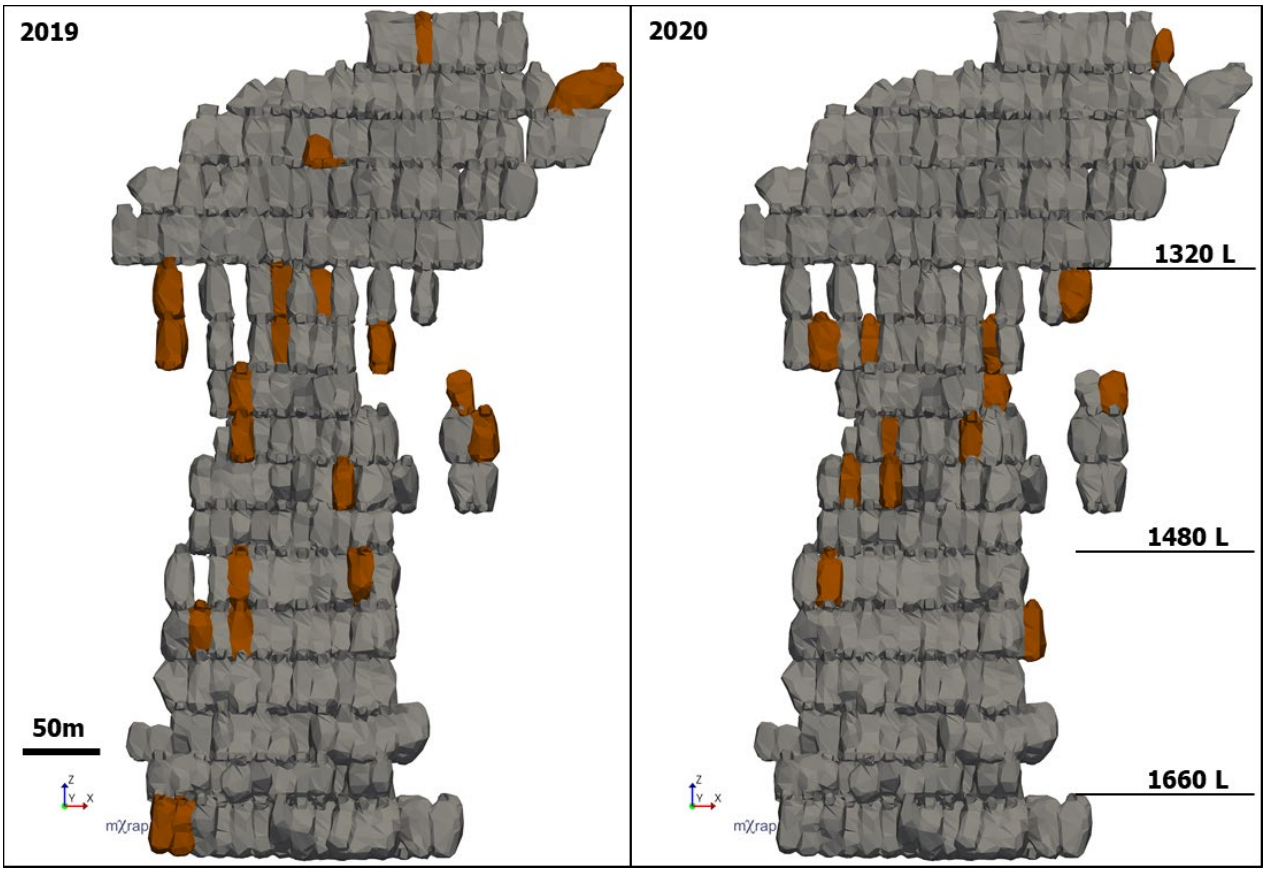

Figure 44 2019-2020 mining shown in brown, looking from HW

Figure 44 shows the lower mining sequence was almost fully extracted by 2020. From 2019-2020, the 1320L sill was mined to near full strike length and secondary mining was initiated in the center.

3.4 Seismic Monitoring

NRS is seismically active and takes measures to manage seismic risk to operations and personnel. This section will give a brief overview of the monitoring hardware, its accuracy, and a broad look at the seismic history of the mine.

3.4.1 Hardware

Unlike many of the historic mines in the Sudbury camp, NRS was discovered and developed after seismic monitoring had become commonplace and was readily available. Seismic activity was

expected at NRS, therefore a seismic system was installed as early as possible and a near complete seismic record for the mine exists.

The NRS sensor array is illustrated in Figure 45.

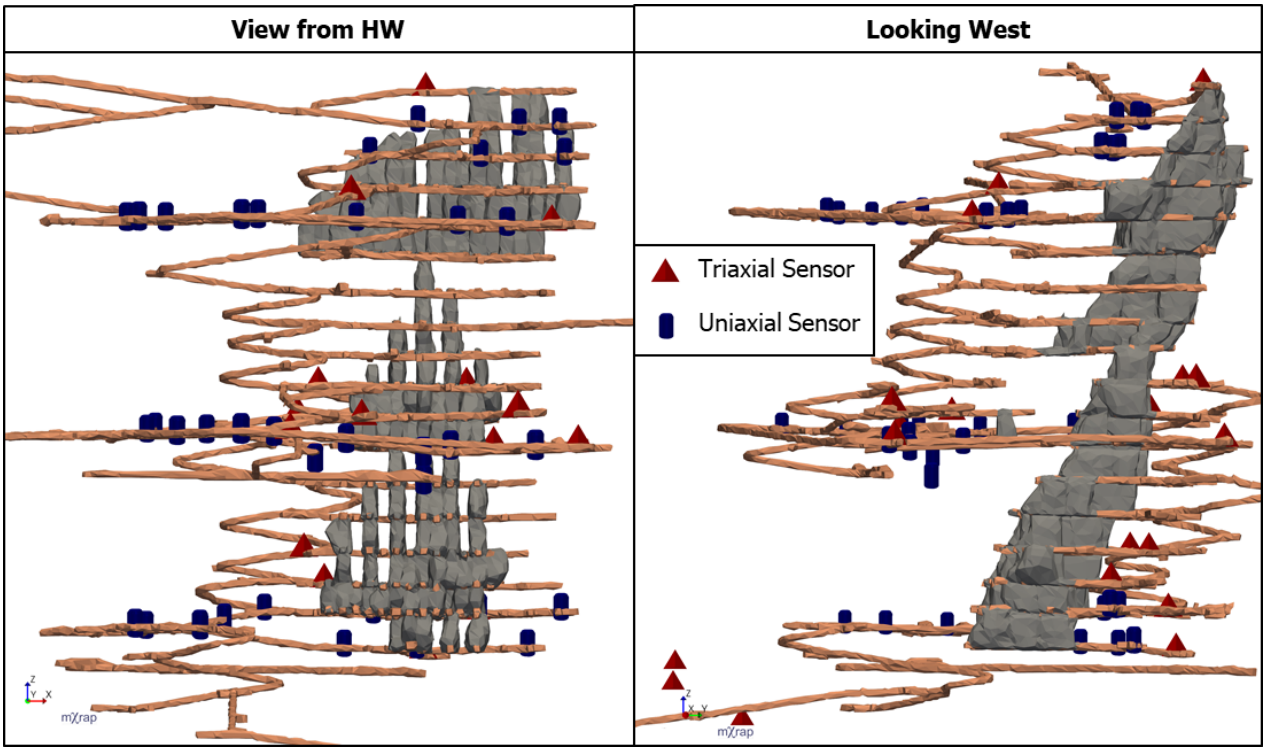

Figure 45 Nickel Rim South Sensor Array

As of late 2017, NRS had an array of forty uniaxial accelerometers, eighteen 15 Hz triaxial geophones and two 4.5 Hz triaxial geophones (Carusone, 2018). Figure 45 shows good 3D sensor coverage of the main mining area, with uniaxial and triaxial sensors in both abutments and in the HW and FW.

3.4.2 Location Accuracy

Location accuracy of seismicity is critical. A poorly located seismic event will result in unreliable source parameters.

Figure 46 shows a chart of cumulative location error for the seismic dataset at NRS.

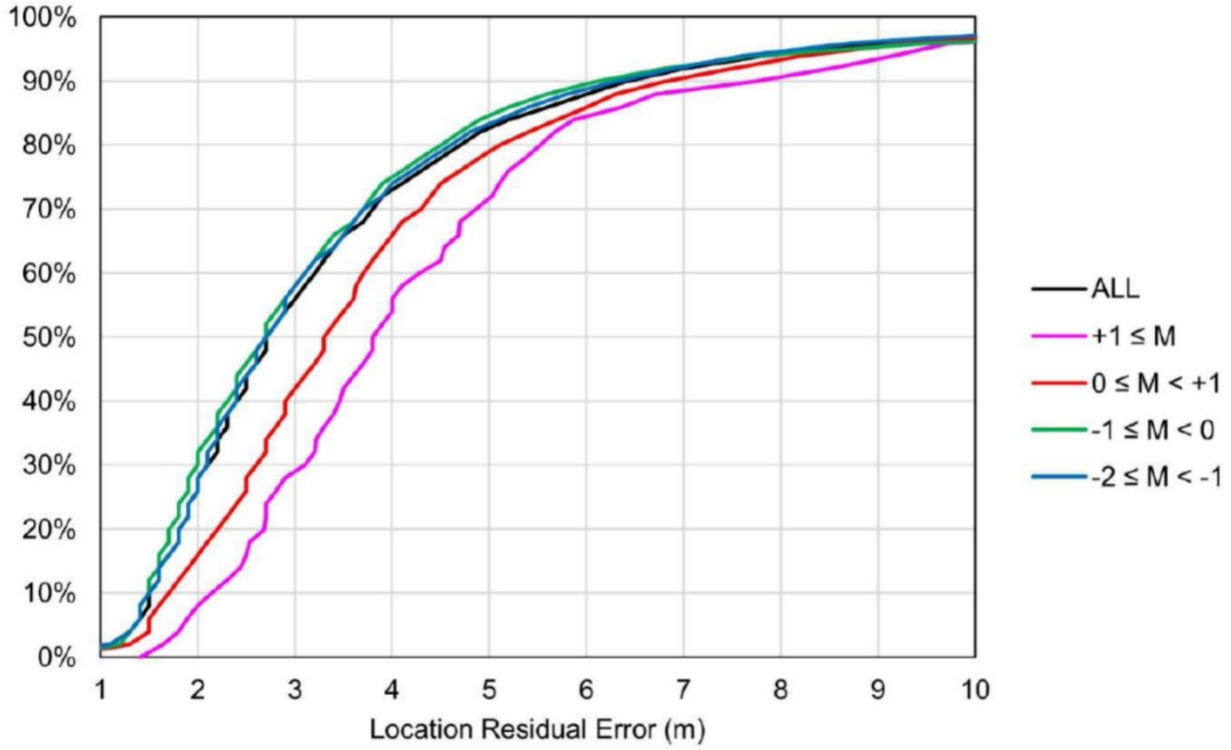

Figure 46 Cumulative distribution of location errors at per moment magnitude range at Nickel Rim South from 2011-2017 (Carusone, 2018)

A 2018 survey showed the median location error for Canadian seismic systems was generally 4-8m (see Figure 16) (Brown and Hudyma, 2018). Figure 46 shows that the median location residual error for NRS is approximately 2.7m, which suggests the NRS seismic system is among the best in Canada.

Events in Figure 46 are grouped by magnitude range, which shows that the larger events often have larger associated errors. The location of seismic events are represented by points in space, when in reality the source of a seismic wave is a fracture or shear with a 3D shape. Larger magnitude seismic events can have larger source regions, therefore the inherent error with the assumption of a point source increases.

3.4.3 Seismic Response to Mining

In the last decade of mining at NRS, hundreds of thousands of seismic events have been recorded. Figure 47 shows a Magnitude-Time graph of Mw ≥ 0.0 events from the onset of production to late 2020.

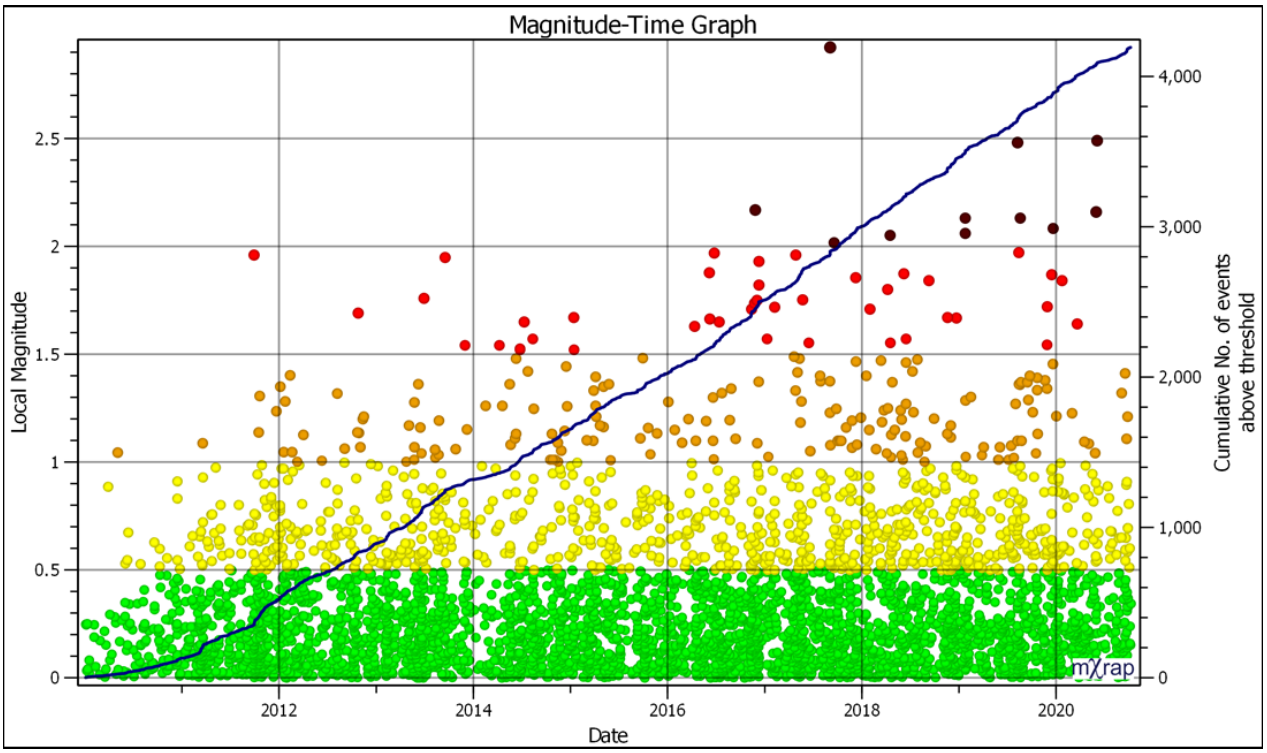

Figure 47 Magnitude Time History chart for all Mw ≥ 0.0 events at Nickel Rim South mine 2010 to late 2020

Though the term "local magnitude" generally refers to Richter Magnitude in earthquake seismology, mine sites commonly use the same term to refer to the magnitude scale local to the mine site. The NRS local magnitude (ML) is actually a true moment magnitude, calculated using seismic moment. In reference to magnitude at NRS, ML and Mw will be used interchangeably, both meaning moment magnitude.

There is a gradual increase in event rate 2010-2012, coinciding with establishment of the three stoping sequences. After 2012, the long term event rate is stable, with several short increases or decreases.

Over the duration of mining, the frequency of large events (Mw ≥ 2.0) increases. Beginning in 2011, M_{max}, which is the largest recorded event, increases 4 times. There are two unusually large increases in M_{max}: the first in late 2011 and the second in late 2017.

3.5 Summary

NRS is located on the eastern side of the Sudbury basin in the Archean Superior Province of the Canadian Shield. The HW and FW of the orebody are strong, competent norite and gneiss with softer ore. The orebody is intersected by 3 brittle fault sets. The principal stress direction is sub-horizontal at a slight angle to the strike of the orebody.

The mine utilizes blasthole open stoping with hydraulic backfill. The dominant sequence is bottom up, primary-secondary mining in a chevron shape with 2 sill pillars.

Like many mines in the Sudbury basin, NRS experiences seismic activity. NRS has a high quality seismic system with good coverage of the mining area. Location error is low. Several large magnitude events have taken place at NRS.

4 Back Analysis of a Mine Scale Event at Nickel Rim South

This chapter will describe a back analysis of the largest magnitude event recorded to date at NRS. The background section gives a description of known factors and identifies several areas where understanding can be improved. A novel tool, Time Distance Analysis, is proposed to help understand factors that lead to the occurrence of the event. Guidelines are presented to use the tool, including spatial, temporal and magnitude filtering. Results and insights into the failure mechanism of the large event are presented.

4.1 MSE Background

4.1.1 MSE Source Parameters

On 2017-09-03 at 12:12:00 a Mn 3.2 occurred at NRS in the HW of 1355L. The event source parameters are given in Table 5.

Table 5 Event Source Parameters

MN [GSC]	Mw [Mine]	Seismic Moment [Nm]	Total Radiated Energy [J]	Apparent Stress [MPa]	Residual [m]	Es:Ep	Source Radius [m]
3.2	2.9	2.4E+13	9.9E+07	0.14	3.3	31	150

Event magnitudes were recorded by the mine seismic system, the Sudbury Regional Seismic System (SRSN) and the Geological Survey of Canada (GSC). Different magnitude scales were used for each system, but have agreement that the event was the largest recorded to date at NRS. The residual error of the event location is low, indicating a good degree of confidence in event location. The ratio of S:P energy is high, indicating the event was likely shear related. The large magnitude and high S:P are both characteristics of fault slip. The estimate for source radius indicated a large spatial area was deformed during the event, possibly involving an area on the scale of a large part of the mine.

Because of the very large magnitude of the event, it will be referred to as a mine scale event (MSE).

4.1.2 MSE Location

The event located close to a mapped, North-south trending fault. The latest nearest stope blast was 18 hours prior to the event, two levels below the MSE hypocenter. Figure 48 to Figure 51 show visualizations of events in 3 time periods around the MSE:

1) Figure 48: Events occurring in a 4-day time span prior to the blast
2) Figure 49: Events occurring between the blast and the MSE
3) Figure 50 - Figure 51: Events occurring in a 4-day time span after the MSE

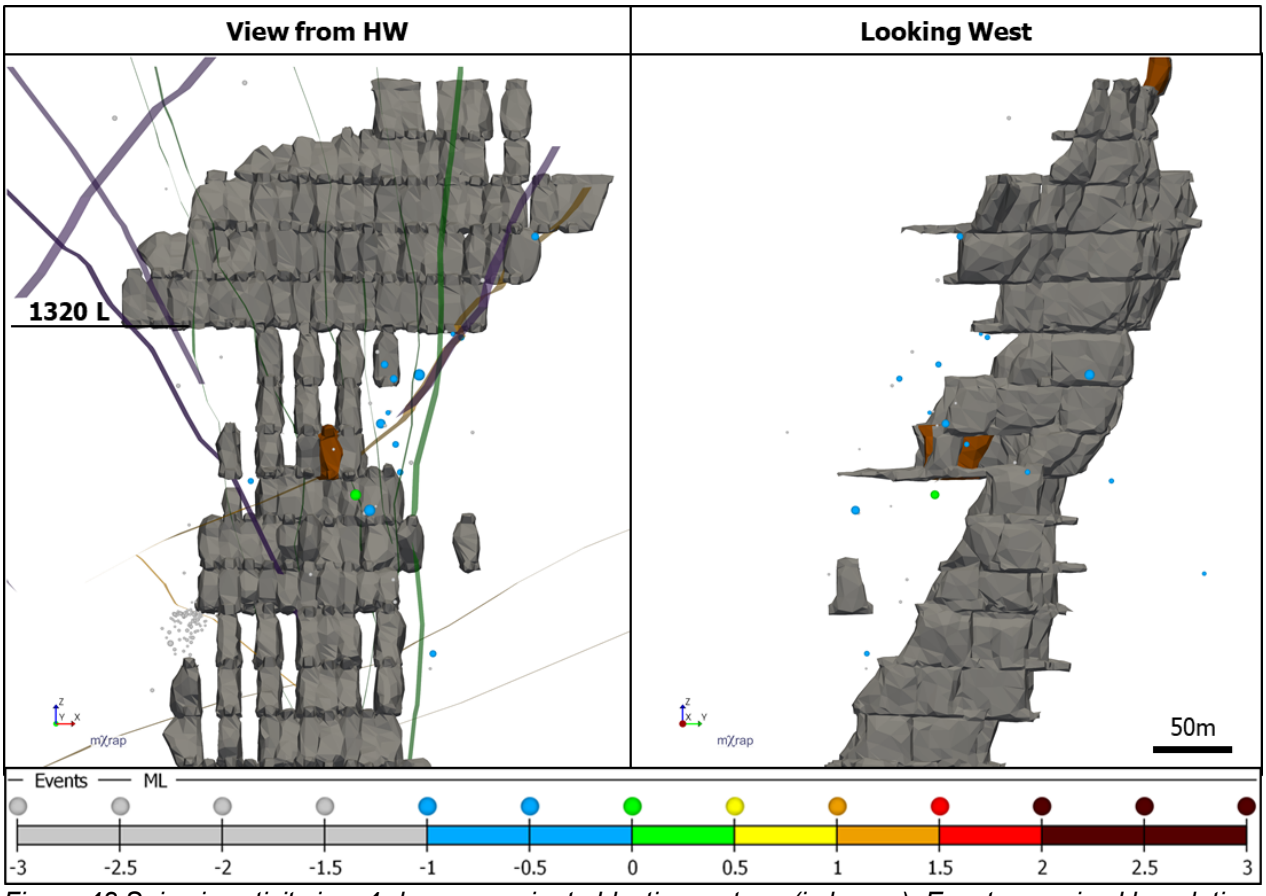

Figure 48 Seismic activity in a 4-day span prior to blasting a stope (in brown). Events are sized by relative source radius.

Significant primary mining had been completed in the 1320L sill pillar prior to the MSE. Mining activities were ongoing in a secondary HW stope, which was bordered by fill to the east and west, below, and to the FW. Visualization of seismic events shows seismic activity in the East abutment of the 1320 sill region. Events somewhat align with vertical and obliquely oriented faults in the abutment.

Figure 49 shows seismic activity between the stope blast (in brown) and the MSE.

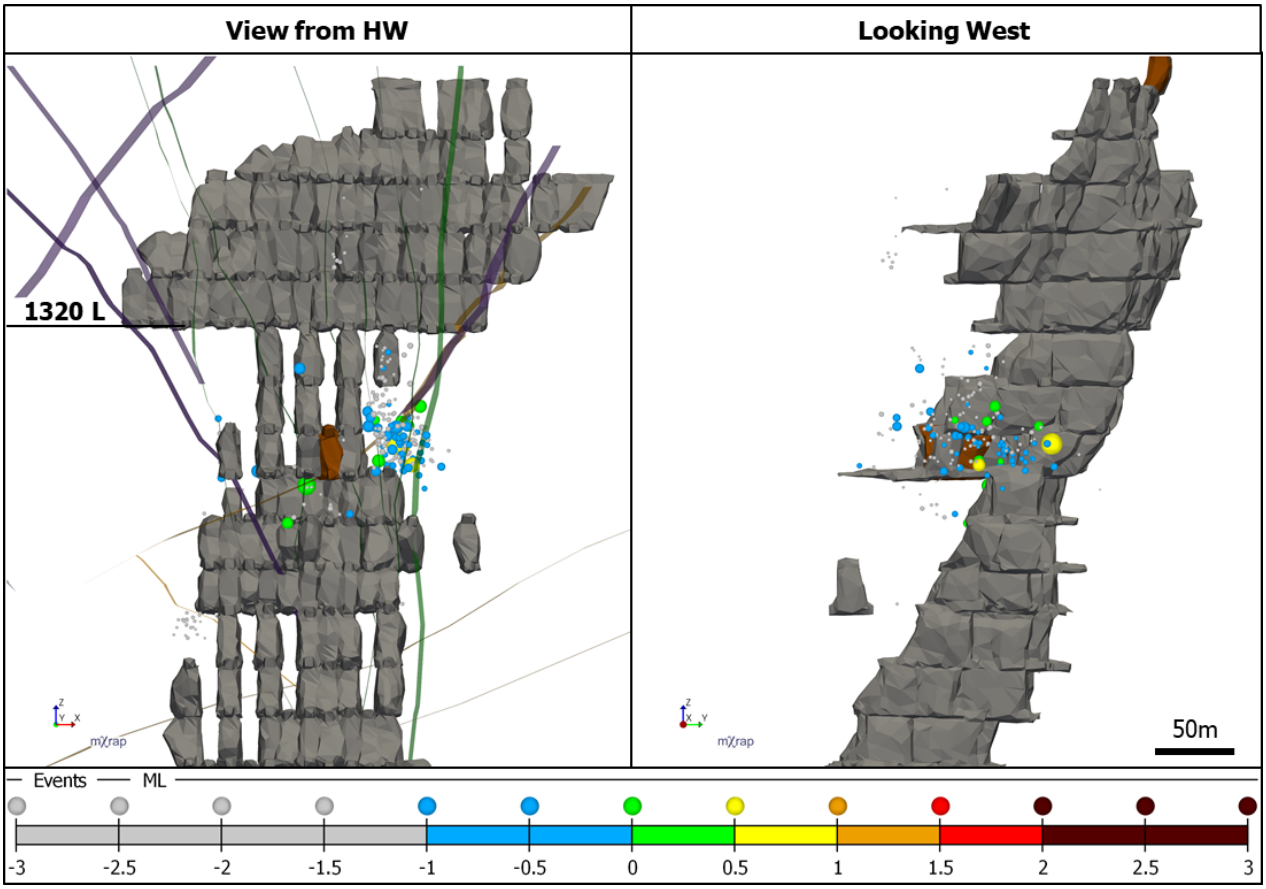

Figure 49 Seismic activity in the 18 hour span between the stope blast (in brown) and the MSE. Events are sized by relative source radius.

After the stope blast, the number of seismic events drastically increased, strongly clustering in the East abutment. Plausible event mechanisms for this cluster are fault slip and abutment stress fracturing.

Figure 50 shows a sequence of events that began with the MSE and continued at a higher than normal event rate for several days.

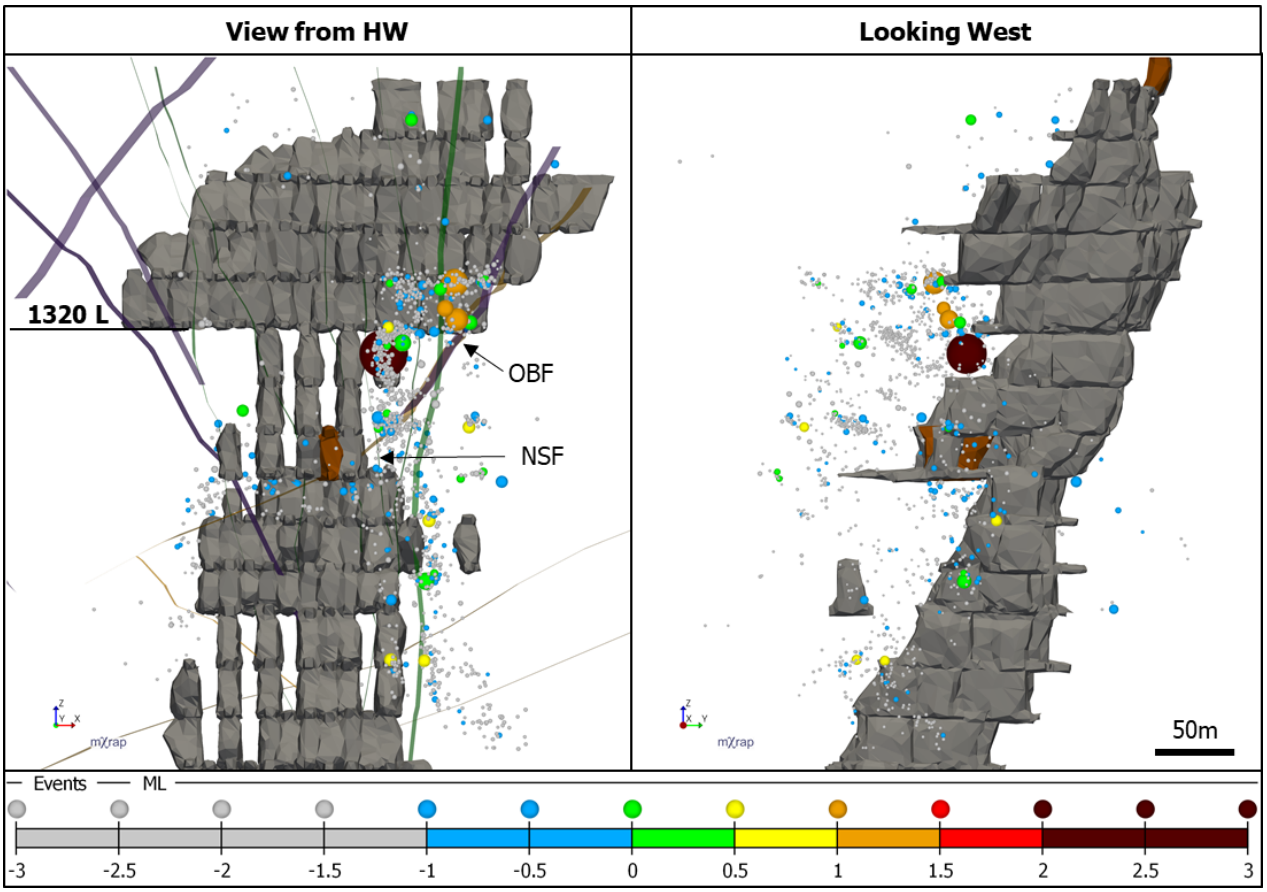

Figure 50 Seismic activity including the MSE and the 4 days following. Events are sized by relative source radius. Abbreviations: OBF – Oblique fault, NSF – North-south fault.

The MSE locates at the top of the 1320 sill in the HW of 1355L, 9m from a sub-vertical, north-south trending fault (NSF). Smaller aftershocks located near three sub vertical faults over 200-300m vertical distance. The largest aftershocks are Mw 1-1.5 that locate close to the northeast-southwest oriented fault (OBF).

The proximity of the recent blast and the increase in seismic activity afterwards would seem to indicate that the blast may have been a contributing factor to the occurrence of the MSE. The stope blast, however, was surrounded by backfill on 4 sides, though only partially on the east side. Backfill is much softer than the surrounding rock and does not transmit any significant

stress, therefore blasting a stope surrounded by backfill usually results in less of a regional stress change than blasting a stope surrounded by intact rock.

The theoretical source radius (150m) (from Table 5) of the MSE and the spatial extent of the aftershocks indicate that it was an event on the scale of a large part of the mine. The MSE locates nearby a sill pillar, which is important considering that sill pillars can result in high stress conditions and elevated rockburst risk (Simser, 2019). A sill pillar resists HW-FW closure and gives stiffness to the loading system. The system stores strain energy while the sill pillar is intact, and releases strain energy while it yields or is being mined. This storage and release of strain energy occurs on the scale of a significant part of the mining sequence and can contribute to large seismic events. The MSE and the largest aftershocks are concentrated near the sill. It is a logical assumption that the ongoing strain energy release during sill mining contributed to the size of the MSE.

Figure 51 shows a plan view of 1355L, the MSE and seismic activity for following 4 days.

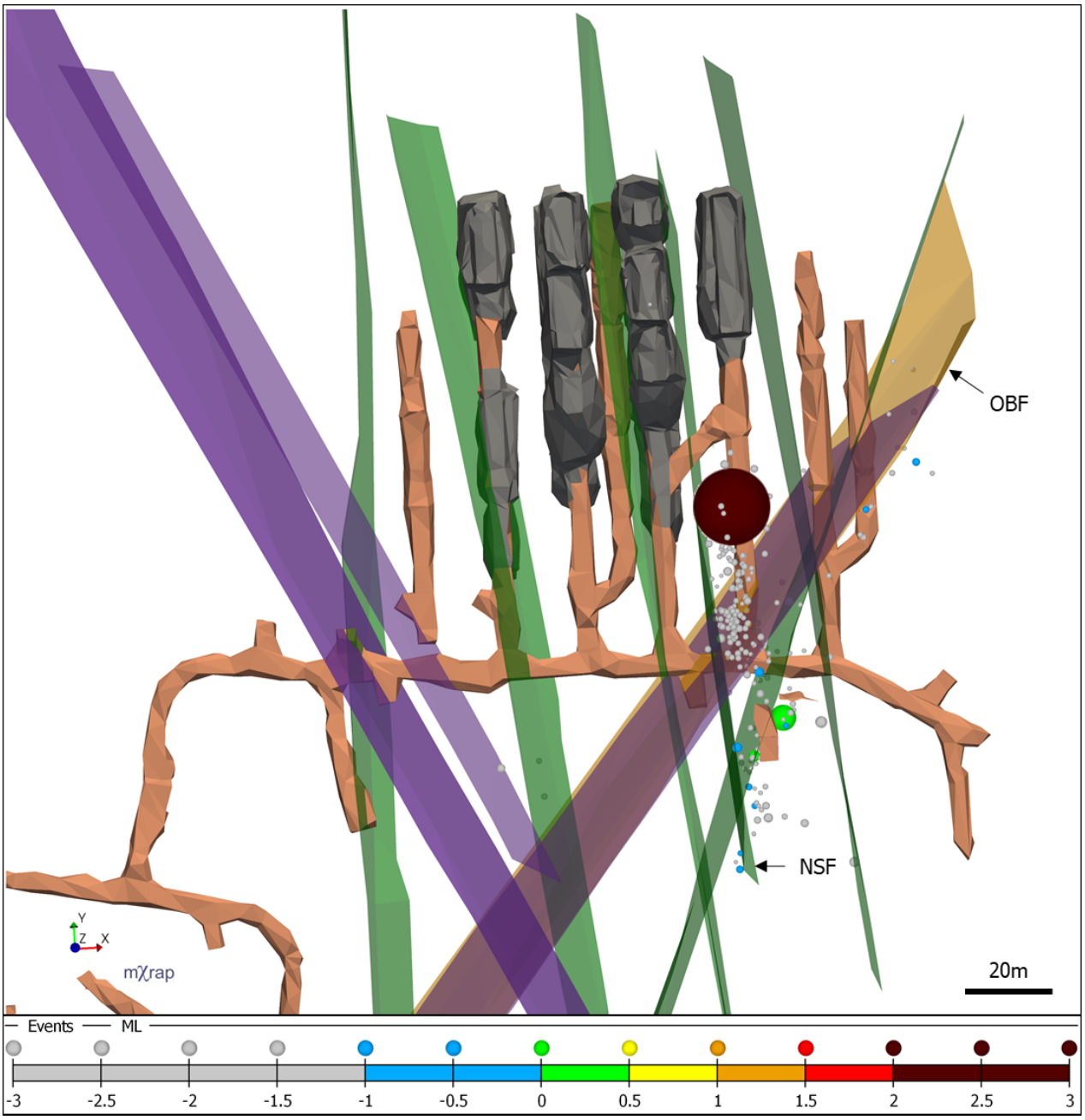

Figure 51 Plan view of 1355L. Faults, excavations and events are clipped at a 20m width above and below 1355L.

From Figure 50 and Figure 51 it can be observed that the MSE and many small aftershocks are proximal to the NSF. The MSE located 9m east of the NSF. The dominant cluster of aftershocks has a planar shape that aligns well with the NSF. Some aftershocks, however, have alignment

with the obliquely oriented structure (OBF) suggesting that this fault was also affected by the MSE.

The location of the MSE and extensive aftershocks on the NSF, the high S:P and the large magnitude are evidence that the source mechanism was fault slip on the NSF. An argument could be made for fault slip on the OBF, however, the MSE located 25m away from the OBF, more than twice as far as the distance from the NSF. The spatial extent of aftershocks was also much larger on the NSF (~280m) than the OBF (~110m), which is consistent with a greater spatial readjustment occurring on the main fault to slip. The three largest aftershocks located on the OBF, which is consistent with secondary triggering of OBF shear slip from stress redistribution. It is not conclusive which fault actually slipped during the MSE, but the evidence seems to be greater for the NSF than the OBF.

Eight primary stopes had been mined on 1355L prior to the occurrence of the MSE. These stopes were extracted from the core of the 1320 sill pillar and would likely have induced a large change in the principal stress orientation near the sill pillar. The NSF had stopes blasted on both sides (East and West), likely daylighting a significant strike length and causing significant stress change on the fault. It seems logical that the timing of a large event is most probable when mining related stress change is the greatest. In this case, the MSE occurred after a blast in a stress shadowed stope two levels below (60m) the hypocenter.

4.1.3 MSE Timing

Figure 52 shows a short term Magnitude-Time graph for a three day time window around the MSE.

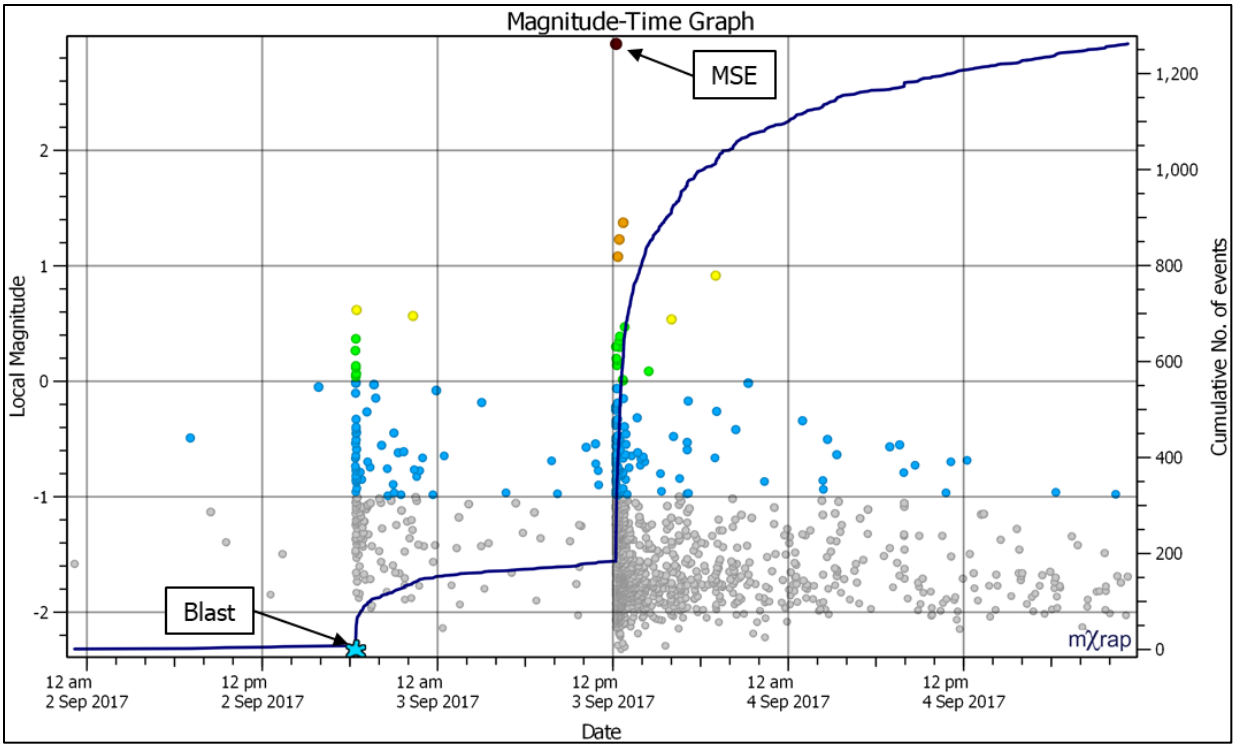

Figure 52 Magnitude-Time History of three days of activity surrounding MSE

There is an increase in the rate of seismicity between the blast and the MSE. Figure 49 showed that these events were located near to the eventual MSE hypocenter, suggesting the blast may have triggered the eventual failure 18 hours later.

A large number of aftershocks followed the MSE, including three events Mw 1.0-2.0 that occurred within the subsequent half hour.

It was assumed that converging mining fronts in the 1320 sill may have contributed to the large magnitude of the MSE. In order to analyze the seismic response to sill blasting, a volumetric filter around the sill pillar, shown in Figure 53, was created.

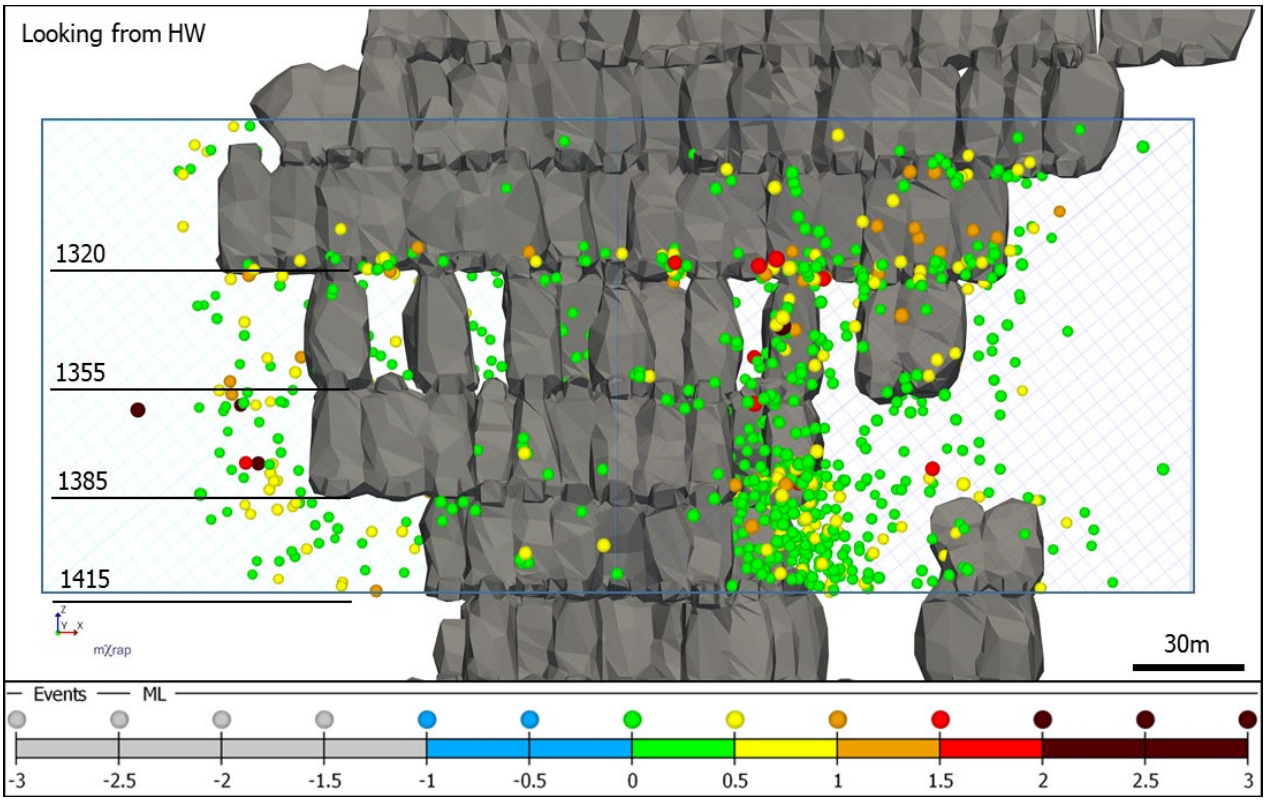

Figure 53 Events Mw ≥ 0.0 occurring in the 1320 sill from 2010-2021

Figure 53 shows large events occurring in the 1320 sill for the entire recorded dataset, which is concurrent with a large part of the sill extraction. Blasts on 1355, 1385 and 1415 levels will be called “sill blasts”.

In order to analyze the timing of changes in the rate of seismicity, the occurrence of large events and the influence of blasting, a Magnitude-Time graph was created for the sill pillar mining period, shown in Figure 54.

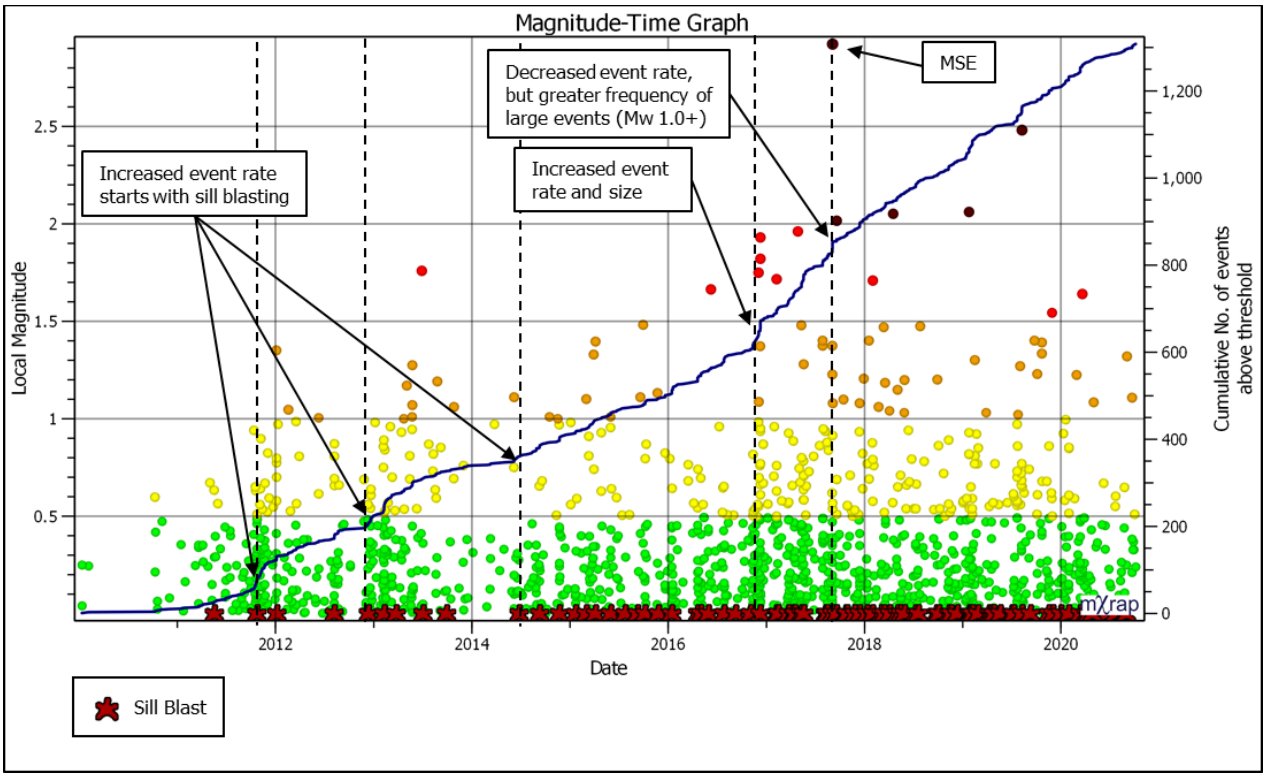

Figure 54 Magnitude-time history of sill events Mw ≥ 0.0.

Blasting is linked to the event rate in the sill, shown by the rate increasing with blasting in late 2011, 2012 and mid-2014. After mid-2014, sill blasting occurs on a fairly routine basis. In late 2016, there is a sharp increase in event rate and the frequency of events Mw ≥ 0.5 that continues until the MSE occurs in late 2017. This change in large event rate is not explainable by an increase in blast frequency. The MSE is an order of magnitude larger than any other previously occurring event. After the MSE occurs in late 2017, the event rate slightly decreases, but events Mw ≥ 1.0 become noticeably more frequent, possibly indicating a change in behavior of sill pillar yield.

4.1.4 MSE Damage

Examination of the damage locations associated with the large event revealed further insights into the mechanism. Figure 55 shows a mapped visualization of 22 damage locations associated with the MSE.

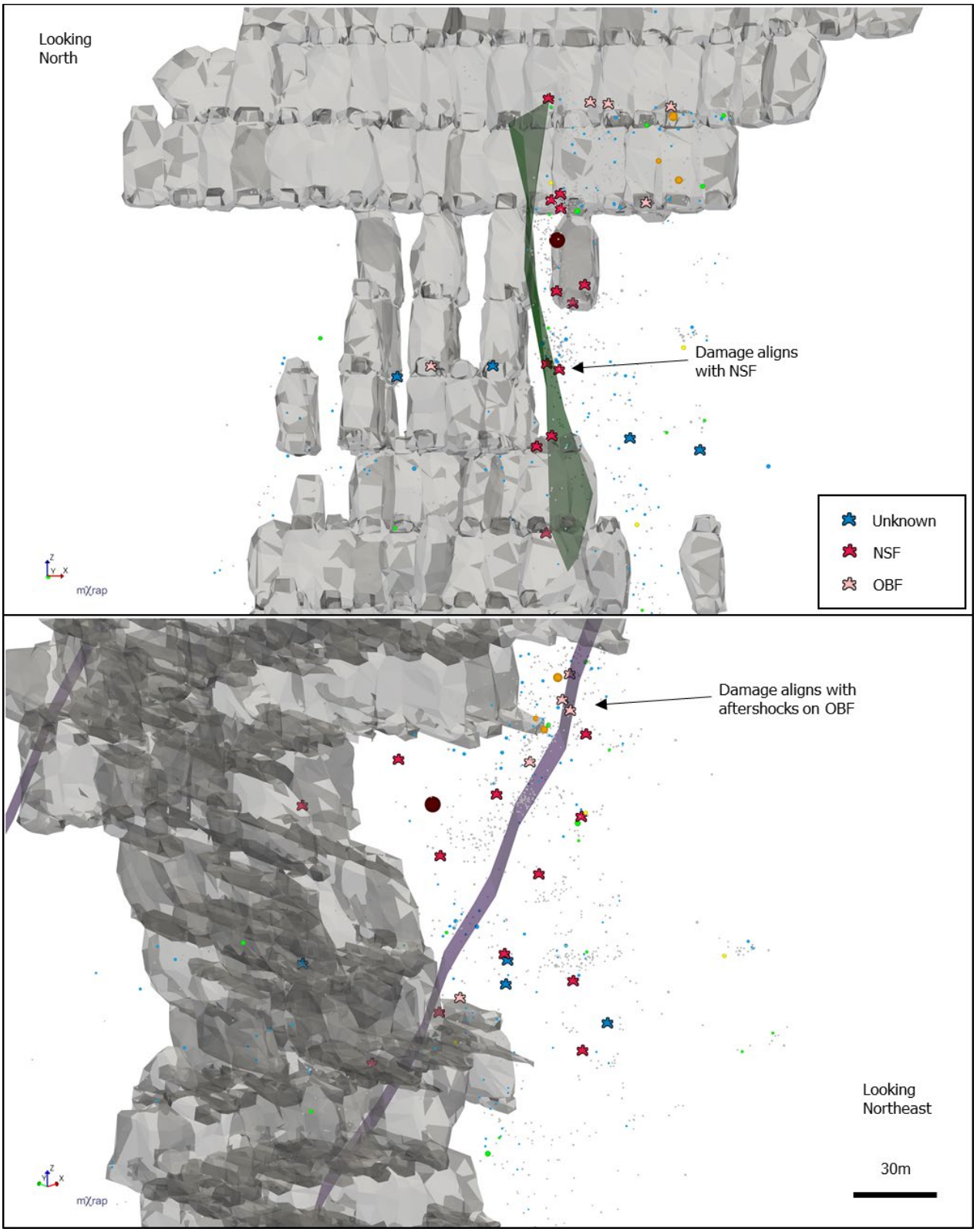

Figure 55 Locations of damage associated with MSE. The top figure looks down strike of the NSF and the bottom figure looks down strike of the OBF.

The locations of damage to development are marked by stars. Damage locations are categorized by proximity to the NSF and the OBF, with those within 20m of the NSF marked as red stars, those within 20m of the OBF by pink stars, and those that are at further distances by blue stars.

Twelve damage locations were within 20m of the NSF over a spatial extent of 190m. Five damage locations were within 20m of the OBF over a spatial extent of 130m. Four damage locations were poorly related to fault locations. The large spatial extent of rock damage and close relation to faults tends to agree with a fault slip mechanism taking place on a large part of the mine. The NSF is again a better candidate than the OBF as the source of the main shock, since damage locations indicate a larger spatial extent of fault deformation on the NSF than the OBF.

4.1.5 Need for Further Analyses

The high magnitude, the high S:P, the location of the MSE and the locations of aftershocks and damage presumably indicate that the MSE was fault slip on the NSF. The location of the MSE in the 1320 sill is evidence that stored strain energy in the sill pillar system may have contributed to the energy release during the large event.

However, several characteristics of the MSE are still poorly understood:

1) The MSE was triggered by a secondary blast that had backfill on 4 sides. The blast should have been almost entirely stress shadowed. Several primary stopes had already been mined that likely induced a greater regional stress change in the sill area, yet the MSE occurred after a relatively low stress change blast. This suggests that blast induced stress change was unlikely to be the primary cause of the MSE and poorly understood geologic factors may have had significant influence on the timing of the MSE.

2) The MSE was an order of magnitude larger than any previously occurring event in the 1320 sill volume. The MSE was the largest event in a sequence of large events in the sill. The significance of the large magnitude of the MSE is unknown.

3) Prior to the MSE, there was a yearlong increase in the magnitude and frequency of events in the sill. The contribution of this precursory trend to the eventual failure is not understood.

4) After the MSE, the total event rate decreased but large events became more frequent. The relation between the MSE and this change in the characteristic of sill seismicity is not understood.

Further investigation is warranted.

4.2 Time Distance Analysis

4.2.1 Conceptual Asperity Model

Aki (1984) suggested that some fault slip events occur due to rupture of strong areas, or asperities on faults. An asperity is essentially defined as an area on a fault that is stronger or more resistant to deformation than weaker, less resistant surrounding areas. Observations from South African mining by Van Aswegen and Mendecki (1993) suggested asperity rupture can be preceded by a period of softening behavior. Strain softening describes deteriorating strength of a loaded element with increased strain, in this case applied to deterioration of the strength of a fault. Figure 56 conceptually illustrates how the softening asperity behavior could lead to a large fault slip event.

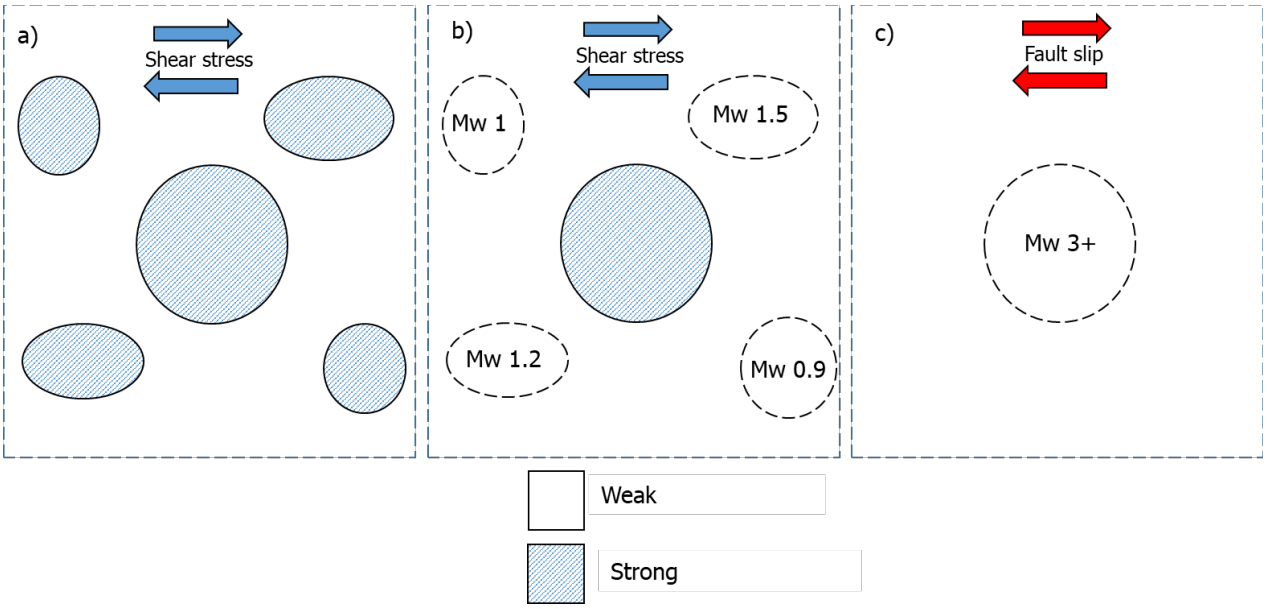

Figure 56 Conceptual illustration of progressive asperity behavior on a fault plane leading to a large event.

a) Fault is stable and stressed. Strength is heterogeneous and several strong asperities resist movement.

b) Some asperities deteriorate and weaken. Some of the deterioration is manifested in seismicity that concentrates around final asperity. The final asperity is subjected to higher shear stress and approaches failure.

c) The final asperity ruptures, generating a large magnitude fault slip event.

If Figure 56 is a valid mechanism for the MSE, then weakening of nearby asperities prior to the MSE should be manifested in seismicity. The eventual source area of the MSE, as the strongest area in the system should anomalously attract stress. Seismicity may spatially and temporally locate around the eventual hypocenter of the MSE as part of an asperity deterioration process. The MSE, as the largest event in the sequence, should effectively represent rupture of the asperity, and unloading of the source region. Continued deformation may be manifested in an increased seismic activity rate elsewhere.

4.2.2 *Time Distance Analysis*

A simple tool, called Time Distance Analysis (TDA) is proposed to investigate the relation between the MSE and other seismic events. Each seismic event has a date and location of occurrence. TDA plots a time history of distance from the hypocenter of a large event to other events of interest. Distance between points with Cartesian coordinates is given by [9].

$$d = [(x_1 - x_2)^2 + (y_1 - y_2)^2 + (z_1 - z_2)^2]^{1/2} \quad [9]$$

Where,

d = distance (m)

(x_1, y_1, z_1) = coordinates of MSE hypocenter

(x_2, y_2, z_2) = coordinates of other events or blasts

Visualization of [9] is illustrated in Figure 57.

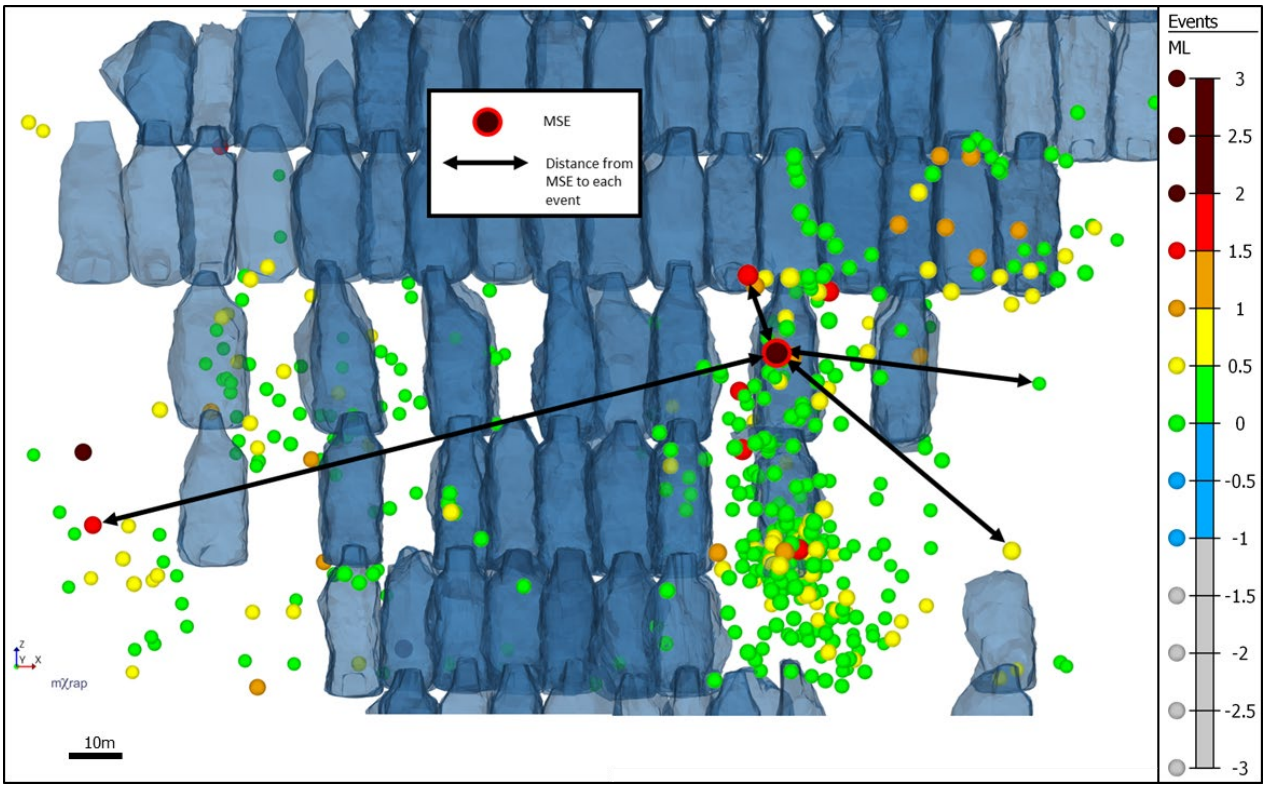

Figure 57 Time Distance Analysis tracks distance from the hypocenter of a large event to locations of other events. Several examples of distances are illustrated by black arrows.

Figure 57 shows locations, distances and magnitudes of seismic events in the 1320 sill. The resultant TDA chart is illustrated in Figure 58.

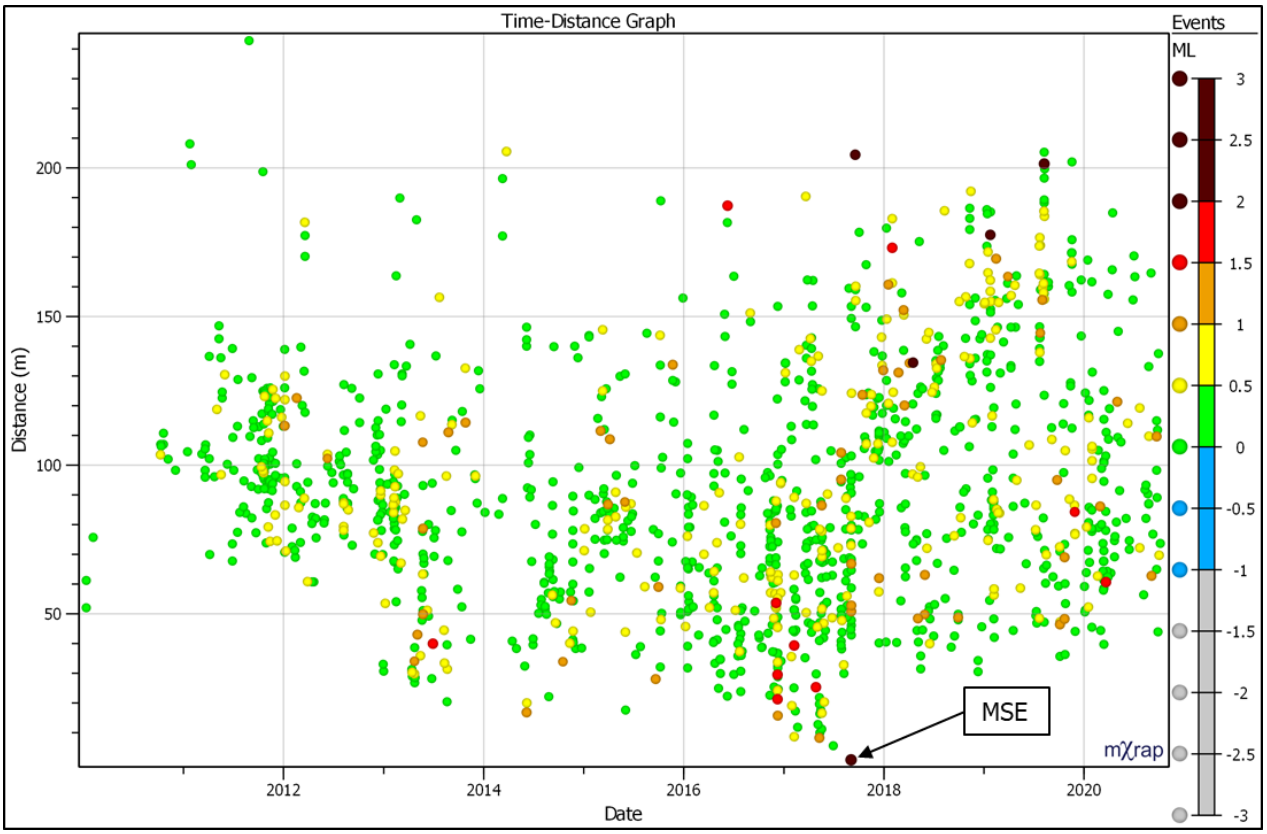

Figure 58 TDA showing the MSE on the horizontal axis in late 2017 and distance to all Mw ≥ 0.0 events in the 1320 sill

Figure 58 shows several interesting trends around the MSE. Beginning in 2016, there is a pattern of seismicity migrating towards the MSE hypocenter including a sequence of large (Mw ≥ 1.5) events. This sequence of events ends with the MSE, suggesting it may be part of the same failure process.

Prior to the MSE, 36 events occurred within 30m of the eventual MSE location. There is a distinct absence of seismicity within 30m of the MSE for the 3 years following the MSE.

Between 40-100m there is a decrease in event occurrence after the MSE. This area begins to become more active again in late 2019.

There is a change in the patterns of seismicity at a significant distance from the MSE. Beyond 100m, there is an increase in the occurrence of Mw ≥ 1.0 events in the time after the MSE. This may suggest a shedding of stress to locations distant to the MSE hypocenter.

There are interesting trends in Figure 58 that will be explored further.

4.2.3 Time Distance Analysis and Blasting

The Magnitude-Time history chart in Figure 47 indicated that there was a link between sill blasting, the rate of seismicity and the occurrence of large events. Since the centroid of a blast can be approximated by a point, distance from the MSE to blasting can be calculated and added to a TDA chart in a similar manner as event distance. Figure 59 shows a TDA chart with blasts and the cumulative number of events.

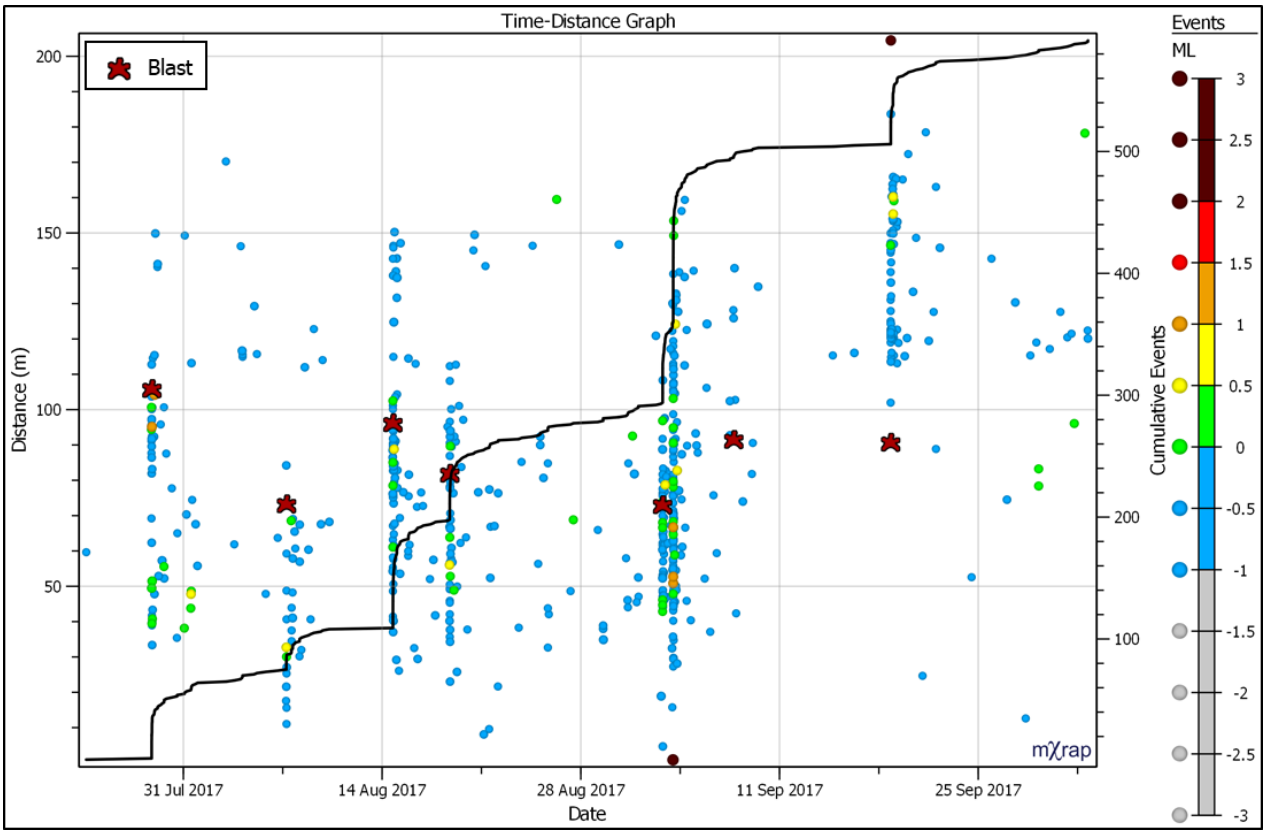

Figure 59 TDA for the sill showing stope blasts and event rate

The shape of the cumulative number of events line gives insight into the event rate (Hudyma, 2008).

- A step in the cumulative number of events signifies an intense period of seismicity, often occurring following blasts or very large events.

- A constant slope of the cumulative number of events line signifies a constant event rate.
- A near flat line signifies a very low event rate.

The addition of blasts and event rate to the TDA chart adds additional insights to the seismic response to mining and the behavior of seismicity around the MSE. Event clusters related to blasting can be observed. Blasting causes an increase in event rate which decreases with time after the blast. After the second last blast (Aug. 14, 2017) before the MSE, the event rate does not return to a quiescent state but continues to be more seismically active than normal. Prior to the MSE, blast related clustering tends to occur closer to the MSE location. After the MSE, blast related clustering occurs further from the MSE than the blast.

4.2.4 Unique Contribution

TDA is a novel contribution to the field of mine seismicity. TDA essentially simplifies a four dimensional (x, y, z, time) problem to two dimensions (distance, time), allowing improved recognition of relations between a MSE, clusters of seismicity and blasting. TDA increases recognition of trends from large spatial and temporal scales. Substantial information can be gained using this method. Application of the method and analyses of the results will be presented in the following sections.

4.3 Spatial, Temporal and Magnitude Filters

This section will describe the use of Time Distance Analysis to interpret seismicity around a MSE.

4.3.1 Analysis Scales

In the analysis of mining induced seismicity, a dataset must be filtered to provide focus and context. The NRS dataset contained of 700,000+ seismic events, ranging from Mw -2 to Mw 3. Not all events were relevant to the back analysis of the MSE and filtering was required to identify meaningful trends.

Three types of filters were used:

- Time
- Space
- Magnitude

Filtering reduces the amount of irrelevant data in analyses. Inadequate filtering can result in too much data to identify meaningful trends, however, if filters are too constraining, not enough data is left to show trends.

This study used similar time scales to those described by van Aswegen (2005):

- Long term analysis coincides with time of mining a sequence of stopes, in the order of several months or a few years.
- Medium term analysis coincides with a mine planning cycle, including several stope blasts over a month or a few months.
- Short term analysis refers to hours and days, including a single blast to a few blasts.

Three spatial scales were used:

- Large scale corresponds to the scale of a mining block, or a large part of the mine.
- Medium scale refers to a local mining area, such as a regional pillar or abutment.
- Small scale refers to a single seismic source, such as a fault, dyke, local pillar, etc.

Event numbers are greater at larger and longer analysis scales. A magnitude filter was used for each analysis scale in order to limit events to a number that would permit trends to be visible.

4.3.2 Temporal Filtering

Temporal filtering attempts to create bounds in time around the rockmass failure process. A MSE occurs in an instant, but potentially can be part of a longer term rockmass failure process. The

relevant time to study the rockmass failure process is dependent on the particular failure process. Long, medium and short term time scales were used for analyses, with the assumption that each time scale could possibly show different but relevant information.

Figure 60 shows a visualization of events and mining that occurred near the sill over a long term time period; the two years preceding the MSE.

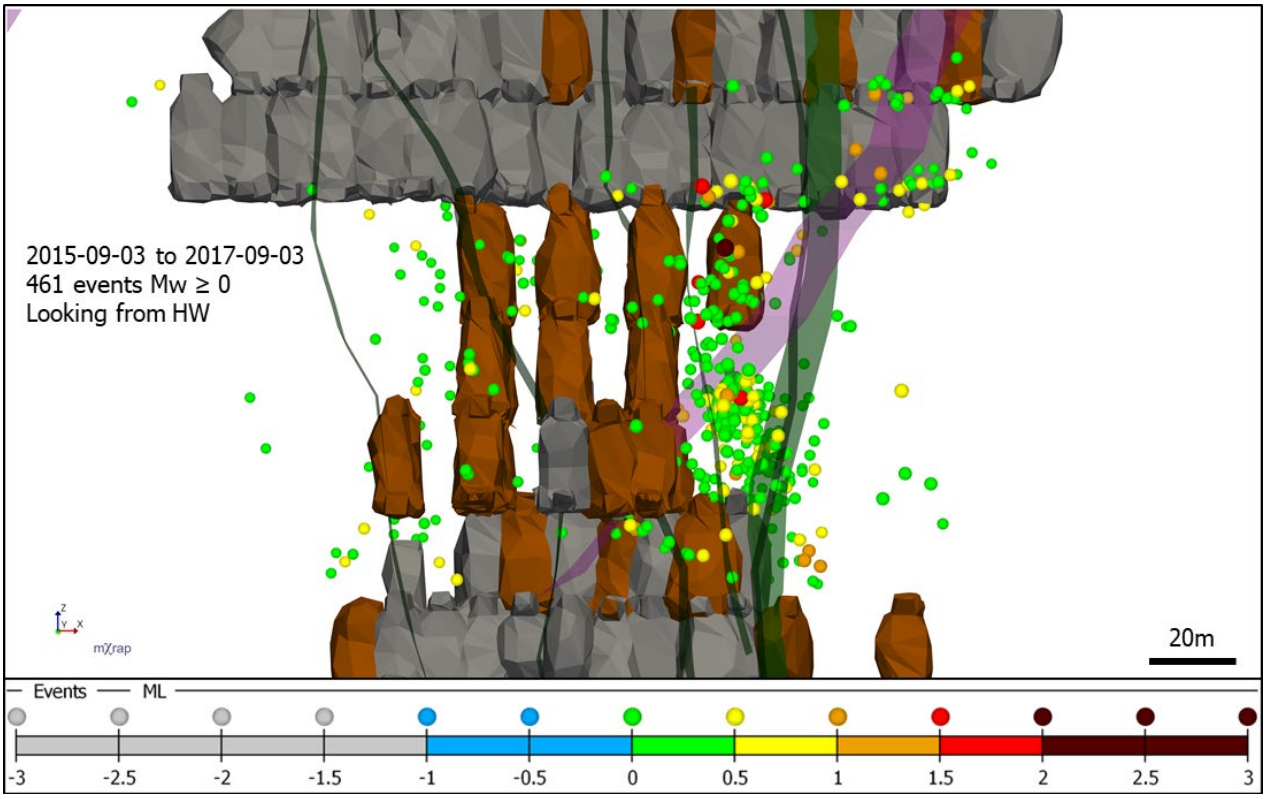

Figure 60 Long term analysis showing a significant part of a stope sequence being mined in the two years prior to the MSE. Stopes mined in this time period are coloured brown.

Long term analysis corresponded with a significant part of the sill sequence being extracted. Past studies have shown that events Mw < 0.0 tend to be related to mining processes, such as ore passes and development mining and are often unrelated to larger scale failure processes. Events Mw < 0.0 often comprise more than 90% of events recorded, obscuring the larger scale failure processes. Since small events were exceedingly numerous, a low magnitude filter of Mw ≥ 0.0 was used to show only the largest events and increase the clarity of the figure. Figure 60 shows

events and mining in a two year span prior to the MSE, during which the 1320 sill pillar was breached and mined to a 7 panel length on strike. It can be observed that while mining was somewhat symmetric, the majority of the large events were located in the East abutment. Several large East abutment events were located near faults, possibly indicating mining induced shear deformation on structure. In comparison, there was a notable absence of events on West abutment faults, possibly indicating stability. Secondary stopes lacked significant clusters of seismicity throughout the time period, indicative of yielded rock (Simser, 2019).

Figure 61 shows a medium term (a few months) visualization of mining and seismicity in the 1320 sill region, including events prior to and immediately after the MSE.

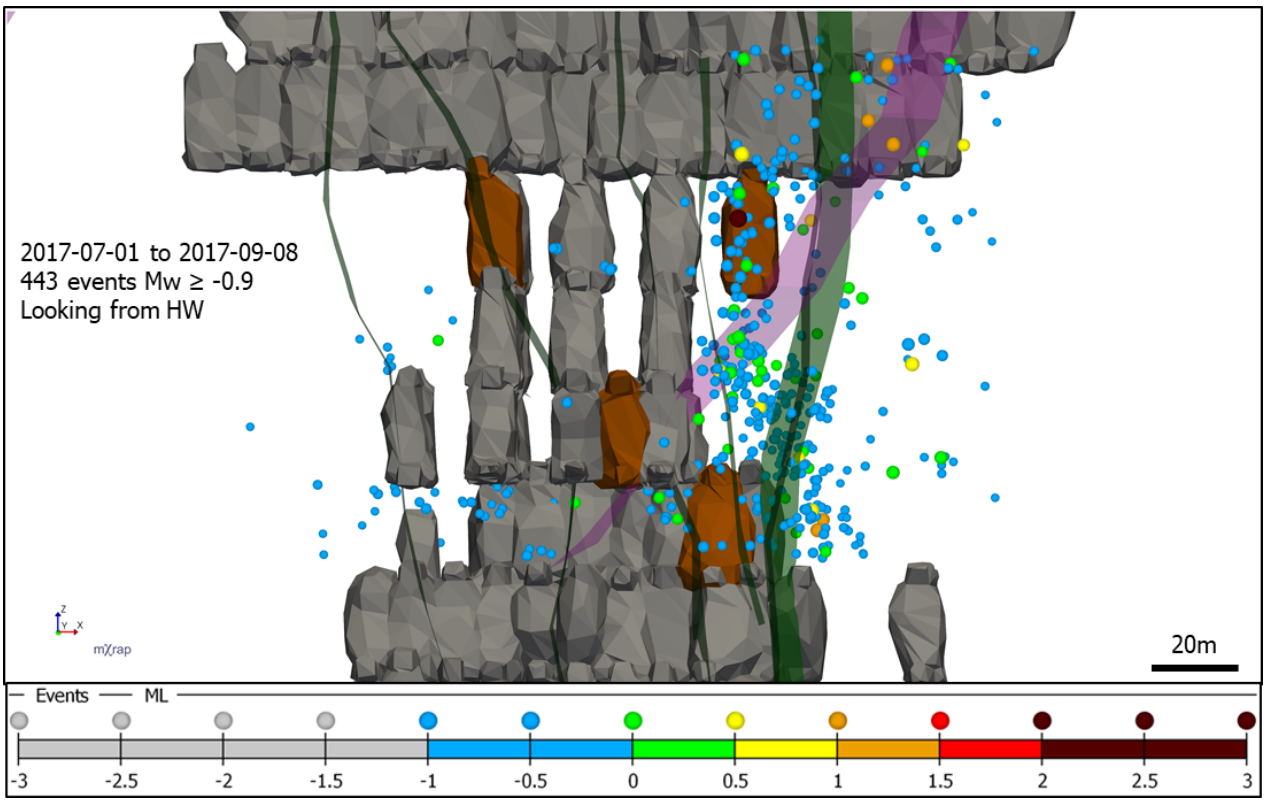

Figure 61 Medium term analysis showing several stopes mined over a period of 3 months prior to and including the MSE

Medium term analysis shows that several stopes were mined in the 3 month time period prior to the MSE. A lower magnitude filter than Figure 60 was needed to include sufficient data, to expose meaningful details.

Mining and seismicity were concentrated in the East abutment during the three month time period prior to the MSE. Locations of seismicity tended to align with structure close to East abutment blasting. The West abutment had low seismic activity during the medium term period, with only one event Mw ≥ 0.0.

Figure 62 shows a short term time period (1 week) centered on the MSE.

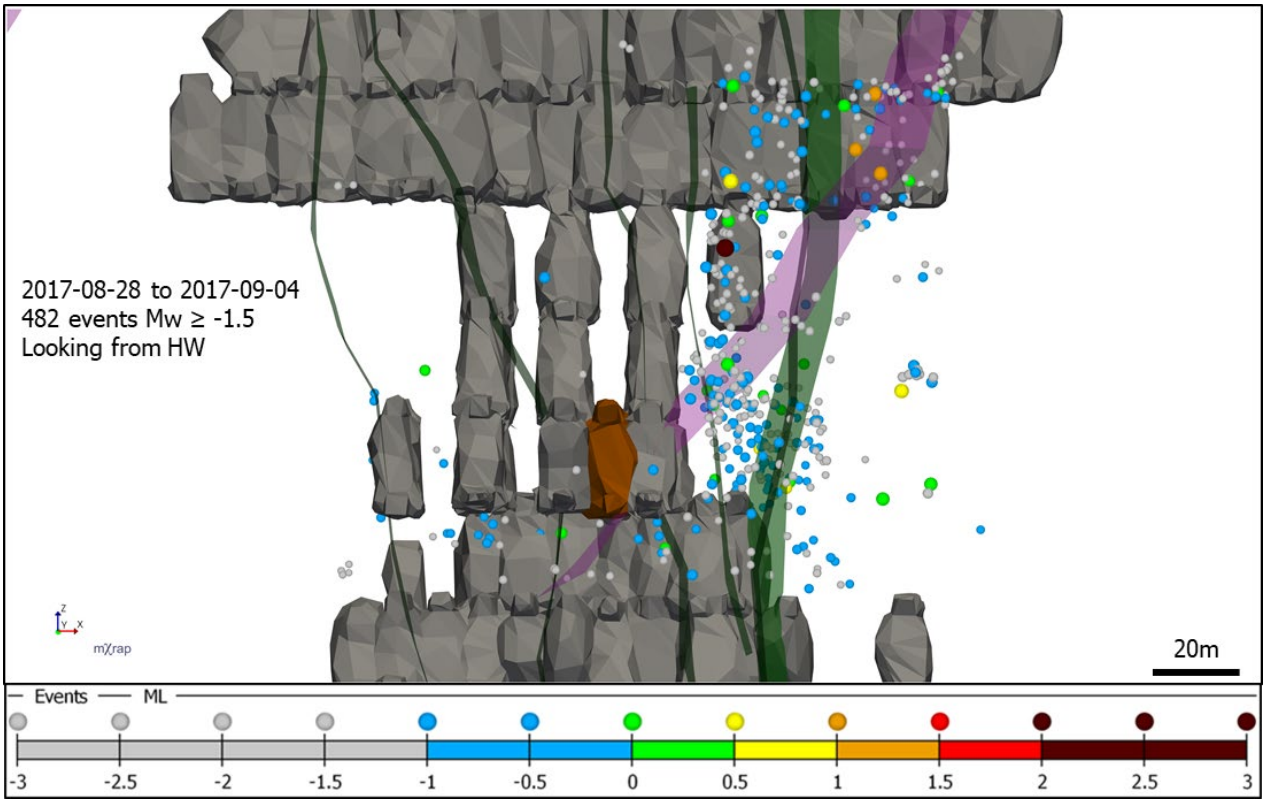

Figure 62 Short term analysis showing a single stope blast prior to the MSE

Less events occurred in the short term time period, making a smaller magnitude filter necessary to provide adequate data.

Short term analysis coincided with a single secondary stope blast in the sill. Seismic activity was concentrated in the East abutment rather than near the stope blast. Events near the MSE show

planar alignment, particularly events Mw ≥ 0.0. The secondary pillars were completely aseismic, likely indicating a yielded rockmass and low relative stress. East abutment event clusters had good agreement with longer term and larger magnitude clusters shown in Figure 60 and Figure 61.

4.3.3 Spatial Filtering

Spatial filtering attempts to place spatial bounds around rockmass failure processes relevant to the MSE. A MSE may potentially be part of a larger rockmass failure process. The spatial extent of changes in the rockmass that contributed to the MSE and was affected by it, is unknown. Multiple spatial analysis scales were necessary to ensure the analyses included relevant information.

Spatial filtering was necessary to limit the back analysis to relevant areas of the mine. No universal guideline exists to give proper spatial filtering around a MSE. Three sizes of spatial filters were selected to ensure relevant failure processes were captured. Figure 63 shows the three spatial filters used.

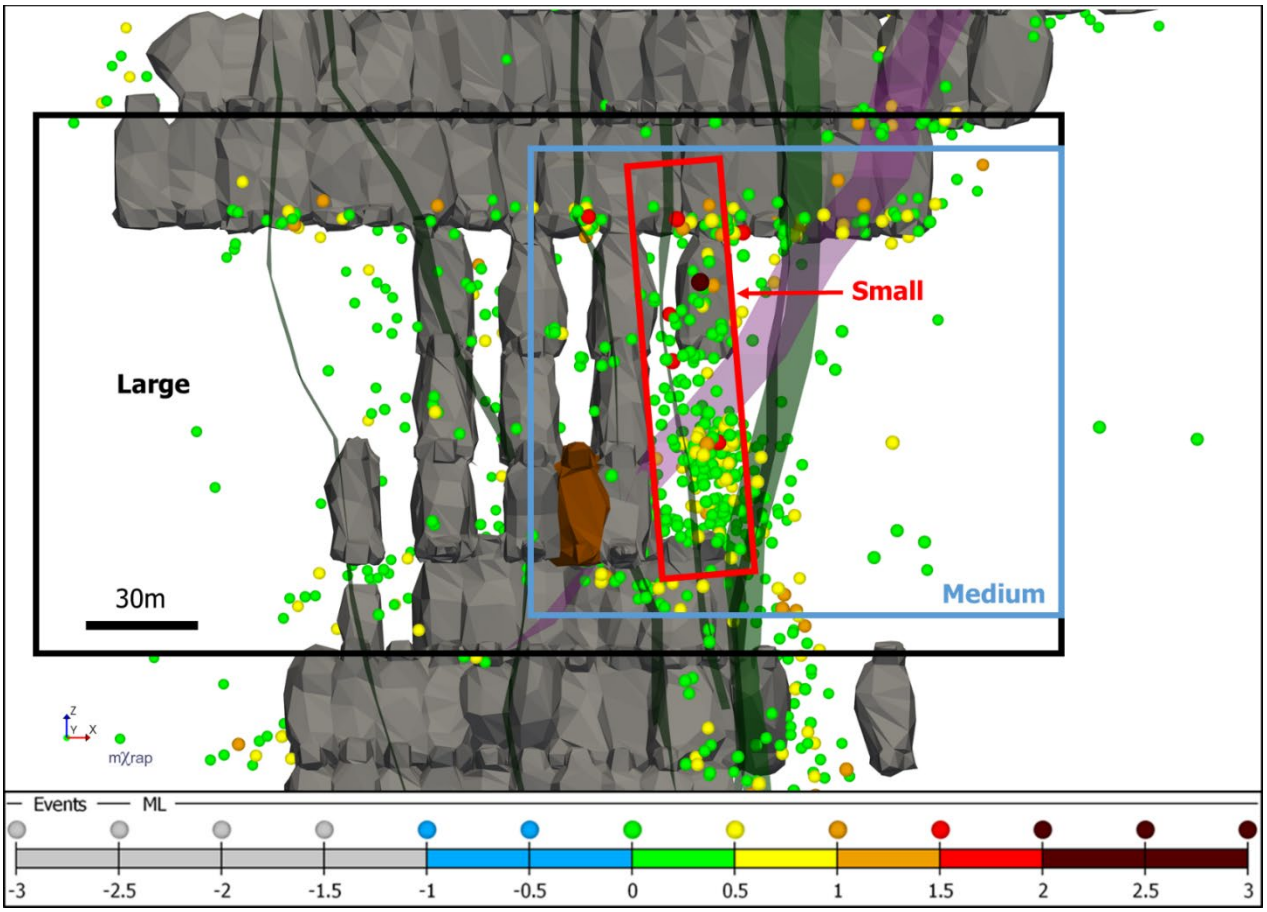

Figure 63 Volumetric filters used for analyses. Visualization shows events from 2012-01-01 to 2017-09-03. The stope blasted 18 hours prior to the MSE is coloured brown.

The large volume filter encompasses five mining levels in the region of the sill. The purpose of this volume was to analyze the rockmass response to the sill mining sequence which was ongoing at the time of the MSE. This volume includes both the East and West abutments, several secondary pillars and seven faults. One hundred and fifty five stopes were blasted in the large volume from 2010-2021.

The purpose of the medium volume was to analyze the response of only the East abutment of the sill region. At the time of the MSE, events Mw ≥ 0.0 were more numerous in the East abutment than the West abutment. The medium volume contained multiple faults, including the NSF and the OBF. Seventy-two stopes were blasted in the medium volume from 2010-2021.

The small volume was created around NSF, which was assumed to have slipped during the MSE. The purpose of the small volume was to exclusively analyze the response of the NSF leading up to and after the MSE. Effort was made to capture the majority of a population of seismic events that located close to the NSF. Seven stopes were blasted in the small volume from 2010-2021.

4.3.4 Magnitude Filtering

The total event number was controlled by spatial, temporal and magnitude filters. Temporal and spatial analysis scales were selected in previous sections. The purpose of this section was to show how additional magnitude filtering was necessary for TDA to show meaningful trends. Figure 64 shows a long term large volume TDA chart for the MSE without magnitude filtering, resulting in more than 200,000 events in the filtered volume.

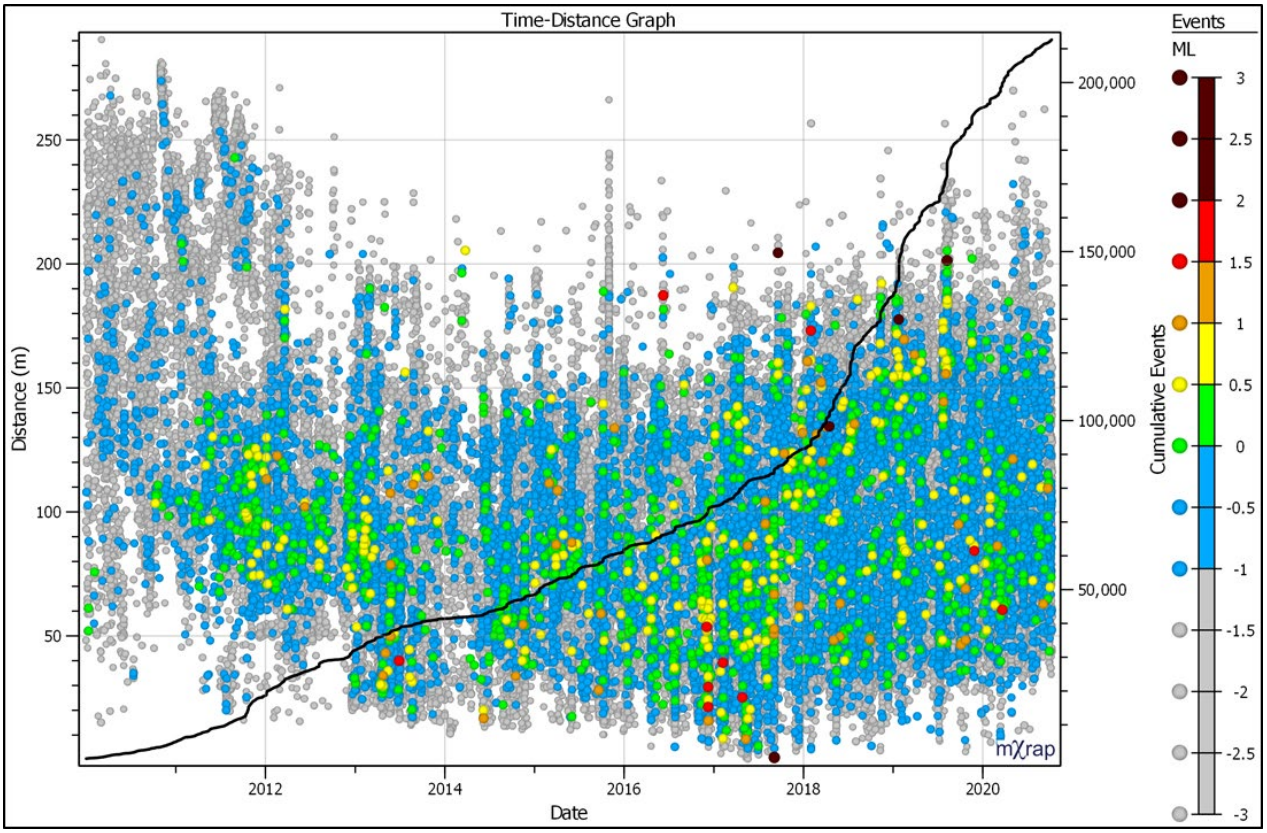

Figure 64 TDA of events in reference to MSE. No magnitude filter results in 212,714 events.

Figure 64 shows a very large number of events. It is difficult to recognize meaningful trends if too many events are included in the analyses. Events tend to overlap and obstruct one another.

Variations in event rate were dominated by the very small and most numerous events. Events below Mw 0.0 do not contribute insights, and obscure trends visible with larger events. It is clear that the number of events in TDA should be limited, underlying the need for multiple analysis scales.

Figure 65 shows improved clarity of TDA with a low magnitude filter (Mw ≥ 0.0).

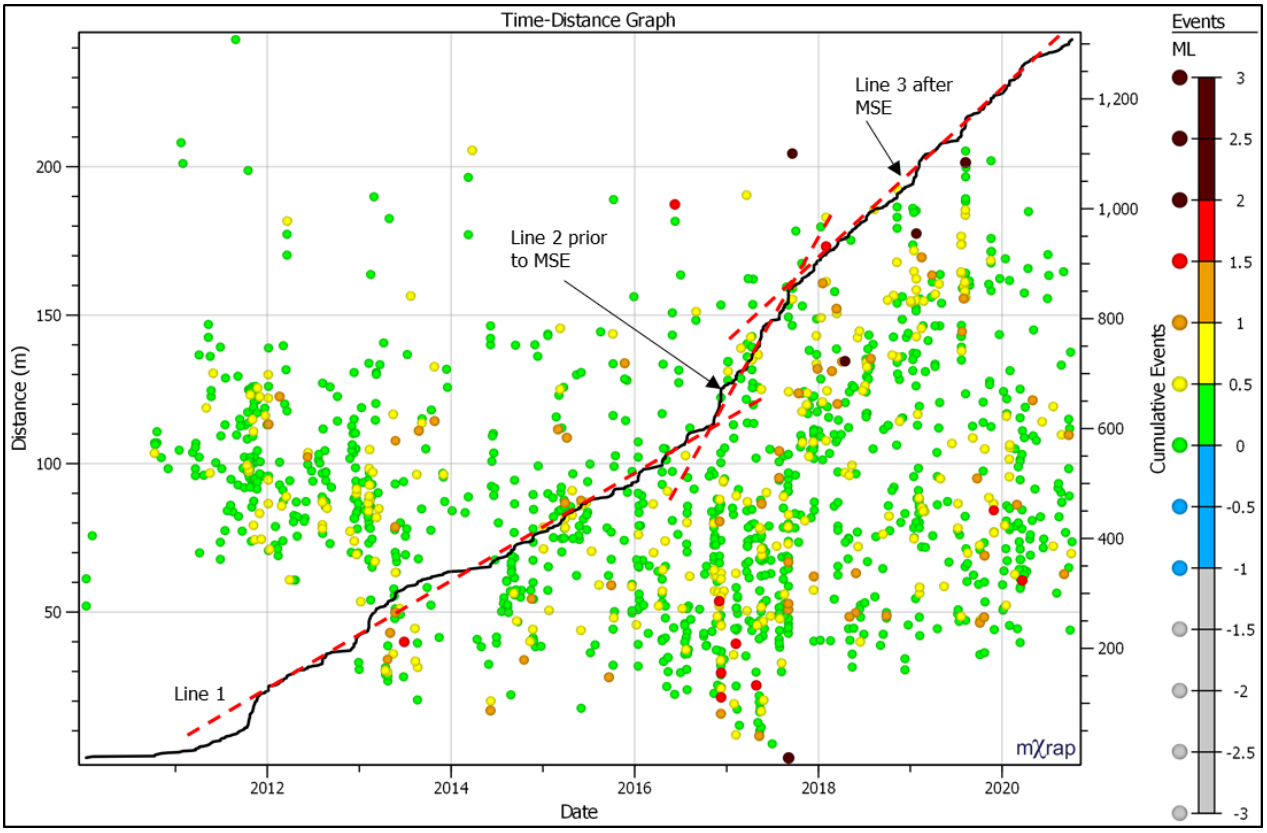

Figure 65 TDA of events in reference to MSE. Mw ≥ 0.0 filter results in 1308 events.

In comparison to Figure 64, the low magnitude filter of Figure 65 shows better clarity. It can be observed that events tend to coalesce around the MSE in the year prior to its occurrence and locate further away from the MSE afterwards. A slight increase in event rate leading up to the MSE is visible starting in early 2017 (Line 2) and decreasing after the MSE (Line 3).

Figure 65 shows that changes are more visible with a higher magnitude cutoff, but Mw 0-0.5 events are still too numerous to add substantial information and tended to obscure some trends.

Figure 66 shows the results of a further increase in event size (Mw ≥ 0.5).

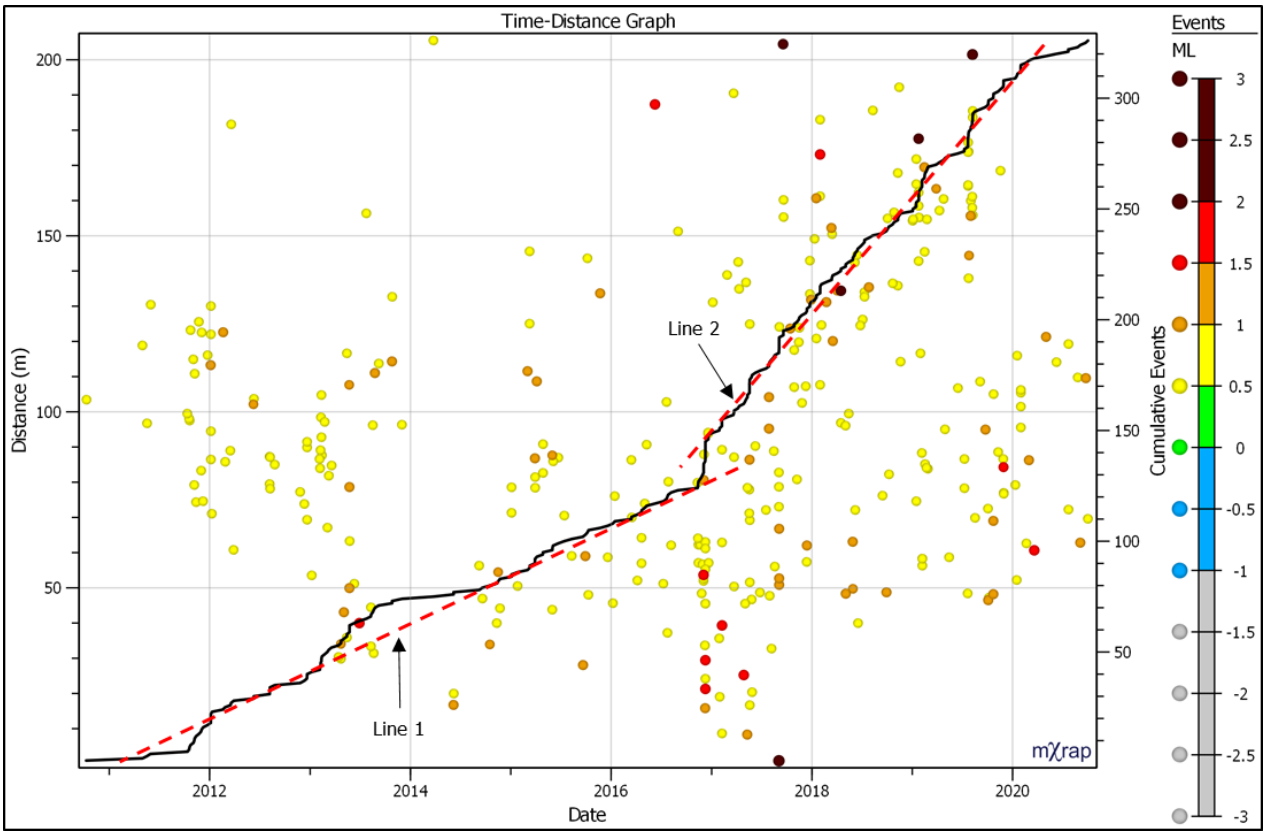

Figure 66 Mw ≥ 0.5 filter results in 328 events. TDA of events in reference to MSE.

A Mw ≥ 0.5 filter decreases the number of events in the analysis to the largest 98th percentile of events in the population. Meaningful trends are more visible. Clusters of events are more visible. Changes in cluster activity at the time of the MSE are more visible. There is a tight cluster of events within 60m of the MSE that begins to be active in late 2016 and ceases after the MSE. There is a loose cluster of events beyond 130m that becomes active after the MSE and becomes inactive in mid-2019. The change in event rate in late 2016 becomes much more distinct and clearly coincides with the occurrence of large events that begin to take place near the MSE. There is no change in the event rate of the entire sill at the time of the MSE, but there is a shift in location of events. The region within 40m of the MSE becomes inactive following the MSE. At distances beyond 100m, Mw ≥ 2.0 events only begin to occur after the MSE.

Figure 67 shows that a further increase in the magnitude cutoff to only include events Mw ≥ 1.0 reduces the clarity of the trends.

Figure 67 Mw ≥ 1.0 filter results in 69 events. TDA of events in reference to MSE.

The Mw ≥ 1.0 filter in Figure 67 does not add any insights that are not already clear with the Mw ≥ 0.5 in Figure 66. The figure shows where the large events locate, but is not very descriptive of the entire population. Changes in the characteristics of seismicity around the MSE are less reliable because the event number is too low.

TDA is not a scale dependent form of analysis, meaning that small events have the same weight as large events. Small events can dominate an analysis because they are much more frequent than large events. If many small events are allowed to be part of a TDA chart, they tend to obscure trends that are visible with larger events.

The volume and time of interest is controlled by spatial and temporal analysis scales. A magnitude filter is necessary to make the analysis useful. Figure 64 - Figure 67 show that a low magnitude filter can be useful for identification of meaningful trends using TDA. There is not an easily identified optimal number of events to use in TDA, therefore upper and lower limits are prescribed. A TDA chart should generally have somewhere in the hundreds of events. It is suggested that 250-1000 events be used for TDA.

4.3.5 Addressing Seismicity Related to Lateral Development

An additional benefit of a low magnitude filter is the elimination of small-scale failure processes that are not related to the MSE. An example is stress fracturing seismicity in the walls of a development heading. Figure 68 shows an example of numerous low magnitude events occurring around a development heading.

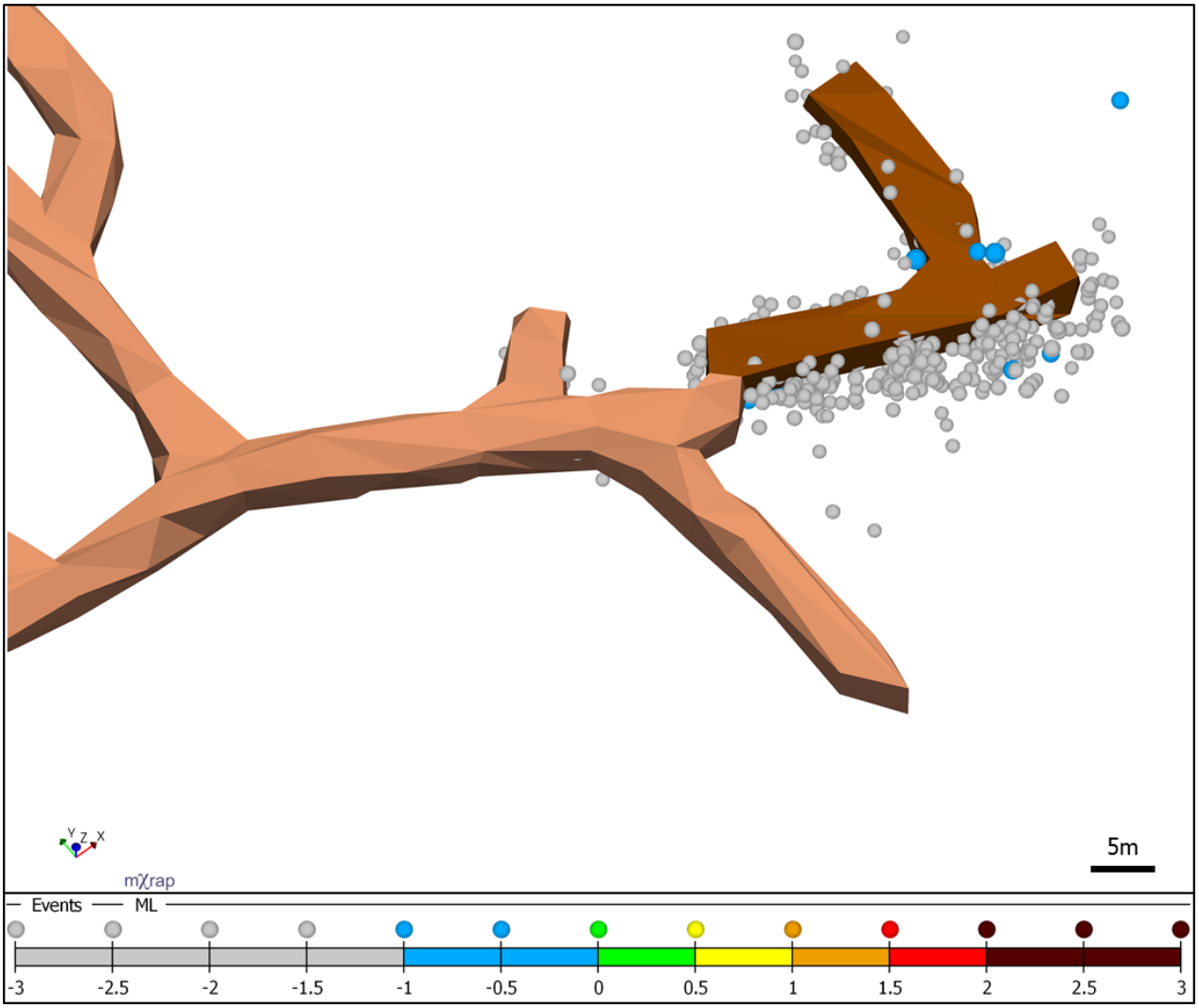

Figure 68 Shows 492 events and new development (dark brown) over a two month span.

Events tend to be clustered around the new development shown in dark brown. These events were strongly related to development blasting, with 75% occurring within hours of a development blast. The source mechanism of these events tends to be related to stress induced fracturing in the walls of the new development.

None of the development related events in Figure 68 are larger than Mw 0.0, underlying the idea that these events are from a smaller scale rockmass failure process may not be relevant to the MSE. Table 1 showed that different source mechanisms tend to have different maximum magnitudes, with fault slip events having a much larger potential magnitude than development

related events. If the relevant population of seismicity to study a fault slip mechanism involves larger events than a development stress fracturing mechanism, then a low magnitude filter may decrease the number of irrelevant development events while retaining larger fault related events.

Development related seismicity can provide learnings about the state of the rockmass during development mining, but adds little to a study of mine-scale failure processes. It can be inferred from Figure 68 that the heading was being developed into a relatively high stress regime, inducing local rockmass failure. After the 90 degree turn (to the left), the rock mass around the development became less seismically active, potentially indicating that the new orientation of development had a more favorable orientation to either the stress direction or the geologic fabric. While development seismicity can provide useful information, the actual rock damage created by development seismicity would tend to have little to do with generation of a MSE. Inclusion of these small events to a TDA chart would add irrelevancy and confusion.

Figure 69 shows a TDA chart that includes the events in Figure 68.

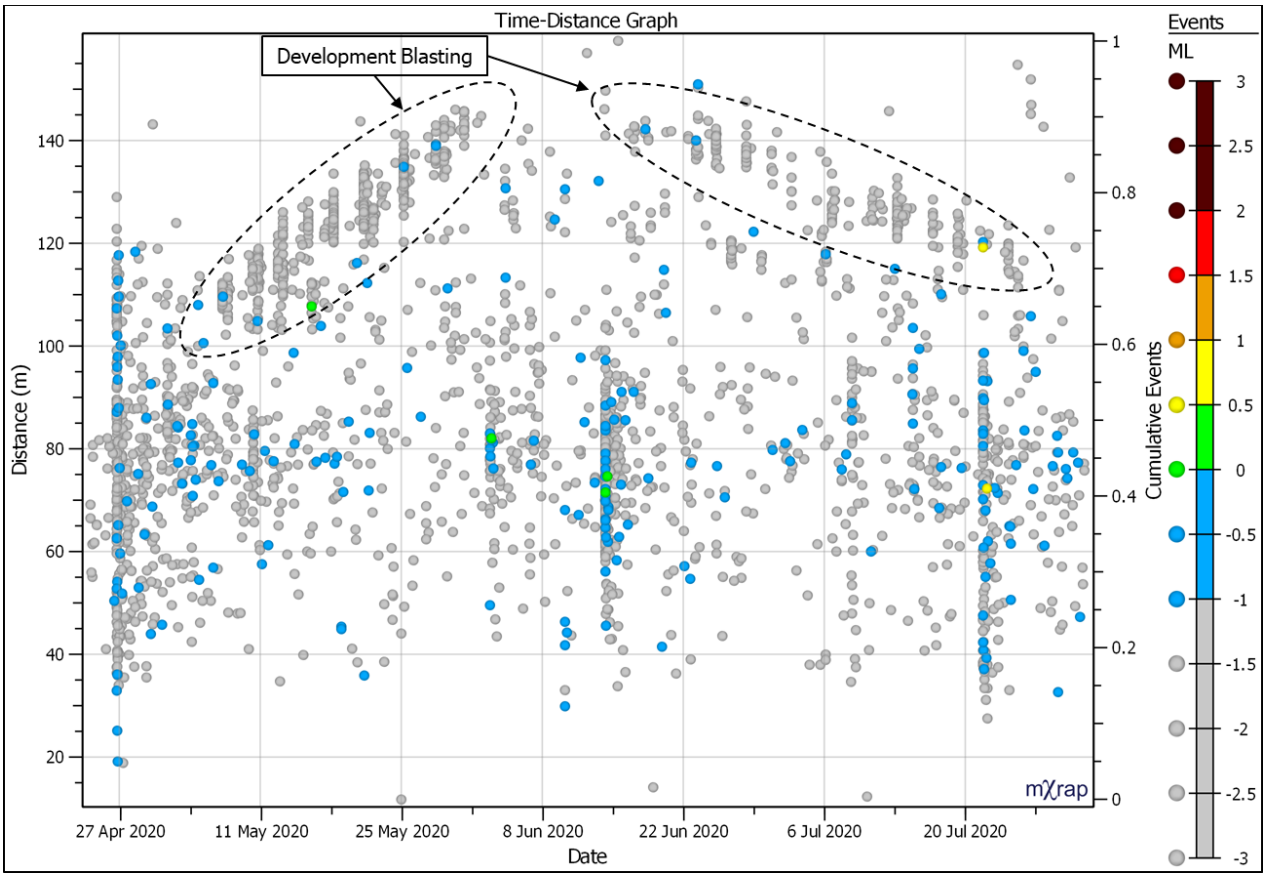

Figure 69 Development blast related seismicity. TDA in reference to MSE hypocenter on Sept. 3, 2017.

Two migrating trends are visible: one moving away from the MSE and one moving towards the MSE. The migrating clusters occur at consistent intervals simply due to regular blasting and progression of the development heading. The two trends are from the same development heading as Figure 68. The 90 degree corner changes the direction of the migrating population. The development heading was initially driven eastwards, away from the MSE hypocenter, which is represented by the event cluster increasing in distance. After the corner was developed, the tunnel was driven to the north, and the distance between the MSE and the event cluster decreases.

These two clusters could be interesting to an analysis of development related seismicity, but are irrelevant to analysis of the MSE. The events are small, likely because they are part of a tunnel

scale failure process. These migrating development trends can be identified in only certain focused analysis scales, and tend to add confusion to long term TDA charts.

4.3.6 Filtering Methodology

Because of the possibility that MSE-related rockmass failure could exist over a range of time, space and magnitudes, a strategy for data filtering was required in order to identify meaningful trends. Magnitude filtering was required to use TDA, with 250-1000 of the largest events tending to be most useful. Three temporal and three spatial analysis scales were used to identify trends related to the MSE.

Combinations of temporal and spatial analysis scales were used to identify trends that were relevant to the MSE. Table 6 illustrates nine combinations of temporal and spatial analysis scales.

Table 6 Analysis scales with approximate bounds for temporal and spatial filters.

	Long Term (years)	**Medium Term (weeks to months)**	**Short Term (hours to days)**
Large (mine scale)	L-LT	L-MT	L-ST
Medium (mining block scale)	M-LT	M-MT	M-ST
Small (stope scale)	S-LT	S-MT	S-ST

The naming convention for each time scale has an abbreviation for the spatial scale before an abbreviation of the temporal scale, e.g. L-LT meaning Large-Long Term.

Seismological data trends prior to and after the MSE were assessed using each of these nine spatial and temporal analysis scales. Long, medium and short term time periods were each assessed using large, medium and small volumetric filters. The intention of using nine different

analysis scales was to widely assess possibilities and look for trends irrespective of time frame and mine volume.

In general, longer and larger analysis scales used higher magnitude filters for increased clarity. The magnitude cutoff limited event numbers to between 250-1000.

Results follow in sections 4.4, 4.5, and 4.6. Sections are organized by primarily by time scale, and secondarily by spatial scale. Trends that improve understanding of the MSE are presented.

4.4 Long Term Time Distance Analysis

The intent of long term analysis was to show the overall process involved in the generation of the MSE. The MSE occurred in the region of a sill, suggesting that stored strain energy due to mining may have been a factor in the magnitude of the event. Long term analysis coincides with mining of the sill, showing the rockmass response to the entire sequence. Volumes used in Long Term TDA are shown in Figure 63.

4.4.1 Use of Trailing Median Distance

Figure 66 showed a shift in the locations of seismicity due to the MSE. In order to quantify this shift over time, a trailing 30 event median distance line was used. L-LT analysis is illustrated in Figure 70.

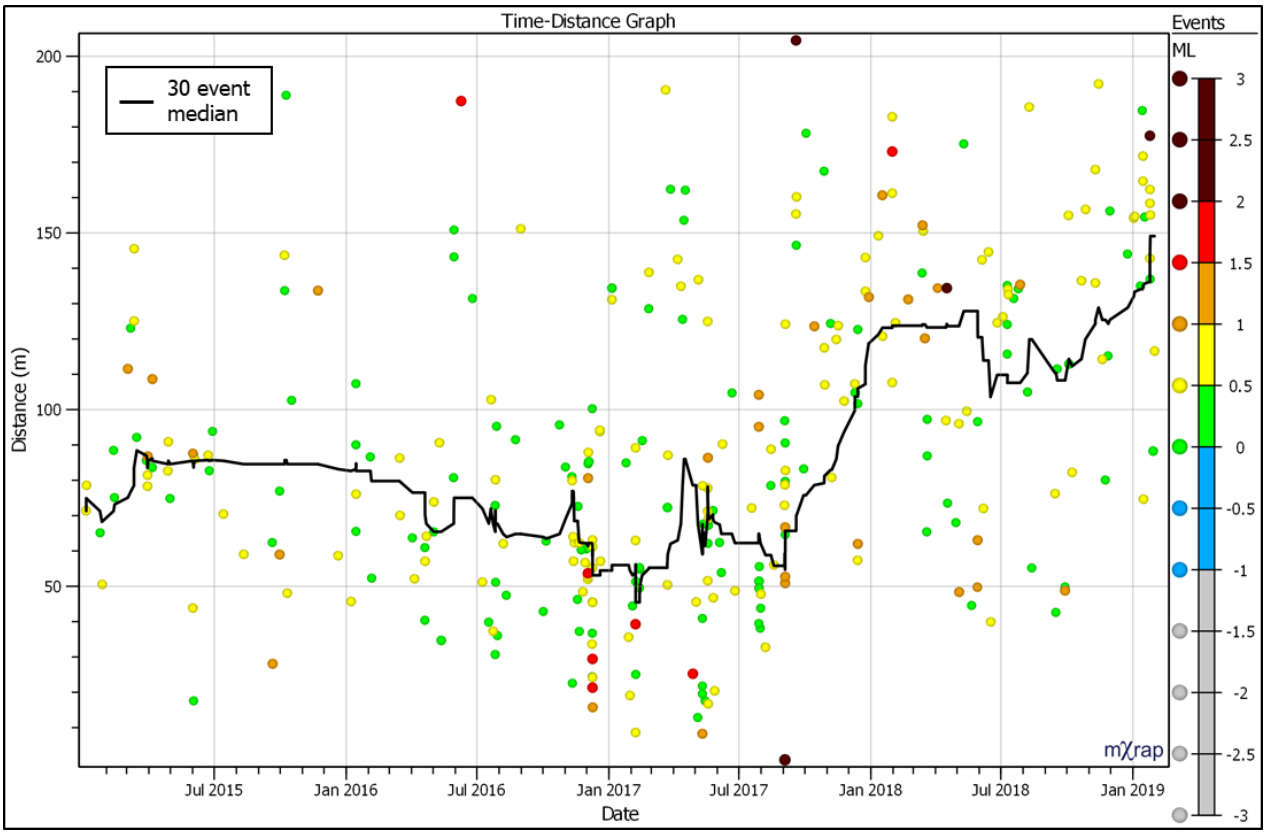

Figure 70 L-LT analysis. 309 events M ≥ 0.3.

A 30 event median distance trend was added to the chart to show changes in locations of seismicity prior to and after the MSE. Only Mw 0.3 events and larger are included. It can be observed that beginning in early 2016, events tended to migrate towards the MSE. This coalescence is particularly obvious with a set of Mw 1.5-2.0 events (red) that occurred within 60m of the MSE. The minimum distance between the MSE and other events decreases from Jan. 2016 to the MSE in Sept. 2017. These events appear to be part of a failure process that leads to the MSE.

Immediately after the MSE occurred, the 30 event median line began to move away from the MSE. The chart shows an absence of seismicity within 60m of the MSE for 8 months afterwards. This behavior was interpreted to mean that the MSE was a part of a rockmass failure process that ended with the MSE. The strain energy in the failure system was released when the MSE occurred, therefore there was no longer excess energy to generate significant seismicity. An

increase in seismicity at a significant distance from the MSE hypocenter immediately afterward could mean that part of the load that was carried by the MSE source region was shifted elsewhere.

The proximal, large precursory events could be interpreted as part of a softening process where seismicity weakens the rockmass and transfers stress onto a final asperity. The rupture of the final asperity, or the MSE, could be interpreted as the unloading of the rockmass, which explains the absence of proximal events afterwards.

The fact that these changes are visible on the scale of the entire mining sequence supports the idea that the MSE is part of a mine-scale failure process.

A median distance line was introduced in Figure 70. The choice of a 30 event trailing median will be justified in Figure 71 and Figure 72.

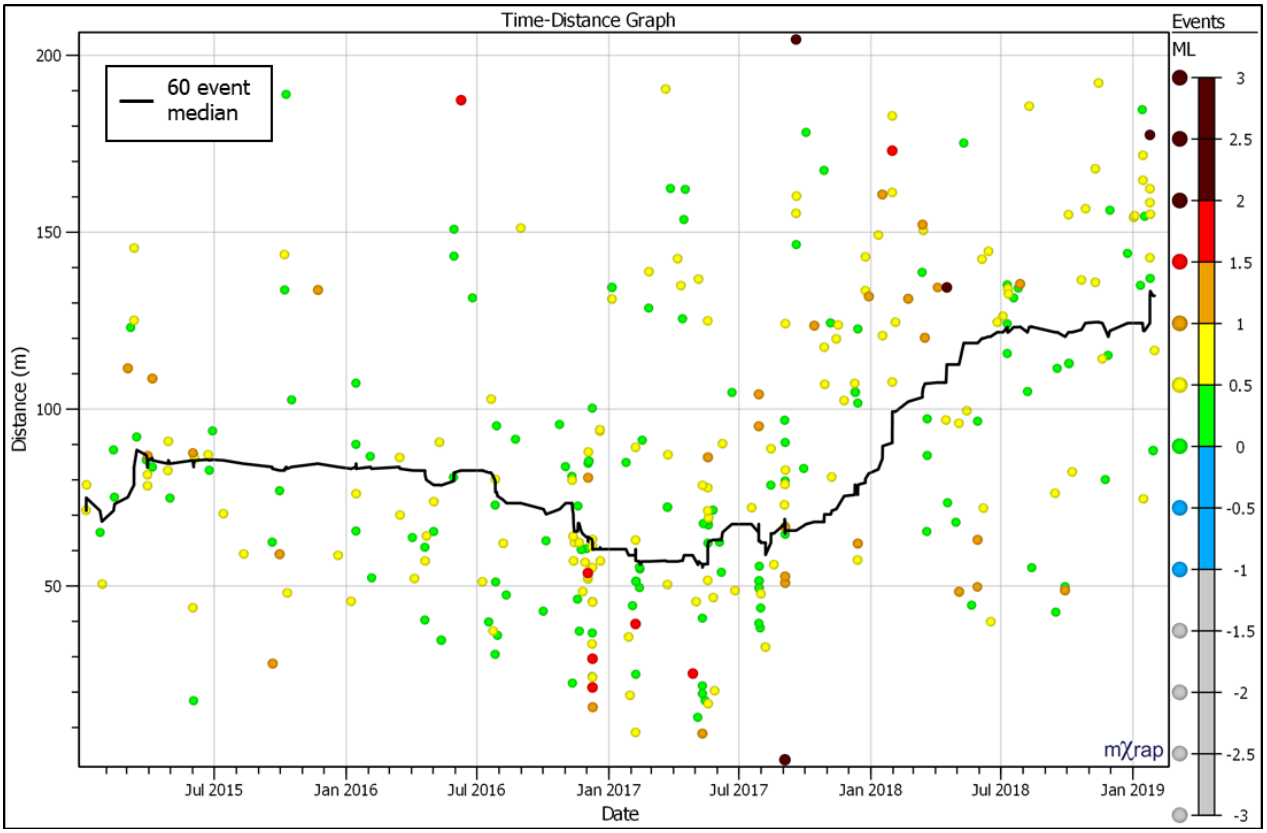

Figure 71 L-LT analysis. 309 events M ≥ 0.3.

A 60 event median tended to be too insensitive. Coalescing behavior can be observed, but with increasing events, the curve becomes more gentle and distinct changes are less visible. After the MSE, the median trend appears to only gradually move away, but a closer look at the actual events reveals the change was more immediate.

Figure 72 shows the L-LT chart with a 10 event trailing median.

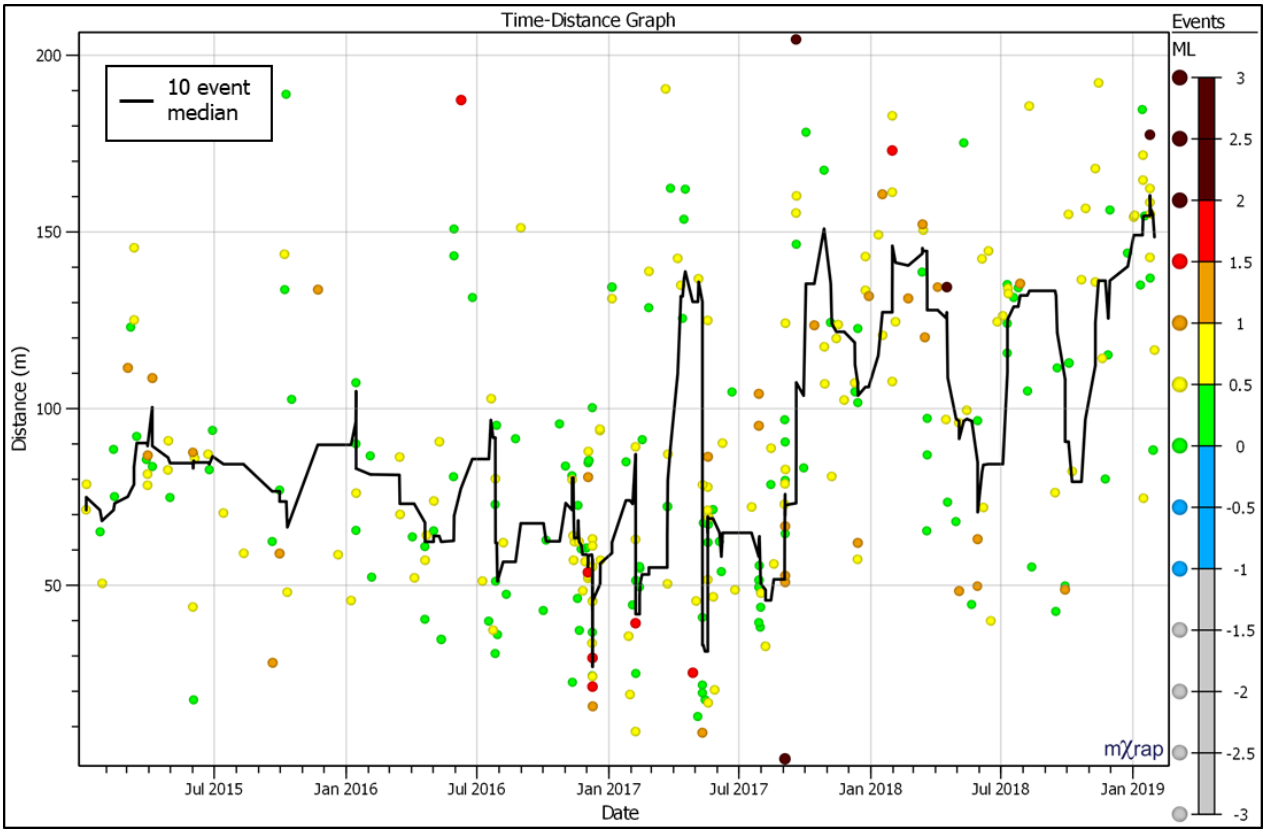

Figure 72 L-LT Analysis. 309 events Mw ≥ 0.3.

The 10 event median was too unstable, and was too influenced by events occurring beyond 100m. The tendency of seismicity to cluster in space and time results in a too short trailing median jumping back and forth to different clusters. The trend still shows precursory coalescing towards the MSE and movement away afterwards, but volatility in the trend does not add insight to the behavior of the MSE.

4.4.2 *Indication of Change in Hazard*

The MSE appeared to have a regional effect on the distribution of seismic hazard. Gibowicz and Kijko (1994) define seismic hazard as the probability of the occurrence of a certain magnitude event in a defined space and time. TDA contains the necessary components to show changes in seismic hazard: space, time and a magnitude threshold. TDA directly indicates changes in seismic hazard, which expedites further analyses. Figure 73 shows how TDA can indicate changes in seismic hazard by comparison of equal space-time windows before and after the MSE.

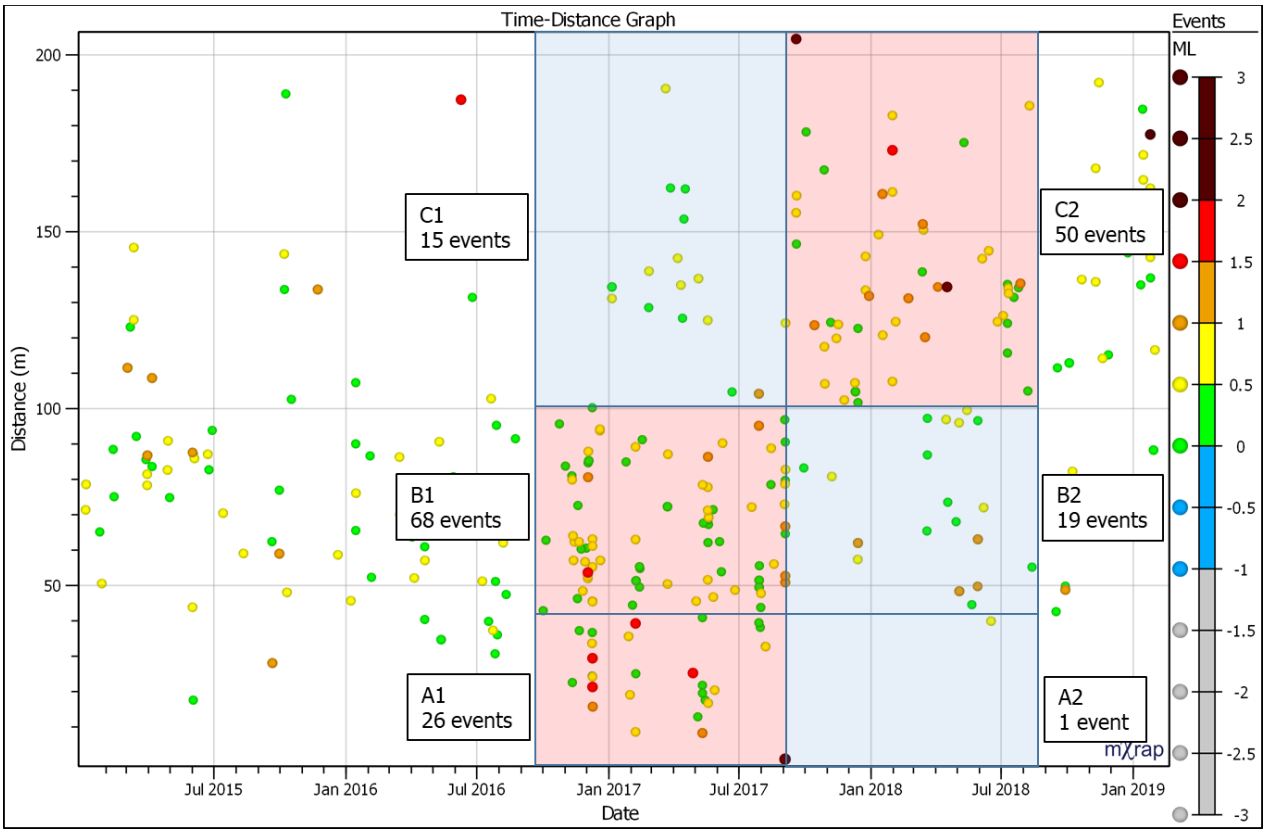

Figure 73 L-LT Analysis showing a change in hazard. Total events in each box is listed in the lower left corners. 309 events Mw ≥ 0.3.

Time-space zones are annotated on Figure 73. Six timeframes are shown, the year preceding the MSE (timeframe 1), and the year after the MSE (timeframe 2). Spatial zones are identified within 40m of the MSE (zone A), 40m to 100m from the MSE (zone B) and events greater than 100m (zone 3).

Changes in event clusters can be observed at the time of the MSE. The affected regions are shown by equal time and distance boxes, coloured red for higher relative hazard and blue for lower. Total number of Mw ≥ 0.3 events in each box can give an estimation of seismic hazard. It can be observed that the "A" and "B" boxes undergo a decrease in seismic hazard while the "C" box increases. This change is consistent with the region closest to the MSE becoming unloaded and the region furthest away becoming critically loaded.

To quantify this apparent change in hazard, frequency-magnitude charts were created for events in boxes A, B and C (Figure 74), boxes A and B combined (Figure 75), and for box C (Figure 76).

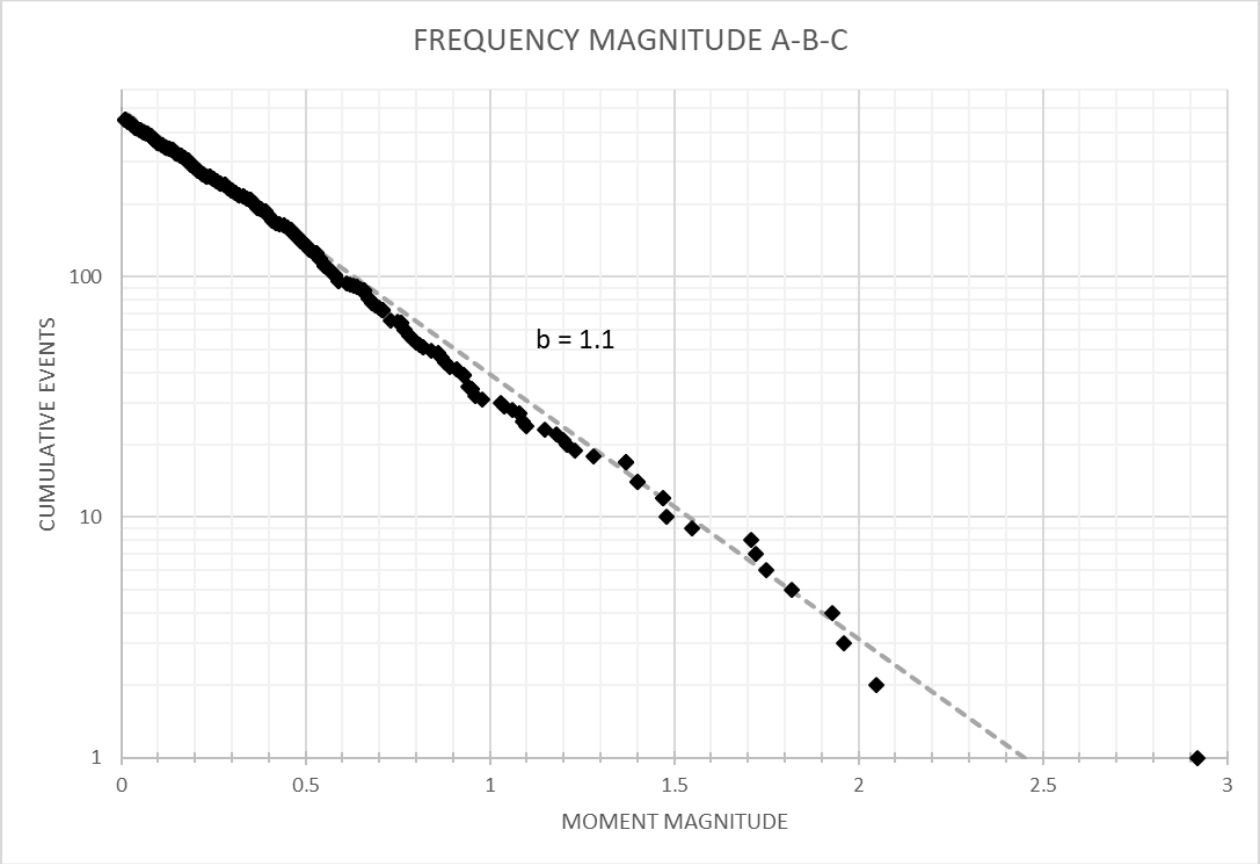

Figure 74 Frequency-Magnitude chart for events in space-time boxes "A," "B," and "C."

A frequency-magnitude relation for was created events highlighted in Figure 73. The grey line shows an approximate line of best fit. The event population is reasonably linear for almost two orders of magnitude, indicating a well behaved data set (Hudyma, 2008). The b-value, or slope,

is shown above the line of best fit. The intercept of the line of best fit with the horizontal axis (a/b), which represents the largest expected event, is approximately Mw 2.4. The largest event in the population, the MSE (Mw 2.9), is larger than a/b by half an order of magnitude.

Comparison of events before and after the MSE reveals further insights into the change in hazard.

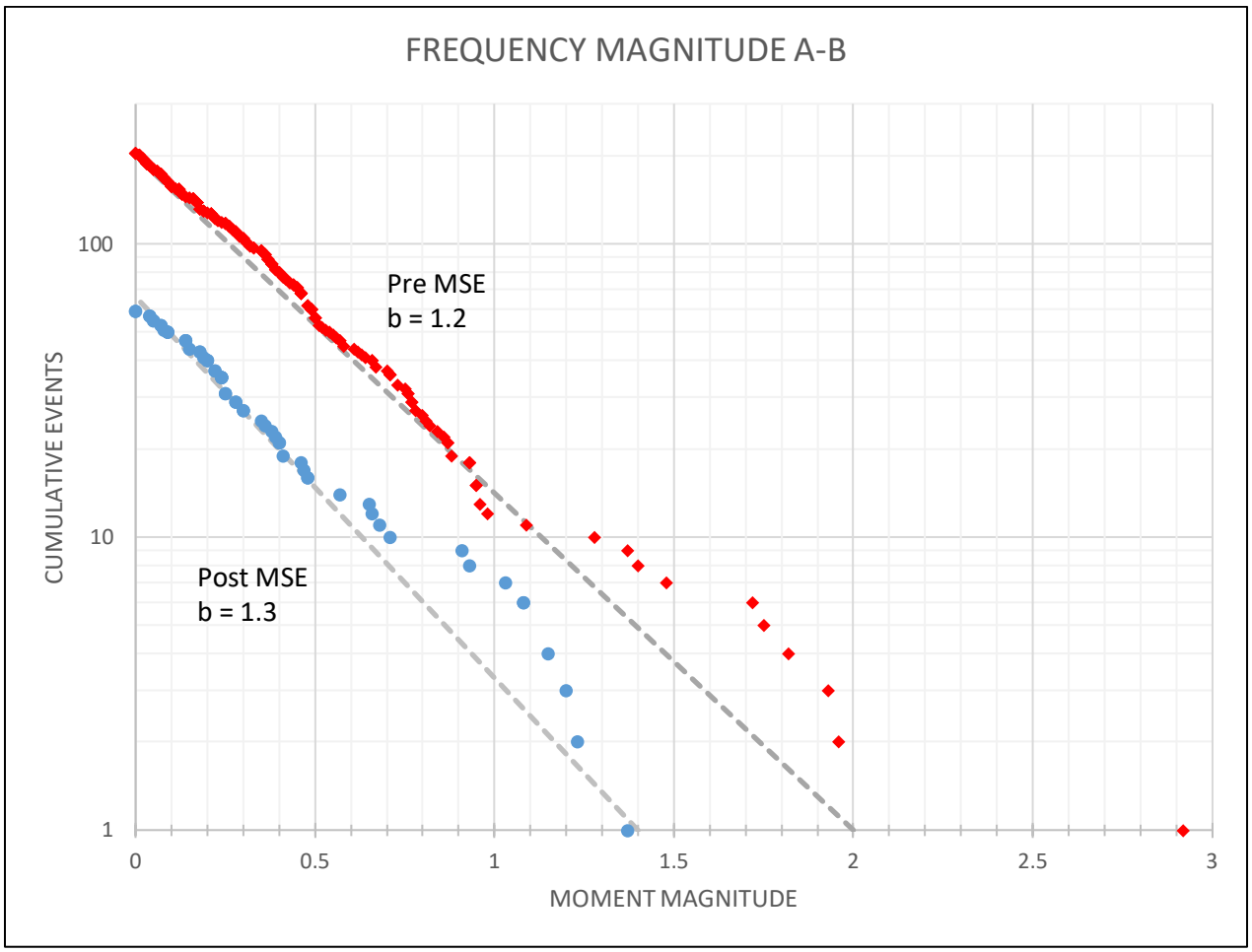

Figure 75 Frequency-Magnitude chart for events in space-time boxes "A" and "B," showing trends before and after the MSE

It can be observed that for areas near to the MSE, in boxes A and B, the hazard decreases after the MSE. The intercept of the line of best fit, thought to give an indication of the seismic hazard of a population, is Mw 2.0 prior to the MSE and Mw 1.4 after the MSE, showing a decrease in hazard. The b-value, which is dependent on the proportion of large events to small events, shows an increase from 1.2 to 1.3 after the MSE, also indicating a decrease in seismic hazard.

Figure 76 shows that box C undergoes a significant change in hazard after the MSE.

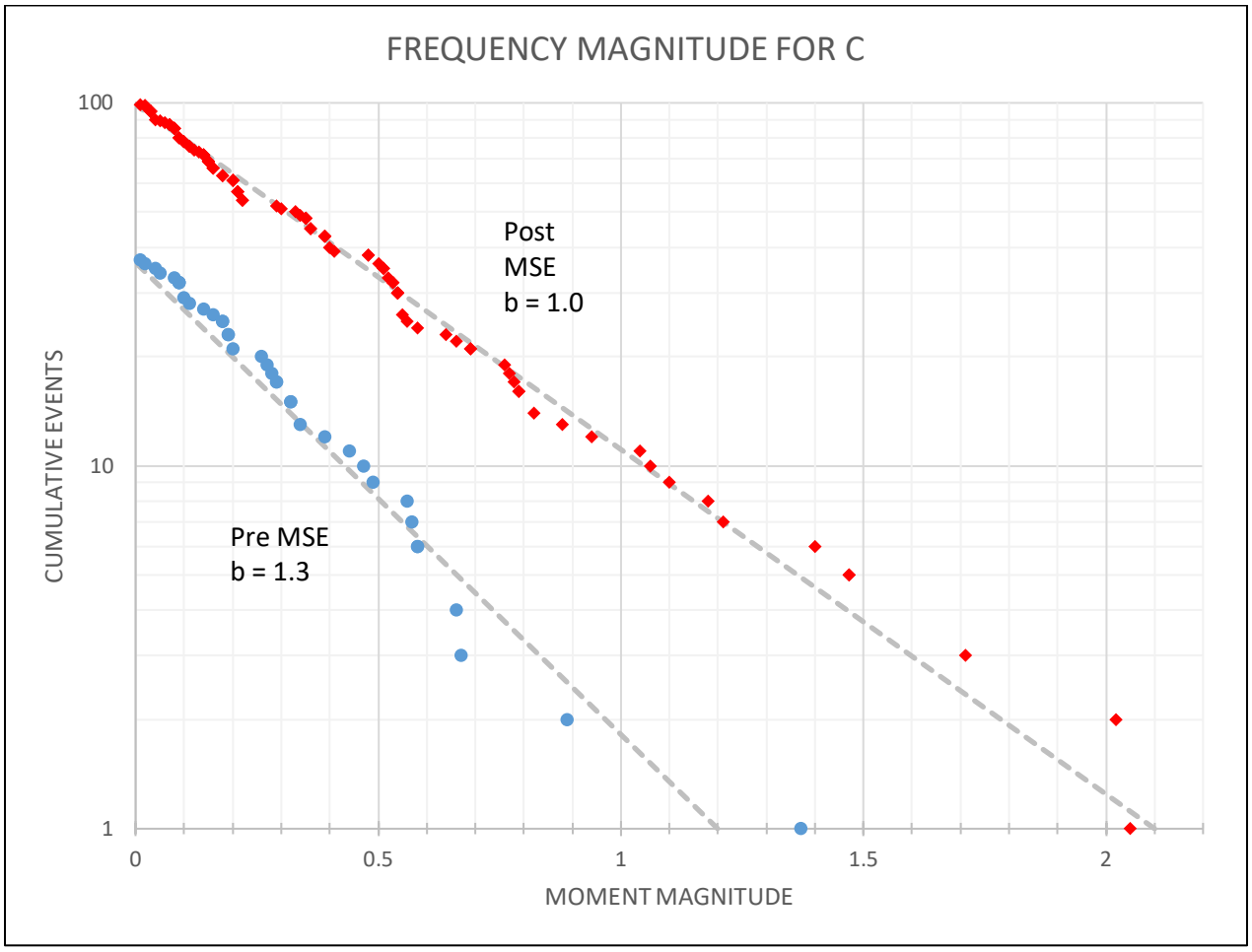

Figure 76 Frequency-Magnitude chart for events in space-time box "C," showing trends before and after the MSE

Box C essentially undergoes the opposite change in hazard to boxes A and B. An increase in a/b from Mw 1.4 to 2.2 after the MSE is the most obvious effect of a change in hazard. The b-value decreases after the MSE from 1.3 to 1.0, showing that less small events are taking place relative to larger events.

An interesting change between the high hazard (red) time periods of Figure 75 and Figure 76 is the fit between a/b and the largest events recorded. In Figure 75, the largest event (MSE), is much larger than a/b, while in Figure 76 the largest events have a much better agreement with a/b. Asperity ruptures are referred to as "catastrophic" failures; larger than the rest of the events

on the fault (Smalley Jr., Turcotte and Solla, 1985). A possible explanation for the difference between boxes A and B and box C is that the MSE was an asperity rupture, and the large events taking place in box C are a different kind of failure mechanism.

To visualize the change in hazard, TDA was used in conjunction with 3D visual analysis to investigate what actual seismic sources may have undergone changes. TDA can show that a change in hazard has occurred, which may not be immediately obvious using other methods. Once trends are observed in the simple, 2D TDA chart, they can be verified and further analyzed in a 3D visualization. The time-distance windows in Figure 73 are represented using 3D visual analysis in Figure 77, which shows events prior to the MSE, and Figure 78, which shows events after the MSE.

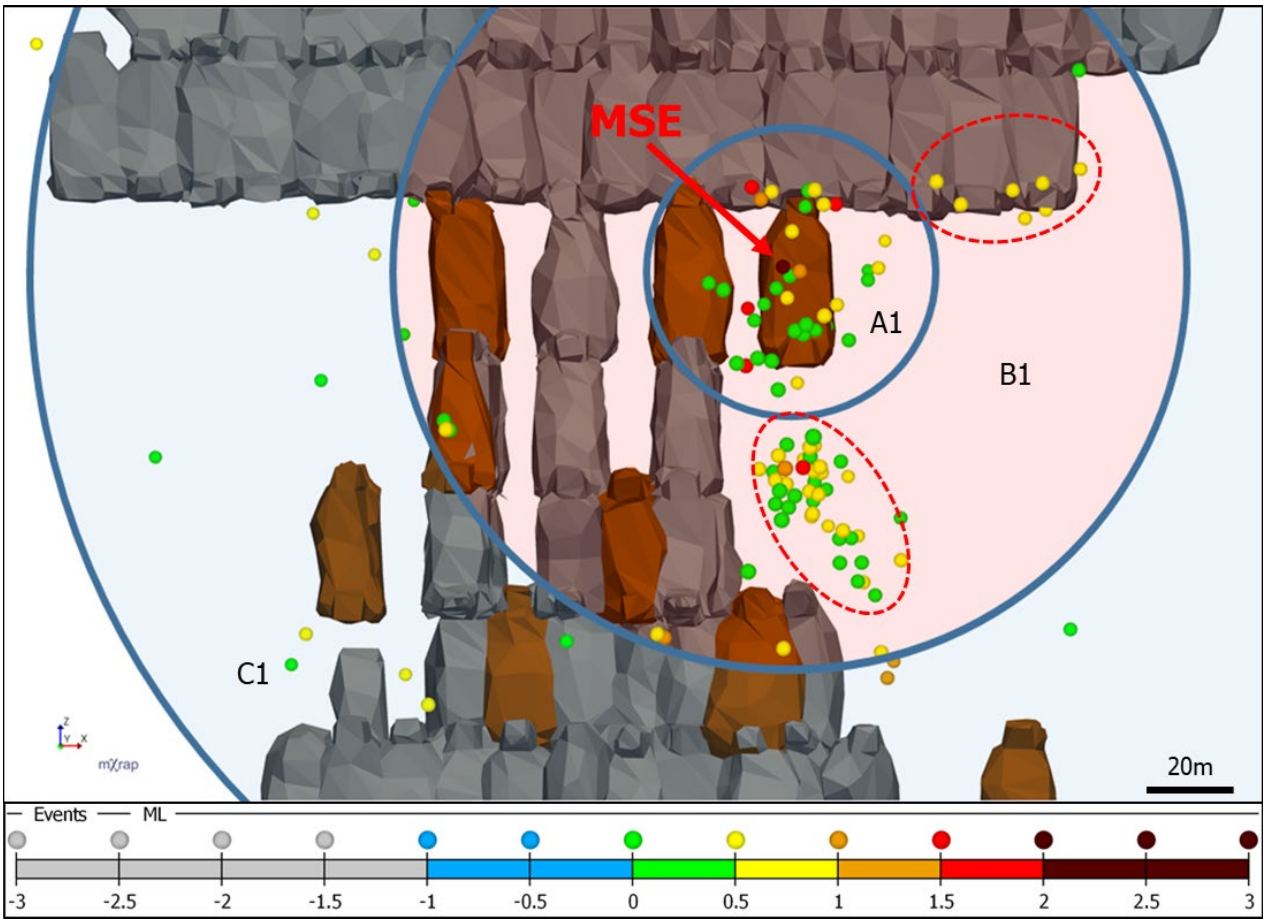

Figure 77 Visualization of zones A, B and C prior to and including the MSE, Sep. 20, 2016 – Sept. 3, 2017

The “boxes” used to compare seismic hazard in TDA are now visualized in 3D as an inner sphere and concentric shell volumes. Several clusters of large events exist. A single cluster of large events exists in A1. It was shown in Figure 70 that the A1 events tended to coalesce around the MSE hypocenter. These events may be related to deformation on the North-South fault (NSF) and Oblique fault (OBF). B1 contains 2 distinct clusters. Directly below A1, there is another cluster that aligns with the NSF. Above and to the right of A1 there is a widely spaced cluster of large events that locates along the OBF. C1 is relatively inactive.

Figure 78 shows a 3D visualization of events occurring after the MSE.

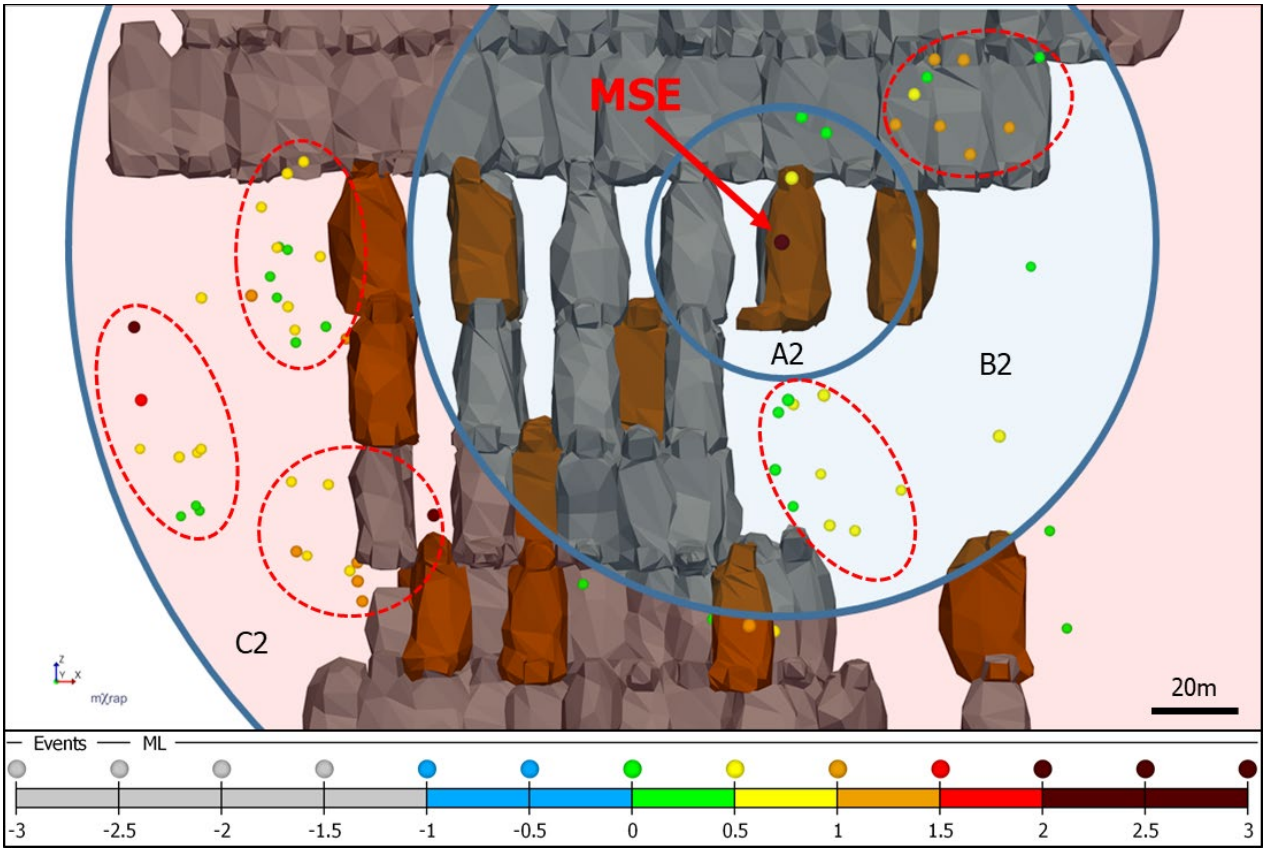

Figure 78 Visualization of zones A, B and C including and after the MSE, Sept. 3, 2017 – Aug. 2018

Significant changes can be observed when comparing Figure 77 to Figure 78. The center sphere, A2, has become aseismic. There are two clusters of events in B2 that were present in B1. In B2,

events became less frequent in the lower cluster, but there was an increase in larger events (Mw 1.0-1.5) in the upper cluster.

C2 is much more seismically active than C1, with several event clusters. Events Mw ≥ 1.0 are much more common in C2 than C1. After the MSE in the East abutment, the seismic hazard of the West abutment increases. The TDA chart in Figure 73 shows that this change initiated with the MSE.

Observation of the changes between Figure 77 and Figure 78 is not immediately obvious using other methods of analysis. TDA indicates if a change has taken place, and what the approximate analysis scales should be used to confirm and further analyze a change.

Mine extraction is somewhat symmetrical on the east and west sides of the orebody. It was expected that similar rockmass failure processes would exist for each abutment. In order to further investigate the hazard change that was identified in the TDA chart in Figure 73, separate Magnitude-Time charts were created for the east and west sides of the sill. Figure 79 shows a change in behavior between the east and west abutments.

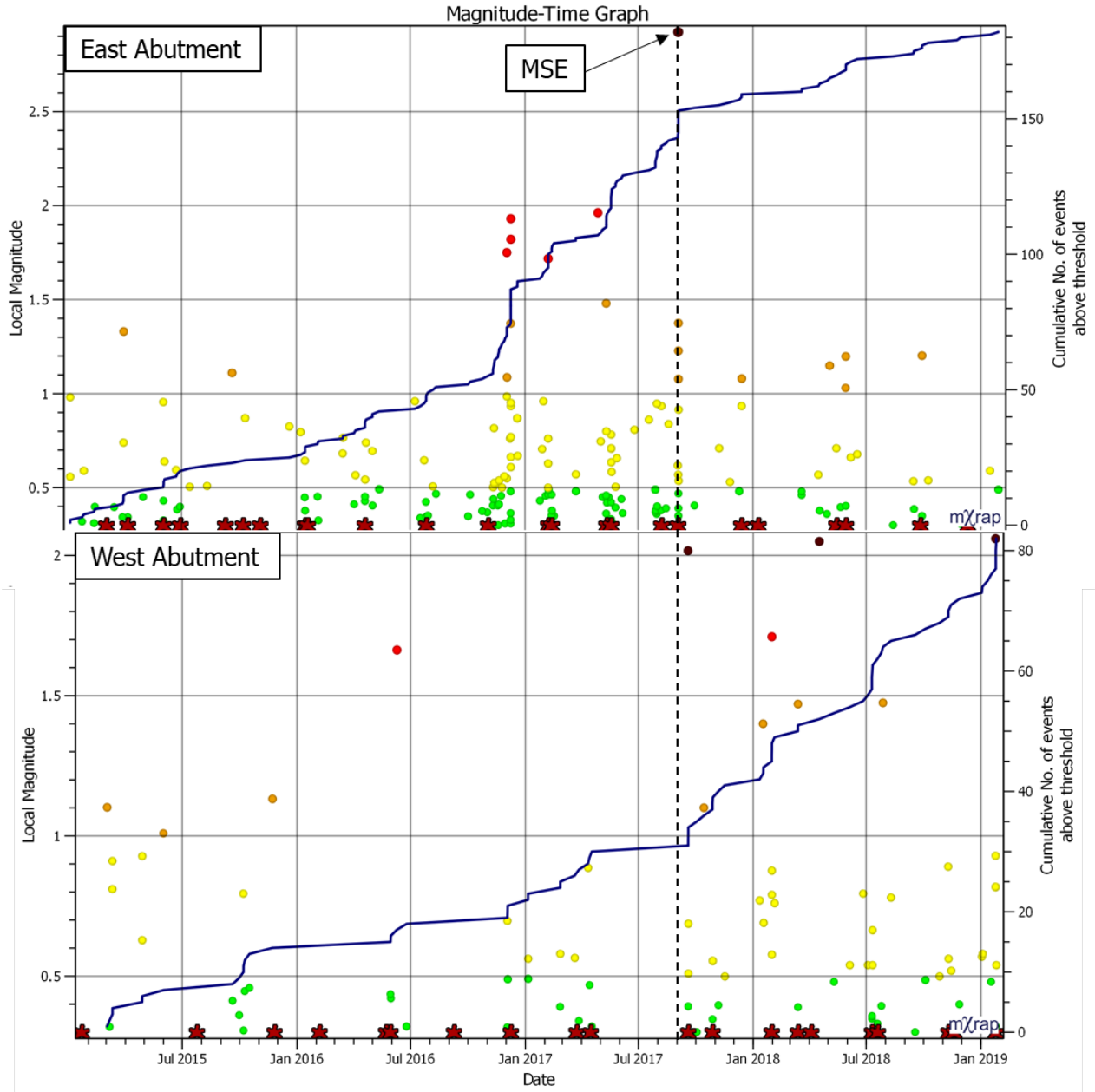

Figure 79 A comparison of Magnitude-Time charts between the East and West abutments

At the time of the MSE, there were opposite trending inflection points in the event rates of the East and West abutments. The East abutment undergoes a decrease in event rate and the West abutment experiences an increase in event rate. The same behavior can be observed with large magnitude events. Prior to the MSE, there is a prevalence of Mw ≥ 1.5 events in the East abutment. After the MSE there are no events greater than Mw 1.5 in the East abutment and there is an increase in Mw ≥ 1.5 events in the West.

Production blasts are visible on the horizontal axis of each chart by brown stars on the x-axis of Figure 79. The mine sequence roughly alternates stopes between the East and West abutments. Prior to the MSE, the East abutment was at a higher level of extraction, with 17 stope blasts observed in the East abutment and 10 blasts in the West. After the MSE, extraction was slightly weighted towards the West abutment, with 10 blasts in the West compared to 6 in the East.

It is clear that the seismic hazard decreased in the East abutment and increased in the West abutment at about the time of the MSE. The cause of the change, however, was not clear. West abutment blasting was likely a factor, but static stress transfer from the MSE to the West abutment may also have been a factor.

4.4.3 S-LT Yield Behavior

Analysis of the smallest volume improved understanding of the yield process. The small volume is shown in Figure 63. The small volume was focused on the NSF in the sill region. Only event Mw -0.3 and greater are included. Figure 80 shows S-LT analysis for the MSE.

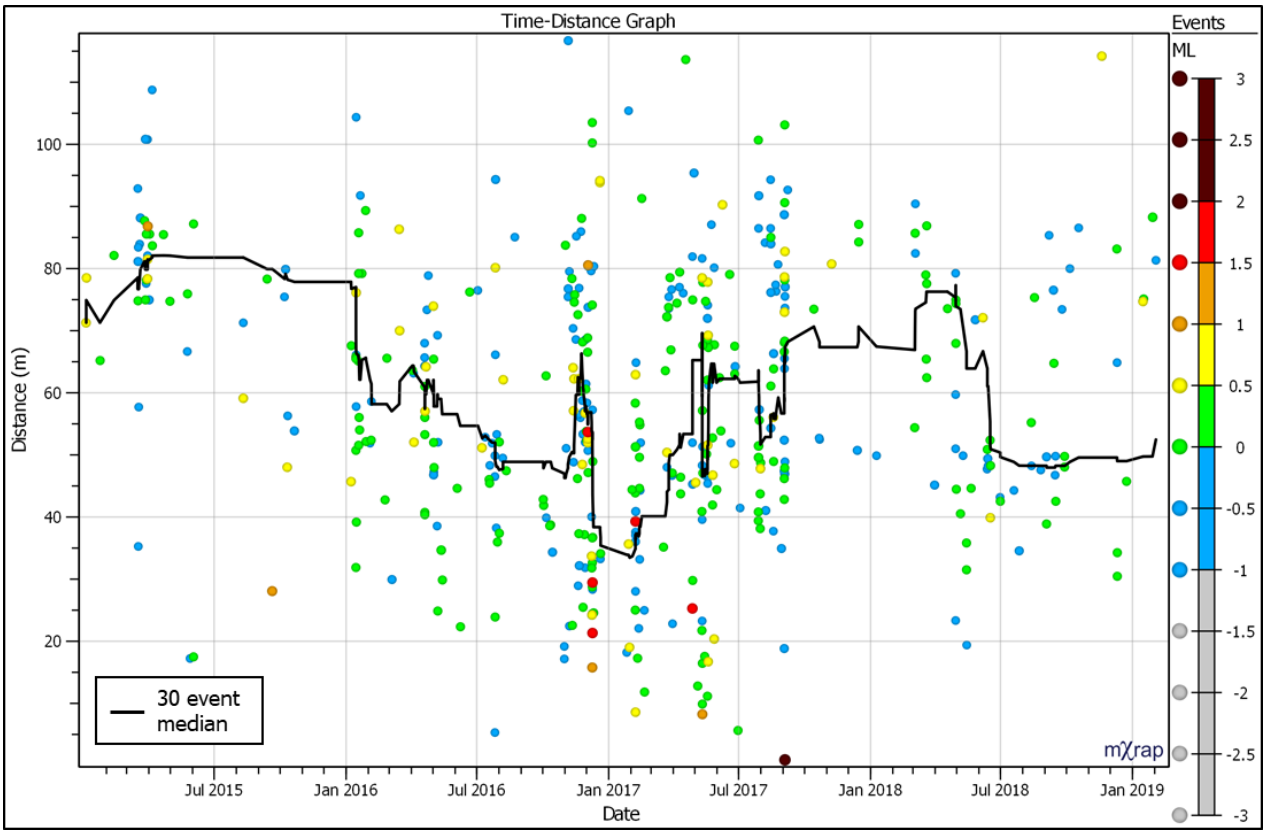

Figure 80 S-LT analysis. 464 events Mw ≥ -0.3.

Use of a small volume, isolating the fault region, shows that the most important processes observed so far occurred near to the NSF, strengthening the confidence that the MSE occurred on the NSF rather than the OBF. The 30 event median line shows that events near the fault coalesce towards the MSE from Jan. 2016 – Feb. 2017. Dispersion of events away from the MSE is observed after its occurrence.

Five Mw ≥ 1.5 events (red), which occurred between Dec. 2016 and Jun. 2017, were noted to be important in L-LT analysis. The fact that these events occurred in the NSF volume is a further indication that the yield process was controlled by the NSF rather than the OBF. Spatial coalescence, such as that shown in Figure 80, may represent damage to or softening of an asperity. Figure 81 shows that long term softening behavior occurred on the fault prior to the MSE.

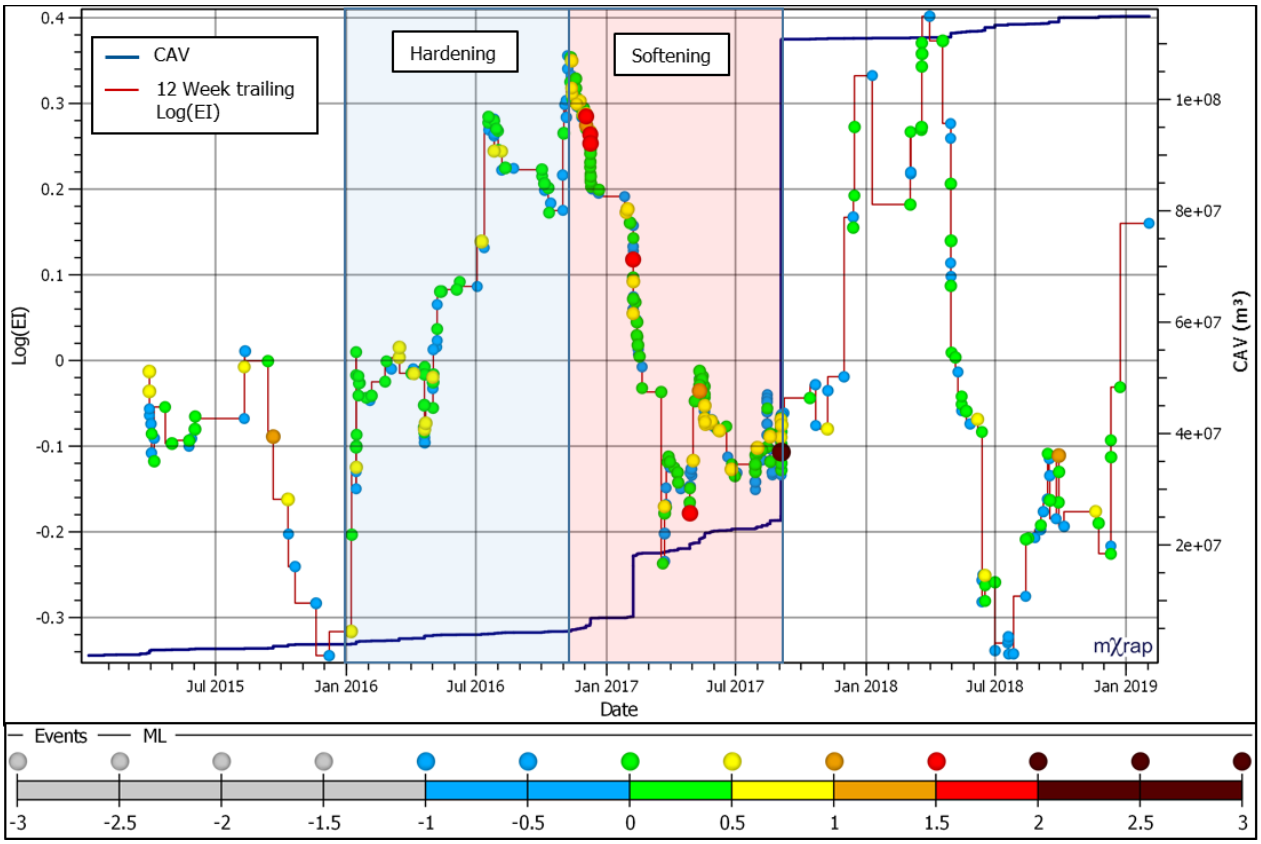

Figure 81 S-LT Instability Analysis chart

Figure 81 is an instability analysis chart for the events in the S-LT analysis in Figure 80. A twelve week trailing average, red log(EI) line is plotted against the left vertical axis with event dates and magnitudes marked on the line. CAV is plotted on the right vertical axis. Jan. 2016 marks the onset of rising EI, which coincides with the start of the coalescing behavior in Figure 80. From Jan. to Nov. 2016 there is an increase in the EI (stress), while CAV (deformation), remains flat. Mendecki and Van Aswegen (1998) described this occurrence as hardening behavior, indicative of high stress and low deformation in an intact rockmass. From Nov. 2016 to the MSE in Sept. 2017, events occurring in the volume change behavior from a hardening regime to a softening regime. The softening regime is characterized by a steep drop off in EI and increases in CAV, which represents decreasing stress and increasing deformation. Strain softening is essentially characterized by a drop in the minimum stress necessary for irreversible plastic deformation to

occur. Seismicity occurring during the softening period can be interpreted as deterioration of the strength of the fault, providing greater mobility for the eventual MSE.

The MSE appears to be the final event in the softening phase. After the MSE, EI increases once more, but CAV remains flat. The increase in EI could be interpreted as the start of another loading cycle in the east abutment, or the onset of a related, but previously stable yield process. In either case, the softening phase that led to the MSE is no longer the dominant failure process.

4.4.4 Visualization of Fault Seismicity

A general coalescence of events towards the MSE and a dispersion of events afterwards was observed in the NSF volume in Figure 80. To further investigate this change in behavior that was identified by TDA, events on the fault were visualized and compared to mining voids in three time periods:

- Prior to coalescence (2010-01 to 2014-09) (Figure 82)
- During coalescence (2014-09 to 2017-09) (Figure 84)
- During dispersion (2017-09 to 2020-10) (Figure 85)

A visual examination of the NSF reveals a change in change in the locations of the largest events. Figure 82 illustrates the locations of large events from the initiation of mining up to three years prior to the MSE.

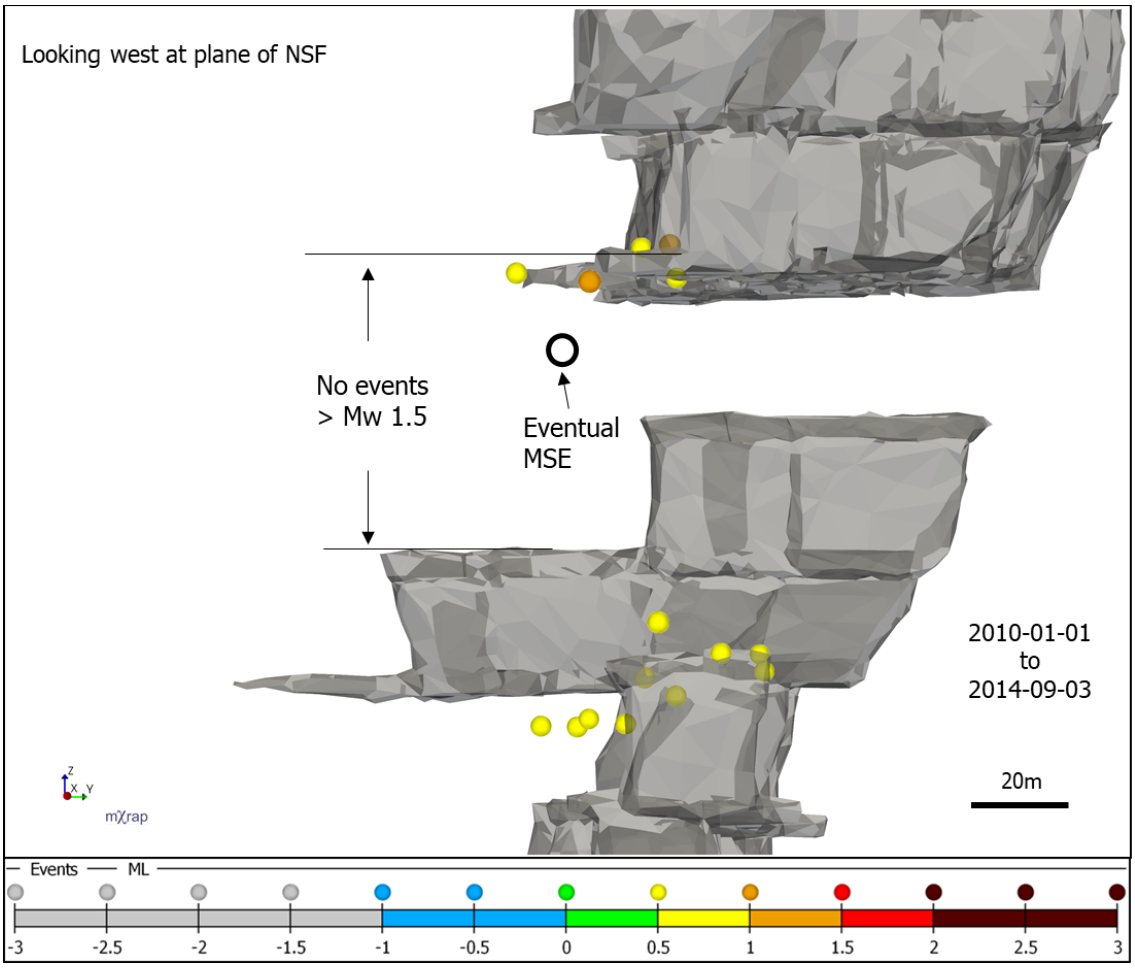

Figure 82 Events in NSF volume prior to sill breakthrough. 15 events Mw ≥ 0.5.

From 2010 to 2014, the sill pillar was established by the convergent mining sequences. In Figure 82, the sill pillar is intact, but encroached upon by mining. During this time period, it is assumed that the pillar is under substantial stress and resists HW-FW convergence. It can be observed that though the pillar should be highly stressed, there is an absence of significant events in the fault volume in the center of the pillar. This absence of events appears to be a seismic gap, in which the absence of events on a fault is explained by stability; the stress on the fault does not exceed the resistance of the fault to slip, therefore there are no significant slip events.

Martin and Maybee (2000) state that as hard rock pillars progress from squat to slender, unloading of the pillar through rock failure becomes increasingly likely. The slenderness of sill pillars constantly increases as the mining fronts converge, which should result in the sill pillar

transitioning from a stable to an unstable state. In this case, the sill pillar was intersected by faulting, with the largest events prior to the MSE taking place near the NSF (Figure 63). This behavior is demonstrated by gradually increasing rate and magnitude of large seismic events (in the large volume, Figure 63), after the sill pillar was breached in 2015-03-02, shown in Figure 83.

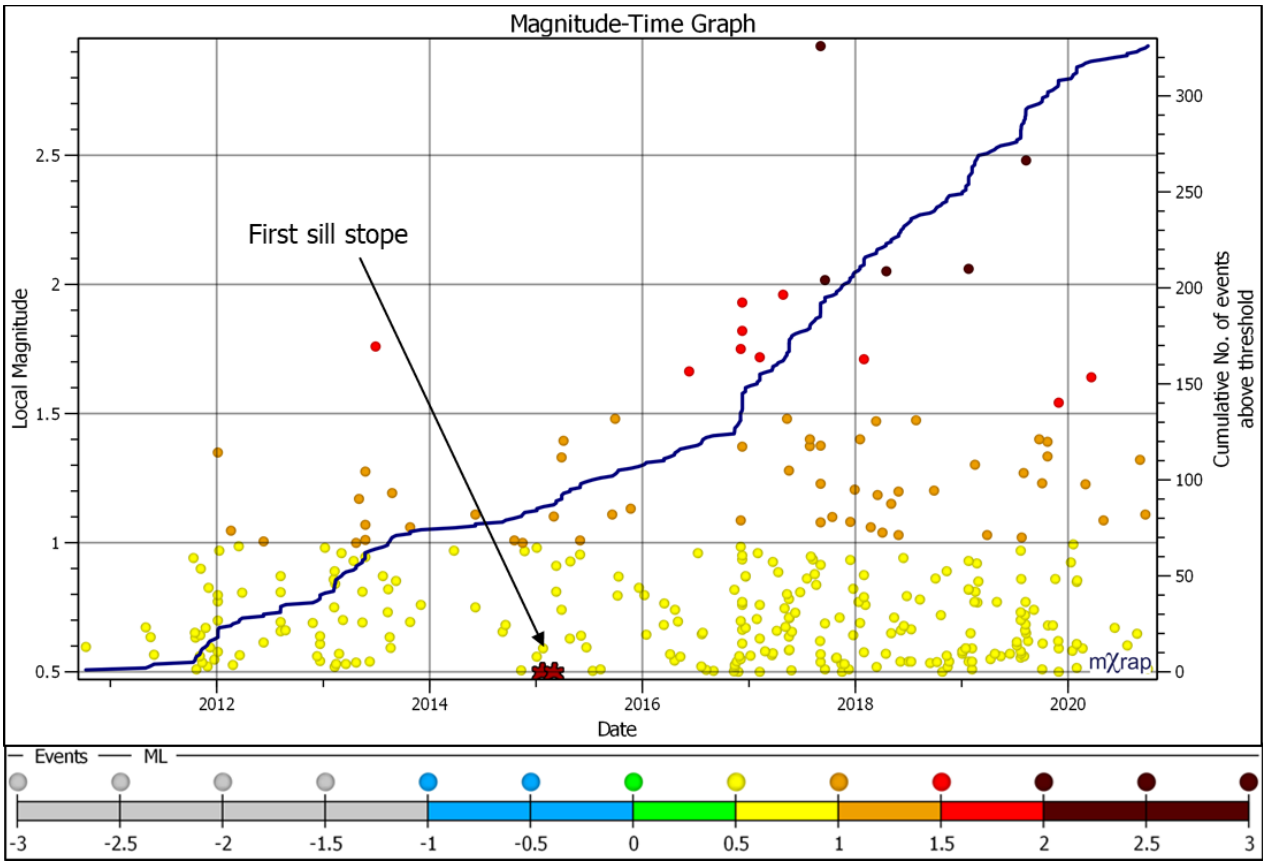

Figure 83 MTH of Mw ≥ 0.5 events in the 1320 sill pillar

The rate of large events is relatively flat in the year prior to breaching the sill. After the sill is breached with the first stope on 1355L, there is a slight uptick in the rate of large events, remaining fairly constant until late 2016. Breaching of the sill was followed by an expansion of stoping along strike.

Figure 84 shows an increase in events in the NSF volume, interpreted to be a sign of release of stored energy in the sill.

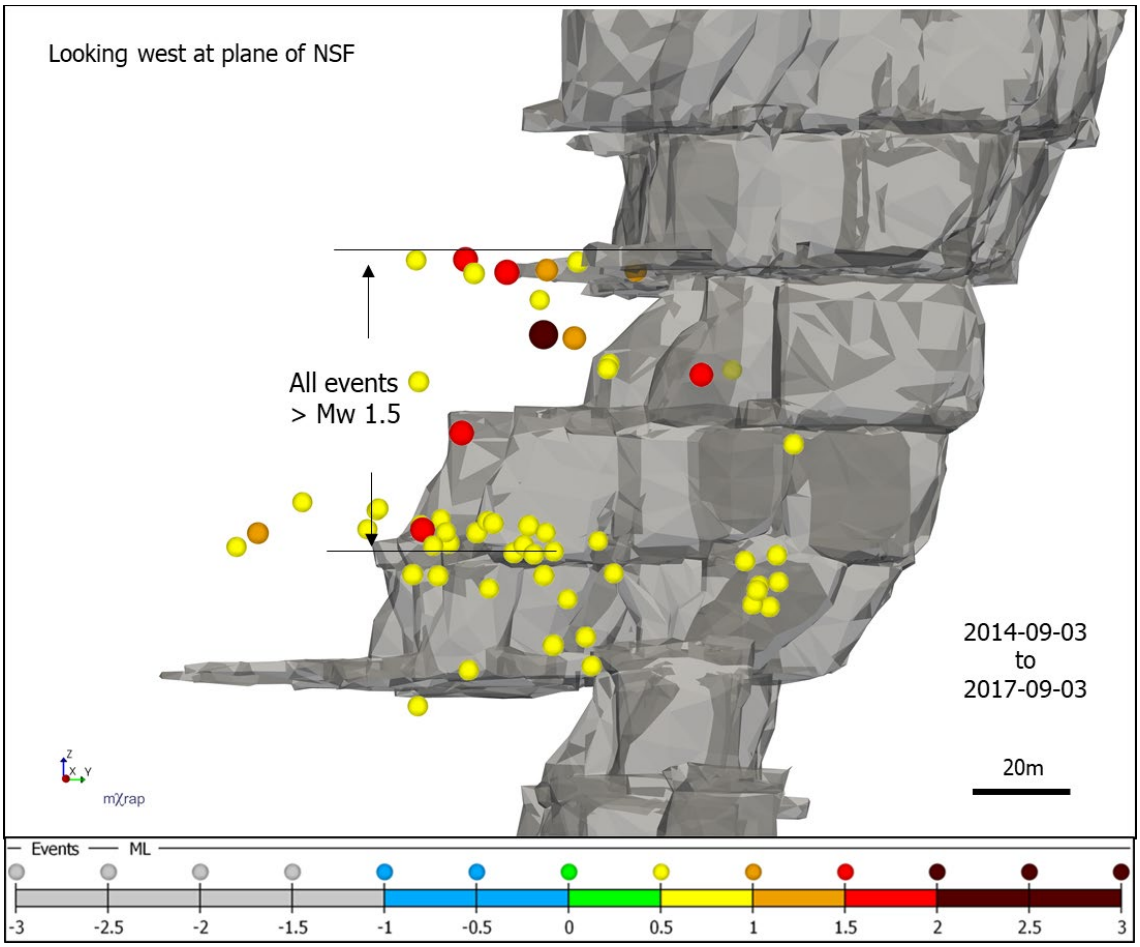

Figure 84 Events in NSF volume in the three years prior to the MSE. 57 events Mw ≥ 0.5.

From Figure 82 to Figure 84, substantial mining takes place in the sill pillar. The region in the NSF volume which was previously aseismic now contains five Mw 1.5 events, shown in red. This is consistent with the fault being previously stable but stressed, with the large events occurring as a softening (de-stressing) process. The sequence of large events culminates in the MSE, which occurs at the center of the red events. TDA (Figure 80) and instability analysis (Figure 81) showed that these events were part of a coalescing, strain-softening process that is interpreted to lead to the final rupture of the asperity in the MSE.

The complete rupture of an asperity should result in a termination of the processes that led to failure. After the asperity is unloaded, the source region should become aseismic, since stored energy has been released and the ruptured area of the fault has become sheared and weaker,

making it less prone to store further energy. Further deformation, however, should still be ongoing on the periphery of the sheared area, caused by continued extraction of the orebody. Figure 85 shows the locations of large events for three years following the MSE.

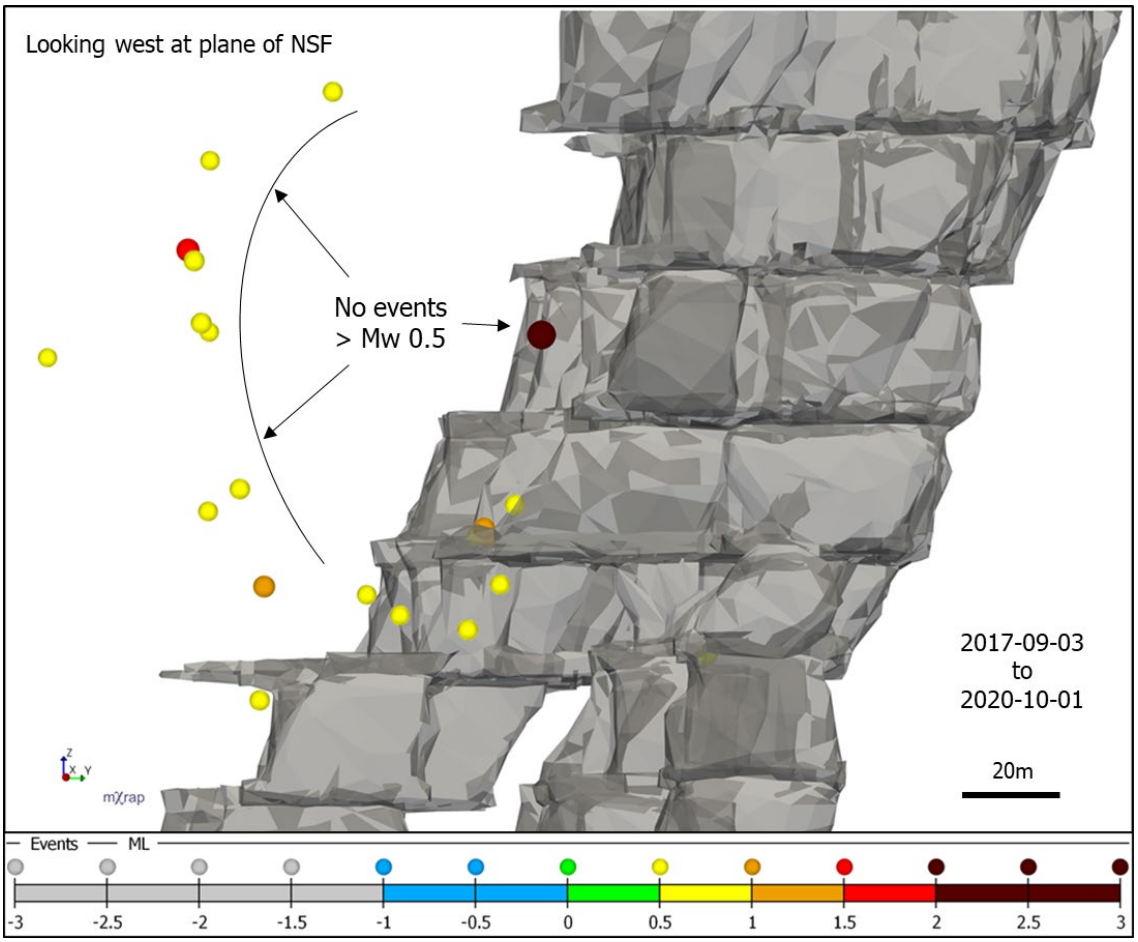

Figure 85 Events in NSF volume after the MSE. 21 events Mw ≥ 0.5.

It can be observed that large events still continue to take place in the NSF volume with continued extraction of the sill. After the MSE, these events are absent from the source region, suggesting the region has been unloaded during the large event. Events begin to take place deeper in the HW than they had previously. It is possible that these events are now occurring on the edge of the MSE source region, representing an expansion of the ruptured area on the fault.

It is interesting that these events form a 60-70m radius arc in the HW of the MSE hypocenter. This arc appears to be centered on the MSE hypocenter. Source size calculations assume a

theoretical circular, planar rupture area. It was assumed that the convergence of the HW towards the FW was the dominant direction of deformation. These later events on the NSF seem to indicate that HW-FW convergence continued further into the HW after the MSE. The MSE hypocenter, explained as a ruptured asperity, could continue to slip aseismically due to a damaged, weaker fault area, unable to store significant energy.

4.5 Medium Term Time-Distance Analysis

The medium volume is shown in Figure 63. Increased detail can be seen using medium term analysis. The response of the rockmass to individual stope blasts becomes increasingly clear. The analysis shows the response of several stopes prior to and after the MSE.

4.5.1 L-MT Analysis

Figure 86 shows L-MT analysis of the MSE using TDA.

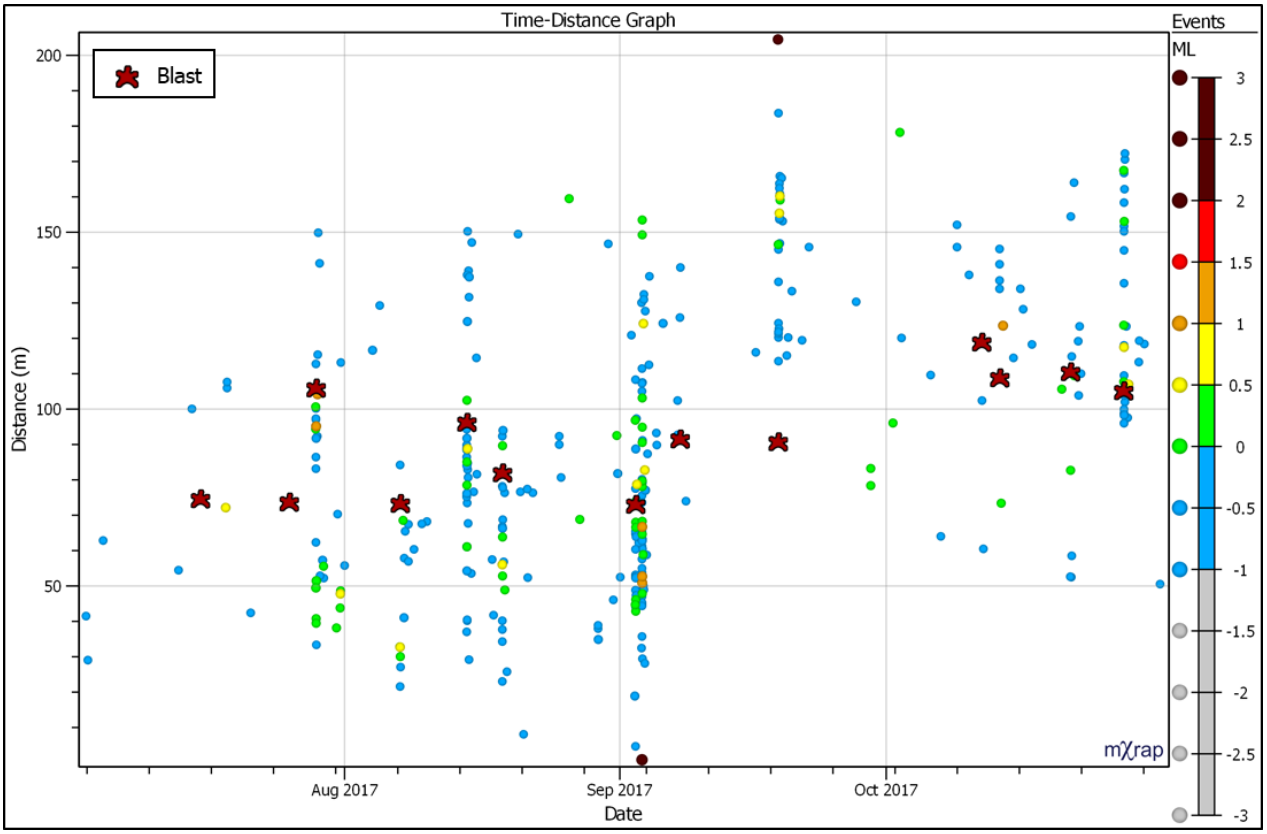

Figure 86 L-MT analysis of sill blasting and seismicity. 332 events Mw ≥ -0.6.

The relation between blasting and seismicity is observable by vertically aligned clusters or "strings" of events. These strings of events show the scale of blast influence with respect to the MSE hypocenter.

Prior to the MSE, there are several blasts within 100m of the MSE, with most events tending to occur closer to the MSE than the blast. After the MSE, the region near to the MSE essentially becomes aseismic and regions beyond 100m become increasingly seismically active. Since seismicity represents damage to the rockmass and release of stored energy, the seismic response near the MSE hypocenter and its absence post MSE may indicate that the precursory events were caused by the same energy release process that resulted in the MSE. Before the MSE, the sub 100m region may have been in an energy release process. Once excess energy has been released, a rockmass should be in a more stable state, lowering the seismic response in the region of the MSE hypocenter. After the MSE, the seismic response beyond 100m is increased, including a large event (Mw 2.0) locating 200m away from the MSE. This large secondary event occurred at the time of a blast, but over 100m away from that blast, suggesting a triggered mechanism.

An additional benefit of showing blast locations is that events with poor temporal relation to blasting can be distinguished. These events may be related to time-dependent rockmass failure processes initiated by a blast, or be related to another failure process entirely. After blasting, events often still occur at similar distances, indicating an ongoing time-dependent failure process.

4.5.2 S-MT Analysis

Figure 87 shows S-MT analysis of events in the small NSF volume (from Figure 63) over a medium time period.

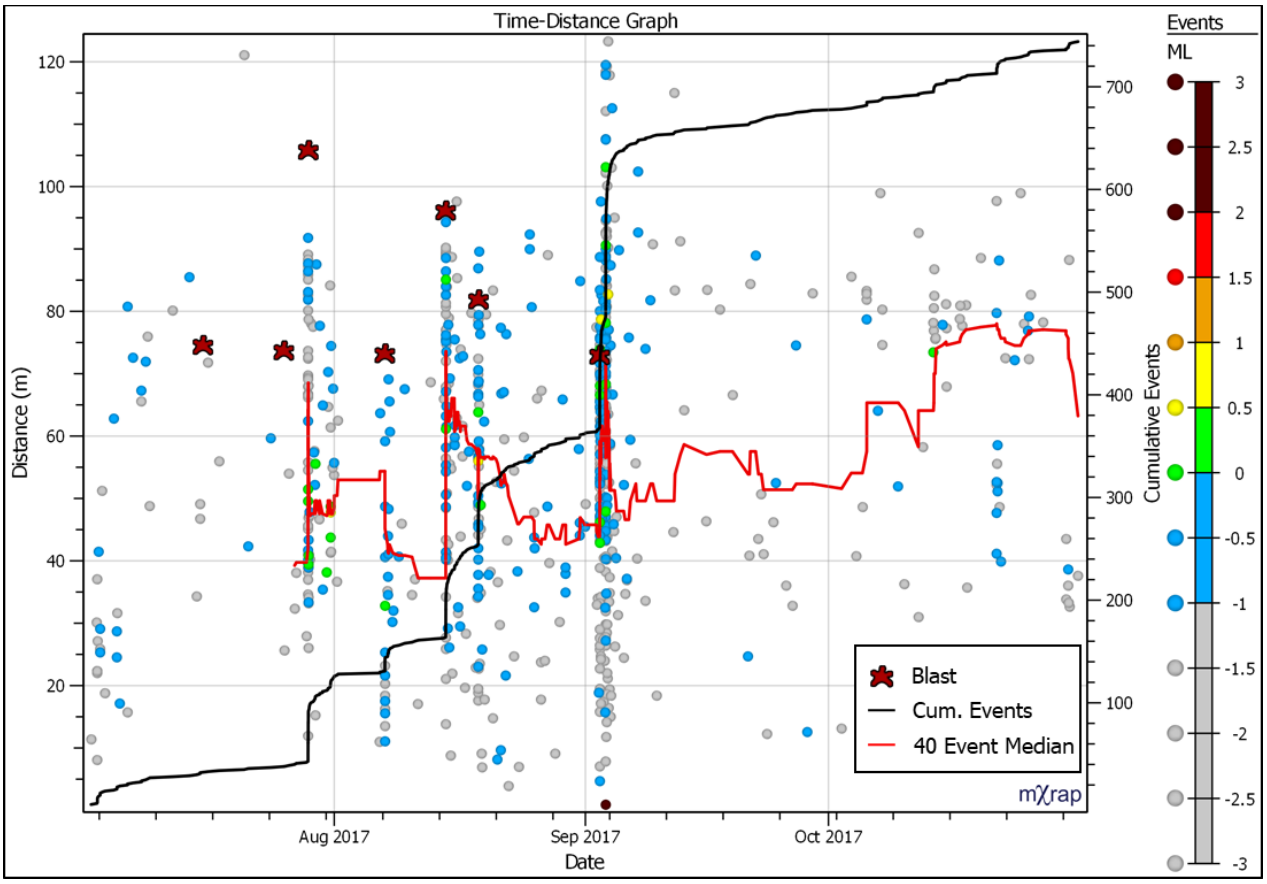

Figure 87 S-MT analysis of seismicity near the NSF. 508 events Mw ≥ -1.5.

Figure 87 shows similar trends to Figure 86. It is useful information to know that the trends occurred in the fault volume because it increases the confidence that the behavior of interest was fault related.

After each blast there is an increase in event rate, characterized by a spike in event rate at the time of a blast, then a gradual decrease to a background rate. The three blasts (Aug. 14, 18 and Sept. 2) prior to the MSE event were unusual. There was a spike in event rate at the blast, but the rate did not return to a background level, but remained high. These three blasts also show coalescing behavior. Beginning with the Aug. 14th blast, the event median migrates 20m towards the MSE hypocenter, showing similar coalescing trends to that in S-LT analysis. The event rate stayed high until the occurrence of the MSE. In the days after the MSE, the event rate returns to

a gentler slope, indicative of a slowed or different failure process. These trends are consistent with increasing deterioration of the fault strength around an asperity.

4.6 Short Term Time Distance Analysis

Short term TDA was useful to identify relevant information in the time frame immediately prior to and after the MSE, including blasting, foreshocks and aftershocks.

4.6.1 M-ST Analysis

M-ST analysis can be viewed in Figure 88.

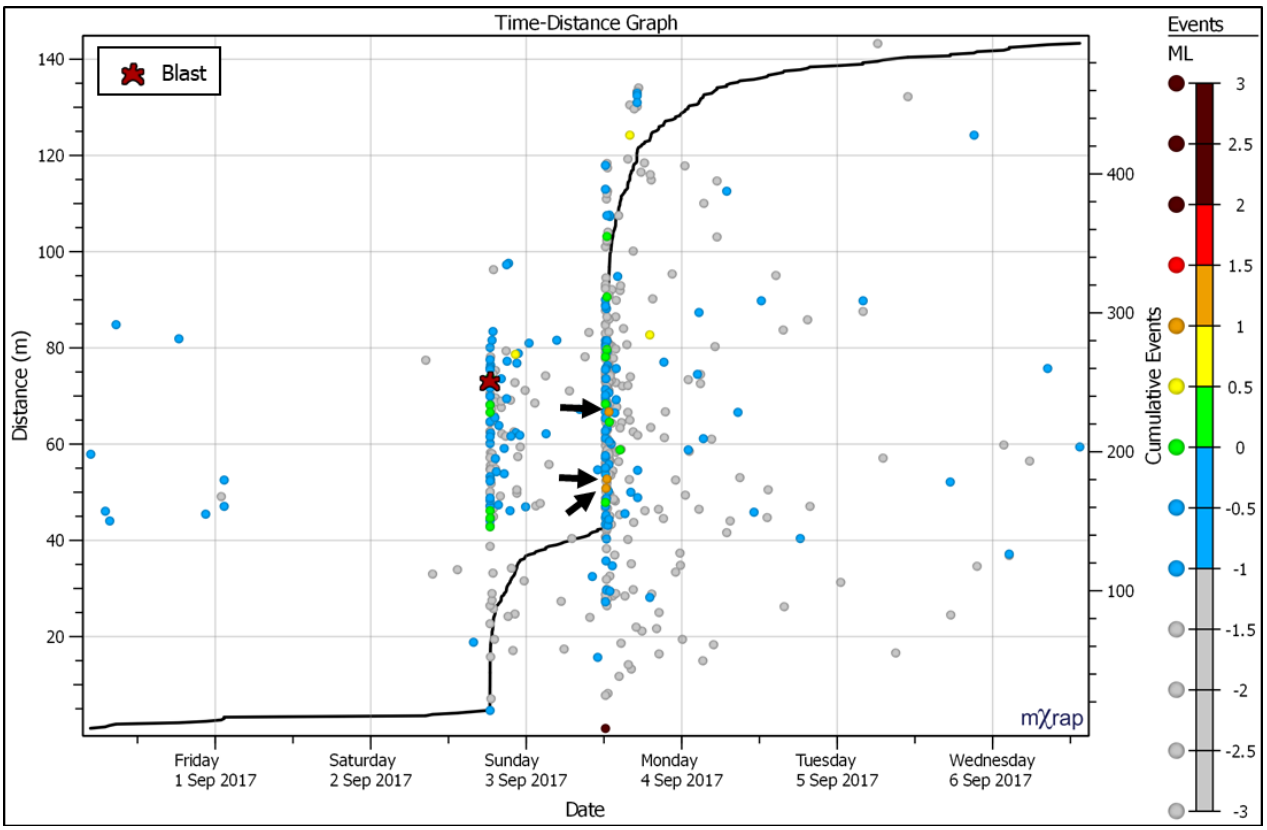

Figure 88 M-ST analysis showing blasting and events in the east abutment of the sill. 494 events Mw ≥ -1.6. The largest three aftershocks are indicated by arrows.

Prior to the blast, the event rate had already been elevated for 19 days, as shown in Figure 87. Eighteen hours prior to the MSE there was a blast at a distance of 75m. After the blast at 18:30 Sept. 2, the event rate increased once more, remaining higher than normal until the MSE

occurred. Since each event represents part of a rockmass failure process and the events appear to be related to the MSE, the increase in event rate can be thought of as an increasing rate of rockmass failure leading up to the MSE.

Three Mw 1-1.5 aftershocks (see black arrows) occurred shortly after the MSE. These large aftershocks occurred 50-75m from the MSE, locating in the sill region on the OBF. Redistribution of strain energy after the main shock is an oft-cited cause of aftershocks (Stein, 1999). It is possible that the energy storage process that resulted in the MSE also contributed to the large aftershocks.

4.6.2 S-ST Analysis

Focus on events in the small fault volume yields additional insights into the MSE failure mechanism. Figure 89 shows S-ST analysis.

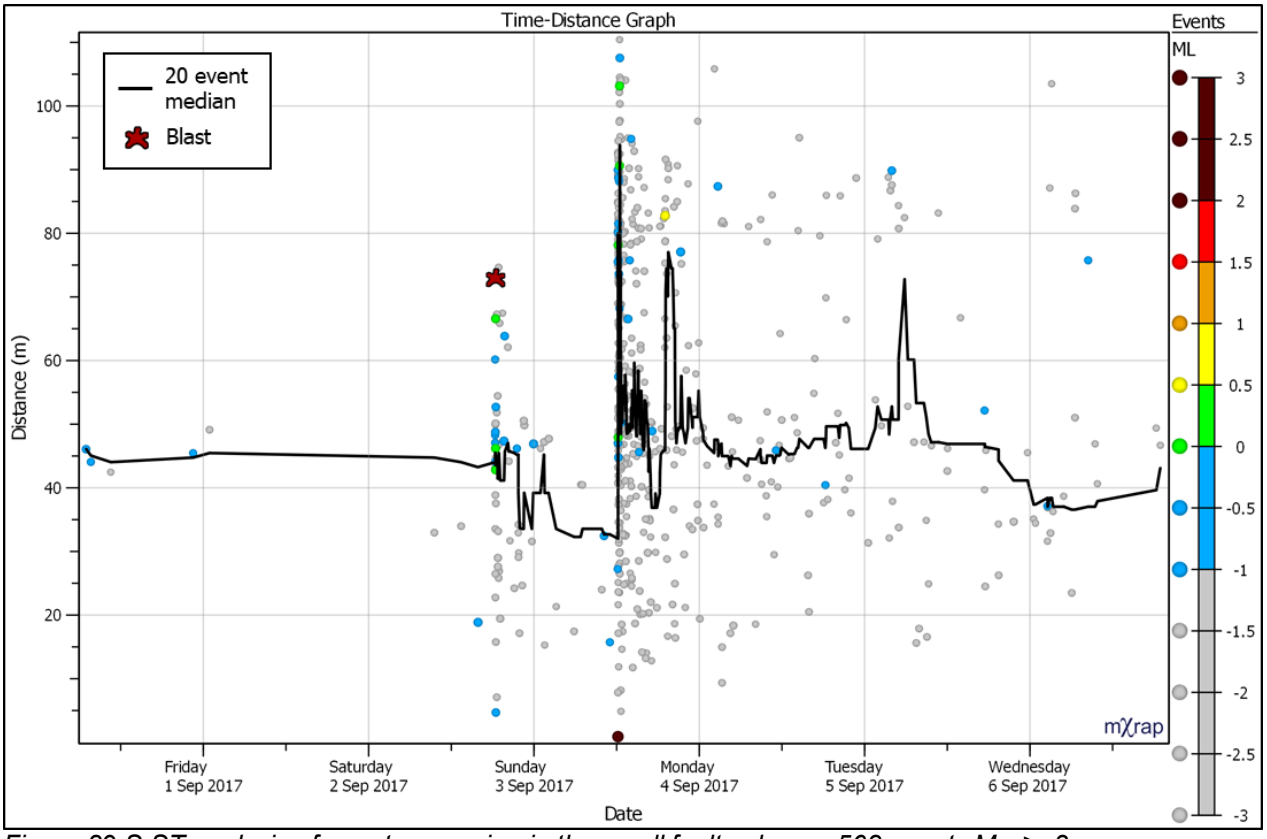

Figure 89 S-ST analysis of events occurring in the small fault volume. 568 events Mw ≥ -3.

S-ST analysis shows trends consistent with other analysis scales. Again, a link between the final blast and the MSE can be observed, evidenced by an increased rate of seismicity. The event median lines shows slight coalescing behavior following the blast, which is a recurring trend through several analysis scales. The blast appears to have triggered the MSE. The possibility of the blast inducing the event is very low, due to the high degree of stress shadowing on 4 sides of the blast. The link between the MSE and this blast is somewhat surprising, but may indicate that the timing of the event may have had more to do with geological factors than blast induced stress change.

Events near the MSE were larger and closer prior to its occurrence than afterwards. Four events Mw -1.0 to 0.0 occurred within 40m in the 20 hours prior to the MSE, but no events greater than Mw -1.0 occurred within the same distance afterwards. No large aftershocks occurred within 50m of the MSE hypocenter, with most aftershocks at distances under 40m being quite small, less than Mw -1.0. The change in behavior is consistent with an asperity being highly stressed prior to the event. Larger, closer precursory events are interpreted as part of an asperity yield or damage process. The absence of significant events near the MSE hypocenter can be explained by looking at the MSE as a de-energizing event. Rupture of the asperity allowed release of stored strain energy to an extent that large seismic events no longer take place in the same region. The many small aftershock events may be the result of stress redistribution or creeping after slip.

4.7 Chapter Summary

4.7.1 Findings Applied to Research Questions

The hypothesis for this study suggested that temporal and spatial variations of seismicity around a MSE hypocenter may provide insights into the proposed asperity failure mode of the event. In Section 4.1.5, four questions were identified for further analyses. These questions are reiterated below, with explanations how the results of the case study may apply.

1) Question: The MSE was triggered by a secondary blast that had backfill on 4 sides. The blast should have been almost entirely stress shadowed. Several primary stopes had already been mined that likely induced greater regional stress change in the sill area. This suggests that the primary cause of the MSE was unlikely to have been blast induced stress change and poorly understood geologic factors may have had significant influence on the timing of the MSE.

New Insight: The results suggest that the deteriorating stability of an asperity controlled the timing of the MSE. Asperity behavior, demonstrated by softening EI/CAV behavior, coalescing foreshocks, and spreading aftershocks were observed in the NSF volume. In order for the MSE to occur, the stability of the asperity had to be lowered to the point where rupture could occur. Generally, failure occurs though either an increase in deviatoric stress or a decrease in strength. The MSE did not occur at times when stress increase was likely the greatest, suggesting a decrease in strength may be the more important factor. Decrease of strength of a fault can occur through coseismic damage to the rockmass. A damage or weakening process was observed prior to the MSE, demonstrated by an increased rate of seismicity, the converging behavior and the occurrence of large events.

2) Question: The MSE was an order of magnitude larger than any previously occurring event in the 1320 sill volume. The MSE was the largest event in a sequence of large events in the sill. The significance of the large magnitude of the MSE is unknown.

New Insight: The results show a converging sequence of events lead up to the MSE, after which, an area around its hypocenter lacked significant seismic events. This sequence is consistent with yield leading to asperity rupture and release of excess stress in the source region. Shear deformation of a large area of the fault was resisted by a smaller strong area, or an asperity. The asperity, as the strongest part of the

fault, attracted seismicity as its strength deteriorated through rock fracture, demonstrated by coalescing foreshock sequences. The rupture of the asperity resulted in mobilization of a larger part of the fault. If the preliminary events are viewed as a failure process that exists only to enable the main fault slip event that occurred with the MSE, the MSE should be the largest magnitude event in the sequence.

3) Question: Prior to the MSE, there was a yearlong increase in the magnitude and frequency of events in the sill. The contribution of this precursory trend to the eventual failure is not understood.

New Insight: The results show that these events predominantly occurred near to the NSF, leading to the assumption that they were fault related. The pre-MSE behaviour of increased magnitude and frequency of events was further understood by the observed coalescence of seismicity towards the MSE and the corresponding strain softening process. These events are interpreted to be part of an asperity yield process.

4) Question: After the MSE, the event rate decreased but large events became more frequent. The relation between the MSE and this change in the characteristic of sill seismicity is unknown.

New Insight: The orebody is somewhat symmetrical, with faults on both sides. After the MSE, the rate of large events decreased in the East abutment and increased in the West abutment. East abutment mining continued with a muted seismic response, consistent with a significant reduction in potential energy. Within 2 weeks of the east abutment Mn 3.2 MSE, the West abutment had a Mn 3.1. West abutment blasting was involved in triggering the second large event, but a link between the two large events seems likely. The results showed that somewhat similar scale failure processes existed for both abutments.

4.7.2 Summary of the Role of TDA and Analysis scales

Table 7 summarizes the analysis scales used in the results sections.

Table 7 Summary of ranges used for analysis scales

Analyses Scale	Spatial Volume	Date Range	Mw ≥ #	# Events Used	Percentile of Total Events	Blast Type
L-LT	Sill	Jan. 2015 - Feb. 2019	0.3	309	99.7	Stope Final
M-LT	East abutment	Jan. 2015 - Feb. 2019	0	403	98.8	Stope Final
S-LT	NSF	Jan. 2015 - Feb. 2019	-0.3	464	97.4	Stope Final
L-MT	Sill	Jun. 2017 - Nov. 2017	-0.6	332	95.0	All Stope Blasts
M-MT	East abutment	Jun. 2017 - Nov. 2017	-1	484	81.6	All Stope Blasts
S-MT	NSF	Jun. 2017 - Nov. 2017	-1.5	508	60.4	All Stope Blasts
L-ST	Sill	Aug. 28 - Sept. 7, 2017	-1.4	467	67.3	All Blasts
M-ST	East abutment	Aug. 28 - Sept. 7, 2017	-1.6	494	58.3	All Blasts
S-ST	NSF	Aug. 28 - Sept. 7, 2017	-2.2	868	0.0	All Blasts

It can be observed that there was a general increase in detail that could be observed at smaller analysis scales. As the spatial volume and time window were decreased, smaller events, and smaller blasts were more useful. In contrast, only large events and larger blasts were useful for large spatial volumes and long term time scales.

A main finding was the coalescence of foreshocks and dispersal of aftershocks. Without use of TDA it would not be obvious that coalescence and dispersal occurred or that they were related to the MSE. Use of multiple spatial scales proved useful, with the large spatial scale showing the shift in seismic hazard from the East to West abutments and the smallest spatial showing evidence of an asperity rupture. Temporal scales identified time periods when unusual patterns of seismicity occurred. The longest temporal scale indicated that the coalescing process was over a year in length while afterwards, the rupture area became permanently absent of significant events (Mw ≥ 0.5). Coloring events by magnitude in TDA indicated the size of the event sequences. Coalescence by larger events tended to exist over the long time period, but was confined to the small NSF volume, indicating the coalescing behavior was likely fault related. Smaller magnitude sequences of coalescing foreshocks could be viewed at shorter time periods.

TDA provided insights into the relation between blasting and seismicity. Induced seismicity is more likely to be spatially and temporally related to blasting than triggered seismicity. Addition of blasts into a TDA chart can give an indication if seismicity is related to blasting. Seismicity that clusters near blasting on a TDA chart are more likely to have been induced by the blast, while events that occur further away are more likely to have been triggered.

It was observed that blasting appeared to accelerate the failure process leading up to the MSE. In the few weeks prior to the MSE, after blasting there was an accelerated rate of seismicity, coinciding with coalescence towards the MSE. After a disturbance, time dependent failure of hard rock tends to accelerate towards failure or decelerate towards stability (Dusseault and Fordham, 1993). Blasting appeared to be an accelerant for the failure process leading to the MSE, in that an increased rate of seismicity was observed to be initiated by the last three blasts, with a migration of seismicity away from the blasts towards the MSE.

Use of TDA and multiple analysis scales enabled and expedited further analyses. Insights provided by TDA helped to identify changes in patterns of seismicity that could be further analyzed through existing tools. One of the main findings was that after the MSE in the East abutment, the seismic hazard of the West abutment increased (Section 4.4.2). This change was observed using L-LT TDA and further explored using other methods. TDA in combination with 3D visual analysis showed exactly where the increased hazard was taking place, which tended to be on faults in the West abutment (Figure 78). The change in hazard was quantified, using the frequency-magnitude relation (Figure 75 - Figure 76), which indicated that after the MSE, the seismic hazard of the East abutment decreased and the seismic hazard of the West abutment increased.

5 Discussion

5.1 Interpretation

5.1.1 Mine Scale Event Failure Process

Coalescence of foreshocks towards the asperity was interpreted to be a sign of asperity weakening. In unconfined compressive testing of rock, fractures have been observed to propagate, join and coalesce as part of a strain softening process (Zhou, Cheng and Feng, 2014; Zhao *et al.*, 2018). Since seismicity is an indirect observation of rock damage, it cannot be explicitly stated what the foreshocks physically mean with regards to rockmass damage; it can only be inferred by drawing parallels to tests and models where a softening process can be observed. In this case study, the coalescence of foreshocks around the MSE hypocenter is conceptually similar to the coalescing damage process in sample scale failure. Sample scale coalescence is a strain softening process. Strain softening is a weakening process in which the strength of a material deteriorates with increased strain. It was shown that the coalescence of foreshocks occurred simultaneously with decreasing EI and increasing CAV, indicative of decreasing stress and increasing deformation, which Mendecki and Van Aswegen (1998) refer to as softening. Source parameters associated with these events, shown in the EI/CAV chart in Figure 81, showed long term softening leading up to the MSE. The presence of the same coalescing weakening process through longer term analysis scales is evidence that the MSE did not occur due to stress change from a single blast but was rather part of a long term failure process in the sill that was ultimately triggered by a blast. The culmination of that failure process in the East abutment was the MSE. After the strongest point in the fault yield system, the asperity, was broken, the source area became unloaded, resulting in stress redistribution and failure processes taking place elsewhere.

An additional sign of asperity weakening was the accelerating event rate around the asperity. In each time scale, an increase in event rate prior to the MSE was observed. Acceleration in the rate of foreshocks is sometimes observed before large events (Nordström, Dineva and Nordlund, 2020). It is not always apparent, however, what an accelerating rate of foreshocks means, whether it is due to a weakening process that permits the large event or a sign of a regional stress increase that concurrently causes the large event (Maeda, 1999). In this case study, the acceleration of foreshocks occurred concurrently with coalescence towards the MSE and long term softening behaviour. Additionally, the MSE was linked to a seemingly low stress change blast. These factors suggest that the foreshocks to the MSE were likely part of the deterioration of the asperity rather than part of a regional stress increase.

The absence of seismicity in the source region after the MSE is consistent with an asperity rupture. The region on the NSF near to the MSE hypocenter area became aseismic after the event, interpreted as de-energized during the asperity rupture. Section 4.4 showed an absence of events Mw ≥ 0.5 within 60-70m of the MSE hypocenter for the three years of available data following the event. The MSE had a source radius of 150m (Table 5), which is much greater than the 60-70m aseismic area. The 150m source radius, however, tends to agree with the extent of fault related damage (Section 4.1.4) aftershocks (Figure 50). The difference between the aseismic area and the calculated source radius leaves ambiguity to the size of the actual source area. Source size models assume a circular source region on a fault, which, while unlikely to be an accurate representation of reality, is a reasonable approach considering the lack of physical information. The maximum displacement at the source takes presumably takes place closest to the hypocenter and decreases towards the outer edges. This assumption is consistent with a greater release of strain energy on the area of the fault closest to the hypocenter, explaining the lack of recorded seismicity in that area in the following years. As mining in the sill continued to progress, so would HW-FW convergence and deformation along structure. After the MSE, there

was an absence of Mw ≥ 0.5 from the fault region surrounding the hypocenter, however, there was an increase in Mw ≥ 0.5 events beyond 60m of the hypocenter into the HW. These events are interpreted to be the outer edges of the MSE rupture area becoming active with significant events, expanding the ruptured area on the fault.

Fifteen days after the East abutment MSE on Sept. 3, a Mn 3.1 occurred at a similar elevation in the opposite abutment on Sept. 18 at a distance of 205 metres. This second event was likely related to the same sill HW-FW convergence process. The influence of a large event triggering other seismicity through static stress change has been observed in both large earthquakes (King, Stein and Lin, 1994) and large mining events (Orlecka-Sikora, 2010). The Sept. 3 MSE likely caused significant stress decrease near the hypocenter, but also may have caused stress increase elsewhere. The West abutment event had a different behaviour than the East abutment event in that there were no foreshocks and it occurred immediately after blasting. It is plausible that the timing of the Sept. 18 Mn 3.1 was coincidental, and independent failure processes existed for each abutment, however, the close timing and similar scale of the failure processes in each abutment suggests otherwise.

5.1.2 Use of the term "Mine Scale"

A multi-year failure process existed on a temporal scale similar to that of a significant part of the mine. Relevant information was gained through analysis of data concurrent with 10 years of mining. Between 2010 and 2015, the sill pillar lacked significant events, but was likely in the process of becoming loaded, evidenced by the excessive release of energy that occurred later. From 2016 to 2017 the asperity failure process occurred, ending with the MSE, which reduced the number of large events in the east abutment. After the MSE, from late 2017 to 2021, a rupture area can be inferred on the NSF around the MSE hypocenter by an absence of significant events, with events taking place on the fault further into the hanging wall, interpreted as the outer edges

of the rupture area. The length of time for the sum of these processes approaches a decade, which is a similar time scale to the mine life.

The MSE was part of a failure process that existed on a spatial scale similar to that of the mine. The geometry of the main mining area at NRS exists over 550m with a footprint of up to 300m on strike and 150m HW-FW. The main orebody of the mine has three stope sequences that merge in two sills, one of which is purported to be a central causational factor in the immense energy release of the MSE. Observations that can give an indication of the spatial scale of the MSE suggest a failure process that existed over a large part of the mine, giving credibility to the use of the term “mine scale” to describe this event. The calculated source radius of the MSE was 150m, suggesting an instance of fault slip on a scale near to the vertical extent of mining. Aftershocks to the MSE were observed near the NSF over a vertical extent of near 300m, which has good agreement with the calculated source size. The aseismic area on the NSF extended approximately 60m into the HW of the MSE hypocenter. Damage was observed near intersections of mine openings with the NSF over five levels, approximately 150m vertical extent. A shift in seismicity was observed from the east abutment of the sill to the west abutment, approximately a 150m distance, again suggesting a mine scale failure process.

The excessive energy released in the MSE appears to be related to a large part of a mining sequence, the extraction of the 1320 sill pillar. Convergent mining fronts, such as sills, are often related to large seismic events (Simser, 2019; Hudyma *et al.*, 1994). The occurrence of the MSE in the region of the sill during sill pillar extraction suggests that mining induced storage of strain energy may have played a large role in the magnitude of the event. The energy release of the MSE, if caused by the convergence of two mining sequences, again suggests that the term “mine scale” is a good term to reference to the energy storage and release process.

5.2 Implications

5.2.1 Analysis scales

This research addresses the problem of selecting appropriate temporal and spatial analysis scales to use to understand large events. Dynamic rock failure exists on a wide range of scales, from the smallest size laboratory acoustic emissions, to mining related microseismicity up to the largest crustal earthquakes. A study of microseismicity related to development blasting needs analysis scales local to the failure region over the duration of the development (Section 4.3.5). In contrast, the spatial and temporal scales needed to analyse the largest megathrust earthquakes can be hundreds of kilometres and hundreds of years (Reddy *et al.*, 2011). The implication is that as the magnitude of a seismic event increases, the spatial and temporal scales needed for analysis must increase. It was shown in this research that for study of a MSE, useful information was gained on similar spatial and temporal scales to a large part of the mine. Changes in the characteristics of seismicity immediately prior to MSEs have been documented to be related to individual blasts or stopes, therefore medium and short term analyses are also necessary to understand contributing factors.

Use of multiple analysis scales can increase understanding of a MSE. In the NRS case study, combinations of three spatial scales and three temporal scales were used to define nine spatial/temporal windows. The purpose of the nine windows were to ensure trends were not missed, and to show the spatial/temporal extent of meaningful trends. Repetition of data and trends was observed, consequently not all nine charts were presented in the results section.

This research also sheds light on appropriate event magnitudes to use for analysis of MSEs. A low magnitude filter was used to limit events to what was considered a reasonable number, using the assumption larger events would be more meaningful to a MSE than smaller events. Analyses with small events tends to contain irrelevant information from multiple failure processes, while on the opposite end of the spectrum, analyses with only the largest events tends to have the problem

of not enough information. In the feature case study, long term changes in rockmass characteristics were especially visible through focus on large events (Mw ≥ 0.0 or higher). Small magnitude seismicity became increasingly useful with smaller temporal/spatial scales, showing a link between blasting, event clusters and converging behavior. Analysis of a subset of the largest events in a population can help reduce the effect of mixed mechanisms and focus on macro scale failure processes.

5.2.2 TDA Importance of Foreshocks

The importance of when and where foreshocks occur may be ambiguous and open to interpretation. TDA provides a simple, easy method to quantitatively analyze foreshocks and aftershocks and identify spatial and temporal trends around the MSE. By simplification of locations of foreshocks and aftershocks to a distance from the hypocenter, TDA makes it easy to observe spatial/temporal changes in seismicity before and after a large event. Foreshocks and aftershocks are often analysed temporally, such as with a MTH chart, or spatially, such as with 3D visual analysis. MTH gives insights into the timing and size of events, but provides little information about where the events are. Three-dimensional visual analysis shows insights into where the events occur relative to mine openings and geologic features, but their timing can be difficult to analyse. TDA transforms (x, y, z) location to distance from a reference point, providing a link between time and location that can be analysed in a simple scatter plot. TDA is simple to understand, which makes potential sources of misinterpretation easy to recognize. While timing and locations of foreshocks can be observed independently through other methods of analysis, only TDA was able to show trends in the relation between time and location, resulting in the observation that foreshocks consistently migrated towards the MSE hypocenter and aftershocks were absent from the rupture area.

Softening behaviour in EI/CAV has been interpreted to be asperity yield, and in South African experience, an early warning of instability (Mendecki and Van Aswegen, 1998). Simultaneous

decrease in EI and increase in CAV has been found to give an indication of dropping stress and increasing deformation, interpreted as initiation of rock failure. This TDA research adds spatial behaviour to the softening process, in this case, showing that softening occurred concurrently with coalescence of foreshocks around the MSE hypocenter.

The coalescence of foreshocks around the MSE is possibly the result of a time dependent yield process. Events appeared to coalesce towards the proposed asperity in space and time. Spatial coalescence suggests decreasing strength of the asperity through gradual deterioration of the remaining strong area on the fault. Temporal coalescence may be evidence that the decrease in strength was a time dependent process. The effect of time dependent failure of hard rock is widely discussed but is still a topic of research. Time dependent failure of hard rock clearly occurs, otherwise all seismicity would occur at the same time as the stress change caused by blasting. The mechanism for time dependency in hard rocks is thought to be driven by propagation of fractures or damage to the rockmass (Dusseault and Fordham, 1993; Malan, 2002). The fact that seismic events occur some time after a stress change suggests the existence of time dependent failure. Large events commonly occur hours or days after blasting, leaving open the question of the role that time dependent processes play in failure. The MSE occurred 18 hours after a blast. The maximum stress increase tends to occur immediately with blasting and this blast was assumed to be a low stress change blast due to stress shadowing of existing stopes. The relation to stress increase from the blast then appears to be low. Any further stress change must then occur through inelastic methods, or fracturing and damage to the rockmass. An asperity damage process has been suggested as the mechanism for the MSE. In this model, the coalescent foreshocks could be part of the time dependent strength decay of the strong asperity. This strength decay appeared to be accelerated by blasting, evidenced by several increases in event rate initiating with blasts.

The scale of this failure process appears to decrease approaching the time of the MSE. It was observed in Sections 4.4-4.6 that a general decrease in the magnitude of converging events occurred with closer time to the MSE. With decreasing time to the MSE, it is plausible that smaller scale damage processes become more influential and yield is controlled by smaller scale fracturing and damage until the final asperity rupture.

5.2.3 TDA with Blasting

While very large events can be related to blasting (Hedley ***et al.***, 2013), the contribution of individual blasts to a MSE is poorly understood. Brown (2018) introduced spatial and temporal parameters to classify events as triggered or induced, those whose magnitudes have similar scales to the stress change from blasting and those that do not. MSEs, by definition, almost always indicate a triggered mechanism, as it is assumed that cumulative mine extraction often plays a key role in generation of the event. TDA provides a simple way to look at relations between blasts and clusters of seismicity over time. Seismic events tend to cluster in space and time, making it possible to simplify event location to a relative distance. Event clusters that are strongly related to blasting tend to have similar distances and times as blasting. Events that are temporally related to blasting but spatially distant are more likely to be triggered. Events that are both temporally and spatially related to blasting tend to be induced. Events that are spatially related but occur long after the blast are possibly part of time dependent failure processes.

An assumption of this research was that blasting contributed to the magnitude of the MSE on the extent of a significant part of the mine, or rather that blasting over a number of years created conditions for excessive energy storage and release associated with a MSE. MSEs have been known to occur simultaneously with blasting or shortly afterwards, have been theorized to be delayed responses to blasting by days or weeks, and have occurred completely without a plausible blast trigger. TDA gives a method to evaluate blast influence or lack of influence. In the feature case study of this thesis, the event appears to have been triggered by a relatively low

stress change blast, demonstrated by a migration of seismicity towards the MSE hypocenter after the blast. Similar converging event sequences were observed to be initiated by blasting over long and medium time periods. Blasts are viewed in this case as contributors to the failure process, but not as individually causational. The failure process can be observed through long, medium and short time scales, with some seismic events being related to blasting and some unrelated to blasting. The contribution of blasting appears to be an acceleration of the failure process, with many blasts over the long term contributing to the eventual asperity failure. The MSE, as a long term failure process, could only occur once conditions for asperity rupture had been reached.

5.2.4 Combining TDA with Other Forms of Analysis

TDA complements other forms of seismic data analysis. This section shows how analysis of spatial and temporal changes in TDA permits insights that are not apparent using common spatial and temporal analysis techniques such as 3D visual analysis and MTH.

Three-dimensional visual analysis is useful to study the relation between event locations, mine openings and geology. After an event occurs, it is often the first and simplest way to get an indication of potential source mechanisms. Figure 90 shows a visualization significant events occurring in the sill from 2015-2020.

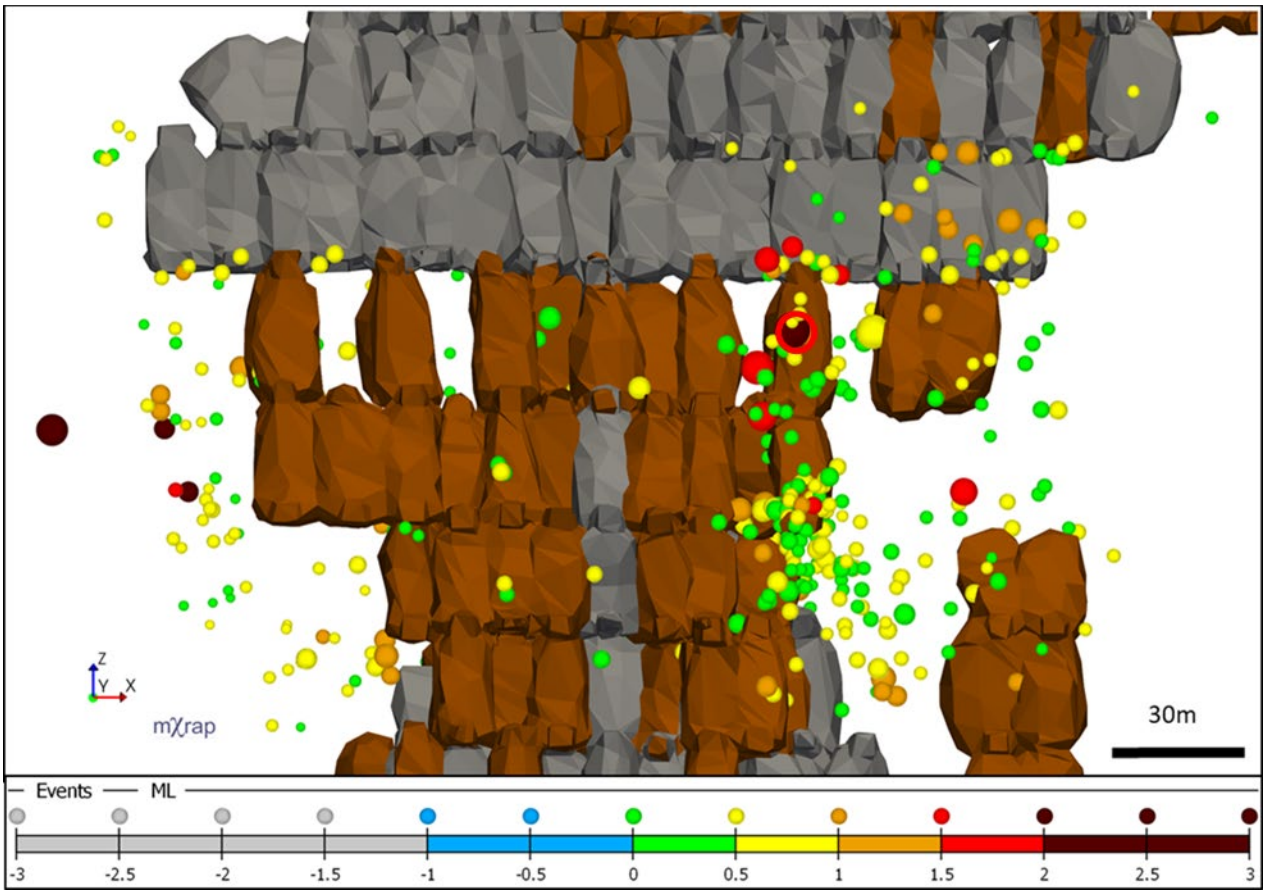

Figure 90 Three-dimensional visual analysis of event locations. 2015-01-01 to 2020-10-01, 415 Mw ≥ 0.3, large sill volumetric filter, mining in period shown in brown, MSE circled in red.

A limitation of 3D visual analysis is that it is difficult to recognize changes in the locations of seismicity over time. Large events can be observed in both abutments of the sill, but the timing of their occurrence and any related failure processes is unknown. Analysis of changes in location is generally done by visual comparison of event locations over subsequent time windows. The length of time window tends to be judgment based and recognition of change requires discernment. If a change is observed, quantification of the change is difficult.

Magnitude time history is a method that can be used to analyse the time, rate and magnitude of seismicity. Figure 91 shows a MTH chart for the same events in Figure 90.

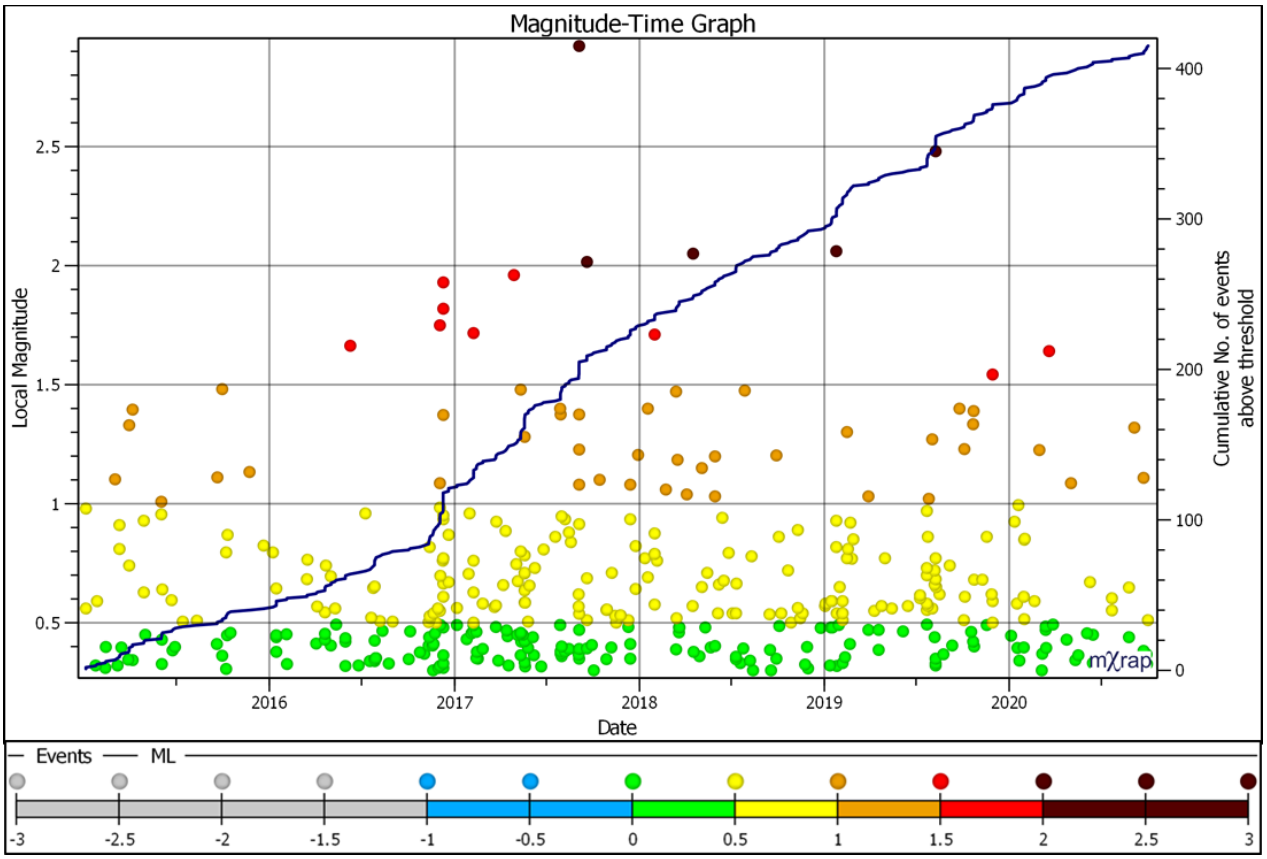

Figure 91 MTH analysis of events. 2015-01-01 – 2020-10-01, 415 Mw ≥ 0.3, Large sill volumetric filter

Insights into the seismic response are gained through looking at MTH. There is a rate increase in late 2016 that coincides with the increased frequency of large events. The frequency of events Mw ≥ 1.0 increases after the MSE. The event rate appears to taper off towards the end date of the chart.

It is only known that events are located in the region of the sill; MTH only provides limited insights into exactly where the events are occurring.

TDA simplifies 4D problem (x,y,z, time) to a 2D problem (distance, time) to permit analysis of spatial changes over time. These changes would be hard to define using any other method. Recognition of these changes can expedite further investigation with other techniques. Figure 92 shows a TDA chart for the events in Figure 90 and Figure 91.

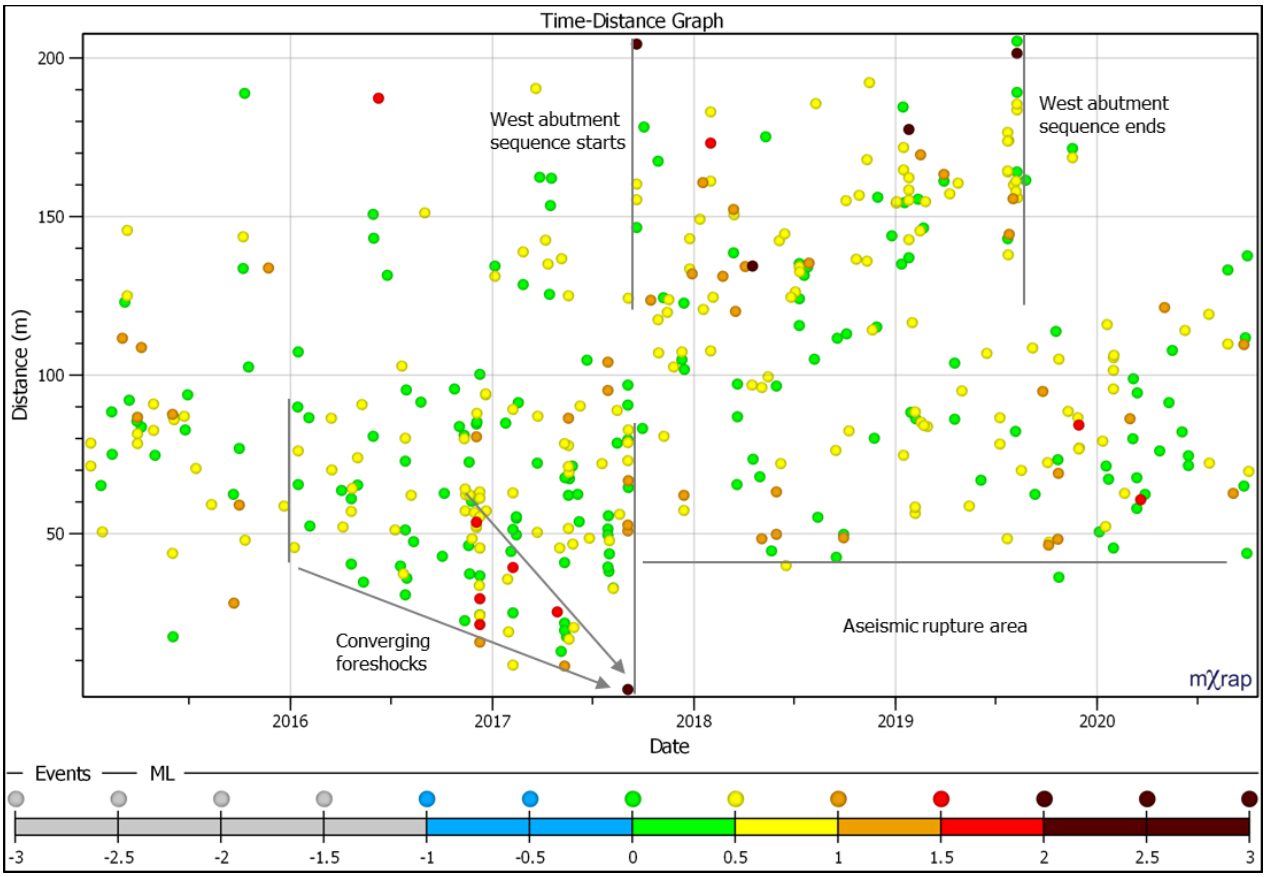

Figure 92 TDA analysis of event locations with reference to the MSE. 2015-01-01 – 2020-10-01, 415 Mw ≥ 0.3, Large sill volumetric filter

Using TDA, it can be observed that events start to coalesce towards the MSE in 2016, increasing in magnitude in late 2016. After the MSE, a region of 40m around the MSE becomes aseismic and a sequence of large events begins in the west abutment, identified in Section 4.4.2. The west abutment sequence continues until mid 2019, ending with another large event.

The benefit of using TDA is that changes in event location can be recognized immediately and can be quantified. It is doubtful that the converging foreshock sequences or the aseismic source region would have been recognized without TDA. Once changes are known to have occurred, they can be further interrogated using other established methods of seismic data analysis.

5.3 Limitations and Assumptions

5.3.1 Assumptions of Stress

Several assumptions were made about stress and deformation in the rockmass based on the geometry of the mine, the in-situ stress direction and knowledge of rockmass yield. A fundamental assumption was that the immense energy released in the MSE was due to excessive stored strain energy in the region of the sill pillar. Generally, the dominant direction of mining induced deformation is towards an extracted orebody. In an orebody elongated along strike, the greatest potential for mining induced elastic deformation tends to be HW-FW convergence. HW-FW deformation is resisted primarily by stiff pillars, pastefill and abutments of the orebody. The regional scale of the sill pillar resulted in a greater resistance to HW-FW deformation over several levels. In the region of the sill, HW-FW convergence lagged behind the rest of other parts of the orebody, resulting in excessive stored strain energy. As the sill was extracted, the amount of load-carrying rock was decreased, resulting in high stress, instability and yield in the remaining rock. The excessive strain energy stored in the rockmass resulted in high magnitude seismic events as the rockmass failure process took place. The largest event at NRS (MSE Mn 3.2 2017-09-03) took place on a fault in the region of the sill. It is assumed that the dominant factor in the high magnitude of this event was stored strain energy in the region of the sill. In essence, the resistance of sill pillar to HW-FW convergence supplied the potential strain energy and the fault provided the path of least resistance to release a large part of that energy.

The research conducted in this NRS case study analyzed seismicity to learn about the rockmass failure process. Seismicity is not prerequisite to deformation, stress or yield, therefore this study was limited to what could be observed and measured through transient seismic waves. It was assumed that in the hard, stiff rockmass at NRS, the most important features of rock yield and rock failure were manifested by seismicity.

It was assumed that if the MSE represented an asperity rupture, the area of rupture would subsequently lack signs of further stress. Long term aseismicity in the region of the hypocenter was observed. Aseismicity simply means the rock is not failing dynamically, and can be associated with two potential rockmass conditions:

1. The rockmass has yielded and further application of stress cannot store enough energy to result in significant seismicity
2. The rockmass is storing energy, but has not yet reached the point of undergoing significant seismicity.

The first condition seems to fit the later observations best. After 2 years and significant mining in the sill, the NSF appeared to react with significant events deeper into the HW. The area on the fault nearby the MSE hypocenter lacked significant events.

5.3.2 Asperity Assumptions

Neither fault asperities nor a rupture area can be entirely physically observed. Asperities are a theoretical model of fault stick-slip that explains behaviour of some types of earthquakes. The properties of the asperity are usually unknown, whether they are caused by a healed fault surface, are related to heterogeneous frictional properties, local area of high clamping stress or other factors. The behaviour of the MSE in this case study was consistent with expected asperity behaviour, but the physical cause of strength heterogeneities on the fault remains unknown.

Temporal converging foreshocks were observed over a several month basis in this case study. It is unknown how pervasive converging foreshocks are in asperity yield.

5.3.3 Limitations of TDA

The primary weakness of TDA is that event clusters in different locations can overlap due to simplification of a location to a distance. TDA graphs distance from a point of interest, such as a MSE, to other events. The distance is indiscriminate, and multiple clusters of seismic events can

overlap, which reduces the meaning and utility of the tool. This overlapping of events can disguise and obscure meaningful trends. Knowledge of where clusters are through simultaneous use of a 3D visual analysis tool, as indicated in Section 4.4.2., minimizes this problem. Clusters in TDA can and should be viewed in a 3D visual analysis in order to improve understanding of the event cluster. Strategic spatially filtering can also be useful to limit the analysis to a known location, for example, in use of the NSF volume to limit events to a planar shape.

Some of the characteristics of this case study that were observed with TDA, such as coalescing foreshocks and outward migration of aftershocks, are unlikely to be behaviours common to all large events. Not all large events or fault events are asperity failures. It is unknown if coalescing foreshocks are only a characteristic of asperity events or if other large events may have similar yield behaviour. Large events occurring without foreshocks being observed is relatively common. It is unlikely that TDA is always useful to analyse MSEs.

5.3.4 Geological Assumptions

This research strongly relied on structural mapping at NRS. There are, however, always unknowns and sources of error in a mine structural geologic model. Faults can only be observed where they intersect tunnels or exploration holes. Interpretation and judgment becomes increasingly necessary in geologically complex environments. Underground structural mapping is typically done by hand on paper, then converted to a 3D electronic model. Creation of the 3D structural model often requires significant assumptions of geological continuity and planarity.

Interpretation of an event mechanism as fault slip is often more difficult than simple location of the event on the plane of the fault. Error and unknowns exist in projection of faults because faults can exist as parallel families or have sets of splays. In a structurally complex system, clear designation of single faults is not always possible. Error exists in event locations, which tends to increase with magnitude. Attempting to filter seismic events to a single fault in a structurally complex system can also be difficult, as seismicity can occur on multiple faults, could be caused

by interaction between faults and could be caused by shear induced fracturing of the sidewalls of the fault.

In the NRS case study, the MSE was inferred to have occurred on the NSF. The evidence for the MSE mechanisms as fault slip is quite strong and most indicators are in agreement. The location, magnitude, S:P, and delayed timing of the event tend to indicate fault slip. The coalescent foreshock sequence occurred within several metres of the projected NSF. The MSE hypocenter was within 10m of the NSF. Aftershocks were more numerous and had a greater spatial extent on the NSF, while the larger aftershocks occurred on the OBF, which is interpreted to be primary slip on the NSF and triggering of slip on the OBF.

Slip direction is a large part of understanding the physical mechanism of the MSE. While TDA can be used to infer some parts of a physical mechanism, it provides no sense of the slip direction. TDA gives some confirmation on which fault slipped, since a coalescing failure process was observed on the NSF. Confidence in which fault actually slipped permits further assumptions to the behaviour of the fault. The occurrence of the MSE in the sill seems to suggest that the shear deformation is dominantly driven by mining induced HW-FW deformation. If this assumption is correct, the side of the fault with the greater amount of void should have a higher relative slip, since it has more freedom to converge. For the MSE occurring on the NSF, a greater amount of mining had taken place at the center of the sill, to the east of the fault, making dextral slip a more reasonable assumption than synstral slip.

5.3.5 MSE Magnitude

The definition of MSEs as mining events that are Mn ≥ 3.0 is somewhat arbitrary. It is possible that events slightly below Mn 3.0 would meet the requirement of being part of a failure process that exists on the scale of the mine. Mn 3.0 was chosen because events of this magnitude are typically recorded by Earthquakes Canada, are uncommon, and have the potential to do extensive

damage. As the magnitude of an event decreases below Mn 3.0, the less likely it is a MSE. As event magnitude increases beyond Mn 3.0, the more likely it is a MSE.

5.4 Data Quality

The consistency, adequacy and completeness of the seismic dataset is critical in using these methods for back analysis. The observations and interpretations made in this research were only possible with the high quality data of NRS. Inference of source mechanism, using even high quality source parameters, is difficult and can be subject to interpretation. Unreliable source parameters in the seismic database adds confusion to an already difficult task.

One of the reasons that made it possible to achieve meaningful results was that NRS has in this case study, a very high quality seismic dataset. Three-dimensional focal coverage of the orebody and an adequate number of triaxial sensors are necessary to ensure good source parameters (Hudyma and Brummer, 2007). NRS is relatively modern for a deep Canadian mine, and unlike most historic mines, was developed after seismic monitoring in mines had become commonplace in the industry. When NRS was developed, the field of mine seismology was established and the collective industry knowledge of how to install a quality seismic array was already high. Canadian mines started prior to 1990 had to gradually improve their seismic systems as hardware, knowledge and need increased. The objectives of seismic monitoring at NRS were clear in the mine planning stage. There was an expectation of seismicity due to experience at similar depth in the Sudbury basin, therefore the seismic system was designed proactively rather than reactively (Simser *et al.*, 2015). The result was that the mine had sensor coverage in place prior to stope blasting, giving the mine an almost complete record of seismicity and good quality source parameters.

The high quality of the seismic dataset has enabled significant research, with numerous publications completed (Jalbout and Simser, 2014; Simser *et al.*, 2015; Abolfazlzadeh and McKinnon, 2017; Carusone and Hudyma, 2017; Butler and Simser, 2018).

The adequacy of source parameters to describe characteristics of rockmass failure was critical in this case study. Location, time, magnitude, energy index, apparent volume, and S:P wave energy were all used to assess factors leading to and after the MSE. These source parameters were in general agreement with the proposed failure mechanism, which increases confidence of their adequacy. Accurate locations are one of the key components in the calculation of source parameters (Hudyma and Brummer, 2007). Figure 16 and Figure 46 indicate that NRS has a very high location accuracy relative to other Canadian mines.

The accuracy of source parameters would be meaningless to this research if there were not continuity of source parameters, meaning there are no subtle shifts in the calculation of source parameters. A survey of 8 mines in Canada, Australia, Sweden and USA showed that all had shifts in calculation of source parameters, leading to the assumption that shifts were fairly commonplace (Morkel, Wesseloo and Harris, 2015). These shifts must be accounted for prior undertaking long term analysis of source parameters. Reprocessing of events to standardize the source parameters is a possible solution. In a time history chart, a shift in calculation of source parameters can be interpreted as a variation in the characteristics of rockmass failure. Because the change is an artefact, any conclusions drawn from the shift are potentially misleading or meaningless. For NRS, there was continuity in source parameters over the time periods in which changes in the characteristics of rockmass failure were inferred.

A complete record of blasting was crucial in understanding the MSE failure process. A stope blast record should at a minimum include times, locations, size, type and a void survey. Without a time, it is unclear whether event rate increases and large events initiate with blasting or are unrelated to blasting. Additionally, the distance from events to blasting cannot be determined without accurate blast locations. The relation of events to blasting can be an indication of source mechanism (Hudyma, 2008). Blasts should be classified by type and ideally by size in order to distinguish high influence from low influence blasts. Type of blast means first blast, second blast,

daylight or slot final, stope final etc. Size is usually measure in blasted tonnage, but blasted volume works just as well. In large and long term analyses, blasts can be too frequent to find meaning. In open stope mining, each stope can have multiple blasts. In large volume and long term analyses, it is difficult to link changes in seismic behaviour to single blasts, but easier to link to a stope life of multiple weeks, therefore only the most important blasts, such as stope final blasts should be analysed. At smaller, shorter analysis scales, meaning can be found from additional detail, and less important blasts such as small production and development blasts can be analysed. If blasts are unlabelled, there is no way to distinguish between more important and less important blasts. Surveys of mining voids are exceptionally helpful to understand the state of the mine sequence at the time of a MSE. In this case study, the location of the MSE in the region of the sill pillar was an important piece of information to understand the location, time and magnitude of the event.

Trustworthy geological information was helpful to understand the mechanism of the MSE. The location of the MSE near the NSF helped to infer a fault slip mechanism and reduced uncertainty about what fault actually slipped. A complete set of mine faults and lithology is important to recognize patterns in seismicity. Without accurate structural geology, it is unlikely this back analysis could have been undertaken.

5.5 Guidance for Use of Analysis Scales

The strategy of combining several spatial and temporal analysis scales in this study is an inelegant but effective approach to back analyze seismic data. What would constitute the most appropriate analysis scales to understand the MSE was unknown; therefore several combinations of spatial and temporal analysis scales were studied. From a starting point with little knowledge of the MSE, it was necessary to err on the side of caution, collecting more rather than less data. Less analysis increases the chances of missing information and more analysis becomes repetitive and tedious. It is likely that when employing this method of combining every temporal analysis scale with every

spatial analysis scale that repetitive information will result. The advantage, however, is a more comprehensive understanding of how the MSE fits into the regional rockmass failure process in space and time.

Selection of specific analysis scales is not completely reproducible and only general guidelines are given, requiring judgment to fine tune temporal and spatial windows to another case study. The overarching approach of using combinations of several temporal and spatial analysis scales attempts to minimize bias and the effect of variability in judgment. It is doubtful that more specific instructions would be useful given the unpredictability of possible conditions of different case studies.

- Large spatial scale: Should be similar in size to a mine sequence. Multiple seismic sources may exist at this scale. The focus should be on spatially capturing the large scale effect of a mining sequence. In the case study, the large spatial scale included the 1320 sill pillar and both abutments.
- Long temporal scale: Should be years in length, similar to the duration of a mine sequence. The purpose of this scale should be to analyze long term affects of mining on the characteristics of seismicity. The length of this scale should coincide with the duration of mining stopes in the large spatial scale.
- Medium spatial scale: Should contain a local mining area of interest, including several stopes. Multiple seismic sources may exist at this scale. The medium spatial scale in this case study was the abutment to the 1320 sill pillar.
- Medium temporal scale: Should be several weeks or months in length, similar to the duration of a 1-2 stope cycles.

- Small spatial scale: Should consist of the volume around the proposed seismic source, such as a single fault and a few stopes or pillars. This spatial scale should attempt to spatially isolate the most probable failure mechanism of the event.
- Small temporal scale: Should be several days and contain 1-2 blasts. Foreshocks, aftershocks and blast triggering mechanisms may be observed.

5.6 Mixed Mechanisms

A primary concern in inferred seismic data analysis is isolation of individual rockmass failure processes. Analysis of seismic events from mixed mechanisms can obscure trends (Rebuli and Kohler, 2014). Common practice in seismic data analysis is to use space-time windows to filter data. These space-time windows can attempt to isolate a single rockmass failure process, such as what was done using the small NSF volume, but occasionally include seismic events from multiple source mechanisms. Attempting to characterise a single source mechanism from a dataset that contains multiple source mechanisms can result in superposition of entirely different trends, resulting in confusing data and difficult or ambiguous interpretation of mechanisms.

The large and medium volumes used in this research likely contained multiple source mechanisms. These volumes were focused on large scale features, the sill pillar in the large volume and the East abutment of the sill pillar in the medium volume. TDA, however, is not necessarily limited by multiple source mechanisms because it can still give an indication of when and where seismic sources are active.

Methods of clustering events have been used to attempt to isolate seismic source mechanisms (Hudyma, 2008; Rebuli and Kohler, 2014; Cortolezzis, 2018). These clustering methods show promise, but are not widely accepted or commonly used at mine sites.

The low magnitude filter used in this case study reduces events from irrelevant source mechanisms. It was demonstrated in Section 4.3.5 that seismicity related to development blasting

had a tendency to be dominated by small events that located close to new development. A fault slip source mechanism has a higher potential magnitude than a development source mechanism, leading to the conclusion the seismogenic failure processes related to each mechanism should exist over different magnitude ranges. Ortlepp and Stacey (1994) proposed ML 0.0 as a maximum magnitude for strainbursting, which is a type of rockbursting that is typically related to a tunnel scale rockmass failure process. It follows that use of a lower ML 0.0 cut-off could eliminate much of the seismicity related to strainbursting. A low magnitude filter, such as used in this research, should reduce the number of events associated with tunnel-scale failure processes, while maintaining a useable number of fault slip events for analysis.

A debated subject in seismicity is if there is a lower magnitude cut-off for fault related events. It has been shown that macro seismicity is not always self similar with micro seismicity (Hudyma, 2008; Amidzic, 2001), but it is not clear whether the lack of self similarity exists across the same source mechanism. Adding complexity is the tendency for fault events to occur without foreshocks, leaving open the question of whether the events related to the fault slip failure process were missed or whether the events occurred at earlier stages in geologic time. Morton, Villaescusa and Thompson, (2019) and Boettcher, McGarr and Johnston, (2009) suggested that completely self similar datasets may include microseismic events for each failure process. It is plausible that the lack of self similarity may be due to mixed mechanisms, with lack of self-similarity occurring due to the difficulty of completely separating seismic populations of differing mechanism.

The existence of coalescent microseismic events in S-ST and S-MT analyses suggest that micro seismic events can play a role in fault slip towards time of the event. These events were observed in the shortest monitoring period prior to the MSE. It is unknown if these smaller events are concealed during time periods when other types of seismicity are more numerous. It is unknown

if the events are actually slip events or part of a rockmass failure process near the fault that may effect the stability of the fault.

It is clear that in S-ST, S-MT and S-LT that while coalescence of foreshocks occurs, not all events in the NSF volume were part of a convergent process. A possible explanation could be that the events are part of a different source mechanism that overlapped the fault. The events could also be a different type of fault event, part of a yield process unrelated to the asperity.

5.7 Finding Meaning in Instability Analysis

EI/CAV can be a difficult form of analysis to use. It has not been found to be a robust predictor of large seismic events, but has in many cases has showed signs of precursory instability (Van Aswegen and Butler, 1993; Mendecki and Van Aswegen, 1998). Classical EI/CAV instability shows a softening process prior to large events. An observable softening process, however, is not a prerequisite to large events. Large events can occur can occur without foreshocks. Large events can occur after increases in driving stress.

In Figure 81 it was observed that EI actually increased for several months after the MSE, signaling high stress events were occurring. In theory, this stress increase should not occur because the MSE should have effectively unloaded the region around the hypocenter. A problem with a region being unloaded, however, is that it releases stress and lack of stress inevitably results in less seismic events from the same source mechanism. Large events have also been found to redistribute static stress (King, Stein and Lin, 1994; Orlecka-Sikora, 2010), which can trigger other source mechanisms existing in the same spatial window, making it possible that the increasing EI events were caused by the initialization of another failure process. Another hypothetical cause is the stabilization and reloading of the source region, similar to the cyclical stick slip process that exists along crustal boundaries.

In this case study, there was confidence in the main findings of EI/CAV for two reasons:

1) EI/CAV exhibited classic softening behaviour; dropping EI and increasing CAV prior to the MSE.

2) The softening events were demonstrated to be part of a coalescent foreshock sequence.

Three factors are thought to contribute to utility of EI/CAV in this case study:

1) A low magnitude cut-off was used was used to limit analysis to the minimum number of the largest events that would still provide meaning, reducing the likelihood of less important failure mechanisms obscuring the trends. As spatial and temporal analysis scales increase, the possibility of mixed mechanisms becomes greater. Inclusion of mixed mechanisms may lead to confused trends, and are more impactful to EI than other source parameters due to EI's lack of scale dependence. A fundamental characteristic of seismicity is the frequency of events decreases with increased magnitude according to a power law (Gutenberg and Richter, 1944). The MSE was the largest magnitude event in the history of the mine. If the MSE can be assumed have a self-similar dataset, that dataset should have a higher proportion of large events than other failure processes. It is likely that as the lower magnitude cut-off increases, the proportion of events related to the MSE will increase relative to unrelated failure processes.

2) EI/CAV was used to recognized changes in seismicity over a long term time frame rather than as a predictor of large events. Lynch and Mendecki (2001) and Jalbout and Simser (2014) both showed meaningful results from pillar yield case studies using EI/CAV over several years. The duration of the EI/CAV analysis in the NRS case study (Figure 81) was 48 months, with a 3 month trailing average used for EI. The long term analysis in the feature case study also showed a long term change in the characteristics of rockmass failure, with a progression from stable to hardening to softening ground conditions. This

progression does not attempt to predict the timing of large events, but rather shows a change in ground conditions that may result in an increase in seismic hazard.

3) The use of the specific NSF volume for instability analysis increased the likelihood that a single rockmass failure process was analysed in the EI/CAV chart. Focus of the NSF volume on a fault increases the likelihood that the events contained in that volume are related to a single fault slip source mechanism. If EI/CAV is purposed to indicate a progression of the rockmass failure from highly stressed → yielding → failed, it should not include other failure processes that can potentially exist at other states of failure.

4) The softening occurred in the NSF volume which was entirely within the region of the sill pillar. Success has been found with EI/CAV in analysing a rockmass that should go through a yield process, such as a diminishing pillar (Lynch and Mendecki, 2001) and a secondary pillar (Jalbout and Simser, 2014). The fault analysed in this case study was part of a large scale pillar that resisted HW-FW convergence. This pillar was under high stress and was expected to undergo a softening regime, with yield and fracturing being manifested in seismicity. It is possible that the softening characteristics observed in the EI/CAV chart in Figure 81 are more pillar characteristics than fault characteristics, with regional softening providing the fault with freedom to slip. The NSF, as an unfavorably oriented pre-existing discontinuity in the sill, had the greatest potential to release stored strain energy in the sill. The behaviour of the NSF could then be thought of as part of the sill pillar failure process rather than as a fault analysed in isolation.

6 Conclusions and Recommendations

6.1 Conclusions

On Sept. 3, 2017 a Mn 3.2 took place at Nickel Rim South mine. The event location was near a north-south trending, steeply dipping fault in the east abutment of a sill pillar. The large magnitude and the spatial extent of aftershocks and damage suggested that this event was part of a failure process that existed over a large part of the mine, leading to the use of the term Mine Scale Event (MSE) to describe the main shock.

The fact that the MSE took place near a fault and was preceded by a significant time period of elevated seismic hazard led to the hypothesis that the MSE may have been caused by the rupture of an asperity. In order to study in seismicity surrounding the MSE, a novel tool was developed called Time-Distance Analysis (TDA), which plots distance from the MSE hypocenter to other seismic events in order to investigate spatial/temporal trends pre and post MSE. Because the spatial and temporal limits of the failure processes that led to the MSE were unknown, a strategy was developed to employ several combinations of spatial and temporal analysis scales in order to systematically interrogate the seismic data.

The results of the back analysis showed that precursory seismicity tended to coalesce around the MSE hypocenter, interpreted as part of a deterioration process. The coalescence occurred simultaneously with trends in EI/CAV that are characteristic of strain softening. Post MSE, significant seismicity was absent on the fault in the region of the hypocenter, and fault seismicity tended to locate further into the mine hanging wall in less disturbed rockmass. The coalescence of seismicity pre MSE and the absence of seismicity post MSE were interpreted to be caused by the rupture of an asperity on the fault, with coalescence representing deterioration of a stressed, failing asperity and absence of seismicity a sign of rupture. Recognition of these spatial/temporal

trends in seismicity was only made obvious by TDA applied methodically through several combinations of analysis scales.

Two novel ideas arose out of this research: TDA and the methodology to apply it to a MSE by filtering seismic data using a combination of analysis scales. TDA showed spatial/temporal changes in seismicity around the MSE that were not obvious using other methods. Use of several combinations of analysis scales for data filtering lead to improved understanding of the processes involved in generation of MSE.

6.2 Recommendations

The methodology proposed in this thesis should be tested with other MSEs of diverse mechanisms. TDA has the potential to reveal trends in time and space around a MSE that are not obvious using other methods. The strategy of using a multiplicity of analysis scales was useful to interrogate seismicity around the event, and will likely be useful when applied to other mine seismicity analysis tools for back analysis of large magnitude seismic events.

Clustering algorithms have been shown to successfully isolate source mechanisms. The approach taken in this research primarily used spatial/volumetric/magnitude filtering to isolate the failure mechanism. The results of this study could potentially be improved or changed by performing TDA on a cluster associate with the MSE.

Coalescent foreshocks seemed to occur in certain magnitude ranges, but was not specifically studied. Foreshock sequences with similar magnitude events converged towards the MSE with somewhat regular spatial/temporal intervals, as visible in Figure 86. These events appear to coalesce towards the time and location of the MSE. If this behaviour is real and pervasive, the implications may be useful to understand asperity failure. Further investigation should determine if converging sequences of events of similar magnitude are common around large asperity events and if they can be identified prior to a large event.

Events were coloured by magnitude in TDA, but the potential exists to use other source parameters such as apparent stress, EI, and S:P to further identify spatio-temporal changes in clustering.

The point of reference used in this study was a point source for a seismic event, but it is possible other references could be used. Use of a blast as a reference point has the potential to show interesting trends between induced and triggered seismicity.

References

Abolfazlzadeh, Y. and McKinnon, S.D. (2017) 'Stress field characterisation in Nickel Rim South Mine using seismic stress inversion', in Wesseloo, J. (ed.) *Deep Mining 2017: Proceedings from the Eighth International Conference on Deep and High Stress Mining*. Perth: Australian Centre for Geomechanics, pp. 247–256.

Aki, K. (1966) 'Generation and propagation of G waves from the Niigata earthquake of June 14, 1964. Part 2. Estimation of earthquake moment, released energy and stress-strain drop from G wave spectrum', *Bulletin of the Earthquake Research Institute*, 44, pp. 73–88.

Aki, K. (1984) 'Asperities, barriers, characteristic earthquakes and strong motion prediction', *Journal of Geophysical Research*, 89(B7), pp. 5867–5872.

Ames, D.E., Davidson, A. and Wodicka, N. (2008) 'Geology of the giant Sudbury polymetallic mining camp, Ontario, Canada', *Economic Geology*, 103(5), pp. 1057–1077.

Amidzic, D. (2001) 'Energy-moment relation and its application', in Van Aswegen, G., Ortlepp, W.D., and Durrheim, R. (eds) *Proceedings of the 5th International Symposium on Rockbursts and Seismicity in Mines*. Johannesburg: South African Institute of Mining and Metallurgy, pp. 509–513.

Berberian, M. (2014) 'Chapter 17 - Earthquake history of Iran', in Berberian, M. (ed.) *Developments in Earth Surface Processes*. New York: Elsevier, pp. 519–628.

Bewick, R. (2013) *Shear Rupture of Massive Brittle Rock under Constant Normal Stress and Stiffness Boundary Conditions*. PhD Thesis. University of Toronto.

Blake, W. and Hedley, D.G.F. (2001) *Rockburst case histories for North American hardrock mines*. Canadian Mining Industry Research Organization.

Boatwright, J. (1984) 'Seismic estimates of stress release', *Journal of Geophysical Research*, 89(B8), pp. 6961–6968.

Boatwright, J. and Fletcher, J. (1984) 'The partition of radiated energy between P and S waves', *Bulletin of the Seismological Society of America*, 74(2), pp. 361–376.

Boettcher, M.S., McGarr, A. and Johnston, M. (2009) 'Extension of Gutenberg-Richter distribution to MW −1.3, no lower limit in sight', *Geophysical Research Letters*, 36(L10307).

Boyd, S. (2021) 'Agnico Eagle Mines provides an update on exploration results for H1 2021: discovery of a new mineralized horizon 400m south of East Gouldie Deposit; additional high-grade gold-copper in footwall zone at Upper Beaver in Kirkland Lake', *Junior Mining Network*, 8 July. Available at: https://www.juniorminingnetwork.com/junior-miner-news/press-releases/1060-tsx/aem/102850-agnico-eagle-provides-an-update-on-exploration-results-for-h1-2021-discovery-of-a-new-mineralized-horizon-400m-south-of-east-gouldie-deposit-additional-high-grade-gold-copper-in-footwall-zone-at-upper-beaver-in-kirkland-lake-exploration-at-hope-bay-confirms-

expansion-potential-of-doris-and-madrid-deposits-drilling-at-kittila-yields-deepest-ore-grade-intersection.html (Accessed: 20 July 2021).

Brady, B.H.G. and Brown, E. (2004) *Rock mechanics for underground mining*. 3rd edn. Dordrecht: Springer.

Brown, L. and Hudyma, M. (2017) 'Identification of stress change within a rock mass through apparent stress of local seismic events', *Rock Mechanics and Rock Engineering*, 50(1), pp. 81–88.

Brown, L. and Hudyma, M. (2018) 'Mining induced seismicity in Canada: a 2017 update', in *Proceedings of Fifty-Second Rock Mechanics/Geomechanics Symposium*. American Rock Mechanics Association, p. 8.

Brown, L.G. (2018) *Quantification of seismic responses to mining using novel seismic response parameters*. PhD Thesis. Laurentian University.

Brummer, R.K. (1999) 'Simple truths about rockbursts keynote lecture', in Hagan, T.O. (ed.) *Second Southern African Rock Engineering Symposium*. Johannesburg: International Society of Rock Mechanics, pp. 6–11.

Brune, J.N. (1970) 'Tectonic stress and the spectra of seismic shear waves from earthquakes', *Journal of Geophysical Research*, 75(26), pp. 4997–5009.

Butler, T. and Simser, B. (2018) 'Early access microseismic monitoring using sensors installed in long boreholes', *Journal of the Southern African Institute of Mining and Metallurgy*, 118(3), pp. 251–257.

Cai, M., Kaiser, P. and Martin, D. (2001) 'Quantification of rock mass damage in underground excavations from microseismic event monitoring', *International Journal of Rock Mechanics and Mining Sciences*, 38(8), pp. 1135–1145.

Carusone, O. (2018) *Interpretation of rock mass yield using apparent stress of microseismic events – examples from Glencore's Nickel Rim South Mine, Sudbury, Ontario*. MASc. Thesis. Laurentian University.

Carusone, O. and Hudyma, M. (2017) 'Variations in apparent stress and energy index as indicators of stress and yielding around excavations', in Hudyma, M. and Potvin, Y. (eds) *First International Conference on Underground Mining Technology*. Perth: Australian Centre for Geomechanics, pp. 205–218.

Castro, L.A.M., Carter, T.G. and Lightfoot, N. (2009) 'Investigating factors influencing fault-slip in seismically active structures', in Diederichs, M.S. and Grasselli, G. (eds) *Proceedings of the 3rd CANUS Rock Mechanics Symposium*, pp. 1–12.

Cook, N.G.W. (1976) 'Seismicity associated with mining', *Engineering Geology*, 10(2), pp. 99–122.

Cormier, V.F. and Gupta, H.K. (1990) 'Seismic attenuation: Observation and measurement', in *Geophysics Encyclopedia of Earth Science*. New York: Springer, pp. 1005–1018.

Cortolezzis, D.M. (2018) *Characterization of seismic sources using sequential spatial clustering and fractal dimension*. PhD Thesis. Laurentian University.

Coulomb, C.A. (1776) 'Essai sur une application des regles des maximis et minimis a quelquels problemesde statique relatifs, a la architecture', *Mem. Acad. Roy. Div. Sav*, 7, pp. 343–387.

Coulson, A. (2009) *Investigation of the pre to post peak strength state and behaviour of confined rock masses using mining induced seismicity*. PhD Thesis. University of Toronto.

Counter, D. (2014) 'Kidd Mine – dealing with the issues of deep and high stress mining – past, present and future', in Hudyma, M. and Potvin, Y. (eds) *Deep Mining 2014: Proceedings from the Seventh International Conference on Deep and High Stress Mining*. Perth: Australian Centre for Geomechanics, pp. 3–22.

Counter, D. (2017) 'Strain and rock bursting at Kidd Creek: support response and recent work on damage measurement systems'. *2017 ACG Strainburst Seminar*, Sudbury.

Diederichs, M.S., Kaiser, P.K. and Eberhardt, E. (2004) 'Damage initiation and propagation in hard rock during tunnelling and the influence of near-face stress rotation', *International Journal of Rock Mechanics and Mining Sciences*, 41(5), pp. 785–812.

Dieterich, J.H. (1972) 'Time-dependent friction in rocks', *Journal of Geophysical Research*, 77(20), pp. 3690–3697.

Dieterich, J.H. (1978) 'Time-dependent friction and the mechanics of stick-slip', *Pure and Applied Geophysics*, 116(4), pp. 790–806.

Disley, N. (2014) 'Seismic risk and hazard management at Kidd Mine', in Hudyma, M. and Potvin, Y. (eds) *Deep Mining 2014: Proceedings from the Seventh International Conference on Deep and High Stress Mining*. Perth: Australian Centre for Geomechanics, pp. 107–121.

Disley, N. (2018) 'Destress stope sequence response in the south abutment of "D" Mine'. *Workshop - Evaluating Seismic Hazard in Canadian Mines*, Laurentian University, 10 October.

Drover, C. and Villaescusa, E. (2019) 'A comparison of seismic response to conventional and face destress blasting during deep tunnel development', *Journal of Rock Mechanics and Geotechnical Engineering*, 11(5), pp. 965–978.

Duan, W., Wesseloo, J. and Potvin, Y. (2015) 'Evaluation of the adjusted rockburst damage potential method for dynamic ground support selection in extreme rockburst conditions', in Potvin, Y. (ed.) *International Seminar on Design Methods in Underground Mining*. Perth: Australian Centre for Geomechanics, pp. 399–418.

Dusseault, M.B. and Fordham, C.J. (1993) 'Chapter 6 - Time-dependent behavior of rocks', in Hudson, J.A. (ed.) *Rock Testing and Site Characterization*. Oxford: Pergamon, pp. 119–149.

Earthquakes Canada (2021) 'Earthquake search (on-line bulletin)'. Natural Resources Canada. Available at: http://earthquakescanada.nrcan.gc.ca/stndon/NEDB-BNDS/bulletin-en.php (Accessed: 22 January 2021).

Gay, N.C. and Ortlepp, W.D. (1978) 'The anatomy of a mining induced fault zone', *Geological Society of America Bulletin*, 90(1), pp. 47–58.

Gibowicz, S. and Kijko, A. (1994) *An introduction to mining seismology*. Cambridge, Massachusetts: Academic Press.

Gibowicz, S. and Lasocki, S. (2001) 'Seismicity induced by mining: ten years later', in *Advances in Geophysics*, pp. 39–181.

Gibowicz, S.J. (1990) 'The mechanism of seismic events induced by mining: a review', in Fairhurst, C. (ed.) *Proceedings of the Second International Symposium on Rockbursts and Seismicity in Mines*. Rotterdam: Blakema, pp. 3–27.

Glencore (2018) *Nickel Rim South Mine Design Document*. Internal report.

Gonzalez-Huizar, H. and Velasco, A.A. (2011) 'Dynamic triggering: stress modeling and a case study', *Journal of Geophysical Research: Solid Earth*, 116(B2), pp. 1–13.

Goodfellow, S.D. and Young, R.P. (2014) 'A laboratory acoustic emission experiment under in situ conditions', *Geophysical Research Letters*, (41), pp. 3422–3430.

Grech, R. (2021) *Glencore approves further drilling in hopes of extending Kidd mine life*, *Timmins Press*. Available at: https://timminspress.com/news/local-news/glencore-approves-further-drilling-in-hopes-of-extending-kidd-mine-life (Accessed: 20 July 2021).

Gudmundsson, A. (2014) 'Elastic energy release in great earthquakes and eruptions', *Frontiers in Earth Sciences*, 2(10), pp. 1–12.

Gutenberg, B. and Richter, C.F. (1944) 'Frequency of earthquakes in California', *Bulletin of the Seismological Society of America*, 34(4), pp. 185–188.

Hanks, T.C. and Kanamori, H. (1979) 'A moment magnitude scale', *Journal of Geophysical Research: Solid Earth*, 84(B5), pp. 2348–2350.

Hanks, T.C. and Thatcher, W. (1972) 'A graphical representation of seismic source parameters', *Journal of Geophysical Research*, 77(23), pp. 4393–4405.

Heal, D., Hudyma, M. and Vezina, F. (2005) 'Seismic hazard at Agnico-Eagle's LaRonde mine using MS-RAP', in *Proceedings of the CIM Maintenance Engineering and Mine Operators Conference*. Canadian Institute of Mining.

Heal, D., Potvin, Y. and Hudyma, M. (2006) 'Evaluating Rockburst Damage Potential in Underground Mining', in *Golden Rocks 2006 - The 41st U.S. Symposium on Rock Mechanics*. American Rock Mechanics Association.

Hedley, D.G.F. (1991) *A Five-year review of the Canada-Ontario industry rockburst project*. CANMET Special Report SP90-4E. Ottawa: Canada Communication Group.

Hedley, D.G.F. (1992) *Rockburst Handbook for Ontario Hardrock Mines*. CANMET Special Report SP92-1E. Ottawa: Canada Communication Group.

Hedley, D.G.F., Blake, W., Andrieux, P.P., Erling, N., Phipps, D., Simser, B. and Swan, G. (2013) *Case studies for update to Canadian rock burst handbook*. Canadian Mining Industry Research Organization.

Helmstetter, A. and Sornette, D. (2003) 'Foreshocks explained by cascades of triggered seismicity', *Journal of Geophysical Research: Solid Earth*, 108(B10), p. 2457.

Henry, C. and Das, S. (2001) 'Aftershock zones of large shallow earthquakes: Fault dimensions, aftershock area expansion and scaling relations', *Geophysical Journal International*, 147(2), pp. 272–293.

Hirata, T., Satoh, T. and Ito, K. (1987) 'Fractal structure of spatial distribution of microfracturing in rock', *Geophysical Journal of the Royal Astronomical Society*, 90(2), pp. 369–374.

Hoek, E., Kaiser, P. and Bawden, W.F. (1995) *Support of underground excavations in hard rock*. Mining Research Directorate and Universities Research Incentive Fund.

Hou, P., Cai, M., Zhang, X. and Feng, X. (2021) 'Post-peak Stress–Strain Curves of Brittle Rocks Under Axial- and Lateral-Strain-Controlled Loadings', *Rock Mechanics and Rock Engineering* [Preprint]. doi:10.1007/s00603-021-02684-9.

Hsu, Y.-J., Simons, M., Avouac, J.-P., Galetzka, J., Sieh, K., Chlieh, M., Natawidjaja, D., Prawirodirdjo, L. and Bock, Y. (2006) 'Frictional afterslip following the 2005 Nias-Simeulue earthquake, Sumatra', *Science*, 312(5782), pp. 1921–1926.

Hudyma, M. (2008) *Analysis and interpretation of clusters of seismic events in mines*. PhD Thesis. University of Western Australia.

Hudyma, M. and Brown, L. (2020) 'Using seismic data to identify temporal increases in mining induced stress', in *Eurock 2020*. International Society of Rock Mechanics.

Hudyma, M., Brown, L. and Cortolezzis, D. (2016) 'Seismic risk in Canadian mines', in *Proceedings of the CIM Maintenance Engineering and Mine Operators Conference*. Canadian Institute of Mining.

Hudyma, M. and Brummer, R. (2007) 'Seismic monitoring in mines - design, operation, tricks and traps', in *1st Canada – U.S. Rock Mechanics Symposium*. American Rock Mechanics Association.

Hudyma, M., Mikula, P. and Heal, D. (2003) 'Seismic monitoring in mines – old technology – new applications', in *Proceedings of the 1st Australasian Ground Control in Mining Conference*. Sydney: University of New South Wales School of Mining Engineering, pp. 201–218.

Hudyma, M. and Potvin, Y. (2010) 'An Engineering Approach to Seismic Risk Management in Hardrock Mines', *Rock Mechanics and Rock Engineering*, 43(6), pp. 891–906.

Hudyma, M., Potvin, Y., Grant, D., Milne, D., Brummer, R.K. and Board, M. (1994) 'Geomechanics of sill pillar mining in rockburst prone conditions', in *Proceedings of the 1st North American Rock Mechanics Symposium*. American Rock Mechanics Association.

Ide, S. and Aochi, H. (2005) 'Earthquakes as multiscale dynamic ruptures with heterogeneous fracture surface energy', *Journal of Geophysical Research: Solid Earth*, 110(B11).

Jalbout, A. and Simser, B. (2014) 'Rock mechanics tools for mining in high stress ground conditions at Nickel Rim South Mine', in Hudyma, M. and Potvin, Y. (eds) *Deep Mining 2014: Proceedings from the Seventh International Conference on Deep and High Stress Mining*. Perth: Australian Centre for Geomechanics, pp. 189–208.

James, J., Rangasamy, T. and Petho, S. (2007) 'Excess shear stress analysis of seismicity associated with dykes', in Potvin, Y. (ed.) *Fourth International Seminar on Deep and High Stress Mining*. Perth: Australian Centre for Geomechanics, pp. 21–30.

Kagan, Y. and Knopoff, L. (1976) 'Statistical search for non-random features of the seismicity of strong earthquakes', *Physics of the Earth and Planetary Interiors*, 12(4), pp. 291–318.

Kagan, Y.Y. and Jackson, D.D. (1991) 'Seismic gap hypothesis: ten years after', *Journal of Geophysical Research: Solid Earth*, 96(B13), pp. 21419–21431.

Kaiser, P.K. and Cai, M. (2013) 'Critical review of design principles for rock support in burst-prone ground – time to rethink!', in Potvin, Y. and Brady, B.H.G. (eds) *Ground Support 2013: Proceedings of the Seventh International Symposium on Ground Support in Mining and Underground Construction*. Perth: Australian Centre for Geomechanics, pp. 3–37.

Kaiser, P.K., McCreath, D. and Tannant, D. (1996) *Rockburst research handbook.* Sudbury: Canadian Mining Industry Research Organization.

Kalenchuk, K.S., Mercer, R. and Williams, E. (2017) 'Large-magnitude seismicity at the Westwood mine, Quebec, Canada', in Wesseloo, J. (ed.) *Deep Mining 2017: Proceedings from the Eighth International Conference on Deep and High Stress Mining*. Perth: Australian Centre for Geomechanics, pp. 89–101.

Kamogawa, M., Nanjo, K.Z., Izutsu, J., Orihara, Y., Nagao, T. and Uyeda, S. (2019) 'Nucleation and cascade features of earthquake mainshock statistically explored from foreshock seismicity', *Entropy*, 21(4), p. 421.

Kanamori, H. and Rivera, L. (2006) 'Energy partitioning during an earthquake', in *Earthquakes: Radiated Energy and the Physics of Faulting*. American Geophysical Union, pp. 3–13.

Kayal, J.R. (2008) *Microearthquake seismology and seismotectonics of South Asia*. New York: Springer.

Kijko, A. and Funk, C. (1994) 'The assessment of seismic hazards in mines', *Journal of the South African Institute of Mining and Metallurgy*, 94(7), pp. 179–185.

King, G., Stein, R. and Lin, J. (1994) 'Static stress changes and the triggering of earthquakes', *Bulletin - Seismological Society of America*, 84(3), pp. 935–953.

Lay, T. and Kanamori, H. (1981) 'An asperity model of large earthquake sequences', in Simpson, D. and Richards, P.G. (eds) *Earthquake prediction: an international review - Maurice Ewing series*. American Geophysical Union, pp. 579–592.

Lebel, G.R., Quesnel, W.J.F. and Glover, W. (1987) 'An analysis of rockburst events during the sinking of Macassa No. 3 shaft', in *89th Annual General Meeting of the CIM*. Canadian Institute of Mining.

Legge, N. and Spottiswoode, S.M. (1987) 'Fracturing and microseismicity ahead of a deep gold mine stope in the pre-remnant and remnant stages of mining', in *Proceedings of the 6th International Conference on Rock Mechanics*. International Society of Rock Mechanics.

Lenhardt, W.A. (1988) 'Some observations regarding the influence of geology on mining induced seismicity at Western Deep Level', in *Proceedings of 1st Regional Conference for Africa - Rock Mechanics in Africa*. South African National Group on Rock Mechanics, pp. 45–48.

Lenhardt, W.A. (1992) 'Seismicity associated with deep-level mining at Western Deep Levels Limited', *Journal of the South African Institute of Mining and Metallurgy*, 92(5).

Lockner, D. (1993) 'The role of acoustic emission in the study of rock fracture', *International Journal of Rock Mechanics and Mining Sciences & Geomechanics Abstracts*, 30(7), pp. 883–899.

Lynch, R. and Mendecki, A. (2001) 'High-resolution seismic monitoring in mines', in *Proceedings of the 5th International Symposium on Rockbursts and Seismicity in Mines*. Johannesburg: South African Institute of Mining and Metallurgy, pp. 19–24.

Ma, X., Westman, E., Slaker, B., Thibodeau, D. and Counter, D. (2018) 'The b-value evolution of mining-induced seismicity and mainshock occurrences at hard-rock mines', *International Journal of Rock Mechanics and Mining Sciences*, 104, pp. 64–70.

Maeda, K. (1999) 'Time distribution of immediate foreshocks obtained by a stacking method', in Wyss, M., Shimazaki, K., and Ito, A. (eds) *Seismicity Patterns, their Statistical Significance and Physical Meaning*. Basel: Birkhäuser (Pageoph Topical Volumes), pp. 381–394.

Malan, D. (2002) 'Simulating the time-dependent behaviour of excavations in hard rock', *Rock Mechanics and Rock Engineering*, 35(4), pp. 225–254.

Martin, C.D. and Chandler, N.A. (1994) 'The progressive fracture of Lac du Bonnet granite', *International Journal of Rock Mechanics and Mining Sciences & Geomechanics Abstracts*, 31(6), pp. 643–659.

Martin, C.D., Christiansson, R. and Soederhaell, J. (2001) *Rock stability considerations for siting and constructing a KBS-3 repository based on experiences from Aespoe HRL, AECL's URL, tunnelling and mining*. Technical Report TR-01-38. Sweden, p. 94.

Martin, C.D. and Maybee, W.G. (2000) 'The strength of hard-rock pillars', *International Journal of Rock Mechanics and Mining Sciences*, 37(8), pp. 1239–1246.

McBeck, J., Mair, K. and Renard, F. (2021) 'Decrypting healed fault zones: how gouge production reduces the influence of fault roughness', *Geophysical Journal International*, 225(2), pp. 759–774.

McCann, W.R., Nishenko, S.P., Sykes, L.R. and Krause, J. (1979) 'Seismic gaps and plate tectonics: seismic potential for major boundaries', *Pure and Applied Geophysics*, 117(6), pp. 1082–1147.

McGarr, A., Simpson, D. and Seeber, L. (2002) 'Case Histories of Induced and Triggered Seismicity', in *International Handbook of Earthquake and Engineering Seismology*. International Association of Seismology & Physics of the Earth's Interior.

McKinnon, S.D. (2006) 'Triggering of seismicity remote from active mining excavations', *Rock Mechanics and Rock Engineering*, 39(3), pp. 255–279.

McLean, S.A., Straub, K.H. and Stevens, K.M. (2005) in Mungall, J.E. (ed.) *Chapter 16 - The discovery and characterization of the Nickel Rim South deposit, Sudbury, Ontario*. Mineralogical Association of Canada, (Exploration for Platinum-Group Elements Deposits).

Mendecki, A. (1993) 'Real time quantitative seismology in mines keynote address', in Young, R.P. (ed.) *Proceedings from the 3rd International Symposium on Rockbursts and Seismicity in Mines*. Rotterdam: Balkema, pp. 287–295.

Mendecki, A., Napier, J., Ilchev, A. and Sellers, E. (2001) 'Fundamental aspects of the integration of seismic monitoring with numerical modelling', in *GAP 603*. Safety in Mines Research Advisory Committee, pp. 1–152.

Mendecki, A. and Van Aswegen, G. (1998) 'System stiffness and seismic characteristics - a case study', in Ando, M. (ed.) *International Workshop on Frontiers in Monitoring Science and Technology for Earthquake Environments*. Japan.

Mendecki, A.J., Lynch, R. and Malovichko, D. (2010) 'Routine micro-seismic monitoring in mines', in *Australian Earthquake Engineering Society 2010 Conference*. Australian Earthquake Engineering Society.

Mendecki, A.J., Malovichko, A. and Malovichko, D. (2013) 'Mine seismology: glossary of selected terms', in *8th International Symposium on Rockbursts and Seismicity in Mines*. Geophysical Survey of the Russian Academy of Sciences.

Mining-technology.com Staff (2019) *The top ten deepest mines in the world*. Available at: https://www.mining-technology.com/features/feature-top-ten-deepest-mines-world-south-africa/ (Accessed: 11 June 2021).

Mogi, K. (1962) 'Magnitude frequency relations for elastic shocks accompanying fractures of various materials and some related problems in earthquakes', *Bulletin of the Earthquake Research Institute*, 40, pp. 831–853.

Mogi, K. (1979) 'Two Kinds of Seismic Gaps', in Wyss, M. (ed.) *Earthquake Prediction and Seismicity Patterns*. Basel: Birkhäuser, pp. 1172–1186.

Mori, J. and Abercrombie, R.E. (1997) 'Depth dependence of earthquake frequency-magnitude distributions in California: implications for rupture initiation', *Journal of Geophysical Research: Solid Earth*, 102(B7), pp. 15081–15090.

Morissette, P. (2015) *A ground support design strategy for deep underground mines subjected to dynamic loading conditions*. Ph.D. Thesis. University of Toronto.

Morkel, I., Wesseloo, J. and Harris, P. (2015) 'Highlighting and quantifying seismic data quality concerns', in Dight, P. (ed.) *Ninth International Symposium on Field Measurements in Geomechanics*. Perth: Australian Centre for Geomechanics, pp. 539–549.

Morkel, I., Wesseloo, J. and Potvin, Y. (2019) 'The validity of Es/Ep as a source parameter in mining seismology', in Joughin, W. (ed.) *Deep Mining 2019: Proceedings of the Ninth International Conference on Deep and High Stress Mining*. Johannesburg: The Southern African Institute of Mining and Metallurgy.

Morton, E., Villaescusa, E. and Thompson, A. (2019) 'Self-similarity in rock fracturing and the behaviour of large-scale faults in the mining environment', in Joughin W (ed.) *Deep Mining 2019: Proceedings of the Ninth International Conference on Deep and High Stress Mining*. Johannesburg: The Southern African Institute of Mining and Metallurgy, pp. 413–425.

Nordström, E., Dineva, S. and Nordlund, E. (2017) 'Source parameters of seismic events potentially associated with damage in block 33/34 of the Kiirunavaara mine (Sweden)', *Acta Geophysca*, 65(6), pp. 1229–1242.

Nordström, E., Dineva, S. and Nordlund, E. (2020) 'Back analysis of short-term seismic hazard indicators of larger seismic events in deep underground mines (LKAB, Kiirunavaara Mine, Sweden)', *Pure and Applied Geophysics*, 177(2), pp. 763–785.

Nuttli, O.W. (1973) 'Seismic wave attenuation and magnitude relations for eastern North America', *Journal of Geophysical Research*, 78(5), pp. 876–885.

Olson, E.L. and Allen, R.M. (2005) 'The deterministic nature of earthquake rupture', *Nature*, 438(7065), pp. 212–215.

Omori, F. (1894) 'On the aftershocks of earthquakes', *Journal of the College of Science, Imperial University of Tokyo*, 7, pp. 111–120.

Orlecka-Sikora, B. (2010) 'The role of static stress transfer in mining induced seismic events occurrence, a case study of the Rudna mine in the Legnica-Glogow Copper District in Poland', *Geophysical Journal International*, 182(2), pp. 1087–1095.

Ortlepp, W. (2005) 'RaSiM comes of age: a review of the contribution to the understanding and control of mine rockbursts', in Potvin, Y. and Hudyma, M. (eds) *Proceedings of the 6th International Symposium on Rockbursts and Seismicity in Mines*. Perth: Australian Centre for Geomechanics, pp. 3–20.

Ortlepp, W.D. (1998) 'Stress and how it leads to seismicity', in *ACG Workshop: Mine Seismicity and Rockburst Risk Management in Underground Mines*. Perth: Australian Centre for Geomechanics.

Ortlepp, W.D. and Stacey, T.R. (1994) 'Rockburst mechanisms in tunnels and shafts', *Tunnelling and Underground Space Technology*, 9(1), pp. 59–65.

Parsons, T. (2005) 'A hypothesis for delayed dynamic earthquake triggering', *Geophysical Research Letters*, 32(4), pp. 1–4.

Rebuli, D. and Kohler, S. (2014) 'Using clustering algorithms to assist short-term seismic hazard analysis in deep South African mines', in Hudyma, M. and Potvin, Y. (eds) *Deep Mining 2014: Proceedings from the Seventh International Conference on Deep and High Stress Mining*. Perth: Australian Centre for Geomechanics, pp. 699–708.

Rebuli, D. and Van Aswegen, G. (2013) 'Short Term Hazard Assessment in S. A. Gold Mines', in Malovichko, A. and Malovichko, D. (eds) *8th International Symposium on Rockbursts and Seismicity in Mines*. Geophysical Survey of the Russian Academy of Sciences, pp. 323–331.

Reddy, C., Arora, S., Sunil, P.S. and Prajapati, S. (2011) 'Earthquake related deformation cycle: perspectives from 2004 Sumatra and 2010 Chile mega-earthquakes', *Disaster Advances*, 4(2), pp. 13–21.

Richter, C.F. (1935) 'An instrumental earthquake magnitude scale', *Bulletin of the Seismological Society of America*, 25(1), pp. 1–32.

Scholz, C.H. (1968) 'The frequency-magnitude relation of microfracturing in rock and its relation to earthquakes', *Bulletin of the Seismological Society of America*, 58(1), pp. 399–415.

Scholz, C.H. (2010) 'Large earthquake triggering, clustering, and the synchronization of faults', *Bulletin of the Seismological Society of America*, 100(3), pp. 901–909.

Scholz, C.H. (2015) 'On the stress dependence of the earthquake b value', *Geophysical Research Letters*, 42(5), pp. 1399–1402.

Schwartz, S.Y. and Ruff, L.J. (1987) 'Asperity distribution and earthquake occurrence in the southern Kurile Islands arc', *Physics of the Earth and Planetary Interiors*, 49(1), pp. 54–77.

Selvadurai, P.A. and Glaser, S.D. (2015) 'Laboratory-developed contact models controlling instability on frictional faults', *Journal of Geophysical Research: Solid Earth*, 120(6), pp. 4208–4236.

Simser, B. (2006) 'Strategic and Tactical Approaches to Mining at Depth at Xstrata Nickel's Craig Mine', in Hadjigeorgiou, J. and Grenon, M. (eds) *Proceedings of the International Conference on Challenges in Deep and High Stress Mining*. Perth: Australian Centre for Geomechanics, p. 14.

Simser, B., Deredin, R., Jalbout, A. and Butler, T. (2015) 'Use of Microseismic Monitoring Data as an Aid to Rock Mechanics Decision Making and Mine Design Verification', in *49th U.S. Rock Mechanics/Geomechanics Symposium*. American Rock Mechanics Association.

Simser, B.P. (2019) 'Rockburst management in Canadian hard rock mines', *Journal of Rock Mechanics and Geotechnical Engineering*, 11(5), pp. 1036–1043.

Smalley Jr., R.F., Turcotte, D.L. and Solla, S.A. (1985) 'A renormalization group approach to the stick-slip behavior of faults', *Journal of Geophysical Research: Solid Earth*, 90(B2), pp. 1894–1900.

Spottiswoode, S.M. (2010) 'Mine seismicity: prediction or forecasting?', *Journal of the Southern African Institute of Mining and Metallurgy*, 110(1), pp. 11–20.

Stein, R.S. (1999) 'The role of stress transfer in earthquake occurrence', *Nature*, 402(6762), pp. 605–609.

Sudbury.com Staff (2020) *Seismic event occurred after development blast at Vale's Creighton Mine*, *Northern Ontario Business*. Available at: https://www.northernontariobusiness.com/regional-news/sudbury/earthquakes-canada-confirms-36mn-seismic-event-at-vales-creighton-mine-2277110 (Accessed: 15 March 2021).

Therriault, A.M., Fowler, A.D. and Grieve, R.A.F. (2002) 'The Sudbury Igneous Complex: a differentiated impact melt sheet', *Economic Geology*, 97(7), pp. 1521–1540.

Townsend, S. and Sampson-Forsythe, A. (2014) 'Mitigation strategies for mining in high stress sill pillars at Coleman Mine – a case study', in Hudyma, M. and Potvin, Y. (eds) *Deep Mining 2014: Proceedings from the Seventh International Conference on Deep and High Stress Mining*. Perth: Australian Centre for Geomechanics, pp. 65–77.

Urbancic, T.I., Bawden, W.F. and Young, R.P. (1992) 'Microseismic source parameters and their use in characterizing rock mass behaviour: considerations from Strathcona mine', in *Proceedings of 94th Annual General Meeting of the CIM: Rock Mechanics and Strata Control Sessions*. Canadian Institute of Mining, pp. 36–47.

Utsu, T. (2002) 'Chapter 43 - Statistical Features of Seismicity', in Lee, W.H.K., Kanamori, H., Jennings, P.C., and Kisslinger, C. (eds) *International Geophysics*. Cambridge, Massachusetts: Academic Press, pp. 719–732.

Van Aswegen, G. (2005) 'Routine seismic hazard assessment in some South African mines', in Potvin, Y. and Hudyma, M. (eds) *Proceedings of the 6th International Symposium on Rockburst and Seismicity in Mines*. Perth: Australian Centre for Geomechanics, pp. 437–444.

Van Aswegen, G. and Butler, A. (1993) 'Applications of quantitative seismology in South African gold mines', in Young, R.P. (ed.) *Proceedings of the 3rd International Symposium on Rockbursts and Seismicity in Mines*. Rotterdam: Balkema, pp. 261–266.

Van Aswegen, G. and Meijer, O. (1994) 'The mechanisms of seismic events around faults in mines', in *Rock Mechanics in Petroleum Engineering*. Society of Petroleum Engineers/International Society of Rock Mechanics, pp. 605–613.

Van Aswegen, G. and Mendecki, A. (1993) 'Mine layout, geological features and seismic hazard', in *GAP 303*. Safety in Mines Research Advisory Committee, pp. 1–113.

de la Vergne, J. (2008) *Hard rock miner's handbook*. Stantec Consulting.

Vezina, F. and Leslie, I. (2001) 'Seismic data analysis in underground mining operations using ESG's Hyperion systems', in *Proceedings of the 16th Quebec Mining Association Ground Control Colloque, Val D'Or*.

Wetzler, N., Lay, T., Brodsky, E.E. and Kanamori, H. (2018) 'Systematic deficiency of aftershocks in areas of high coseismic slip for large subduction zone earthquakes', *Science Advances*, 4(2), pp. 1–9.

White, B. and Whyatt, J. (1999) 'Role of fault slip on mechanisms of rock burst damage, Lucky Friday Mine, Idaho, USA', in Hagan, T.O. (ed.) *Second Southern African Rock Engineering Symposium, ISRM Regional Symposium*. International Society of Rock Mechanics, pp. 169–178.

Woodward, K. and Wesseloo, J. (2015) 'Observed spatial and temporal behaviour of seismic rock mass response to blasting', *Journal of the Southern African Institute of Mining and Metallurgy*, 115(11), pp. 1044–1056.

Wyss, M. and Brune, J.N. (1968) 'Seismic moment, stress and source dimensions for earthquakes in the California-Nevada region', *Journal of Geophysical Research*, 73, pp. 4681–4694.

Wyss, M. and Wiemer, S. (1999) 'How can one test the seismic gap hypothesis? The case of repeated ruptures in the Aleutians', in Wyss, M., Shimazaki, K., and Ito, A. (eds) *Seismicity Patterns, their Statistical Significance and Physical Meaning*. Basel: Birkhäuser, pp. 259–278.

Zhao, Cheng, Zhou, Y., Zhao, Chun and Bao, C. (2018) 'Cracking processes and coalescence modes in rock-like specimens with two parallel pre-existing cracks', *Rock Mechanics and Rock Engineering*, 51(11), pp. 3377–3393.

Zhou, X.P., Cheng, H. and Feng, Y.F. (2014) 'An experimental study of crack coalescence behaviour in rock-like materials containing multiple flaws under uniaxial compression', *Rock Mechanics and Rock Engineering*, 47(6), pp. 1961–1986.